Mesoscopic Rings

Yury Holubeu *

November 28, 2024

This draft is not aimed for distribution.
Links below show the contents of problems.

Contents

*https://yuriholubeu.github.io/, yuri.holubev@gmail.com

1 Preface and main motivation

Amazing facts

(I'll reveal it later)

Puzzles for motivation

(I'll reveal it later)

2 Mesoscopic Rings in a Nutshell

2.1 Main Formulas and Ideas (?)

2.1.1 Mesoscopic rings with Spin-Orbit interactions by Berche et. al.

Abstract

A didactic description of charge and spin equilibrium currents on mesoscopic rings in the presence of Spin-Orbit interaction is presented. Emphasis is made on the non trivial construction of the correct Hamiltonian in polar coordinates, the calculation of eigenvalues and eigenfunctions and the symmetries of the ground state properties. Spin currents are derived following an intuitive definition and then a more thorough derivation is built upon the canonical Lagrangian formulation that emphasizes the SU(2) gauge structure of the transport problem of spin 1/2 fermions in spin-orbit active media. The quantization conditions that follow from the constraint of single-valued Pauli spinors are also discussed. The targeted students are those of a graduate Condensed Matter Physics course.

Introduction

$$\begin{aligned}\mathbf{H} &= \Big[\frac{(\vec{p}-e\vec{\mathrm{A}})^2}{2m}-e\phi\Big]\mathbf{1}_{2\times 2}-\Big[\frac{\vec{p}^{\,4}}{8m^3c^2}-\frac{e\hbar^2}{8m^2c^2}\vec{\nabla}\cdot\vec{\mathrm{E}}\Big]\mathbf{1}_{2\times 2}\\ &\quad -\frac{e\hbar}{2m}\vec{\boldsymbol{\sigma}}\cdot\vec{\mathrm{B}}+\frac{e\hbar\vec{\boldsymbol{\sigma}}\cdot(\vec{p}-e\vec{\mathrm{A}})\times\vec{\mathrm{E}}}{4m^2c^2}.\end{aligned} \tag{2.1}$$

$\vec{\boldsymbol{\mu}} = g\frac{e}{2m}\vec{\mathbf{s}} = -\frac{|e|\hbar}{2m}\vec{\boldsymbol{\sigma}}$

$$\vec{\mathrm{B}}_{\text{rest fr.}} = \frac{1}{c^2}(-\vec{v})\times\vec{\mathrm{E}} = -(mc^2)^{-1}(\vec{p}\times\vec{\mathrm{E}}), \tag{2.2}$$

$$\begin{aligned}H_{\mathrm{SO}} &= -\frac{|e|\hbar}{2m^2c^2}\vec{\boldsymbol{\sigma}}\cdot(\vec{p}\times\vec{\mathrm{E}}),\\ &= \frac{|e|}{m^2c^2}\frac{1}{r}\frac{\partial\phi(r)}{\partial r}\vec{\mathbf{s}}\cdot\vec{L},\end{aligned} \tag{2.3}$$

$\vec{\mathrm{E}} = -\vec{\nabla}\phi = \frac{1}{r}\frac{\partial\phi(r)}{\partial r}\vec{r}$ and the interaction is proportional to $\vec{\mathbf{s}}\cdot\vec{L}$.

$$\mathbf{V}_{Rashba} = \text{const. }\vec{\boldsymbol{\sigma}}\cdot(\vec{\mathrm{E}}\times\vec{p}) = \alpha(\boldsymbol{\sigma}_y p_x - \boldsymbol{\sigma}_x p_y). \tag{2.4}$$

$$\mathbf{V}_{D,3d} = \text{const. } k_x(k_y^2-k_z^2)\boldsymbol{\sigma}_x + \text{c.p.} \tag{2.5}$$

$$\mathbf{V}_{Dresselhaus} = \beta(\boldsymbol{\sigma}_x p_x - \boldsymbol{\sigma}_y p_y), \tag{2.6}$$

Derivation of the ring Hamiltonian

The argument of Meijer, Morpurgo and Klapwijk for the Rashba SO interaction

$$\begin{aligned}\mathbf{H}_{2d} &= -\frac{\hbar^2}{2m}\left(\partial_\rho^2+\rho^{-1}\partial_\rho+\rho^{-2}\partial_\varphi^2\right)\mathbf{1}_{2\times 2}\\ &\quad +\alpha\rho^{-1}(\boldsymbol{\sigma}_x\cos\varphi+\boldsymbol{\sigma}_y\sin\varphi)i\hbar\partial_\varphi+\alpha(\boldsymbol{\sigma}_x\sin\varphi-\boldsymbol{\sigma}_y\cos\varphi)i\hbar\partial_\rho.\end{aligned} \tag{2.7}$$

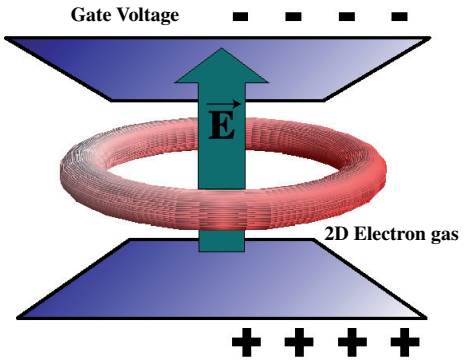

Figure 1: The typical Rashba situation with an electric field, created by a gate voltage, perpendicular to a ring fabricated on a two dimensional electron gas.

$\partial_x = -(\rho)^{-1}\sin\varphi\,\partial_\varphi + \cos\varphi\,\partial_\rho$
$\partial_y = (\rho)^{-1}\cos\varphi\,\partial_\varphi + \sin\varphi\,\partial_\rho.$

$$\mathbf{H'}_{1d} = \frac{\hbar^2}{2ma^2}(i\partial_\varphi)^2 + \alpha\hbar a^{-1}(\boldsymbol{\sigma}_x\cos\varphi + \boldsymbol{\sigma}_y\sin\varphi)i\partial_\varphi. \tag{2.8}$$

In [33], the authors note that the last term in (4.8) is non-Hermitian, since

$$\begin{aligned}\langle F|(\boldsymbol{\sigma}_x\cos\varphi + \boldsymbol{\sigma}_y\sin\varphi)i\partial_\varphi|G\rangle^* &= \left(\int_0^{2\pi} d\varphi\,(F_\uparrow^*\ F_\downarrow^*)\begin{pmatrix}0 & ie^{-i\varphi}\partial_\varphi\\ ie^{i\varphi}\partial_\varphi & 0\end{pmatrix}\begin{pmatrix}G_\uparrow\\ G_\downarrow\end{pmatrix}\right)^*\\ &= \left[-iF_\uparrow e^{i\varphi}G_\downarrow^* - iF_\downarrow e^{-i\varphi}G_\uparrow^*\right]_0^{2\pi} + \int_0^{2\pi} d\varphi\,(G_\uparrow^*\ G_\downarrow^*)\begin{pmatrix}0 & ie^{-i\varphi}\partial_\varphi\\ ie^{i\varphi}\partial_\varphi & 0\end{pmatrix}\begin{pmatrix}F_\uparrow\\ F_\downarrow\end{pmatrix}\\ &\quad + \int_0^{2\pi} d\varphi\,(G_\uparrow^*\ G_\downarrow^*)\begin{pmatrix}0 & e^{-i\varphi}\\ -e^{i\varphi} & 0\end{pmatrix}\begin{pmatrix}F_\uparrow\\ F_\downarrow\end{pmatrix}.\\ &= \langle G|(\boldsymbol{\sigma}_x\cos\varphi + \boldsymbol{\sigma}_y\sin\varphi)i\partial_\varphi|F\rangle - i\langle G|(\boldsymbol{\sigma}_x\sin\varphi - \boldsymbol{\sigma}_y\cos\varphi)|F\rangle,\end{aligned} \tag{2.9}$$

$\langle\varphi + 2\pi|F\rangle = \langle\varphi|F\rangle.$
$\mathbf{V} = \alpha\hbar a^{-1}\mathbf{W}$

$$\mathbf{W} = (\boldsymbol{\sigma}_\mathbf{x}\cos\varphi + \boldsymbol{\sigma}_\mathbf{y}\sin\varphi)\mathbf{i}\partial_\varphi - \mathbf{iA}(\boldsymbol{\sigma}_\mathbf{x}\sin\varphi - \boldsymbol{\sigma}_\mathbf{y}\cos\varphi), \tag{2.10}$$

since

$$\begin{aligned}\langle F|\mathbf{W}|\mathbf{G}\rangle^* \ =\ & \langle G|(\boldsymbol{\sigma}_x\cos\varphi + \boldsymbol{\sigma}_y\sin\varphi)i\partial_\varphi|F\rangle\\ & -i(1-A^*)\langle G|(\boldsymbol{\sigma}_x\sin\varphi - \boldsymbol{\sigma}_y\cos\varphi)|F\rangle,\end{aligned} \tag{2.11}$$

and

$$\begin{aligned}\langle G|\mathbf{W}|\mathbf{F}\rangle \ =\ & \langle G|(\boldsymbol{\sigma}_x\cos\varphi + \boldsymbol{\sigma}_y\sin\varphi)i\partial_\varphi|F\rangle\\ & -iA\langle G|(\boldsymbol{\sigma}_x\sin\varphi - \boldsymbol{\sigma}_y\cos\varphi)|F\rangle.\end{aligned} \tag{2.12}$$

$$H_\rho = \mathrm{KE} + V(\rho) = -\frac{\hbar^2}{2m}\left(\partial_\rho^2 + \rho^{-1}\partial_\rho\right) + V(\rho), \tag{2.13}$$

$$\mathbf{H}^{\mathrm{ring}}_{Rashba} = \langle R_0|\mathbf{H}_{2d} - \mathrm{KE}\,\mathbf{1}_{2\times2}|R_0\rangle, \tag{2.14}$$

$$\begin{aligned}\mathbf{H}^{\mathrm{ring}}_{Rashba} \ =\ & \frac{\hbar^2}{2ma^2}(i\partial_\varphi)^2\mathbf{1}_{2\times2}\\ & +\alpha\hbar a^{-1}(\boldsymbol{\sigma}_x\cos\varphi + \boldsymbol{\sigma}_y\sin\varphi)i\partial_\varphi - i\alpha\hbar(2a)^{-1}(\boldsymbol{\sigma}_x\sin\varphi - \boldsymbol{\sigma}_y\cos\varphi).\end{aligned} \tag{2.15}$$

Symmetrization of the original Hamiltonian

$\vec{\alpha} = \alpha\vec{e}_z$,

$$\vec{\boldsymbol{\sigma}} \cdot (\vec{\alpha} \times \vec{p}) = -\alpha(\boldsymbol{\sigma}_\rho p_\varphi - \boldsymbol{\sigma}_\varphi p_\rho), \tag{2.16}$$

$\boldsymbol{\sigma}_\rho = \boldsymbol{\sigma}_x \cos\varphi + \boldsymbol{\sigma}_y \sin\varphi$ and $\boldsymbol{\sigma}_\varphi = -\boldsymbol{\sigma}_x \sin\varphi + \boldsymbol{\sigma}_y \cos\varphi$
$p_\rho = -i\hbar(\partial_\rho - (2\rho)^{-1})$ and $p_\varphi = -i\hbar a^{-1}\partial_\varphi$.

$$\mathbf{V}^{\text{ring}}_{Rashba} = -\frac{1}{2}\alpha\{\boldsymbol{\sigma}_\rho, p_\varphi\} = i\hbar\alpha a^{-1}(\boldsymbol{\sigma}_\rho\partial_\varphi + \frac{1}{2}\partial_\varphi\boldsymbol{\sigma}_\rho), \tag{2.17}$$

$\partial_\varphi\boldsymbol{\sigma}_\rho = \boldsymbol{\sigma}_\varphi$,

$$\mathbf{H}^{\text{ring}}_{Rashba} = \frac{\hbar^2}{2ma^2}(i\partial_\varphi)^2\mathbf{1}_{2\times2} + i\hbar\alpha a^{-1}(\boldsymbol{\sigma}_\rho\partial_\varphi + \frac{1}{2}\boldsymbol{\sigma}_\varphi). \tag{2.18}$$

Hamiltonian in the rotated spin basis

$$|F'\rangle = e^{i\frac{\varphi}{2}\boldsymbol{\sigma}_z}|F\rangle = \big(\cos\frac{\varphi}{2}\mathbf{1}_{2\times2} + i\sin\frac{\varphi}{2}\boldsymbol{\sigma}_z\big)|F\rangle. \tag{2.19}$$

$$|\uparrow'\rangle = e^{i\frac{\varphi}{2}}|\uparrow\rangle, \quad |\downarrow'\rangle = e^{-i\frac{\varphi}{2}}|\downarrow\rangle. \tag{2.20}$$

$$\mathbf{H}' = e^{i\frac{\varphi}{2}\boldsymbol{\sigma}_z}\mathbf{H}e^{-i\frac{\varphi}{2}\boldsymbol{\sigma}_z}. \tag{2.21}$$

$\boldsymbol{\sigma}_\rho\boldsymbol{\sigma}_z = -i\boldsymbol{\sigma}_\varphi$,

$$\mathbf{H}^{\text{ring}}_{Rashba} = \frac{\hbar^2}{2ma^2}(i\partial_\varphi)^2\mathbf{1}_{2\times2} + i\hbar\alpha a^{-1}\boldsymbol{\sigma}_\rho(\partial_\varphi + \frac{i}{2}\boldsymbol{\sigma}_z). \tag{2.22}$$

$$e^{i\frac{\varphi}{2}\boldsymbol{\sigma}_z}\mathbf{H}^{\text{ring}}_{Rashba}e^{-i\frac{\varphi}{2}\boldsymbol{\sigma}_z} = \frac{\hbar^2}{2ma^2}(i\partial_\varphi\mathbf{1}_{2\times2} + \frac{1}{2}\boldsymbol{\sigma}_z)^2 + i\hbar\alpha a^{-1}\boldsymbol{\sigma}_x\partial_\varphi, \tag{2.23}$$

$\boldsymbol{\sigma}'_\rho \equiv e^{i\frac{\varphi}{2}\boldsymbol{\sigma}_z}\boldsymbol{\sigma}_\rho e^{-i\frac{\varphi}{2}\boldsymbol{\sigma}_z} = \boldsymbol{\sigma}_x$.

Eigenenergies and Eigenvectors on a ring

The Rashba SO interaction

$$\left(i\partial_\varphi\mathbf{1}_{2\times2} + \frac{ma\alpha}{\hbar}\boldsymbol{\sigma}_\rho\right)^2 = (i\partial_\varphi)^2\mathbf{1}_{2\times2} + \frac{2ma\alpha}{\hbar}\boldsymbol{\sigma}_\rho(i\partial_\varphi) + \frac{ma\alpha}{\hbar}i\boldsymbol{\sigma}_\varphi + \left(\frac{ma\alpha}{\hbar}\right)^2\mathbf{1}_{2\times2}. \tag{2.24}$$

$$\mathbf{H}^{\text{ring}}_{Rashba} = \frac{\hbar^2}{2ma^2}\left[\left(i\partial_\varphi\mathbf{1}_{2\times2} + \frac{ma\alpha}{\hbar}\boldsymbol{\sigma}_\rho\right)^2 - \left(\frac{ma\alpha}{\hbar}\right)^2\mathbf{1}_{2\times2}\right]. \tag{2.25}$$

$$\left(i\partial_\varphi\mathbf{1}_{2\times2} + \frac{ma\alpha}{\hbar}\boldsymbol{\sigma}_\rho\right)\Psi = \varepsilon\Psi, \tag{2.26}$$

$$\begin{pmatrix} i\partial_\varphi & \frac{ma\alpha}{\hbar}\mathrm{e}^{-i\varphi} \\ \frac{ma\alpha}{\hbar}\mathrm{e}^{i\varphi} & i\partial_\varphi \end{pmatrix}\begin{pmatrix}\psi_\uparrow \\ \psi_\downarrow\end{pmatrix} = \varepsilon\begin{pmatrix}\psi_\uparrow \\ \psi_\downarrow\end{pmatrix}. \tag{2.27}$$

$$\Psi^\lambda_{n,s} = \mathrm{e}^{i\lambda n\varphi}\begin{pmatrix} A_{\lambda,s}\mathrm{e}^{-i\varphi/2} \\ B_{\lambda,s}\mathrm{e}^{i\varphi/2}\end{pmatrix}, \tag{2.28}$$

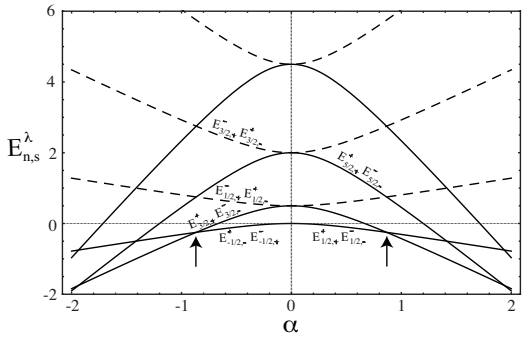

Figure 2: Energies of electrons on a ring with spin-orbit interaction as a function of the SO interaction strength α. The energy is in units of $\hbar^2/ma^2$ while α is in units of $\hbar/ma$. Indicated are the eigenvalue labels for the first five levels (note the ground state is fourfold degenerate). The graph shows how the limit $\alpha = 0$ is fourfold degenerate as expected since the time inversion symmetry turns into independent space and spin inversion symmetry. Arrows indicate change in lowest energy level.

$$\varepsilon^{\lambda}_{n,s} = \frac{s}{2}\sqrt{1+4\left(\frac{ma\alpha}{\hbar}\right)^2} - \lambda n, \tag{2.29}$$

where n is a half odd integer as will be seen below when we address the wavefunctions. The eigenvalues of (4.25) then simply follow

$$E^{\lambda}_{n,s} = \frac{\hbar^2}{2ma^2}\left[\left(n - \frac{\lambda s}{2}\sqrt{1+4\left(\frac{ma\alpha}{\hbar}\right)^2}\right)^2 - \left(\frac{ma\alpha}{\hbar}\right)^2\right]. \tag{2.30}$$

$E^{\lambda}_{n,s} = E^{-\lambda}_{n,-s}$
$E^{\lambda}_{n,s} = \hbar^2(n-\lambda s/2)^2/2ma^2 = \hbar^2 N^2/2ma^2$ (with n half odd integers).

$$B_{+,s} = \frac{\hbar}{2ma\alpha}\left(\frac{s}{\cos\theta} - 1\right)A_{+,s}, \tag{2.31}$$

$\cos\theta = 1/\sqrt{1+4(ma\alpha/\hbar)^2}$.
$B_{+,+} = \sin\theta/2$

$$\frac{\hbar}{2ma\alpha}\left(\frac{1-\cos\theta}{\cos\theta}\right)\cos\frac{\theta}{2} = \sin\frac{\theta}{2}, \tag{2.32}$$

$$\tan\theta = \frac{2ma\alpha}{\hbar}. \tag{2.33}$$

$$\Psi^{+}_{n,+} = e^{in\varphi}\begin{pmatrix}\cos\frac{\theta}{2}e^{-i\varphi/2}\\ \sin\frac{\theta}{2}e^{i\varphi/2}\end{pmatrix}, \Psi^{+}_{n,-} = e^{in\varphi}\begin{pmatrix}-\sin\frac{\theta}{2}e^{-i\varphi/2}\\ \cos\frac{\theta}{2}e^{i\varphi/2}.\end{pmatrix} \tag{2.34}$$

$$\Psi^{-}_{n,+} = e^{-in\varphi}\begin{pmatrix}\cos\frac{\theta}{2}e^{-i\varphi/2}\\ \sin\frac{\theta}{2}e^{i\varphi/2}\end{pmatrix}, \Psi^{-}_{n,-} = e^{-in\varphi}\begin{pmatrix}-\sin\frac{\theta}{2}e^{-i\varphi/2}\\ \cos\frac{\theta}{2}e^{i\varphi/2}\end{pmatrix} \tag{2.35}$$

$\Psi^{+}_{n,+} = \Theta\Psi^{-}_{n,-}$ and $\Psi^{+}_{n,-} = \Theta\Psi^{-}_{n,+}$.

Charge and spin currents in the ground state

Direct calculation

$$I_{charge} = -\sum_{n,s} \frac{\partial E^{\lambda}_{n,s}}{\partial \Phi} \tag{2.36}$$

$\vec{j}(\vec{r}) = n(\vec{r})e\vec{v}$,

$$\vec{J}_{charge} = \Psi^{\dagger} e\vec{\mathbf{v}}\ \Psi. \tag{2.37}$$

$$\mathbf{v}_{\varphi} = \frac{ia}{\hbar}[\mathbf{H}, \varphi] = \frac{\hbar}{ima}\partial_{\varphi}\mathbf{1}_{2\times 2} - \alpha\boldsymbol{\sigma}_{\rho}. \tag{2.38}$$

$$\begin{aligned} J_{\varphi} &= -\frac{e}{4}(\Psi^{+}_{1/2,+})^{\dagger}\mathbf{v}_{\varphi}\Psi^{+}_{1/2,+} - \frac{e}{4}(\Psi^{-}_{1/2,-})^{\dagger}\mathbf{v}_{\varphi}\Psi^{-}_{1/2,-} \\ &- \frac{e}{4}(\Psi^{-}_{-1/2,+})^{\dagger}\mathbf{v}_{\varphi}\Psi^{-}_{-1/2,+} - \frac{e}{4}(\Psi^{+}_{-1/2,-})^{\dagger}\mathbf{v}_{\varphi}\Psi^{+}_{-1/2,-} \qquad (2.39) \\ &= -\frac{e\hbar}{4ma}\left[\frac{1}{2} - \frac{1}{2\cos\theta}\right] - \frac{e\hbar}{4ma}\left[-\frac{1}{2} + \frac{1}{2\cos\theta}\right] \\ &- \frac{e\hbar}{4ma}\left[-\frac{1}{2} - \frac{1}{2\cos\theta}\right] - \frac{e\hbar}{4ma}\left[\frac{1}{2} + \frac{1}{2\cos\theta}\right] = 0 \qquad (2.40) \end{aligned}$$

$$\vec{\mathcal{J}}^{a} = \frac{1}{2}\Psi^{\dagger}\{\vec{\mathbf{v}}, \mathbf{s}^{a}\}\Psi, \tag{2.41}$$

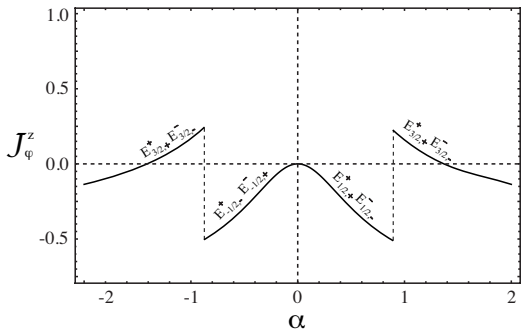

Figure 3: Spin current in units of $\hbar^2/4ma$ from the lowest lying degenerate level indicated in Fig.28 as a function of α. Between the arrows in Fig.28 the lowest level is fourfold degenerate so there are four terms in the spin current. Outside that range, other two-fold degenerate level take over causing a jump in the spin current as indicated. The graph shows how the limit $\alpha = 0$ indicates zero spin current because up down spin symmetry along with inversion symmetry are restored.

$$\begin{aligned} \mathcal{J}^{a}_{\varphi} &= \frac{\hbar^2}{2ma}(\lambda n - 1/2)[|A_{\lambda s}|^2\sigma^{a}_{11} + B^{*}_{\lambda s}A_{\lambda s}e^{-i\varphi}\sigma^{a}_{21}] \\ &+ \frac{\hbar^2}{2ma}(\lambda n + 1/2)[A^{*}_{\lambda s}B_{\lambda s}e^{i\varphi}\sigma^{a}_{12} + |B_{\lambda s}|^2\sigma^{a}_{22}] \\ &- \frac{\hbar}{2}\alpha\left(\cos\varphi\ \delta_{x,a} + \sin\varphi\ \delta_{y,a}\right), \end{aligned} \tag{2.42}$$

$$\begin{aligned}
\mathcal{J}^z_\varphi &= \frac{1}{4}(\Psi^+_{1/2,+})^\dagger \frac{1}{2}\{\mathbf{v}_\varphi, \mathbf{s}^z\}\Psi^+_{1/2,+} + \frac{1}{4}(\Psi^-_{1/2,-})^\dagger \frac{1}{2}\{\mathbf{v}_\varphi, \mathbf{s}^z\}\Psi^-_{1/2,-} \\
&+ \frac{1}{4}(\Psi^-_{-1/2,+})^\dagger \frac{1}{2}\{\mathbf{v}_\varphi, \mathbf{s}^z\}\Psi^-_{-1/2,+} + \frac{1}{4}(\Psi^+_{-1/2,-})^\dagger \frac{1}{2}\{\mathbf{v}_\varphi, \mathbf{s}^z\}\Psi^+_{-1/2,-} \qquad (2.43) \\
&= \frac{\hbar^2}{8ma}\left(\frac{1}{2}\cos\theta - \frac{1}{2}\right) + \frac{\hbar^2}{8ma}\left(\frac{1}{2}\cos\theta - \frac{1}{2}\right) \\
&- \frac{\hbar^2}{8ma}\left(-\frac{1}{2}\cos\theta + \frac{1}{2}\right) - \frac{\hbar^2}{8ma}\left(-\frac{1}{2}\cos\theta + \frac{1}{2}\right), \qquad (2.44) \\
&= \frac{\hbar^2}{4ma}(\cos\theta - 1)\,. \qquad (2.45)
\end{aligned}$$

$$\begin{aligned}
\mathcal{J}^x_\varphi &= \frac{1}{2}\hbar\alpha(\cos\theta - 1)\cos\varphi, \\
\mathcal{J}^y_\varphi &= \frac{1}{2}\hbar\alpha(\cos\theta - 1)\sin\varphi. \qquad (2.46)
\end{aligned}$$

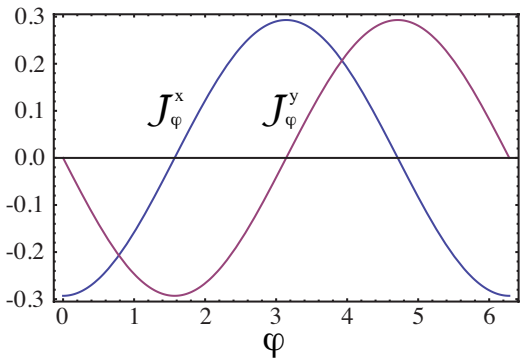

Figure 4: Spin currents for the x, y polarizations in units of $\hbar^2/4ma$ from the lowest lying degenerate levels indicated in Fig.28 as a function of φ and for $\alpha = \frac{\hbar}{2ma}$. Between the arrows in Fig.28, the lowest level is fourfold degenerate so there are four terms in each of the spin currents.

The Dresselhaus SO interaction

$$\begin{aligned}
\mathbf{V}^{\rm ring}_{Dresselhaus} &= -\tfrac{1}{2}\beta(\boldsymbol{\sigma}_x\{\sin\varphi, p_\varphi\} + \boldsymbol{\sigma}_y\{\cos\varphi, p_\varphi\}) \\
&= i\hbar\beta a^{-1}[(\boldsymbol{\sigma}_x\sin\varphi + \boldsymbol{\sigma}_y\cos\varphi)\partial_\varphi + \tfrac{1}{2}(\boldsymbol{\sigma}_x\cos\varphi - \boldsymbol{\sigma}_y\sin\varphi)],
\end{aligned} \qquad (2.47)$$

$$\mathbf{W} = (\boldsymbol{\sigma}_\mathbf{x}\sin\varphi + \boldsymbol{\sigma}_\mathbf{y}\cos\varphi)\mathbf{i}\partial_\varphi + \mathbf{iA}(\boldsymbol{\sigma}_\mathbf{x}\cos\varphi - \boldsymbol{\sigma}_\mathbf{y}\sin\varphi), \qquad (2.48)$$

$$\mathbf{W}^\dagger = (\boldsymbol{\sigma}_x\sin\varphi + \boldsymbol{\sigma}_y\cos\varphi)i\partial_\varphi + i(1 - A^*)(\boldsymbol{\sigma}_x\cos\varphi - \boldsymbol{\sigma}_y\sin\varphi), \qquad (2.49)$$

hermiticity requires $A^* = A = \frac{1}{2}$.

$$\mathbf{H}^{\rm ring}_{Dresselhaus} = \frac{\hbar^2}{2ma^2}\left[\left(i\partial_\varphi \mathbf{1}_{2\times 2} + \frac{ma\beta}{\hbar}(\boldsymbol{\sigma}_x \sin\varphi + \boldsymbol{\sigma}_y \cos\varphi)\right)^2 - \left(\frac{ma\beta}{\hbar}\right)^2 \mathbf{1}_{2\times 2}\right]. \quad (2.50)$$

$$E^\lambda_{n,s} = \frac{\hbar^2}{2ma^2}\Big[\Big(n - \frac{\lambda s}{2}\sqrt{1+4(ma\beta/\hbar)^2}\Big)^2 - (ma\beta/\hbar)^2\Big], \quad (2.51)$$

$$\Psi^+_{n,+} = e^{in\varphi}\begin{pmatrix}\sin\frac{\theta}{2}e^{i\varphi/2}\\ -i\cos\frac{\theta}{2}e^{-i\varphi/2}\end{pmatrix}, \Psi^+_{n,-} = e^{in\varphi}\begin{pmatrix}-\cos\frac{\theta}{2}e^{i\varphi/2}\\ -i\sin\frac{\theta}{2}e^{-i\varphi/2}\end{pmatrix} \quad (2.52)$$

$$\Psi^-_{n,+} = e^{-in\varphi}\begin{pmatrix}\sin\frac{\theta}{2}e^{i\varphi/2}\\ -i\cos\frac{\theta}{2}e^{-i\varphi/2}\end{pmatrix}, \Psi^-_{n,-} = e^{-in\varphi}\begin{pmatrix}-\cos\frac{\theta}{2}e^{i\varphi/2}\\ -i\sin\frac{\theta}{2}e^{-i\varphi/2}\end{pmatrix} \quad (2.53)$$

where now $\cos\theta = 1/\sqrt{1+4(ma\beta/\hbar)^2}$.

$$\mathcal{J}^z_\varphi = \frac{\hbar^2}{4ma}(1-\cos\theta). \quad (2.54)$$

Spin current and the non-Abelian gauge formalism

$$\begin{aligned} L &\equiv \int ad\varphi\, \mathcal{L}, \\ &= \langle\Psi|i\hbar\partial_t \mathbf{1}_{2\times 2} - \mathbf{H}|\Psi\rangle, \\ &= \int ad\varphi\, [i\hbar\Psi^\dagger\dot{\Psi} - \Psi^\dagger \mathbf{H}\Psi]. \end{aligned} \quad (2.55)$$

$$\begin{aligned} &i\hbar\Psi^\dagger\dot{\Psi} \\ &-\frac{1}{2m}\left[\Psi^\dagger(i\hbar a^{-1}\overleftarrow{\partial}_\varphi \mathbf{1}_{2\times 2} - \frac{1}{2}gW^a_\varphi\boldsymbol{\sigma}_a))\right]\left[(-i\hbar a^{-1}\overrightarrow{\partial}_\varphi \mathbf{1}_{2\times 2} - \frac{1}{2}gW^a_\varphi\boldsymbol{\sigma}_a))\Psi\right] \\ &+\frac{1}{8m}g^2\Psi^\dagger(W^b_\varphi\boldsymbol{\sigma}_b)(W^c_\varphi\boldsymbol{\sigma}_c)\Psi, \end{aligned} \quad (2.56)$$

$$\frac{1}{2}gW^a_\varphi\boldsymbol{\sigma}_a = m\alpha\boldsymbol{\sigma}_\rho, \quad (2.57)$$

$$\mathcal{J}^a_\varphi = \frac{\partial\mathcal{L}}{\partial W^a_\varphi} \quad (2.58)$$

$$\begin{aligned} \mathcal{J}_{(1)}{}^a_\varphi &= -\frac{1}{2m}\Psi^\dagger(-\frac{1}{2}\hbar\sigma_a)(-i\hbar a^{-1}\partial_\varphi \mathbf{1}_{2\times 2} - m\alpha\boldsymbol{\sigma}_\rho)\Psi \\ &\quad -\frac{1}{2m}\Psi^\dagger(i\hbar a^{-1}\partial_\varphi \mathbf{1}_{2\times 2} - m\alpha\boldsymbol{\sigma}_\rho)(-\frac{1}{2}\hbar\sigma_a)\Psi, \end{aligned} \quad (2.59)$$

$$\mathcal{J}_{(1)}{}^x_\varphi = -\frac{i\hbar^2}{4ma}[\Psi^\dagger\boldsymbol{\sigma}_x\partial_\varphi\Psi - (\partial_\varphi\Psi^\dagger)\boldsymbol{\sigma}_x\Psi] - \frac{1}{2}\hbar\alpha\Psi^\dagger\cos\varphi\Psi, \quad (2.60)$$

$$\mathcal{J}_{(1)}{}^y_\varphi = -\frac{i\hbar^2}{4ma}[\Psi^\dagger\boldsymbol{\sigma}_y\partial_\varphi\Psi - (\partial_\varphi\Psi^\dagger)\boldsymbol{\sigma}_y\Psi] - \frac{1}{2}\hbar\alpha\Psi^\dagger\sin\varphi\Psi, \quad (2.61)$$

$$\mathcal{J}_{(1)}{}^z_\varphi = -\frac{i\hbar^2}{4ma}[\Psi^\dagger\boldsymbol{\sigma}_z\partial_\varphi\Psi - (\partial_\varphi\Psi^\dagger)\boldsymbol{\sigma}_z\Psi]. \quad (2.62)$$

$$\mathcal{J}_{(2)}{}_{\varphi}^{a} = \frac{1}{8m}g^2\Psi^\dagger\left(\sigma_a W_\varphi^b\sigma_b + W_\varphi^b\sigma_b\sigma_a\right)\Psi, \tag{2.63}$$

$$= \frac{1}{4}\hbar\alpha\Psi^\dagger\{\sigma_a,\sigma_\rho\}\Psi, \tag{2.64}$$

$$\mathcal{J}_{(2)}{}_{\varphi}^{x} = \frac{1}{2}\hbar\alpha\Psi^\dagger\cos\varphi\Psi, \tag{2.65}$$

$$\mathcal{J}_{(2)}{}_{\varphi}^{y} = \frac{1}{2}\hbar\alpha\Psi^\dagger\sin\varphi\Psi, \tag{2.66}$$

$$\mathcal{J}_{(2)}{}_{\varphi}^{z} = 0, \tag{2.67}$$

$$\mathcal{J}_\varphi^a = -\frac{i\hbar^2}{4ma}[\Psi^\dagger\boldsymbol{\sigma}_a\partial_\varphi\Psi - (\partial_\varphi\Psi^\dagger)\boldsymbol{\sigma}_a\Psi], \tag{2.68}$$

Path integral on the ring and voltage quantization

$\sim -\vec{\boldsymbol{\sigma}}\cdot\vec{\mathrm{B}}_{\mathrm{eff.}}$.

$$\vec{\mathrm{B}}_{Rashba}^{\mathrm{eff.}} = \alpha p_\varphi\vec{e}_\rho \tag{2.69}$$

$$\hbar^{-1}\oint\frac{1}{2}g\vec{W}^a\boldsymbol{\sigma}_a d\vec{r} = \frac{m\alpha}{\hbar}\int_0^{2\pi} a\,d\varphi\,\boldsymbol{\sigma}_\rho. \tag{2.70}$$

$$(-i\hbar a^{-1}\partial_\varphi)\mathbf{1}_{2\times2} - m\alpha\boldsymbol{\sigma}_\rho, \tag{2.71}$$

where $m\alpha\boldsymbol{\sigma}_\rho \equiv \frac{1}{2}g\vec{W}^a\boldsymbol{\sigma}_a$ is a non-Abelian $SU(2)-$gauge field introduced in equation (4.57).

$\exp\left(i\hbar^{-1}\oint\frac{1}{2}g\vec{W}^a\boldsymbol{\sigma}_a d\vec{r}\right)$

$\Psi = \psi_\uparrow|+\rangle_\rho + \psi_\downarrow|-\rangle_\rho$,

$$\cos\tfrac{2\pi ma\alpha}{\hbar}\mathbf{1}_{2\times2}\Psi + i\boldsymbol{\sigma}_\rho\sin\tfrac{2\pi ma\alpha}{\hbar}\Psi = \Psi \tag{2.72}$$

$$\frac{2\pi ma\alpha}{\hbar} = 2\pi\times\texttt{integer}. \tag{2.73}$$

$$\frac{V}{4\pi mc^2/e} = \texttt{integer}, \tag{2.74}$$

$\langle\varphi+2\pi|n\rangle = \langle\varphi|n\rangle$ and $\int_0^{2\pi}d\varphi|\langle\varphi|n\rangle|^2 = 1$. We have

$$\langle\varphi|n\rangle = (2\pi)^{-1/2}e^{in\varphi},\quad n\in\mathbb{Z}. \tag{2.75}$$

$$\mathcal{A}(\varphi,\sigma;t\to\varphi',\sigma';t') = \prod_{i=1}^{N-1}\langle\varphi_{i+1},\sigma_{i+1}|e^{-i\Delta t\mathbf{H}/\hbar}|\varphi_i,\sigma_i\rangle, \tag{2.76}$$

$$i\partial_\varphi\mathbf{1}_{2\times2}|\varphi,\sigma\rangle = \sum_{n\in\mathbb{Z}}(-n)(2\pi)^{-1/2}e^{-in\varphi}\mathbf{1}_{2\times2}|n,\sigma\rangle, \tag{2.77}$$

$$\langle\varphi',\sigma'|\mathbf{H}|\varphi,\sigma\rangle = \frac{\hbar^2}{2ma^2}\sum_{n\in\mathbb{Z}}\frac{1}{2\pi}[n^2\delta_{\sigma,\sigma'} - 2n\frac{ma\alpha}{\hbar}(\boldsymbol{\sigma}_\rho)_{\sigma,\sigma'}]e^{in(\varphi'-\varphi)}. \tag{2.78}$$

$$\langle\varphi',\sigma'|\mathbf{1}_{2\times2}-\frac{i\Delta t}{\hbar}\mathbf{H}|\varphi,\sigma\rangle=\langle\varphi'|\varphi\rangle\delta_{\sigma,\sigma'}-\frac{i\Delta t}{\hbar}\langle\varphi',\sigma'|\mathbf{H}|\varphi,\sigma\rangle, \tag{2.79}$$

$\langle\varphi'|\varphi\rangle=\sum_{n\in\mathbb{Z}}\frac{1}{2\pi}e^{in(\varphi'-\varphi)}$

$$\langle\varphi',\sigma'|\mathbf{1}_{2\times2}-\frac{i\Delta t}{\hbar}\mathbf{H}|\varphi,\sigma\rangle=\sum_{n\in\mathbb{Z}}\frac{1}{2\pi}\left[e^{-\frac{i\hbar}{2ma^2}\Delta t[n^2\mathbf{1}_{2\times2}-2n\frac{ma\alpha}{\hbar}\boldsymbol{\sigma}_\rho]}\right]_{\sigma,\sigma'}e^{in(\varphi'-\varphi)}. \tag{2.80}$$

$v_\varphi=a(\varphi'-\varphi)/\Delta t$,

$$\langle\varphi_{i+1},\sigma_{i+1}|e^{-i\Delta t\mathbf{H}/\hbar}|\varphi_i,\sigma_i\rangle=\text{const}\ \left[e^{\frac{i}{\hbar}[\frac{1}{2}m(v_\varphi\mathbf{1}_{2\times2}-\alpha\boldsymbol{\sigma}_\rho)^2]\Delta t}\right]_{\sigma,\sigma'}, \tag{2.81}$$

such that extended to the whole path, we get the symbolic expression

$$\mathcal{A}(\varphi,\sigma;t\to\varphi',\sigma';t')=\int\mathcal{D}\varphi(t)\mathbf{T}\left[e^{\frac{i}{\hbar}\int\frac{1}{2}m(v_\varphi\mathbf{1}_{2\times2}-\alpha\boldsymbol{\sigma}_\rho)^2dt}\right]_{\sigma,\sigma'}, \tag{2.82}$$

$$\mathbf{L}=\frac{1}{2}m(v_\varphi\mathbf{1}_{2\times2}-\alpha\boldsymbol{\sigma}_\rho)^2. \tag{2.83}$$

$$\frac{1}{\hbar}\int_0^{2\pi}\frac{1}{2}\ mv_\varphi ad\varphi\,\delta_{\sigma,\sigma'}=\frac{\pi mv_\varphi a}{\hbar}\delta_{\sigma,\sigma'}. \tag{2.84}$$

$$\frac{1}{\hbar}\int_0^{2\pi}\ mv_\varphi\alpha(\boldsymbol{\sigma}_\rho)_{\sigma,\sigma'}dt=\frac{2\pi m\alpha(\boldsymbol{\sigma}_\rho)_{\sigma,\sigma'}a}{\hbar}, \tag{2.85}$$

or, using α and V defined above,

$$\frac{V}{2mc^2/e}(\boldsymbol{\sigma}_\rho)_{\sigma,\sigma'}. \tag{2.86}$$

$$\frac{1}{\hbar}\int_0^{2\pi}\frac{1}{2}\ m\alpha^2(\boldsymbol{\sigma}_\rho^2)_{\sigma,\sigma'}dt=\frac{\pi m\alpha^2\delta_{\sigma,\sigma'}a}{\hbar v_\varphi}. \tag{2.87}$$

$$\mathcal{A}(\varphi;t\to\varphi';t')=\int\mathcal{D}\varphi(t)e^{\frac{i}{\hbar}\int\left(\frac{1}{2}mv_\varphi^2+ev_\varphi A_\varphi\right)dt}, \tag{2.88}$$

2.1.2 Derivation of the correct Hamiltonian for 1D ring by Meijer et. al.

$$\hat{H}=\frac{1}{2m}(\mathbf{p}-e\mathbf{A})^2+\alpha\hat{\sigma}\cdot\mathbf{E}\times(\mathbf{p}-e\mathbf{A})+\mu\hat{\sigma}\cdot\mathbf{B},$$

$$\begin{aligned}\hat{H}(r,\phi)=-\frac{\hbar^2}{2m}&\left[\frac{\partial^2}{\partial r^2}+\frac{1}{r}\frac{\partial}{\partial r}-\frac{1}{r^2}\left(i\frac{\partial}{\partial\phi}+\frac{\Phi}{\Phi_0}\right)^2\right]\\&-\frac{\alpha}{r}\left(\cos\phi\sigma_x+\sin\phi\sigma_y\right)\left(i\frac{\partial}{\partial\phi}+\frac{\Phi}{\Phi_0}\right)\\&+i\alpha\left(\cos\phi\sigma_y-\sin\phi\sigma_x\right)\frac{\partial}{\partial r}+\frac{\hbar\omega_B}{2}\sigma_z\end{aligned}$$

$$\hat{H}(\phi) = -\frac{\hbar^2}{2ma^2}\left(i\frac{\partial}{\partial\phi}+\frac{\Phi}{\Phi_0}\right)^2+\frac{\hbar\omega_B}{2}\sigma_z-\frac{\alpha}{a}\left(\cos\phi\sigma_x+\sin\phi\sigma_y\right)\left(i\frac{\partial}{\partial\phi}+\frac{\Phi}{\Phi_0}\right)$$

$$\hat{H}_0 = -\frac{\hbar^2}{2m}\left[\frac{\partial^2}{\partial r^2}+\frac{1}{r}\frac{\partial}{\partial r}\right]+V(r)$$

$$\hat{H}_1 = \frac{\hbar^2}{2mr^2}\left(i\frac{\partial}{\partial\phi}+\frac{\Phi}{\Phi_0}\right)^2+\frac{\hbar\omega_B}{2}\sigma_z-\frac{\alpha}{r}\left(\cos\phi\sigma_x+\sin\phi\sigma_y\right)\left(i\frac{\partial}{\partial\phi}+\frac{\Phi}{\Phi_0}\right)+i\alpha\left(\cos\phi\sigma_y-\sin\phi\sigma_x\right)\frac{\partial}{\partial r}$$

$$a_{mn} = \langle\Phi_m(\phi)|\langle R_0(r)|\hat{H}_1(r,\phi)|R_0(r)\rangle|\Phi_n(\phi)\rangle,$$

$$\hat{H}_{1\mathrm{D}}(\phi) = \langle R_0(r)|\hat{H}_1(r,\phi)|R_0(r)\rangle.$$

$$-\frac{\hbar^2}{2m}\left[\frac{\partial^2 R(r)}{\partial r^2}+\frac{1}{r}\frac{\partial R(r)}{\partial r}\right]+\frac{1}{2}K(r-a)^2R(r) = ER(r).$$

$$R_0(r) = \left(\frac{\gamma}{a\sqrt{\pi}}\right)^{1/2}e^{-(1/2)\gamma^2(r-a)^2}$$

$\gamma^4 = mK/\hbar^2$

$$\langle R_0(r)|\frac{1}{r}|R_0(r)\rangle = \int_0^\infty R_0^2(r)dr = \frac{1}{a}$$

$$\langle R_0(r)|\frac{\partial}{\partial r}|R_0(r)\rangle = \int_0^\infty R_0(r)\frac{\partial R_0(r)}{\partial r}rdr = -\frac{1}{2a}.$$

$|\rho_0'(r)\rangle = (1/\sqrt{r})|\rho_0(r)\rangle$.

$\langle\rho_0|(1/2r)+(\partial/\partial r)|\rho_0\rangle = \langle\rho_0'|(1/r)(\partial/\partial r)|\rho_0'\rangle = 1/\,2\rho_0'^2|_0^\infty = 1/\,2r\rho_0^2|_0^\infty = 0$. We then obtain $\langle\rho_0|\partial/\partial r|\rho_0\rangle = -\langle\rho_0|1/2r|\rho_0\rangle$.

$\langle\rho_0|\partial/\partial r|\rho_0\rangle = -(1/2a)$,

$$\hat{H}_{1\mathrm{D}}(\phi) = \frac{\hbar^2}{2ma^2}\left(i\frac{\partial}{\partial\phi}+\frac{\Phi}{\Phi_0}\right)^2+\frac{\hbar\omega_B}{2}\sigma_z-\frac{\alpha}{a}\left(\cos\phi\sigma_x+\sin\phi\sigma_y\right)\left(i\frac{\partial}{\partial\phi}+\frac{\Phi}{\Phi_0}\right)- \\ -i\frac{\alpha}{2a}\left(\cos\phi\sigma_y-\sin\phi\sigma_x\right)$$

2.1.3 Spin states and persistent currents in mesoscopic rings: spin-orbit interactions by Sheng, Chang

Abstract

We investigate theoretically electron spin states in one dimensional (1D) and two dimensional (2D) hard-wall mesoscopic rings in the presence of both the Rashba spin-orbit interaction (RSOI) and the Dresselhaus spin-orbit interaction (DSOI) in a perpendicular magnetic field. The Hamiltonian of the RSOI alone is mathematically equivalent to that of the DSOI alone using an SU(2) spin rotation transformation. Our theoretical results show that the interplay between the RSOI and DSOI results in an effective periodic potential, which consequently leads to gaps in the energy spectrum. This periodic potential also weakens and smoothens the oscillations of the persistent charge current (CC) and spin current (SC) and results in the localization of electrons. For a 2D ring with a finite width, higher radial modes destroy the periodic oscillations of persistent currents.

Theoretical model

Hamiltonian

$$H = \frac{\hbar^2 k^2}{2m^*} + \alpha(\sigma_x k_y - \sigma_y k_x) + \beta(\sigma_x k_x - \sigma_y k_y) + \frac{1}{2} g^* \mu_B B \sigma_z + V(r), \tag{2.89}$$

$\boldsymbol{k} = -i\nabla + e\boldsymbol{A}/\hbar$. $\boldsymbol{A}(\boldsymbol{r}) = B/2(-y, x, 0)$

$$V(r) = \begin{cases} 0 & r_1 \leqslant r \leqslant r_2 \\ \infty & \text{otherwise} \end{cases}, \tag{2.90}$$

$$H = \begin{bmatrix} H_k + V(r) + \bar{g}b/2 & \bar{\beta}k_+ + i\bar{\alpha}k_- \\ \bar{\beta}k_- - i\bar{\alpha}k_+ & H_k + V(r) - \bar{g}b/2 \end{bmatrix}, \tag{2.91}$$

$H_k = (\boldsymbol{e}_r k_r + \boldsymbol{e}_\varphi k_\varphi)^2$
$k_\pm = k_x \pm i k_y = e^{\pm i\varphi}(k_r \pm i k_\varphi)$, with $k_r = -i\frac{\partial}{\partial r}$ and $k_\varphi = -\frac{i}{r}\frac{\partial}{\partial \varphi} + \frac{b}{4}r$; $b = \hbar e B/m^* E_0$
$\bar{\alpha}(\bar{\beta}) = \alpha(\beta)/E_0 a$

$$\Psi(\boldsymbol{r}) = \sum_{nm\sigma} a_{nm\sigma} R_n(r) \Theta_m(\varphi) \chi_\sigma(s_z), \tag{2.92}$$

$$R_n(r)\Theta_m(\varphi)\chi_\sigma(s_z) = \sqrt{\frac{2}{dr}} \sin\left[\frac{n\pi}{d}(r - r_1)\right] \cdot \frac{1}{\sqrt{2\pi}} e^{im\varphi} \cdot \chi_\sigma(s_z), \tag{2.93}$$

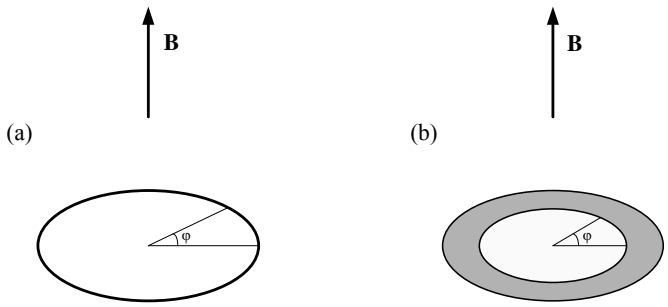

Figure 5: Schematic diagrams for 1D ideal ring (a) and 2D hard-wall ring (b).

$$H\Psi = E\Psi. \tag{2.94}$$

$$H = \left[-i\frac{\partial}{\partial\varphi} + \frac{\Phi}{\Phi_0} + \frac{\bar{\alpha}}{2}\sigma_r - \frac{\bar{\beta}}{2}\sigma_\varphi(-\varphi)\right]^2 - \frac{\bar{\alpha}^2 + \bar{\beta}^2}{4} + \frac{\bar{\alpha}\bar{\beta}}{2}\sin 2\varphi + \frac{1}{2}\bar{g}b\sigma_z, \tag{2.95}$$

$\sigma_r = \cos\varphi\sigma_x + \sin\varphi\sigma_y$,
$\sigma_\varphi = \cos\varphi\sigma_y - \sin\varphi\sigma_x$,
$\Phi = B\pi a^2$

$$S(\boldsymbol{r}) = \Psi^\dagger \boldsymbol{s} \Psi = \Psi^\dagger s_x \Psi \mathbf{e}_x + \Psi^\dagger s_y \Psi \mathbf{e}_y + \Psi^\dagger s_z \Psi \mathbf{e}_z. \tag{2.96}$$

Persistent currents

$$\begin{aligned}\hat{\rho}(\boldsymbol{r}') &= -e\delta(\boldsymbol{r}'-\boldsymbol{r})\\ \hat{\boldsymbol{j}}_c(\boldsymbol{r}') &= \frac{1}{2}[\hat{\rho}(\boldsymbol{r}')\hat{\boldsymbol{v}}+\hat{\boldsymbol{v}}\hat{\rho}(\boldsymbol{r}'))],\end{aligned} \tag{2.97}$$

$$\begin{aligned}\hat{\boldsymbol{S}}(\boldsymbol{r}') &= \frac{\hbar}{2}\hat{\boldsymbol{\sigma}}\delta(\boldsymbol{r}'-\boldsymbol{r})\\ \hat{\boldsymbol{j}}_s(\boldsymbol{r}') &= \frac{1}{2}[\hat{\boldsymbol{S}}(\boldsymbol{r}')\hat{\boldsymbol{v}}+\hat{\boldsymbol{v}}\hat{\boldsymbol{S}}(\boldsymbol{r}')],\end{aligned} \tag{2.98}$$

$\hat{\boldsymbol{\sigma}} = \hat{\sigma}_x\mathbf{e}_x + \hat{\sigma}_y\mathbf{e}_y + \hat{\sigma}_z\mathbf{e}_z$

$$\begin{aligned}\boldsymbol{j}_c(\boldsymbol{r}') &= \langle\Psi|\,\hat{\boldsymbol{j}}_c\,|\Psi\rangle = -e\,\mathrm{Re}\left\{\Psi^\dagger(\boldsymbol{r}')\hat{\boldsymbol{v}}'\Psi(\boldsymbol{r}')\right\}\\ \boldsymbol{j}_s(\boldsymbol{r}') &= \langle\Psi|\,\hat{\boldsymbol{j}}_s\,|\Psi\rangle = \mathrm{Re}\left\{\Psi^\dagger(\boldsymbol{r}')\hat{\boldsymbol{v}}'\hat{\boldsymbol{s}}\Psi(\boldsymbol{r}')\right\},\end{aligned} \tag{2.99}$$

$$\hat{\boldsymbol{v}}_\varphi = \mathbf{e}_\varphi\left[\frac{\hbar}{im^*r}\frac{\partial}{\partial\varphi}+\frac{eBr}{2m^*}+\frac{\alpha}{\hbar}\sigma_r-\frac{\beta}{\hbar}\sigma_\varphi(-\varphi)\right]. \tag{2.100}$$

$$I_\varphi = \frac{1}{2\pi}\int_0^{2\pi}\mathrm{d}\varphi\int_{r_1}^{r_2}\mathrm{d}r j_\varphi(\boldsymbol{r}). \tag{2.101}$$

Results and discussion

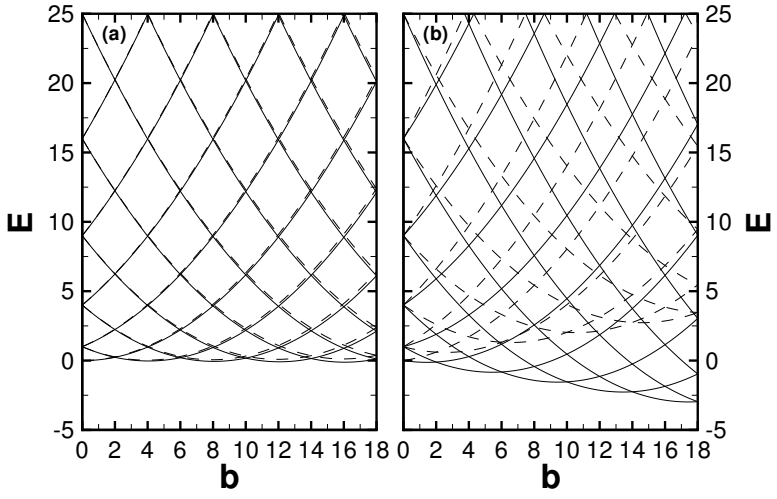

Figure 6: (a) The energy spectrum for 1D GaAs rings. $\bar{\alpha} = \bar{\beta} = 0$, $\bar{g} = -0.01474$; (b) The energy spectrum for 1D InSb ring. $\bar{\alpha} = \bar{\beta} = 0$, $\bar{g} = -0.357$. In Fig. 32(a) and Fig. 32(b) the solid (dashed) lines denote spin-up (spin-down) levels.

Table 1: Parameters used in our calculation are from Ref. [26].

	$m^*(m_e)$	g^*
GaAs	0.067	-0.44
InSb	0.014	-51

1D ring with RSOI alone

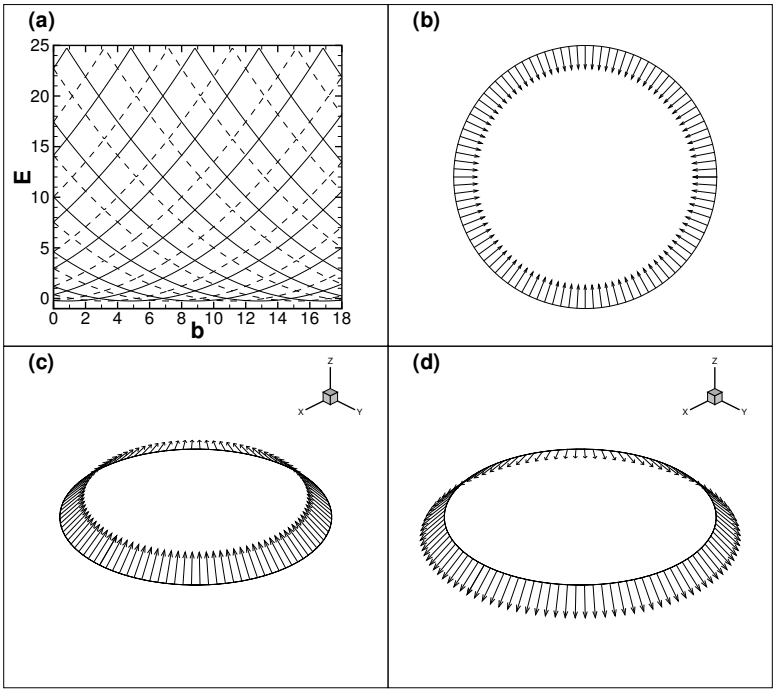

Figure 7: (a) Energy spectrum of 1D ring in the presence of RSOI alone, where the solid lines (dashed lines) denote the spin-up (spin-down) levels; (b) The projection of $S(\boldsymbol{r})^R_\uparrow$ onto the x-y plane; (c) Local spin orientation for all the spin-up levels $S(\boldsymbol{r})^R_\uparrow$; (d) Local spin orientation for all the spin-down levels $S(\boldsymbol{r})^R_\downarrow$. $\bar{\alpha} = 1$, $\bar{\beta} = 0$ and $\bar{g} = 0$.

$$E_{n,\sigma} = \left(n + \frac{b}{4} + \frac{\sigma}{2} - \frac{\sigma}{2\cos\theta}\right)^2 - \frac{\tan^2\theta}{4}, \tag{2.102}$$

$\theta = \arctan(\bar{\alpha})$

$$\begin{aligned} S(\boldsymbol{r})^R_\uparrow &= \Psi^{R\dagger}_{n,\uparrow} s_x \Psi^R_{n,\uparrow} \mathbf{e}_x + \Psi^{R\dagger}_{n,\uparrow} s_y \Psi^R_{n,\uparrow} \mathbf{e}_y + \Psi^{R\dagger}_{n,\uparrow} s_z \Psi^R_{n,\uparrow} \mathbf{e}_z \\ &= \frac{\hbar}{4\pi a} \left[\sin(-\theta)(\cos\varphi \mathbf{e}_x + \sin\varphi \mathbf{e}_y) + \cos(-\theta)\mathbf{e}_z\right]. \end{aligned} \tag{2.103}$$

$$I_{n,\sigma} = -\left(n + \frac{b}{4} + \frac{\sigma}{2} - \frac{\sigma}{2\cos\theta}\right), \tag{2.104}$$

$$I^{s_z}_{n,\sigma} = \left(n + \frac{b}{4} + \frac{\sigma}{2} - \frac{\sigma}{2\cos\theta}\right)\sigma\cos\theta. \tag{2.105}$$

$I_{n,\sigma}$ ($I^{s_z}_{n,\sigma}$) denotes the contribution to the persistent CC (SC) from the eigenstate $\Psi_{n,\sigma}$. $I_{n,\sigma}$ ($I^{s_z}_{n,\sigma}$) is in the units of $2E_0/\Phi_0$ ($E_0/2\pi$).

$I_n = -\partial E_n/\partial\Phi$.

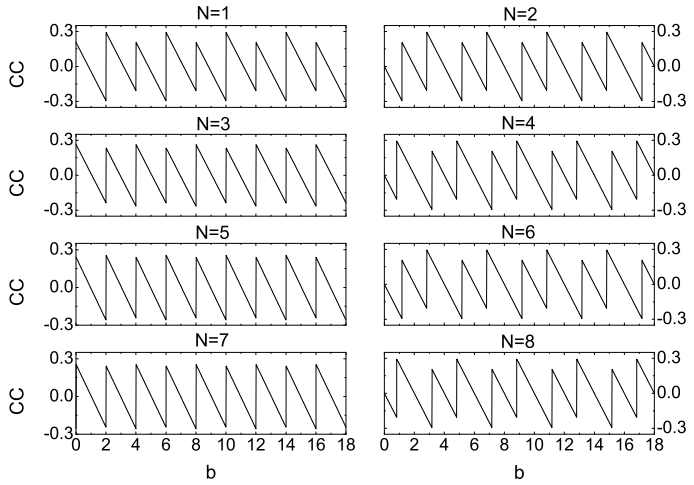

Figure 8: The persistent CC in a 1D ring with different numbers of electrons N *vs* magnetic field b while $\bar{\alpha} = 1$, $\bar{\beta} = 0$, $\bar{g} = 0$. The persistent CC is in units of $2NE_0/\Phi_0$.

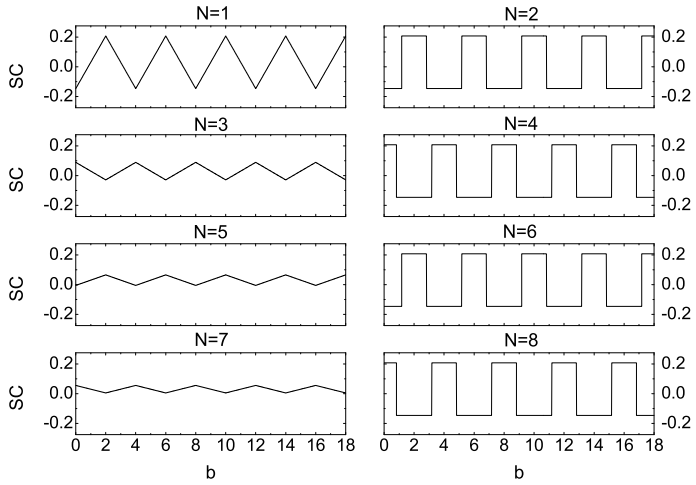

Figure 9: Same as Fig. 34, but for the persistent SC. The persistent SC is in units of $NE_0/2\pi$.

1D ring with DSOI alone

$$E^D_{n,\sigma} = E^R_{n,-\sigma}, \tag{2.106}$$

$$\Psi^D_{n,\uparrow} = \exp[i\pi/4]T\Psi^R_{n,\downarrow}, \tag{2.107}$$

$$\Psi^D_{n,\downarrow} = \exp[-i\pi/4]T^\dagger\Psi^R_{n,\uparrow}. \tag{2.108}$$

$$
\begin{aligned}
&S(\boldsymbol{r})^D_{\uparrow} \\
&= \Psi^{D\dagger}_{n,\uparrow} s_x \Psi^D_{n,\uparrow} \mathbf{e}_x + \Psi^{D\dagger}_{n,\uparrow} s_y \Psi^D_{n,\uparrow} \mathbf{e}_y + \Psi^{D\dagger}_{n,\uparrow} s_z \Psi^D_{n,\uparrow} \mathbf{e}_z \\
&= \Psi^{R\dagger}_{n,\downarrow} T^\dagger s_x T \Psi^R_{n,\downarrow} \mathbf{e}_x + \Psi^{R\dagger}_{n,\downarrow} T^\dagger s_y T \Psi^R_{n,\downarrow} \mathbf{e}_y \\
&+ \Psi^{R\dagger}_{n,\downarrow} T^\dagger s_z T \Psi^R_{n,\downarrow} \mathbf{e}_z \\
&= -\Psi^{R\dagger}_{n,\downarrow} s_y \Psi^R_{n,\downarrow} \mathbf{e}_x - \Psi^{R\dagger}_{n,\downarrow} s_x \Psi^R_{n,\downarrow} \mathbf{e}_y - \Psi^{R\dagger}_{n,\downarrow} s_z \Psi^R_{n,\downarrow} \mathbf{e}_z \\
&= \Psi^{R\dagger}_{n,\uparrow} s_y \Psi^R_{n,\uparrow} \mathbf{e}_x + \Psi^{R\dagger}_{n,\uparrow} s_x \Psi^R_{n,\uparrow} \mathbf{e}_y + \Psi^{R\dagger}_{n,\uparrow} s_z \Psi^R_{n,\uparrow} \mathbf{e}_z \\
&= \frac{\hbar}{4\pi a} \left[\sin(-\theta)(\sin\varphi \mathbf{e}_x + \cos\varphi \mathbf{e}_y) + \cos(-\theta)\mathbf{e}_z \right]. \qquad (2.109)
\end{aligned}
$$

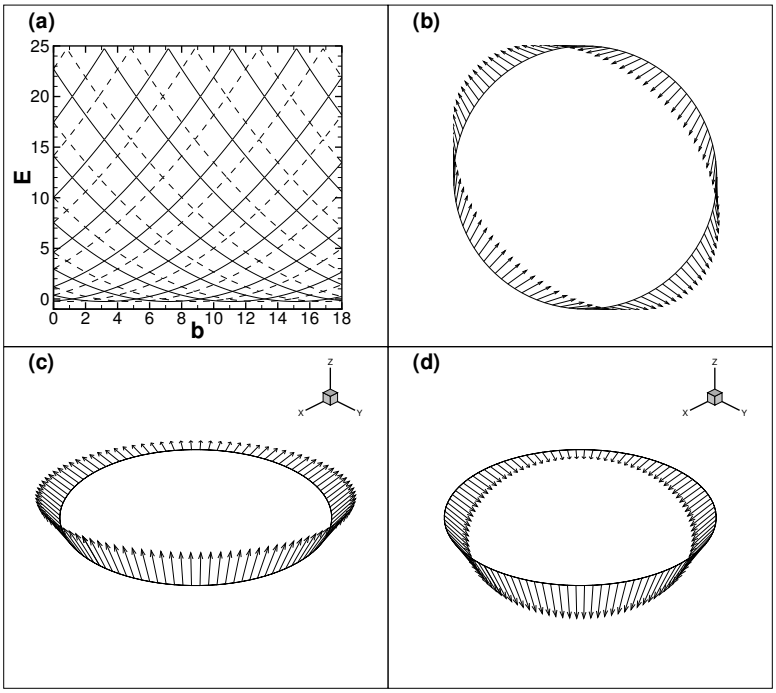

Figure 10: (a) Energy spectrum of 1D ring in the presence of DSOI alone, where the solid lines (dashed lines) denote the spin-up (spin-down) levels; (b) The projection of $S(\boldsymbol{r})^D_{\uparrow}$ onto the x-y plane; (c) Local spin orientation for all the spin-up levels $S(\boldsymbol{r})^D_{\uparrow}$; (d) Local spin orientation for all the spin-down levels $S(\boldsymbol{r})^D_{\downarrow}$. $\bar{\alpha} = 0$, $\bar{\beta} = 1$ and $\bar{g} = 0$.

1D ring with equal strength RSOI and DSOI

$$
D(\mathbf{n}, \varphi) = e^{-i\varphi \mathbf{n}\cdot\boldsymbol{L}/\hbar} \otimes e^{-i\varphi \mathbf{n}\cdot\boldsymbol{s}/\hbar}, \qquad (2.110)
$$

$$
T = D(\mathbf{n}_1, \pi). \qquad (2.111)
$$

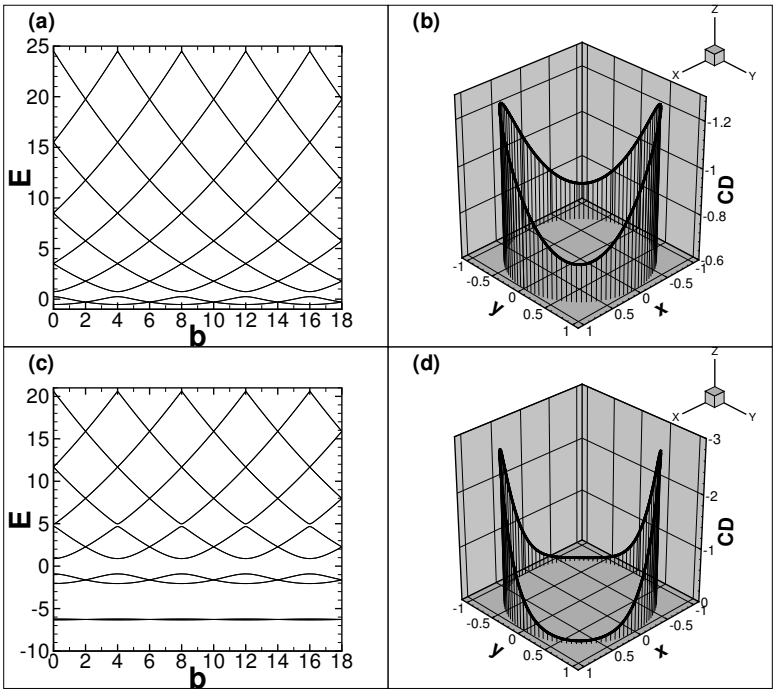

Figure 11: (a) Energy spectrum of 1D ring while $\bar{\alpha} = \bar{\beta} = 1$, $\bar{g} = 0$; (b) The charge density (CD) distribution of the lowest single electron state in a 1D ring while $\bar{\alpha} = \bar{\beta} = 1$, $\bar{g} = 0$, $b = 0$; (c) Energy spectrum of 1D ring while $\bar{\alpha} = \bar{\beta} = 3$, $\bar{g} = 0$; (d) The charge density (CD) distribution of the lowest single electron state in a 1D ring while $\bar{\alpha} = \bar{\beta} = 3$, $\bar{g} = 0$, $b = 0$. The charge density is in units of $e/2\pi a$.

$$A = \frac{1}{\sqrt{2}} \cdot \begin{bmatrix} \exp[-i\bar{\alpha}f(\varphi)] & \exp[i\bar{\alpha}f(\varphi)] \\ \exp[-i\pi/4]\exp[-i\bar{\alpha}f(\varphi)] & -\exp[-i\pi/4]\exp[i\bar{\alpha}f(\varphi)] \end{bmatrix}, \tag{2.112}$$

$f(\varphi) = \sin(\varphi + \pi/4)$.

$$H = \left[-i\frac{\partial}{\partial\varphi} + \frac{b}{4} + \frac{\bar{\alpha}}{2}\sigma_r - \frac{\bar{\alpha}}{2}\sigma_\varphi(-\varphi)\right]^2 - \frac{\bar{\alpha}^2}{2} + \frac{\bar{\alpha}^2}{2}\sin 2\varphi. \tag{2.113}$$

$$H' = A^\dagger H A = \left(-i\frac{\partial}{\partial\varphi} + \frac{b}{4}\right)^2 - \frac{\bar{\alpha}^2}{2} + \frac{\bar{\alpha}^2}{2}\sin 2\varphi. \tag{2.114}$$

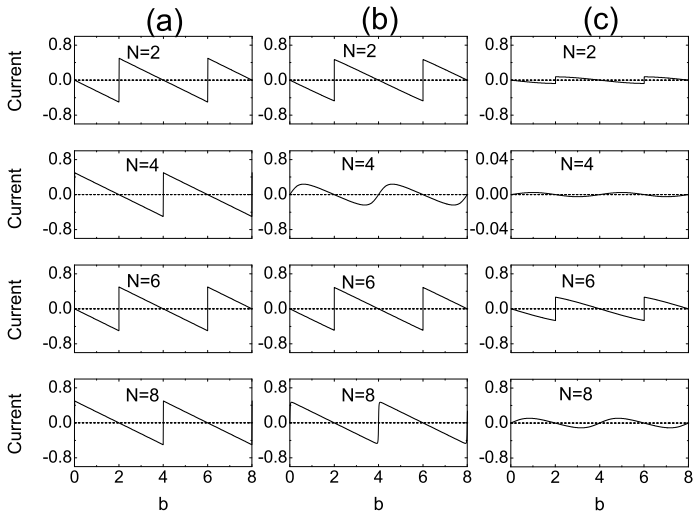

Figure 12: The persistent CC (solid lines) and SC (dashed lines) with different even numbers of electrons N *vs* magnetic field in the degenerate cases (a) $\bar{\alpha} = \bar{\beta} = \bar{g} = 0$; (b) $\bar{\alpha} = \bar{\beta} = 1$, $\bar{g} = 0$; (c) $\bar{\alpha} = \bar{\beta} = 3$, $\bar{g} = 0$. The persistent CC (SC) is in units of $2NE_0/\Phi_0$ ($NE_0/2\pi$).

1D ring with different strength RSOI and DSOI

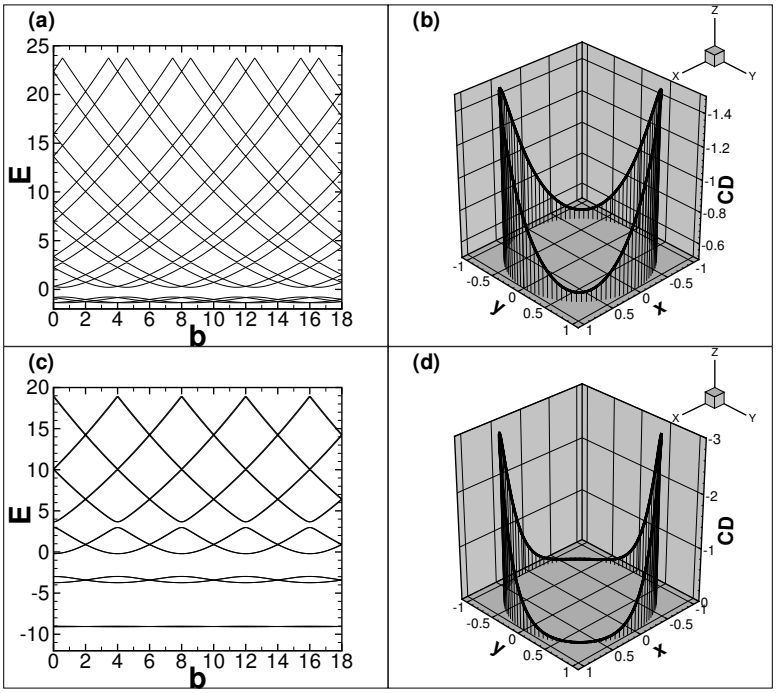

Figure 13: (a) Energy spectrum of 1D ring while $\bar{\alpha} = 2$, $\bar{\beta} = 1$, $\bar{g} = 0$; (b) The charge density (CD) distribution of the lowest single electron state in a 1D ring while $\bar{\alpha} = 2$, $\bar{\beta} = 1$, $\bar{g} = 0$, $b = 0$; (c) Energy spectrum of 1D ring while $\bar{\alpha} = 4$, $\bar{\beta} = 3$, $\bar{g} = 0$; (d) The charge density (CD) distribution of the lowest single electron state in a 1D ring while $\bar{\alpha} = 4$, $\bar{\beta} = 3$, $\bar{g} = 0$, $b = 0$. The charge density is in units of $e/2\pi a$.

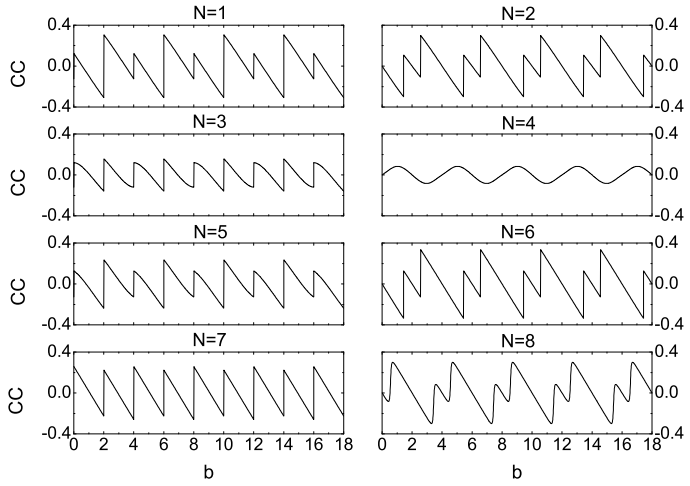

Figure 14: The persistent CC in a 1D ring with different numbers of electrons N *vs* magnetic field b while $\bar{\alpha} = 2$, $\bar{\beta} = 1$, $\bar{g} = 0$. The persistent CC is in units of $2NE_0/\Phi_0$.

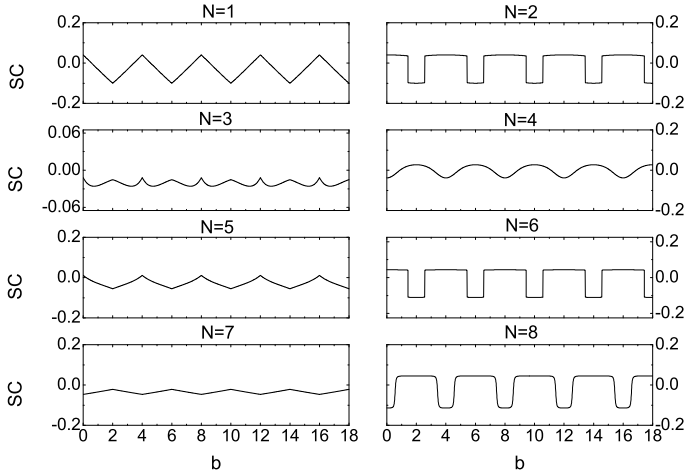

Figure 15: Same as Fig. 40, but for the persistent SC. The persistent SC is in units of $NE_0/2\pi$.

$\frac{\bar{\alpha}}{2}\sigma_r - \frac{\bar{\beta}}{2}\sigma_\varphi(-\varphi)$

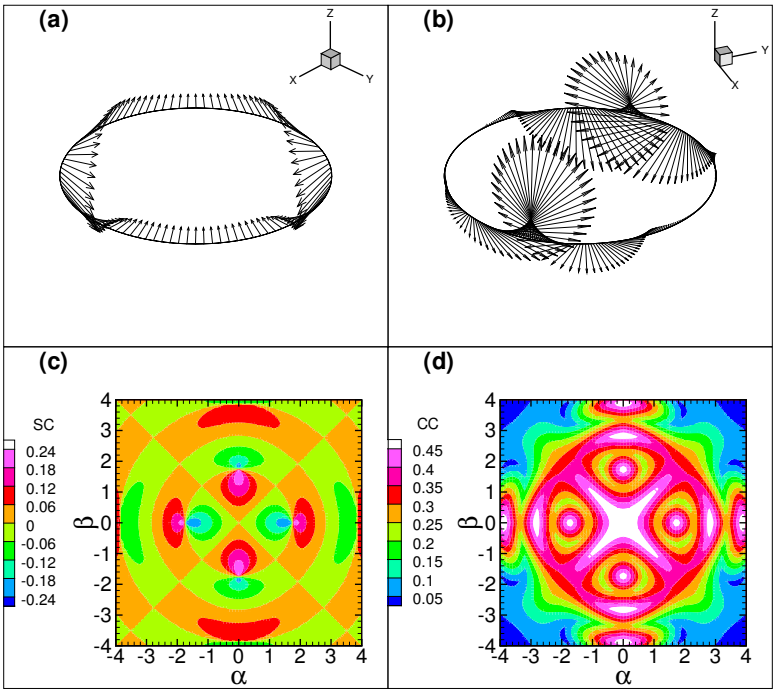

Figure 16: (color online) (a) Local spin orientation $S(\boldsymbol{r})$ for the lowest spin-up level while $\bar{\alpha} = 2$, $\bar{\beta} = 1$, $\bar{g} = 0$, $b = 2$; (b) Local spin orientation $S(\boldsymbol{r})$ for the lowest spin-up level while $\bar{\alpha} = 4$, $\bar{\beta} = 3$, $\bar{g} = 0$, $b = 2$; (c) The persistent SC in a 1D ring with different RSOI and DSOI strengths when the magnetic field b is 2; (d) The oscillation amplitude of the persistent CC in a 1D ring with different RSOI and DSOI strengths. In Fig. 42(c) and Fig. 42(d) we set $\bar{g} = 0$ and $N = 8$. The persistent CC (SC) is in units of $2NE_0/\Phi_0$ ($NE_0/2\pi$).

Finite width effects

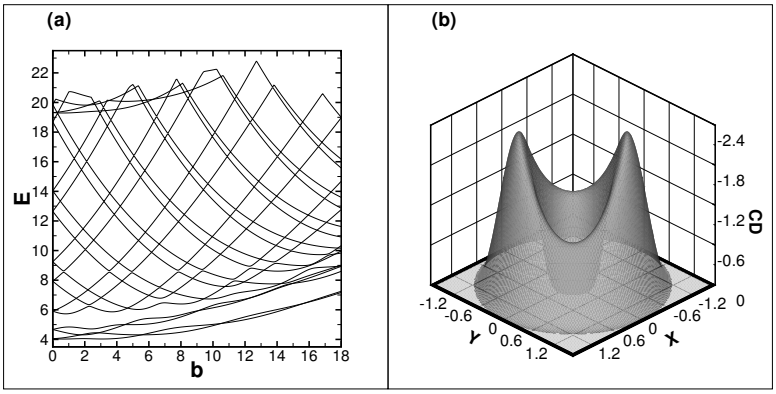

Figure 17: (a) Energy spectrum for 2D hard wall ring with width $d = 1.33$ while $\bar{\alpha} = 2$, $\bar{\beta} = 1$, $\bar{g} = 0$; (b) The charge density (CD) distribution of the lowest single electron state in a 2D hard wall ring with $d = 1.33$ while $\bar{\alpha} = 2$, $\bar{\beta} = 1$, $\bar{g} = 0$, $b = 0$. The charge density is in units of $e/2\pi a^2$.

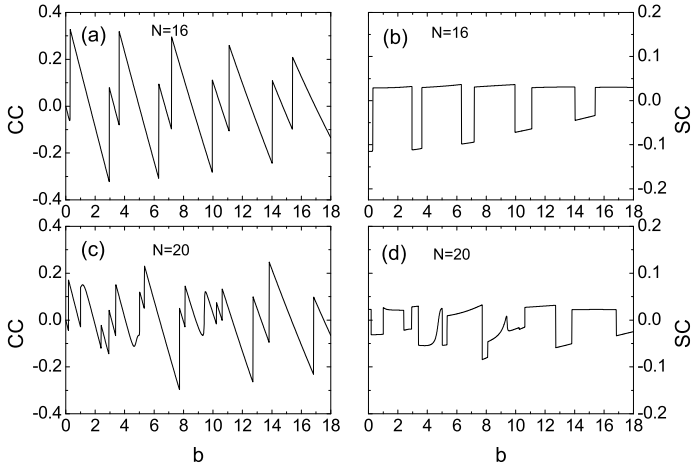

Figure 18: (a) The perisistent CC in a 2D ring *vs* magnetic field b while $\bar{\alpha}=2$, $\bar{\beta}=1$, $\bar{g}=0$, the width $d=1.33$ and $N=16$; (b) Same as (a) but for the persistent SC; (c) Same as (a) except $N=20$; (d) Same as (b) except $N=20$. The persistent CC (SC) is in units of $2NE_0/\Phi_0$ ($NE_0/2\pi$).

The Hamiltonian and available analytical solutions

The dimensionless Hamiltonian for a 2D ring reads

$$H_{2D}=H_k+H_R+H_D+H_Z+V(r), \tag{2.115}$$

where the kinetic term $H_k=(\boldsymbol{e}_r k_r+\boldsymbol{e}_\varphi k_\varphi)^2$, the Rashba term $H_R=\bar{\alpha}(\sigma_r k_\varphi-\sigma_\varphi k_r)$, the Dresselhaus term $H_D=\bar{\beta}[\sigma_r(-\varphi)k_r-\sigma_\varphi(-\varphi)k_\varphi]$, and the Zeeman term $H_Z=\bar{g}b\sigma_z/2$. $V(r)$ is the radial confining potential.

$$\begin{aligned}
H_{2D}=&-\frac{\partial^2}{\partial r^2}-\frac{1}{r}\frac{\partial}{\partial r}+V(r)+k_\varphi^2+\left[\bar{\alpha}\sigma_r-\bar{\beta}\sigma_\varphi(-\varphi)\right]k_\varphi+\frac{i}{2r}\left[-\bar{\alpha}\sigma_\varphi+\bar{\beta}\sigma_r(-\varphi)\right]+\\
&+\frac{1}{2}\bar{g}b\sigma_z+\left(k_r-\frac{i}{2r}\right)\left[-\bar{\alpha}\sigma_\varphi+\bar{\beta}\sigma_r(-\varphi)\right]=\\
=&-\frac{\partial^2}{\partial r^2}-\frac{1}{r}\frac{\partial}{\partial r}+V\left(r\right)+\left(k_r-\frac{i}{2r}\right)\left[-\bar{\alpha}\sigma_\varphi+\bar{\beta}\sigma_r(-\varphi)\right]+\\
&+\left[k_\varphi+\frac{\bar{\alpha}}{2}\sigma_r-\frac{\bar{\beta}}{2}\sigma_\varphi\left(-\varphi\right)\right]^2-\left[\frac{\bar{\alpha}}{2}\sigma_r-\frac{\bar{\beta}}{2}\sigma_\varphi(-\varphi)\right]^2+\frac{1}{2}\bar{g}b\sigma_z=\\
=&-\frac{\partial^2}{\partial r^2}-\frac{1}{r}\frac{\partial}{\partial r}+V(r)+\left(k_r-\frac{i}{2r}\right)\left[-\bar{\alpha}\sigma_\varphi+\bar{\beta}\sigma_r(-\varphi)\right]+\\
&+\left[k_\varphi+\frac{\bar{\alpha}}{2}\sigma_r-\frac{\bar{\beta}}{2}\sigma_\varphi(-\varphi)\right]^2-\frac{\bar{\alpha}^2+\bar{\beta}^2}{4}+\frac{\bar{\alpha}\bar{\beta}}{2}\sin 2\varphi+\frac{1}{2}\bar{g}b\sigma_z.
\end{aligned} \tag{2.116}$$

Specifically we write $H_{2D}=H_0+H_1$, where $H_0=-\frac{\partial^2}{\partial r^2}-\frac{1}{r}\frac{\partial}{\partial r}+V(r)$.

$$\langle\rho_0|\,\frac{\partial}{\partial r}+\frac{1}{2r}\,|\rho_0\rangle=0. \tag{2.117}$$

$$H=\left[-i\frac{\partial}{\partial\varphi}+\frac{b}{4}+\frac{\bar{\alpha}}{2}\sigma_r-\frac{\bar{\beta}}{2}\sigma_\varphi(-\varphi)\right]^2-\frac{\bar{\alpha}^2+\bar{\beta}^2}{4}+\frac{\bar{\alpha}\bar{\beta}}{2}\sin 2\varphi+\frac{1}{2}\bar{g}b\sigma_z. \tag{2.118}$$

$$T = \begin{bmatrix} 0 & \exp[-i\pi/4] \\ -\exp[i\pi/4] & 0 \end{bmatrix}$$

$$THT^\dagger = \left[-i\frac{\partial}{\partial\varphi} + \frac{b}{4} + \frac{\bar\beta}{2}\sigma_r - \frac{\bar\alpha}{2}\sigma_\varphi(-\varphi)\right]^2 - \frac{\bar\alpha^2+\bar\beta^2}{4} + \frac{\bar\alpha\bar\beta}{2}\sin 2\varphi - \frac{1}{2}\bar g b\sigma_z. \tag{2.119}$$

$$\begin{aligned} H &= \begin{bmatrix} H_{11} & H_{12} \\ H_{21} & H_{22} \end{bmatrix}, \text{ where} \\ H_{11} &= \left(-i\frac{\partial}{\partial\varphi} + \frac{b}{4}\right)^2 + \bar g b/2, \\ H_{12} &= \bar\alpha e^{-i\varphi}\left(-i\frac{\partial}{\partial\varphi} + \frac{b}{4} - \frac{1}{2}\right) + i\bar\beta e^{i\varphi}\left(-i\frac{\partial}{\partial\varphi} + \frac{b}{4} + \frac{1}{2}\right), \\ H_{21} &= \bar\alpha e^{i\varphi}\left(-i\frac{\partial}{\partial\varphi} + \frac{b}{4} + \frac{1}{2}\right) - i\bar\beta e^{-i\varphi}\left(-i\frac{\partial}{\partial\varphi} + \frac{b}{4} - \frac{1}{2}\right), \\ H_{22} &= \left(-i\frac{\partial}{\partial\varphi} + \frac{b}{4}\right)^2 - \bar g b/2. \end{aligned} \tag{2.120}$$

$\Psi = \begin{pmatrix}\Psi_1\\ \Psi_2\end{pmatrix} = \sum_m \begin{pmatrix} a_m \\ b_m\end{pmatrix}\Theta_m(\varphi)$, where $\Theta_m(\varphi) = \frac{1}{\sqrt{2\pi}}\exp[im\varphi]$.

$$\begin{cases} b_{m+1}\bar\alpha(m+\frac{b}{4}+\frac12) + ib_{m-1}\bar\beta(m+\frac{b}{4}-\frac12) = \left[E - (m+\frac{b}{4})^2 - \bar g b/2\right] a_m \\ a_{m-1}\bar\alpha(m+\frac{b}{4}-\frac12) - ia_{m+1}\bar\beta(m+\frac{b}{4}+\frac12) = \left[E - (m+\frac{b}{4})^2 + \bar g b/2\right] b_m \end{cases}. \tag{2.121}$$

$$\begin{bmatrix} \ddots & \ddots & 0 & \ddots & 0 & 0 & 0 & 0 \\ \ddots & \left(\frac{b}{4}-1\right)^2 + \frac{\bar g b}{2} & 0 & 0 & \bar\alpha\left(\frac{b}{4}-\frac12\right) & 0 & 0 & 0 \\ 0 & 0 & \left(\frac{b}{4}-1\right)^2 - \frac{\bar g b}{2} & -i\bar\beta\left(\frac{b}{4}-\frac12\right) & 0 & 0 & 0 & 0 \\ \ddots & 0 & i\bar\beta\left(\frac{b}{4}-\frac12\right) & \left(\frac{b}{4}\right)^2 + \frac{\bar g b}{2} & 0 & 0 & \bar\alpha\left(\frac{b}{4}+\frac12\right) & 0 \\ 0 & \bar\alpha\left(\frac{b}{4}-\frac12\right) & 0 & 0 & \left(\frac{b}{4}\right)^2 - \frac{\bar g b}{2} & -i\bar\beta\left(\frac{b}{4}+\frac12\right) & 0 & \ddots \\ 0 & 0 & 0 & 0 & i\bar\beta\left(\frac{b}{4}+\frac12\right) & \left(\frac{b}{4}+1\right)^2 + \frac{\bar g b}{2} & 0 & 0 \\ 0 & 0 & 0 & \bar\alpha\left(\frac{b}{4}+\frac12\right) & 0 & 0 & \left(\frac{b}{4}+1\right)^2 - \frac{\bar g b}{2} & \ddots \\ 0 & 0 & 0 & 0 & \ddots & 0 & \ddots & \ddots \end{bmatrix} \begin{bmatrix} \vdots \\ a_{-1} \\ b_{-1} \\ a_0 \\ b_0 \\ a_1 \\ b_1 \\ \vdots \end{bmatrix} = E \begin{bmatrix} \vdots \\ a_{-1} \\ b_{-1} \\ a_0 \\ b_0 \\ a_1 \\ b_1 \\ \vdots \end{bmatrix}. \tag{2.122}$$

a) $\bar\alpha \neq 0$, $\bar\beta = 0$;

$$\begin{bmatrix} (m+b/4)^2 + \bar g b/2 & \bar\alpha(m+b/4+1/2) \\ \bar\alpha(m+b/4+1/2) & (m+b/4+1)^2 - \bar g b/2 \end{bmatrix} \begin{bmatrix} a_m \\ b_{m+1} \end{bmatrix} = E \begin{bmatrix} a_m \\ b_{m+1} \end{bmatrix}. \tag{2.123}$$

The eigenvalues are

$$E^R_{n,\sigma} = \left(n + \frac{b}{4} + \frac{\sigma}{2} - \frac{\sigma}{2\cos\theta_{n,\sigma}}\right)^2 - \frac{\tan^2\theta_{n,\sigma}}{4} + \sigma\frac{\bar g b}{2\cos\theta_{n,\sigma}}, \tag{2.124}$$

$\tan\theta_{n,\sigma} = \frac{\bar\alpha(n+b/4+\sigma/2)}{n+b/4+\sigma/2-\bar g b/2}$.

$$\Psi^R_{n,\uparrow} = \frac{1}{\sqrt{2\pi}} e^{i(n+1/2)\varphi}\begin{pmatrix} \cos\frac{\theta_{n,\uparrow}}{2} e^{-i\varphi/2} \\ -\sin\frac{\theta_{n,\uparrow}}{2} e^{i\varphi/2}\end{pmatrix} \tag{2.125}$$

and

$$\Psi^R_{n,\downarrow} = \frac{1}{\sqrt{2\pi}} e^{i(n-1/2)\varphi} \begin{pmatrix} \sin\frac{\theta_{n,\downarrow}}{2} e^{-i\varphi/2} \\ \cos\frac{\theta_{n,\downarrow}}{2} e^{i\varphi/2} \end{pmatrix}. \tag{2.126}$$

$$S(\boldsymbol{r})^R_{n,\uparrow} = \frac{\hbar}{4\pi a} \left[\sin(-\theta_{n,\uparrow})(\cos\varphi \mathbf{e}_x + \sin\varphi \mathbf{e}_y) + \cos(-\theta_{n,\uparrow})\mathbf{e}_z\right] \tag{2.127}$$

and

$$S(\boldsymbol{r})^R_{n,\downarrow} = \frac{\hbar}{4\pi a} \left[\sin(\pi - \theta_{n,\downarrow})(\cos\varphi \mathbf{e}_x + \sin\varphi \mathbf{e}_y) + \cos(\pi - \theta_{n,\downarrow})\mathbf{e}_z\right]. \tag{2.128}$$

b) $\bar{\alpha} = 0$, $\bar{\beta} \neq 0$;

$$\begin{bmatrix} (m+b/4+1)^2 + \bar{g}b/2 & i\bar{\beta}(m+b/4+1/2) \\ -i\bar{\beta}(m+b/4+1/2) & (m+b/4)^2 - \bar{g}b/2 \end{bmatrix} \begin{bmatrix} a_{m+1} \\ b_m \end{bmatrix} = E \begin{bmatrix} a_{m+1} \\ b_m \end{bmatrix}. \tag{2.129}$$

The eigenvalues are

$$E^D_{n,\sigma} = \left(n + \frac{b}{4} - \frac{\sigma}{2} + \frac{\sigma}{2\cos\eta_{n,\sigma}}\right)^2 - \frac{\tan^2\eta_{n,\sigma}}{4} + \sigma\frac{\bar{g}b}{2\cos\eta_{n,\sigma}}, \tag{2.130}$$

$\tan\eta_{n,\sigma} = \frac{\bar{\beta}(n+b/4-\sigma/2)}{n+b/4-\sigma/2+\bar{g}b/2}$.

$$\Psi^D_{n,\uparrow} = \frac{1}{\sqrt{2\pi}} e^{i(n-1/2)\varphi} \begin{pmatrix} \cos\frac{\eta_{n,\uparrow}}{2} e^{i\varphi/2} \\ -i\sin\frac{\eta_{n,\uparrow}}{2} e^{-i\varphi/2} \end{pmatrix} \tag{2.131}$$

and

$$\Psi^D_{n,\downarrow} = \frac{1}{\sqrt{2\pi}} e^{i(n+1/2)\varphi} \begin{pmatrix} -i\sin\frac{\eta_{n,\downarrow}}{2} e^{i\varphi/2} \\ \cos\frac{\eta_{n,\downarrow}}{2} e^{-i\varphi/2} \end{pmatrix}. \tag{2.132}$$

$$S(\boldsymbol{r})^D_{n,\uparrow} = \frac{\hbar}{4\pi a} \left[\sin(-\eta_{n,\uparrow})(\sin\varphi \mathbf{e}_x + \cos\varphi \mathbf{e}_y) + \cos(-\eta_{n,\uparrow})\mathbf{e}_z\right] \tag{2.133}$$

and

$$S(\boldsymbol{r})^D_{n,\downarrow} = \frac{\hbar}{4\pi a} \left[\sin(\pi - \eta_{n,\downarrow})(\sin\varphi \mathbf{e}_x + \cos\varphi \mathbf{e}_y) + \cos(\pi - \eta_{n,\downarrow})\mathbf{e}_z\right]. \tag{2.134}$$

c) $\bar{\alpha} \neq 0$, $\bar{\beta} \neq 0$.

2.1.4 Persistent current in ballistic mesoscopic rings with Rashba spin-orbit coupling

Janine Splettstoesser, Michele Governale, Ulrich Zülicke

Abstract

The presence of spin–orbit coupling affects the spontaneously flowing persistent currents in mesoscopic conducting rings. Here we analyze their dependence on magnetic flux with emphasis on identifying possibilities to prove the presence and extract the strength of Rashba spin splitting in low–dimensional systems. Effects of disorder and mixing between quasi–onedimensional ring subbands are considered. The spin-orbit coupling strength can be inferred from the values of flux where sign changes occur in the persistent charge current. As an important consequence of the presence of spin splitting, we identify a nontrivial persistent spin current that is not simply proportional to the charge current. The different flux dependences of persistent charge and spin currents are a *unique* signature of spin–orbit coupling affecting the electronic structure of the ring.

Model of a mesoscopic ring with Rashba spin–orbit coupling

$$H_{\rm so} = \frac{\alpha}{\hbar}\left(\sigma_x\,(\vec{p} - e\vec{A})_y - \sigma_y\,(\vec{p} - e\vec{A})_x\right). \tag{2.135}$$

$l_{\rm so} = \pi\hbar^2/(m\alpha)$.

$$H = \frac{(\vec{p} - e\vec{A})_x^2 + (\vec{p} - e\vec{A})_y^2}{2m} + V_{\rm c}(r) + H_{\rm so} + \hbar\omega_{\rm z}\sigma_z, \tag{2.136}$$

$$H = -\frac{\hbar^2}{2m}\left[\frac{\partial^2}{\partial r^2} + \frac{1}{r}\frac{\partial}{\partial r} - \frac{1}{r^2}\left(i\frac{\partial}{\partial\varphi} + \frac{\Phi}{\Phi_0}\right)^2\right] + V_{\rm c}(r) - \frac{\alpha}{r}\sigma_r\left(i\frac{\partial}{\partial\varphi} + \frac{\Phi}{\Phi_0}\right) + i\alpha\sigma_\varphi\frac{\partial}{\partial r} + \hbar\omega_{\rm z}\sigma_z,$$

$\sigma_r = \cos\varphi\,\sigma_x + \sin\varphi\,\sigma_y$ and $\sigma_\varphi = -\sin\varphi\,\sigma_x + \cos\varphi\,\sigma_y$.
$H_0 = -\frac{\hbar^2}{2m}\left[\frac{\partial^2}{\partial r^2} + \frac{1}{r}\frac{\partial}{\partial r}\right] + V_{\rm c}(r)$.

$$V_{\rm c}(r) = \frac{1}{2}m\omega^2(r-a)^2, \tag{2.137}$$

$$H_0 = -\frac{\hbar^2}{2m}\left[\frac{\partial^2}{\partial r^2}\right] + \frac{1}{2}m\omega^2(r-a)^2. \tag{2.138}$$

$$H_{n,n} = \tfrac{\hbar^2}{2ma^2}\left(i\tfrac{\partial}{\partial\varphi} + \tfrac{\Phi}{\Phi_0}\right)^2 - \tfrac{\alpha}{a}\sigma_r\left(i\tfrac{\partial}{\partial\varphi} + \tfrac{\Phi}{\Phi_0}\right) - i\tfrac{\alpha}{2a}\sigma_\varphi + \hbar\omega_{\rm z}\sigma_z + \hbar\omega(n+\tfrac{1}{2}). \tag{2.139}$$

$$H_{n,n+1} = H^\dagger_{n+1,n} = i\sigma_\varphi\sqrt{\frac{n+1}{2}}\frac{\alpha}{l_\omega}. \tag{2.140}$$

Properties of ideal 1D rings

Energy spectrum of 1D ring with impurity

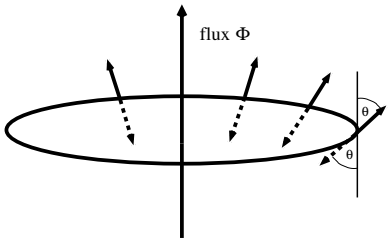

Figure 19: Schematic illustration of the spin texture exhibited by the eigenstates of the ideal one-dimensional ring.

$$E_{q,\pm} = \hbar\omega_{\rm a}\left(q - \frac{\Phi}{\Phi_0} + \frac{1}{2} \mp \frac{1}{2\cos\theta_q}\right)^2 + \frac{\hbar\omega_{\rm a}}{4}\left(1 - \frac{1}{\cos^2\theta_q}\right) \pm \frac{\hbar\omega_{\rm z}}{\cos\theta_q}. \tag{2.141}$$

$$\Psi_{q,\pm} = e^{i(q+\frac{1}{2})\varphi}\chi_{q,\pm}, \tag{2.142}$$

with the spinors

$$\chi_{q,+} = \begin{pmatrix} \cos(\frac{\theta_q}{2})e^{-i\frac{1}{2}\varphi} \\ \sin(\frac{\theta_q}{2})e^{i\frac{1}{2}\varphi} \end{pmatrix}, \tag{2.143a}$$

$$\chi_{q,-} = \begin{pmatrix} -\sin(\frac{\theta_q}{2})e^{-i\frac{1}{2}\varphi} \\ \cos(\frac{\theta_q}{2})e^{i\frac{1}{2}\varphi} \end{pmatrix}. \tag{2.143b}$$

The angle θ_q is given by[13]

$$\tan(\theta_q) = -\frac{\frac{\alpha}{a}(q - \frac{\Phi}{\Phi_0} + \frac{1}{2})}{\hbar\omega_{\rm a}(q - \frac{\Phi}{\Phi_0} + \frac{1}{2}) - \hbar\omega_{\rm z}}. \tag{2.144}$$

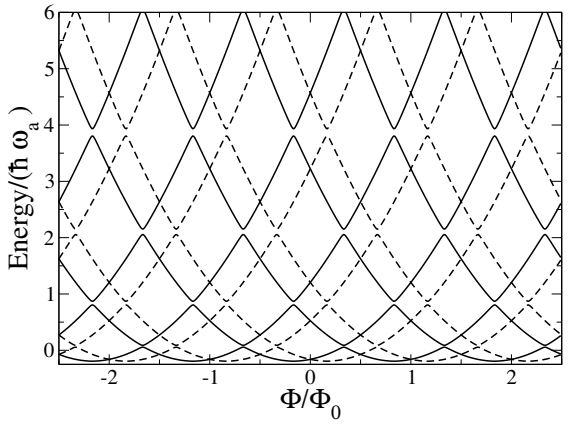

Figure 20: Single-particle energy spectrum of an ideal 1D ring with a model delta–barrier impurity. Parameters are $\cos\theta = 2/5$, and $A = 0.1$. Energy levels for states corresponding to spin-up (solid line) and spin-down (dashed line) in the local-spin-frame basis are shifted, in flux direction, by $1/\cos\theta$.

The spinors $\chi_{q,\pm}$ are the eigenstates of the operator

$$\sigma_{\theta_q} = \sigma_z \cos\theta_q + \sigma_r \sin\theta_q, \tag{2.145}$$

$\left|\hbar\omega_{\rm a}(q - \frac{\Phi}{\Phi_0} + \frac{1}{2})\right| \gg \hbar\omega_{\rm z}$.
$\theta_q \to \theta = \lim_{\omega_z \to 0}\theta_q$.

$$\mathcal{U} = \begin{pmatrix} e^{-i\varphi/2}\cos\frac{\theta}{2} & -e^{-i\varphi/2}\sin\frac{\theta}{2} \\ e^{i\varphi/2}\sin\frac{\theta}{2} & e^{i\varphi/2}\cos\frac{\theta}{2} \end{pmatrix}. \tag{2.146}$$

This yields $H_{\rm 1D} \equiv \mathcal{U}^\dagger \left(H_{0,0} - \hbar\omega/2\right)_{\omega_z=0} \mathcal{U}$ where

$$H_{\rm 1D} = \hbar\omega_{\rm a}\left(-i\frac{\partial}{\partial\varphi} - \frac{\Phi}{\Phi_0} - \frac{1}{2\cos\theta}\sigma_z\right)^2 + \frac{\hbar\omega_{\rm a}}{4}(1 - \frac{1}{\cos^2\theta}). \tag{2.147}$$

$$|t|\cos\left[2\pi\left(\frac{\Phi}{\Phi_0} \pm \frac{1}{2\cos(\theta)}\right)\right] = -\cos\left(2\pi\kappa_\pm + \delta\right), \tag{2.148}$$

$$E_\pm = \hbar\omega_{\rm a}\left[\kappa_\pm^2 + \frac{1}{4}(1 - \frac{1}{\cos^2\theta})\right]. \tag{2.149}$$

$\exp(i\kappa\varphi)|\pm\rangle$ is $t = 2\kappa/[2\kappa + iV_0/(\hbar\omega_{\rm a})]$.

$$\cos\left(2\pi\frac{\Phi_\pm}{\Phi_0}\right) = \cos\left(2\pi\kappa_\pm\right) + \mathrm{sign}(\kappa_\pm) A \sin\left(2\pi\kappa_\pm\right), \tag{2.150}$$

$A = V_0/(\hbar\omega_a\mathcal{N})$,

$$\Phi_\pm = \Phi + \Phi_0\left(\frac{1}{2} \pm \frac{1}{2\cos(\theta)}\right). \tag{2.151}$$

$$\kappa_{q,\pm} = q + \frac{1}{2\pi}\arccos\left[\frac{\cos(2\pi\frac{\Phi_\pm}{\Phi_0}) - \mathrm{sign}(q)\sqrt{A^2\left(\sin^2(2\pi\frac{\Phi_\pm}{\Phi_0}) + A^2\right)}}{1+A^2}\right]. \tag{2.152}$$

Persistent charge currents

$$I = -\frac{\partial E_{\mathrm{gs}}}{\partial\Phi} = -\sum_{i\in\mathrm{occupied}}\frac{\partial E_i}{\partial\Phi}, \tag{2.153}$$

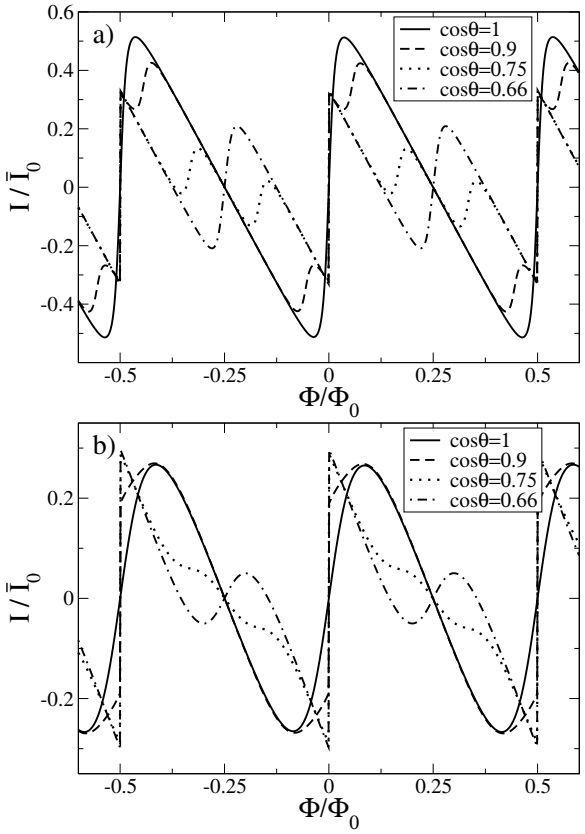

Figure 23: Average persistent charge current for an ensemble of identical rings with different electron numbers, shown as function of magnetic flux for different values of the spin-orbit coupling strength. The impurity parameter is $A = 0.1$ in panel a) and $A = 0.5$ in panel b). The current unit is $\bar{I}_0 = \hbar\omega_a\bar{\mathcal{N}}/\Phi_0$, where $\bar{\mathcal{N}}$ denotes the average number of electrons.

Persistent spin currents

$s_\nu(\vec{r}) = \sigma_\nu(\vec{r'})\,\delta(\vec{r}-\vec{r'})$, with σ_ν

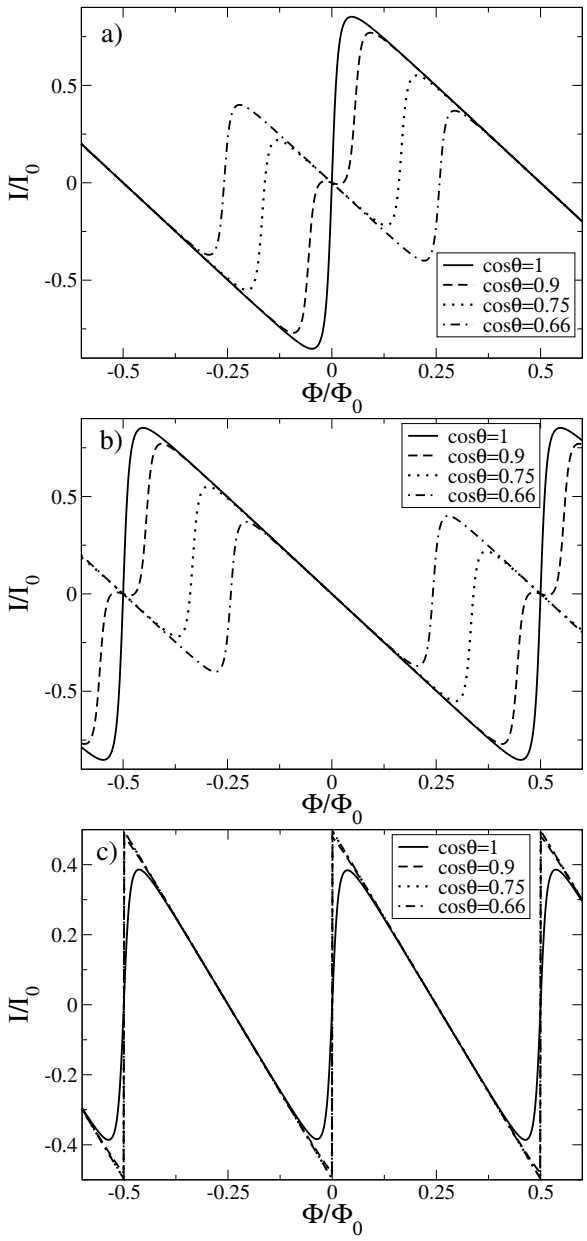

Figure 21: Persistent charge current vs. magnetic flux for a set of values for the spin-orbit coupling strength. The total number of electrons is set to $4N$ in panel a), to $4N+2$ in panel b), and to $2N+1$ in panel c) in the regime of large-enough N such that the persistent current is universal. A dimensionless barrier strength of $A = 0.1$ was assumed. The persistent current is measured in units of $I_0 = \hbar\omega_{\rm a}\mathcal{N}/\Phi_0$.

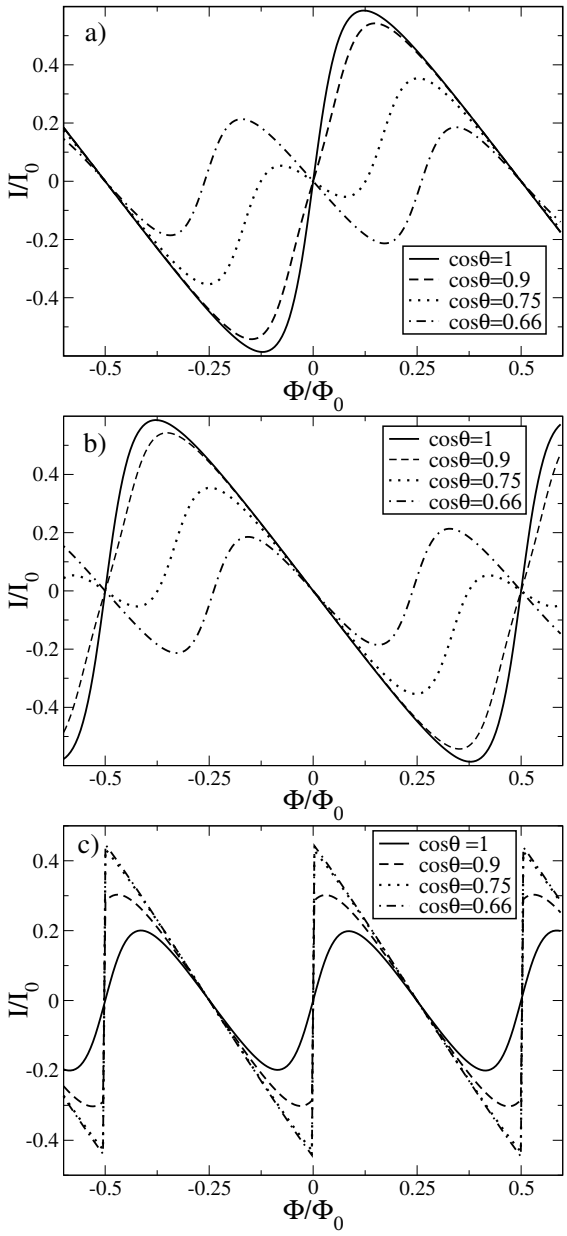

Figure 22: Same as Fig. 65 but with different impurity parameter $A = 0.5$. Note the remaining sharpness of jumps in the case of odd electron number even at this rather large value of A.

$$\frac{d}{dt}\, s_\nu(\vec{r}) = \frac{i}{\hbar}\, [H\,,\, s_\nu(\vec{r})]\,, \tag{2.154a}$$

$$= \left(\frac{d}{dt}\, \sigma_\nu(\vec{r'})\right)\, \delta(\vec{r}-\vec{r'}) - \vec{\nabla}_{\vec{r}} \cdot \left(\sigma_\nu(\vec{r'})\, \vec{v}(\vec{r})\right). \tag{2.154b}$$

$\vec{v} = \vec{v}_0 + \alpha(\hat{z}\times\vec{\sigma})/\hbar.$

$$\frac{d}{dt}\, s_\nu(\vec{r}) + \vec{\nabla}\cdot\vec{j}_\nu(\vec{r}) = \frac{2\alpha}{\hbar^2}\, (\hat{\nu}\times(\hat{z}\times\vec{\sigma}))\cdot\left(\vec{p}-e\vec{A}\right), \tag{2.155a}$$

$$\vec{j}_\nu(\vec{r}) = \vec{v}(\vec{r})\, \sigma_\nu. \tag{2.155b}$$

$$\frac{d}{dt}\, s_z(\varphi) + \frac{1}{a}\frac{\partial}{\partial\varphi}\, j_z^\varphi(\varphi) = 2\omega_{\rm a}\, \sigma_y \left(i\frac{\partial}{\partial\varphi} + \frac{\phi}{\phi_0}\right)\tan\theta. \tag{2.156a}$$

$$\begin{aligned} j_z^\varphi(\varphi) \;\; = \;\; & \frac{\hbar}{ma}\left\{\left(-i\frac{\partial}{\partial\varphi} - \frac{\phi}{\phi_0} - \frac{1}{2\cos\theta}\,\sigma_z\right)\sigma_z\cos\theta \right. \\ & \left. - \left(-i\frac{\partial}{\partial\varphi} - \frac{\phi}{\phi_0}\right)\sigma_x\sin\theta\right\}. \end{aligned} \tag{2.156b}$$

$$I_z^{(q\sigma)} = \frac{1}{2\pi a}\, \langle j_z^\varphi(\varphi)\rangle_{q\sigma} = -\frac{1}{e}\frac{\partial E_{q,\sigma}}{\partial\Phi}\, \sigma\cos\theta, \tag{2.157}$$

$\sigma_\nu(\vec{r'}) = \sigma_\theta(\varphi).$

$$\frac{d}{dt}\, s_\theta(\varphi) + \frac{1}{a}\frac{\partial}{\partial\varphi}\, j_\theta^\varphi(\varphi) = 0, \tag{2.158a}$$

with the current

$$j_\theta^\varphi(\varphi) = \frac{\hbar}{ma}\left(-i\frac{\partial}{\partial\varphi} - \frac{\phi}{\phi_0} - \frac{1}{2\cos\theta}\,\sigma_z\right)\sigma_z. \tag{2.158b}$$

$$I_\theta^{(q\sigma)} = -\frac{1}{e}\frac{\partial E_{q,\sigma}}{\partial\Phi}\, \sigma. \tag{2.159}$$

$I_z^{(q\sigma)} = I_\theta^{(q\sigma)}\cos\theta,$
$I_r^{(q\sigma)} = I_\theta^{(q\sigma)}\sin\theta.$

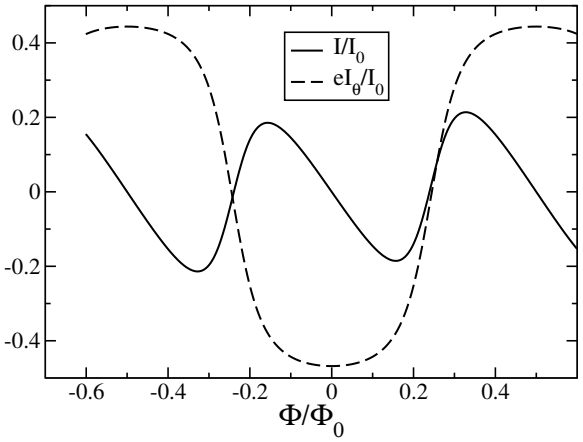

Figure 24: Persistent spin current for spin projection onto the local spin frame (dashed curve) and persistent charge current (solid curve) vs. magnetic flux for the case with electron number $4N+2$. The barrier strength is $A = 0.5$, and $\cos\theta = 0.66$. The current is measured in units of $I_0 = \hbar\omega_{\rm a}\mathcal{N}/\Phi_0$.

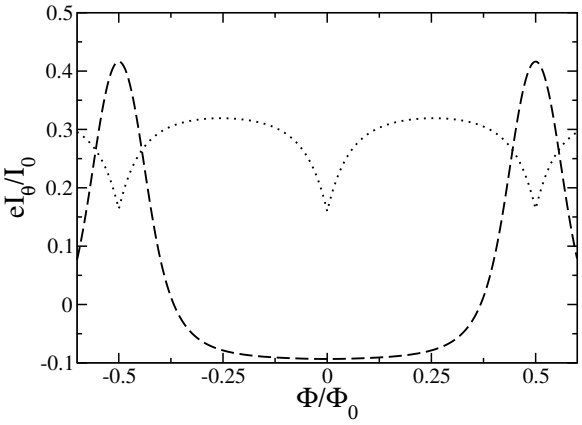

Figure 25: Comparison of persistent spin currents for electron number equal to $4N+2$ (dashed curve) and $2N+1$ (dotted curve). The barrier strength is $A = 0.5$, and $\cos\theta = 0.9$ corresponding to a small spin-orbit coupling strength. The magnitude of persistent spin current decreases rapidly for odd electron number as $\cos\theta$ approaches 0.66.

$$\phi(z) \approx \frac{\mu_0}{4\pi}\, g\mu_{\rm B}\, I_\theta\, \sin\theta\, \frac{a}{z^2}, \tag{2.160}$$

Effect of many radial subbands

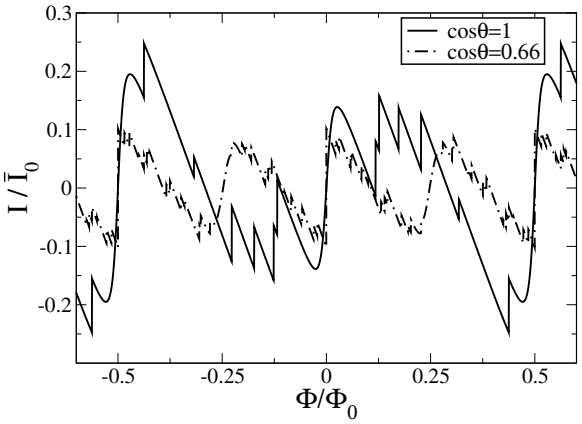

Figure 26: Average persistent current vs. magnetic flux for a ring with two occupied radial subbands. The barrier strength is $A = 0.1$. The average is performed on an ensemble containing rings with occupancy ranging from 60 to 80 electrons.

$$E_{q,\pm,n} = \hbar\omega_{\rm a}\left[\kappa_{q,\pm}^2 + \frac{1}{4}(1 - \frac{1}{\cos^2\theta})\right] + \hbar\omega\left(n + \frac{1}{2}\right), \tag{2.161}$$

3 Theory

4 Mesoscopic rings with Spin-Orbit interactions

Bertrand Berche[(a,b)], Christophe Chatelain[(a)] and Ernesto Medina[(b,c,a)]

Abstract

A didactic description of charge and spin equilibrium currents on mesoscopic rings in the presence of Spin-Orbit interaction is presented. Emphasis is made on the non trivial construction of the correct Hamiltonian in polar coordinates, the calculation of eigenvalues and eigenfunctions and the symmetries of the ground state properties. Spin currents are derived following an intuitive definition and then a more thorough derivation is built upon the canonical Lagrangian formulation that emphasizes the SU(2) gauge structure of the transport problem of spin 1/2 fermions in spin-orbit active media. The quantization conditions that follow from the constraint of single-valued Pauli spinors are also discussed. The targeted students are those of a graduate Condensed Matter Physics course.

4.1 Summary and Conclusions

We have presented an overview of the analytical treatment and role of spin-orbit interactions in the problem of mesoscopic ideal rings. For the benefit of the student, we have placed particular importance to the subtleties of deriving the correct Hamiltonian to the problem when posing it in terms of cylindrical coordinates. Such details had been overlooked in the literature for some time until reference[33] clarified this point. Besides the derivation given in the latter reference we have presented two other appealing approaches that may offer a simpler procedure for more involved problems. Once the correct Hamiltonian was posed we set out to explicitly derive the ground state properties in terms of the charge and spin currents as a function of the spin-orbit strength, pointing out the symmetries of the problem, and making such symmetries explicit both for the wavefunctions and the spectrum. Careful attention was paid to the correct limiting behavior as the spin-orbit interaction was sent to zero, the level degeneracies and all polarization components of the spin current for the lowest filling of the ring.

Using the Lagrangian formulation of the problems we formally derived the equilibrium currents, making a connection with recently reported *color currents*[40]. Such an approach also permitted assessing the role of the naturally ocurring gauge symmetry breaking term in the Rashba Hamiltonian, that is absent from the intuitive formulation of the current in terms of the velocity-spin anticommutator. The results point to a physical distinction of the gauge symmetry breaking contribution in the x, y polarization components of the spin current.

We finally addressed topological considerations on the spin-orbit ring. A voltage quantization condition was derived due to uniqueness of the wavefunction around the ring. A path integral approach to the problem was also formulated in order to formally derive a quadratic in spin-orbit strength contribution to the geometrical phase around the ring.

Every one of the topics discussed has been an opportunity to convey to the student the subtleties of the quantum formulation of the problem of spin transport on mesoscopic rings, detailing the calculations involved and making emphasis on physical insight, and not just bare technicalities.

There are many roads that begin from the material treated here. It is interesting to point out that the exact solutions derived are valid both for the limits: i) Slow rotation of the Rashba magnetic field with respect to a rapid precession of the spin and ii) Rapid rotation of the Rashba field in relation to the precession of the spin. The first is the adiabatic limit where Berry phase effects are dominant, while the latter relates to the sudden perturbation limit. Understanding physically the full range of such behaviors in the presence of a confining potential introduces the

physics of lateral subbands that may render many interesting effects for mesoscopic spin-orbit rings as quantum circuit elements.

4.2 Introduction

The study of spin transport properties in materials, especially in semi-conductors where two-dimensional electron gases (2DEG) can be fabricated, has become an important field of research both theoretically and experimentally in the last decade. One of the key concept there is the Spin-Orbit (SO) interaction which allows for spin manipulations. Mesoscopic rings are very simple laboratories for the investigation of various quantum effects [1] in the presence of spin-orbit interactions. They are the subject of intensive interest, both for fundamental reasons and potential applications in spintronics devices. Let us only mention a few fundamental studies in connection with phase effects, such as Aharonov-Casher effect [2, 3] or Sagnac phase shifts [4], spin interferences and spin filtering [5, 6, 7, 8, 9] or in the fashionable subject of graphene band structure [10]. On the more applied side, we can cite spin manipulations [11, 12, 13, 14], studies of spin related transport properties [15, 16, 17] and persistent currents [18, 19, 20], spin filtering in arrays of SO quantum rings [21] that operate on principles of spin interferometry analogous to their optical counterparts [22] and concepts for the elaboration of qubits gates [23].

Many of the concepts involved in spin transport are rooted in very basic quantum mechanics but in contexts that may be unfamiliar for the beginner, such as multiply connected geometries like closed loops or rings. This paper will serve to sort out such uncommon applications opening the scope of understanding forefront topics such as spintronics.

In this paper, we present an analysis of spin transport in a mesoscopic ring. The exposition is suitable for a course in condensed matter physics at the graduate level. We carefully present the details of the non trivial construction of the correct Hamiltonian in polar coordinates, the calculation of eigenvalues and eigenfunctions and the symmetries of the ground state properties with respect to time reversal symmetry. Charge and spin currents are derived following an intuitive and heuristic definition and then a more thorough derivation is built upon the canonical Lagrangian formulation that emphasizes the $SU(2)$ gauge structure of the transport problem. The path integral approach and the quantization conditions that follow from the constraint of single-valued Pauli spinors are also discussed for the benefit of a full picture that will be valuable to the student.

The Spin-Orbit interaction finds its origin in the Pauli equation, which follows from the non-relativistic limit of the Dirac equation,

$$\begin{aligned}\mathbf{H} \;=\; & \Big[\frac{(\vec{p}-e\vec{\mathrm{A}})^2}{2m}-e\phi\Big]\mathbf{1}_{2\times 2}-\Big[\frac{\vec{p}^{\,4}}{8m^3c^2}-\frac{e\hbar^2}{8m^2c^2}\vec{\nabla}\cdot\vec{\mathrm{E}}\Big]\mathbf{1}_{2\times 2}\\ & -\frac{e\hbar}{2m}\vec{\boldsymbol{\sigma}}\cdot\vec{\mathrm{B}}+\frac{e\hbar\vec{\boldsymbol{\sigma}}\cdot(\vec{p}-e\vec{\mathrm{A}})\times\vec{\mathrm{E}}}{4m^2c^2}.\end{aligned} \tag{4.1}$$

Here we consider electrons, $e=-|e|$. Ordinary vectors are denoted by arrows and bold face characters are used for 2×2 matrices. The first term in the first line corresponds to the usual Schrödinger equation including the kinetic energy with a mininal coupling to the electromagnetic gauge field $\vec{\mathrm{A}}$ and a scalar potential contribution $-e\phi$. The second term in the first line describes the first relativistic correction to the kinetic energy and the Darwin term, where $\vec{\mathrm{E}}$ is the electric field and c the speed of light. These first two terms are proportional to the 2×2 identity matrix in spin space $\mathbf{1}_{2\times 2}$. The second line comprises explicitly spin-dependent terms, first the Zeeman interaction[24] where $\vec{\mathrm{B}}$ is the magnetic field and $\vec{\boldsymbol{\sigma}}$ is the vector of Pauli matrices[24] and the second term is the Spin-Orbit interaction, written with the minimal coupling to the gauge vector. We have assumed a static potential so that the rotor of the electric field is absent and the Spin-Orbit interaction is limited to the term mentioned here [25].

Forgetting about the magnetic field, the Spin-Orbit interaction has a simple interpretation in terms of the interaction of the spin magnetic moment of the particles, (here supposed to be electrons of Landé factor[26] $g \simeq 2$ and spin $\vec{\mathbf{s}} = \frac{1}{2}\hbar\vec{\boldsymbol{\sigma}}$), $\vec{\boldsymbol{\mu}} = g\frac{e}{2m}\vec{\mathbf{s}} = -\frac{|e|\hbar}{2m}\vec{\boldsymbol{\sigma}}$, with the magnetic field produced by all external moving charges in the electron rest frame. Assuming a uniform electric field $\vec{\mathrm{E}}$ acting on the moving electrons, the SO contribution to the Hamiltonian results from the interaction $-\vec{\boldsymbol{\mu}} \cdot \vec{\mathrm{B}}_{\text{rest fr.}}$ of $\vec{\boldsymbol{\mu}}$ with the effective magnetic field experienced by the particles in their rest frame. In the case of a Lorentz change of reference frame, one has

$$\vec{\mathrm{B}}_{\text{rest fr.}} = \frac{1}{c^2}(-\vec{v}) \times \vec{\mathrm{E}} = -(mc^2)^{-1}(\vec{p} \times \vec{\mathrm{E}}), \tag{4.2}$$

where $\vec{v}$ and $\vec{p}$ refer to the dynamical variables of the electron. This expression is corrected by a similar contribution with a factor $-\frac{1}{2}$ due to the Thomas precession in the case of a closed orbit. Such a term appears when the proper Lorentz transformation for the fields is considered[26]. In such a way, the resulting SO interaction is usually written (e.g. in atoms)

$$\begin{aligned} H_{\text{SO}} &= -\frac{|e|\hbar}{2m^2c^2}\vec{\boldsymbol{\sigma}} \cdot (\vec{p} \times \vec{\mathrm{E}}), \\ &= \frac{|e|}{m^2c^2}\frac{1}{r}\frac{\partial\phi(r)}{\partial r}\vec{\mathbf{s}} \cdot \vec{L}, \end{aligned} \tag{4.3}$$

were we have substituted a spherically symmetric potential, $\vec{\mathrm{E}} = -\vec{\nabla}\phi = \frac{1}{r}\frac{\partial\phi(r)}{\partial r}\vec{r}$ and the interaction is proportional to $\vec{\mathbf{s}} \cdot \vec{L}$. It is clear now why, in the context of atoms, the interaction is christened the Spin-Orbit interaction i.e. $\vec{L}$ pertains to the angular momentum of the orbit while $\vec{s}$ pertains to intrinsic angular momentum, the spin.

The prefactor in this expression depends on the details of the problem (Landé factor, effective mass, ...) its sign even depends on the nature of the particles involved. In semiconductor physics, one usually introduces the notations α or β for this coefficient, which is determined perturbatively in the $\vec{k} \cdot \vec{p}$ theory by a matrix element in the Bloch wave functions basis. In the case of a two-dimensional electron gas with a gate voltage applied perpendicular to the $2d$ sample (with a non-symmetric confining potential generating a space inversion assymmetry (SIA)), this term is known as the Rashba SO interaction [27, 28],

$$\mathbf{V}_{Rashba} = \text{const. } \vec{\boldsymbol{\sigma}} \cdot (\vec{\mathrm{E}} \times \vec{p}) = \alpha(\boldsymbol{\sigma}_y p_x - \boldsymbol{\sigma}_x p_y). \tag{4.4}$$

Note that the Rashba SO amplitude can be tuned experimentally using a gate voltage, since the prefactor α is proportional to the electric field (see figure 27).

The calculation of matrix elements leading to α is generally a hard task and one usually uses phenomenological expressions compatible with the crystal symmetries or computes them directly from experiment[29]. The Rashba interaction applies in the case of SIA. When there is bulk inversion asymmetry (BIA) i.e. the crystal unit cell lacks inversion symmetry, we have the Dresselhaus 'flavor' of the SO interaction in $3d$ systems [30],

$$\mathbf{V}_{D,3d} = \text{const. } k_x(k_y^2 - k_z^2)\boldsymbol{\sigma}_x + \text{c.p.} \tag{4.5}$$

where c.p. stands for cyclic permutations. In the case of electrons confined in two dimensions, the expectation value along the confinement, quantized dimension should be considered. If that direction is z, then $\langle k_z \rangle \simeq 0$, $\langle k_z^2 \rangle \simeq (\pi/\ell)^2$, ℓ being the typical confinement length or spatial width of the confinement potential. The Dresselhaus SO interaction thus takes the simple form, here written in a notation closer to equation (4.4),

$$\mathbf{V}_{Dresselhaus} = \beta(\boldsymbol{\sigma}_x p_x - \boldsymbol{\sigma}_y p_y), \tag{4.6}$$

where we neglect cubic terms in k and the average values computed are lumped in the definition of β. For more details on SO interactions in semi-conductors, see Refs. [30, 31, 32].

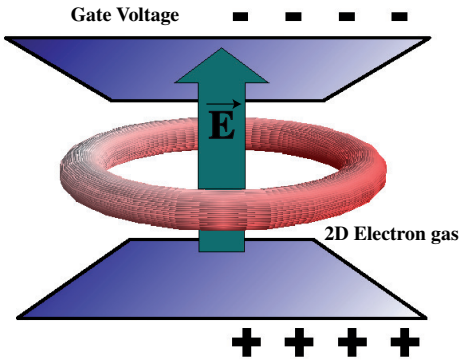

Figure 27: The typical Rashba situation with an electric field, created by a gate voltage, perpendicular to a ring fabricated on a two dimensional electron gas.

4.3 Derivation of the ring Hamiltonian

4.3.1 The argument of Meijer, Morpurgo and Klapwijk for the Rashba SO interaction

To make the discussion simpler, we neglect any magnetic field effect, which is well discussed in the literature. Here we discuss the non-trivial point of designing a Hermitian Hamiltonian when it is not in cartesian coordinates. We explain in detail such construction so the student can understand the pitfalls generally avoided in quantum mechanics courses because of a preferential system of coordinates. Many researchers overlooked this hermiticity problem until the recent paper by Meijer, Morpurgo and Klapwijk [33].

The classical argument in reference [33] is essentially the following. We consider a 2DEG, neglecting interactions between electrons and add the Rashba SO interaction in cylindrical coordinates (ρ, φ, z),

$$\begin{aligned} \mathbf{H}_{2d} \;=\; & -\frac{\hbar^2}{2m}\left(\partial_\rho^2 + \rho^{-1}\partial_\rho + \rho^{-2}\partial_\varphi^2\right)\mathbf{1}_{2\times 2} \\ & +\alpha\rho^{-1}(\boldsymbol{\sigma}_x\cos\varphi + \boldsymbol{\sigma}_y\sin\varphi)i\hbar\partial_\varphi + \alpha(\boldsymbol{\sigma}_x\sin\varphi - \boldsymbol{\sigma}_y\cos\varphi)i\hbar\partial_\rho. \end{aligned} \tag{4.7}$$

The Rashba SO interaction in the second line comes from equation (4.4) with the definitions $p_x = -i\hbar\partial_x$ and $p_y = -i\hbar\partial_y$ after the substitutions $\partial_x = -(\rho)^{-1}\sin\varphi\,\partial_\varphi + \cos\varphi\,\partial_\rho$ and $\partial_y = (\rho)^{-1}\cos\varphi\,\partial_\varphi + \sin\varphi\,\partial_\rho$. Fixing the radial distance ρ to the ring radius a and neglecting the radial derivatives leads to a "1d" Hamiltonian (called $\mathbf{H}'_{1d}$ for the moment) for the ring,

$$\mathbf{H}'_{1d} = \frac{\hbar^2}{2ma^2}(i\partial_\varphi)^2 + \alpha\hbar a^{-1}(\boldsymbol{\sigma}_x\cos\varphi + \boldsymbol{\sigma}_y\sin\varphi)i\partial_\varphi. \tag{4.8}$$

In [33], the authors note that the last term in (4.8) is non-Hermitian, since

$$\begin{aligned} \langle F|(\boldsymbol{\sigma}_x\cos\varphi + \boldsymbol{\sigma}_y\sin\varphi)i\partial_\varphi|G\rangle^* &= \left(\int_0^{2\pi} d\varphi\,(F_\uparrow^*\;F_\downarrow^*)\begin{pmatrix} 0 & ie^{-i\varphi}\partial_\varphi \\ ie^{i\varphi}\partial_\varphi & 0\end{pmatrix}\begin{pmatrix} G_\uparrow \\ G_\downarrow\end{pmatrix}\right)^* \\ &= \left[-iF_\uparrow e^{i\varphi}G_\downarrow^* - iF_\downarrow e^{-i\varphi}G_\uparrow^*\right]_0^{2\pi} + \int_0^{2\pi} d\varphi\,(G_\uparrow^*\;G_\downarrow^*)\begin{pmatrix} 0 & ie^{-i\varphi}\partial_\varphi \\ ie^{i\varphi}\partial_\varphi & 0\end{pmatrix}\begin{pmatrix} F_\uparrow \\ F_\downarrow\end{pmatrix} \\ &\quad + \int_0^{2\pi} d\varphi\,(G_\uparrow^*\;G_\downarrow^*)\begin{pmatrix} 0 & e^{-i\varphi} \\ -e^{i\varphi} & 0\end{pmatrix}\begin{pmatrix} F_\uparrow \\ F_\downarrow\end{pmatrix}. \\ &= \langle G|(\boldsymbol{\sigma}_x\cos\varphi + \boldsymbol{\sigma}_y\sin\varphi)i\partial_\varphi|F\rangle - i\langle G|(\boldsymbol{\sigma}_x\sin\varphi - \boldsymbol{\sigma}_y\cos\varphi)|F\rangle, \end{aligned} \tag{4.9}$$

where $|F\rangle$ and $|G\rangle$ are Pauli spinors, and the integrated terms vanish if we impose single-valued spinors, i.e. $\langle\varphi+2\pi|F\rangle = \langle\varphi|F\rangle$. From the property given in equation (4.9), we may infer that a Hermitian operator could be formed by the combination $\mathbf{V} = \alpha\hbar a^{-1}\mathbf{W}$ where

$$\mathbf{W} = (\boldsymbol{\sigma}_\mathbf{x}\cos\varphi + \boldsymbol{\sigma}_\mathbf{y}\sin\varphi)\mathbf{i}\partial_\varphi - \mathbf{iA}(\boldsymbol{\sigma}_\mathbf{x}\sin\varphi - \boldsymbol{\sigma}_\mathbf{y}\cos\varphi), \tag{4.10}$$

since

$$\begin{aligned}\langle F|\mathbf{W}|\mathbf{G}\rangle^* &= \langle G|(\boldsymbol{\sigma}_x\cos\varphi + \boldsymbol{\sigma}_y\sin\varphi)i\partial_\varphi|F\rangle \\ &\quad -i(1-A^*)\langle G|(\boldsymbol{\sigma}_x\sin\varphi - \boldsymbol{\sigma}_y\cos\varphi)|F\rangle,\end{aligned} \tag{4.11}$$

and

$$\begin{aligned}\langle G|\mathbf{W}|\mathbf{F}\rangle &= \langle G|(\boldsymbol{\sigma}_x\cos\varphi + \boldsymbol{\sigma}_y\sin\varphi)i\partial_\varphi|F\rangle \\ &\quad -iA\langle G|(\boldsymbol{\sigma}_x\sin\varphi - \boldsymbol{\sigma}_y\cos\varphi)|F\rangle.\end{aligned} \tag{4.12}$$

The r.h.s. of equations (4.11) and (4.12) are equal provided that $A^* = A = \frac{1}{2}$. This value in equation (4.10) gives the correct expression that renders the Rashba SO interaction on the ring Hermitian.

The method used in Ref. [33] to build hermiticity into the SO Hamiltonian, consists in the introduction of a confining potential $V(\rho)$ in equation (4.7) in order to localize the particle on a circle of radius a. If this potential is steep enough, the particles will lie in the ground state $R_0(\rho)$ of

$$H_\rho = \mathrm{KE} + V(\rho) = -\frac{\hbar^2}{2m}\left(\partial_\rho^2 + \rho^{-1}\partial_\rho\right) + V(\rho), \tag{4.13}$$

where KE is the contribution of the radial motion to the kinetic energy and the correct $1d$ Hamiltonian ($\mathbf{H}^{\mathrm{ring}}_{Rashba}$) is defined by the projection, on this ground state, of the angular dependence of $\mathbf{H}_{2d}$,

$$\mathbf{H}^{\mathrm{ring}}_{Rashba} = \langle R_0|\mathbf{H}_{2d} - \mathrm{KE}\,\mathbf{1}_{2\times2}|R_0\rangle, \tag{4.14}$$

where $|R_0\rangle$ is extended to a two-component object. Note the very peculiar situation in polar coordinates, KE does not simply coincide with $p_\rho^2/2m$ (see e.g. Ref. [34] for a discussion on this unrecognized point). The calculation is now made specific by considering a circular Harmonic potential $V(\rho) = \frac{1}{2}m\omega^2(\rho-a)^2$ and by the explicit calculation of the matrix elements $\langle R_0|\rho^{-1}|R_0\rangle = a^{-1}$ and $\langle R_0|\partial_\rho|R_0\rangle = -(2a)^{-1}$. The resulting Hamiltonian $\mathbf{H}^{\mathrm{ring}}_{Rashba}$ then follows from the substitutions $\rho \to a$, $\partial_\rho \to -(2a)^{-1}$ in $\mathbf{H}_{2d} + \frac{\hbar^2}{2m}\left(\partial_\rho^2 + \rho^{-1}\partial_\rho\right)$. Thus

$$\begin{aligned}\mathbf{H}^{\mathrm{ring}}_{Rashba} &= \frac{\hbar^2}{2ma^2}(i\partial_\varphi)^2\mathbf{1}_{2\times2} \\ &\quad +\alpha\hbar a^{-1}(\boldsymbol{\sigma}_x\cos\varphi + \boldsymbol{\sigma}_y\sin\varphi)i\partial_\varphi - i\alpha\hbar(2a)^{-1}(\boldsymbol{\sigma}_x\sin\varphi - \boldsymbol{\sigma}_y\cos\varphi).\end{aligned} \tag{4.15}$$

It can be checked that the Hamiltonian is now Hermitian, since it coincides with the choice $A^* = A = \frac{1}{2}$, according to the procedure outlined in Eqs. (4.10-4.12).

4.3.2 Symmetrization of the original Hamiltonian

Although the previous derivation is of course correct, it is instructive to propose another, probably more straightforward derivation. The SO interaction in cylindrical coordinates with a perpendicular electric field, $\vec{\alpha} = \alpha\vec{e}_z$, takes the form

$$\vec{\boldsymbol{\sigma}}\cdot(\vec{\alpha}\times\vec{p}) = -\alpha(\boldsymbol{\sigma}_\rho p_\varphi - \boldsymbol{\sigma}_\varphi p_\rho), \tag{4.16}$$

with $\boldsymbol{\sigma}_\rho = \boldsymbol{\sigma}_x\cos\varphi + \boldsymbol{\sigma}_y\sin\varphi$ and $\boldsymbol{\sigma}_\varphi = -\boldsymbol{\sigma}_x\sin\varphi + \boldsymbol{\sigma}_y\cos\varphi$ treated for the moment as classical variables (i.e. we forget about possible commutation problems). In order to make the

corresponding expression Hermitian in Quantum Mechanics, one has to use the correspondence principle, i.e. add inequivalent orders of non-commuting operators, and symmetrize the "classical" expression, using also $p_\rho = -i\hbar(\partial_\rho - (2\rho)^{-1})$ and $p_\varphi = -i\hbar a^{-1}\partial_\varphi$. Let us also note that when the electrons are confined on a ring, then $\langle p_\rho\rangle = \langle R_0|p_\rho|R_0\rangle = 0$ (*and not* $\langle R_0|\partial_\rho|R_0\rangle = 0$ as it was done to get equation (4.8)) and $\rho = a$. This leads to

$$\mathbf{V}^{\text{ring}}_{Rashba} = -\frac{1}{2}\alpha\{\boldsymbol{\sigma}_\rho, p_\varphi\} = i\hbar\alpha a^{-1}(\boldsymbol{\sigma}_\rho\partial_\varphi + \frac{1}{2}\partial_\varphi\boldsymbol{\sigma}_\rho), \tag{4.17}$$

where $\{\boldsymbol{\sigma}_\rho, p_\varphi\}$ denotes the anticommutator $\boldsymbol{\sigma}_\rho p_\varphi + p_\varphi\boldsymbol{\sigma}_\rho$. Using $\partial_\varphi\boldsymbol{\sigma}_\rho = \boldsymbol{\sigma}_\varphi$, equation (4.15) eventually follows,

$$\mathbf{H}^{\text{ring}}_{Rashba} = \frac{\hbar^2}{2ma^2}(i\partial_\varphi)^2\mathbf{1}_{2\times 2} + i\hbar\alpha a^{-1}(\boldsymbol{\sigma}_\rho\partial_\varphi + \frac{1}{2}\boldsymbol{\sigma}_\varphi). \tag{4.18}$$

Let us emphasize on the fact that the condition $\langle p_\rho\rangle = 0$ is equivalent to Meijer et al's derivation, since it implies $-i\hbar\langle R_0|\partial_\rho - (2\rho)^{-1}|R_0\rangle = 0$ with a radial wave function strongly localized on $\rho \simeq a$. Our proposed derivation, nevertheless, has the merit of being simpler and more general, since it does not rely on any particular assumption on the confining potential (except the fact that it enforces the particles to move along a ring).

4.3.3 Hamiltonian in the rotated spin basis

In the previous sections, the Rashba Hamiltonian (4.18), initially expressed in Cartesian coordinates, has been rewritten in polar coordinates. To preserve the hermiticity of the Hamiltonian, it has been shown that an extra term should be added if the expression is not properly symmetrized prior to quantization. In the following, we give a more physical picture that gives rise to this extra term.

We first start by noting that the change of coordinates $(x, y) \to (\rho, \varphi)$ induces a rotation by an angle φ of the local frame: $(\vec{e}_x, \vec{e}_y) \to (\vec{e}_\rho, \vec{e}_\varphi)$. All vector fields, including $\boldsymbol{\sigma}$ are now expressed in this local frame. However, *no such rotation* has been applied to the spinor basis which thus remains the same at any point of the circle. The notations $\boldsymbol{\sigma}_\rho$ and $\boldsymbol{\sigma}_\varphi$ may thus be misleading. Let us introduce such a rotation of the spinor basis:

$$|F'\rangle = e^{i\frac{\varphi}{2}\boldsymbol{\sigma}_z}|F\rangle = \big(\cos\frac{\varphi}{2}\mathbf{1}_{2\times 2} + i\sin\frac{\varphi}{2}\boldsymbol{\sigma}_z\big)|F\rangle. \tag{4.19}$$

Since the rotation axis is (Oz), the quantification axis is not changed during the transformation. The two spin components simply get a phase

$$|\uparrow'\rangle = e^{i\frac{\varphi}{2}}|\uparrow\rangle, \quad |\downarrow'\rangle = e^{-i\frac{\varphi}{2}}|\downarrow\rangle. \tag{4.20}$$

In the new local spinor basis, the Hamiltonian becomes

$$\mathbf{H}' = e^{i\frac{\varphi}{2}\boldsymbol{\sigma}_z}\mathbf{H}e^{-i\frac{\varphi}{2}\boldsymbol{\sigma}_z}. \tag{4.21}$$

Using the identity $\boldsymbol{\sigma}_\rho\boldsymbol{\sigma}_z = -i\boldsymbol{\sigma}_\varphi$, the correct Hermitian Rashba Hamiltonian can be cast as

$$\mathbf{H}^{\text{ring}}_{Rashba} = \frac{\hbar^2}{2ma^2}(i\partial_\varphi)^2\mathbf{1}_{2\times 2} + i\hbar\alpha a^{-1}\boldsymbol{\sigma}_\rho(\partial_\varphi + \frac{i}{2}\boldsymbol{\sigma}_z). \tag{4.22}$$

Under the change of spinor basis, the new rotated Hamiltonian becomes

$$e^{i\frac{\varphi}{2}\boldsymbol{\sigma}_z}\mathbf{H}^{\text{ring}}_{Rashba}e^{-i\frac{\varphi}{2}\boldsymbol{\sigma}_z} = \frac{\hbar^2}{2ma^2}(i\partial_\varphi\mathbf{1}_{2\times 2} + \frac{1}{2}\boldsymbol{\sigma}_z)^2 + i\hbar\alpha a^{-1}\boldsymbol{\sigma}_x\partial_\varphi, \tag{4.23}$$

since $\boldsymbol{\sigma}'_\rho \equiv e^{i\frac{\varphi}{2}\boldsymbol{\sigma}_z}\boldsymbol{\sigma}_\rho e^{-i\frac{\varphi}{2}\boldsymbol{\sigma}_z} = \boldsymbol{\sigma}_x$. Interestingly, after rotation of the spinor basis the potential energy recovers a form $\propto \boldsymbol{\sigma}'_\rho p_\varphi$ similar to the original Rashba Hamiltonian *before symmetrization* in (4.16). From the physical point of view, one indeed expects the potential energy to be the same in all local orthonormal frames. This implies that, starting from the original Rashba Hamiltonian, the change of coordinates should be accompanied by a change of the local vector and spinor frames. The spin-orbit term then keeps the same form. When expressed in the original spin basis, the additional term needed for symmetrization appears naturally. In contradistinction to the potential energy, additional terms may appear in the kinetic energy when one changes the spinor basis. They are interpreted as inertial forces due to the fact that the local frame is not inertial. This is the origin of the extra term $\frac{1}{2}\boldsymbol{\sigma}_z$ in the Hamiltonian (4.23) (note the appearance of the z component of the total angular momentum, $\mathbf{L_z} + \mathbf{s_z}$). When the particle moves along the circle, the local spinor basis turns by the same angle. Consider for example a constant spinor. To accommodate the change of local basis along the circle, it should have φ-dependent spin-components. Since no kinetic energy is associated to the spin, a term involving derivatives ∂_φ would produce a term which is precisely cancelled by the additional contribution $\frac{1}{2}\boldsymbol{\sigma}_z$.

4.4 Eigenenergies and Eigenvectors on a ring

4.4.1 The Rashba SO interaction

Once the correct Hermitian Hamiltonian has been written in polar coordinates we can confidently derive the eigenvalues and eigenvectors for the strictly one dimensional ring. This section will benefit the student by explicitly obtaining the eigenfunctions and eigenvalues of the system, from which we can obtain all observables or actually measurable quantities in experiments. We will also make some basic symmetry considerations that will illuminate details of why the wavefunction and energies take their particular form.

First we rewrite the Hamiltonian in a clever way in order to arrive rapidly at the eigenvalues and introduce physical insight by pointing out the existence of a gauge field associated to topological phenomena connected to spin transport. An alternative form of the Hamiltonian (4.18) was given in Ref. [35]. We observe that

$$\left(i\partial_\varphi \mathbf{1}_{2\times 2} + \frac{ma\alpha}{\hbar}\boldsymbol{\sigma}_\rho\right)^2 = (i\partial_\varphi)^2\mathbf{1}_{2\times 2} + \frac{2ma\alpha}{\hbar}\boldsymbol{\sigma}_\rho(i\partial_\varphi) + \frac{ma\alpha}{\hbar}i\boldsymbol{\sigma}_\varphi + \left(\frac{ma\alpha}{\hbar}\right)^2\mathbf{1}_{2\times 2}. \tag{4.24}$$

The factor of two in the second term on the right accounts for the appropriate action of an derivative operator. Such form allows one to recast the Hamiltonian as

$$\mathbf{H}^{\text{ring}}_{Rashba} = \frac{\hbar^2}{2ma^2}\left[\left(i\partial_\varphi \mathbf{1}_{2\times 2} + \frac{ma\alpha}{\hbar}\boldsymbol{\sigma}_\rho\right)^2 - \left(\frac{ma\alpha}{\hbar}\right)^2\mathbf{1}_{2\times 2}\right]. \tag{4.25}$$

In order to find the eigenstates of the Hamiltonian (4.25), one first solves the eigenvalue equation

$$\left(i\partial_\varphi \mathbf{1}_{2\times 2} + \frac{ma\alpha}{\hbar}\boldsymbol{\sigma}_\rho\right)\Psi = \varepsilon\Psi, \tag{4.26}$$

or

$$\begin{pmatrix} i\partial_\varphi & \frac{ma\alpha}{\hbar}\mathrm{e}^{-i\varphi} \\ \frac{ma\alpha}{\hbar}\mathrm{e}^{i\varphi} & i\partial_\varphi \end{pmatrix}\begin{pmatrix}\psi_\uparrow \\ \psi_\downarrow\end{pmatrix} = \varepsilon\begin{pmatrix}\psi_\uparrow \\ \psi_\downarrow\end{pmatrix}. \tag{4.27}$$

It follows that the general form for the eigenfuctions should be

$$\Psi^\lambda_{n,s} = \mathrm{e}^{i\lambda n\varphi}\begin{pmatrix} A_{\lambda,s}\mathrm{e}^{-i\varphi/2} \\ B_{\lambda,s}\mathrm{e}^{i\varphi/2}\end{pmatrix}, \tag{4.28}$$

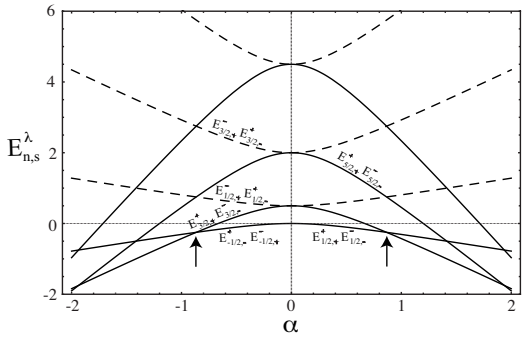

Figure 28: Energies of electrons on a ring with spin-orbit interaction as a function of the SO interaction strength α. The energy is in units of $\hbar^2/ma^2$ while α is in units of $\hbar/ma$. Indicated are the eigenvalue labels for the first five levels (note the ground state is fourfold degenerate). The graph shows how the limit $\alpha = 0$ is fourfold degenerate as expected since the time inversion symmetry turns into independent space and spin inversion symmetry. Arrows indicate change in lowest energy level.

where n is the main quantum number and we account for the two eigenvalues that will arise, $s = \pm$, for each wave propagation direction $\lambda = \pm$. So, assuming such a wavefunction we obtain the corresponding eigenvalues

$$\varepsilon^{\lambda}_{n,s} = \frac{s}{2}\sqrt{1 + 4\left(\frac{ma\alpha}{\hbar}\right)^2} - \lambda n, \tag{4.29}$$

where n is a half odd integer as will be seen below when we address the wavefunctions. The eigenvalues of (4.25) then simply follow

$$E^{\lambda}_{n,s} = \frac{\hbar^2}{2ma^2}\left[\left(n - \frac{\lambda s}{2}\sqrt{1 + 4\left(\frac{ma\alpha}{\hbar}\right)^2}\right)^2 - \left(\frac{ma\alpha}{\hbar}\right)^2\right]. \tag{4.30}$$

Note that left and right propagating waves with the same s-index are not degenerate but time reversal symmetry is satisfied i.e. $E^{\lambda}_{n,s} = E^{-\lambda}_{n,-s}$ (simultaneous change of λ and s). This symmetry reflects the fact that the SO interaction is not space inversion symmetric, but only time reversal symmetric. When the spin-orbit interaction is absent ($\alpha = 0$), space and spin inversion symmetry is recovered and energies of both clockwise and counterclockwise modes are degenerate independent of the spin label. Figure 28 shows the energy levels as a function of the SO strength. The ordering of the levels are indicated according to the spin orientation and sense of the current. The free electron on a ring is recovered for all levels as one can see from the fourfold degeneracy at $\alpha = 0$, rendering all possible combinations of the values of λ, s for a fixed integer value of N in the relation $E^{\lambda}_{n,s} = \hbar^2(n - \lambda s/2)^2/2ma^2 = \hbar^2 N^2/2ma^2$ (with n half odd integers). Table 1 shows the energies for the first three levels in the limit of $\alpha = 0$ and how degeneracies are broken when the SO interaction is turned on.

Now we compute the eigenfunctions. In order to deal with the subtleties associated with the change in sign of spin and propagation direction we explicitly do the $\lambda = +$ case. Using equations (4.27) and (4.28) we find from the secular equation

$$B_{+,s} = \frac{\hbar}{2ma\alpha}\left(\frac{s}{\cos\theta} - 1\right)A_{+,s}, \tag{4.31}$$

where $\cos\theta = 1/\sqrt{1 + 4(ma\alpha/\hbar)^2}$. In order to conform to a canonical spinor we choose $A_{+,+} =$

Table 2: Energies (in units of $\hbar^2/2ma^2$) for the first three levels and their degeneracies according to values of the quantum numbers n, λ and s in the limit of zero spin orbit, and the corresponding values of the free electron integer quantum number N. Also shown is how degeneracies occur when the SO interaction is turned on leaving only time reversal symmetry.

E $(\hbar^2/2ma^2)$	n	λ	s	N	$\alpha \neq 0$
0	$-1/2$	$+$	$-$	0	deg
0	$-1/2$	$-$	$+$	0	
0	$1/2$	$+$	$+$	0	
0	$1/2$	$-$	$-$	0	
1	$1/2$	$+$	$-$	1	deg
1	$1/2$	$-$	$+$	1	
1	$3/2$	$+$	$+$	1	deg
1	$3/2$	$-$	$-$	1	
4	$3/2$	$+$	$-$	2	deg
4	$3/2$	$-$	$+$	2	
4	$5/2$	$+$	$+$	2	deg
4	$5/2$	$-$	$-$	2	

$\cos\theta/2$, and thus $B_{+,+} = \sin\theta/2$ for normalization, so we have

$$\frac{\hbar}{2ma\alpha}\left(\frac{1-\cos\theta}{\cos\theta}\right)\cos\frac{\theta}{2} = \sin\frac{\theta}{2}, \tag{4.32}$$

from which we have the condition

$$\tan\theta = \frac{2ma\alpha}{\hbar}. \tag{4.33}$$

The choice for the second eigenfunction is $A_{+,-} = -\sin\theta/2$, and doing the same exercise we arrive at the two eigenspinors

$$\Psi^{+}_{n,+} = e^{in\varphi}\begin{pmatrix}\cos\frac{\theta}{2}\mathrm{e}^{-i\varphi/2}\\ \sin\frac{\theta}{2}\mathrm{e}^{i\varphi/2}\end{pmatrix}, \Psi^{+}_{n,-} = e^{in\varphi}\begin{pmatrix}-\sin\frac{\theta}{2}\mathrm{e}^{-i\varphi/2}\\ \cos\frac{\theta}{2}\mathrm{e}^{i\varphi/2}.\end{pmatrix} \tag{4.34}$$

The corresponding eigenfunctions for $\lambda = -$ are

$$\Psi^{-}_{n,+} = e^{-in\varphi}\begin{pmatrix}\cos\frac{\theta}{2}\mathrm{e}^{-i\varphi/2}\\ \sin\frac{\theta}{2}\mathrm{e}^{i\varphi/2}\end{pmatrix}, \Psi^{-}_{n,-} = e^{-in\varphi}\begin{pmatrix}-\sin\frac{\theta}{2}\mathrm{e}^{-i\varphi/2}\\ \cos\frac{\theta}{2}\mathrm{e}^{i\varphi/2}\end{pmatrix} \tag{4.35}$$

Using the time reversal operator for spin 1/2 particles $\boldsymbol{\Theta} = -i\boldsymbol{\sigma}_y K$ where $\boldsymbol{\sigma}_y$ is the corresponding Pauli matrix and K is the conjugation operator [36], one can readily show that $\Psi^{+}_{n,+} = \boldsymbol{\Theta}\Psi^{-}_{n,-}$ and $\Psi^{+}_{n,-} = \boldsymbol{\Theta}\Psi^{-}_{n,+}$. As one would expect from the time reversal invariance $\Psi^{-}_{n,+}$ is degenerate with $\Psi^{+}_{n,-}$ and $\Psi^{-}_{n,-}$ with $\Psi^{+}_{n,+}$. With these properties in mind the student can guess that expectation values taken with corresponding time reversed wavefunctions must be added together since there energies are degenerate. This fact will have surprising consequences in the next section.

4.5 Charge and spin currents in the ground state

4.5.1 Direct calculation

Having found the eigenfunctions, one can now compute equilibrium properties such as persistent charge and spin currents on the ring. The student might be accustomed to expecting

a current only when an external force is applied to the system, such as a potential difference. Nevertheless we will show that when symmetry breaking fields exist that can do no work, such as a magnetic field, currents can exist as equilibrium properties borne from the nature of the wavefunctions. In a sense the system can distinguish between clockwise moving current and a counterclockwise moving current, one of them corresponding to a lower energy. These currents are long lived in the absence of perturbations. This is very counterintuitive for the classical line of thought.

There are charge currents in equilibrium only when time reversal symmetry breaking perturbations are present, such as a magnetic field[37, 1], for an experimental review see [38] and references therein. The charge currents can be derived directly from the ground state energy as

$$I_{charge} = -\sum_{n,s} \frac{\partial E^{\lambda}_{n,s}}{\partial \Phi} \tag{4.36}$$

where Φ is the magnetic flux and the λ quantum number is chosen by the direction of the magnetic field. An alternative form of computing the currents is by using the definition of the current operator. These current densities are fields usually defined from a continuity equation rather than from matrix elements of some operators. In order to generalize the classical definition of the current density $\vec{j}(\vec{r}) = n(\vec{r})e\vec{v}$, we take the expectation value of the velocity operator

$$\vec{J}_{charge} = \Psi^{\dagger} e\vec{\mathbf{v}}\ \Psi. \tag{4.37}$$

where e is the electron charge and $\vec{\mathbf{v}}$ is the velocity operator. Note that the current is defined in such a way that its dimension is a charge times a velocity. In the presence of the spin-orbit interaction, the velocity operator is not simply $\vec{\mathbf{p}}/m$. There arises what is known as an additional anomalous velocity term. We start from the quantum mechanical definition of the velocity (which is now a 2×2 matrix due to the presence of the spin-dependent terms in the Hamiltonian) $\vec{\mathbf{v}} = \frac{i}{\hbar}[\mathbf{H}, \vec{r}]$. Since we are interested in the azimuthal velocity component $\dot{\varphi}$, it is more convenient to calculate

$$\mathbf{v}_{\varphi} = \frac{ia}{\hbar}[\mathbf{H}, \varphi] = \frac{\hbar}{ima}\partial_{\varphi}\mathbf{1}_{2\times 2} - \alpha\boldsymbol{\sigma}_{\rho}. \tag{4.38}$$

rather than working in Cartesian coordinates. Note that the Hamiltonian takes a simple form when expressed in terms of the velocity: $\mathbf{H} = \frac{1}{2}m(\mathbf{v}_{\varphi}^2 - \alpha^2\mathbf{1}_{2\times 2})$. Here, we do not consider symmetry breaking magnetic fields, so there can be no persistent charge currents on the ring. If we compute the charge currents for the fourfold degenerate lowest energy levels from which one forms a totally symmetric linear combination, one gets

$$\begin{aligned} J_{\varphi} &= -\frac{e}{4}(\Psi^{+}_{1/2,+})^{\dagger}\mathbf{v}_{\varphi}\Psi^{+}_{1/2,+} - \frac{e}{4}(\Psi^{-}_{1/2,-})^{\dagger}\mathbf{v}_{\varphi}\Psi^{-}_{1/2,-} \\ &- \frac{e}{4}(\Psi^{-}_{-1/2,+})^{\dagger}\mathbf{v}_{\varphi}\Psi^{-}_{-1/2,+} - \frac{e}{4}(\Psi^{+}_{-1/2,-})^{\dagger}\mathbf{v}_{\varphi}\Psi^{+}_{-1/2,-} \qquad (4.39) \\ &= -\frac{e\hbar}{4ma}\left[\frac{1}{2} - \frac{1}{2\cos\theta}\right] - \frac{e\hbar}{4ma}\left[-\frac{1}{2} + \frac{1}{2\cos\theta}\right] \\ &- \frac{e\hbar}{4ma}\left[-\frac{1}{2} - \frac{1}{2\cos\theta}\right] - \frac{e\hbar}{4ma}\left[\frac{1}{2} + \frac{1}{2\cos\theta}\right] = 0 \qquad (4.40) \end{aligned}$$

provided the SO strength is within the arrows in Fig. 28, since outside the interval the computation involves a different two-fold degenerate level. The result above applies to any normalized linear combination of the fourfold ground states satisfying the time-reversal symmetry. Charge current cancellation happens level by level and for all α values, rendering them zero as expected. The effect of an external magnetic field (playing the role of a time-reversal symmetry breaking

field) and the ensuing charge persistent currents in the presence of a simple scalar potential and the spin-orbit interaction were examined in ref.[18]. The small scalar potential breaks the degeneracy at the edge of the Brillouin zone that limits the charge persistent currents to a maximum value for each band.

On the other hand, there can exist currents that don't break time reversal symmetry i.e. spin currents. In order to make an explicit calculation of the current, here we sidestep the consideration of a scalar potential and use the empty lattice approximation[39]. The spin current density, denoted as $\vec{\mathcal{J}}^a$ in order not to get confused with the charge current density $\vec{J}$, follows from the same approach as above. Note that the spin current $\vec{\mathcal{J}}^a$ is a tensor (two indices) while $\vec{J}$ is a vector. We define now a local "spin velocity" operator, properly symmetrized

$$\vec{\mathcal{J}}^a = \frac{1}{2}\Psi^\dagger\{\vec{\mathbf{v}}, \mathbf{s}^a\}\Psi, \tag{4.41}$$

where $\mathbf{s^a} = \hbar\boldsymbol{\sigma}^a/2$. The reader should note that the time reversal operation applied to such an operator (in the absence of a magnetic field) reverses both the velocity and the spin, so the current is not changed by such an operation, so this intuitive definition materializes our earlier expectation.

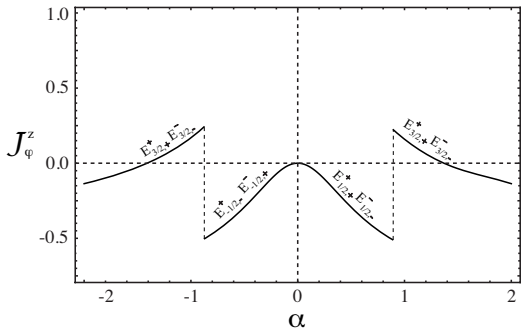

Figure 29: Spin current in units of $\hbar^2/4ma$ from the lowest lying degenerate level indicated in Fig.28 as a function of α. Between the arrows in Fig.28 the lowest level is fourfold degenerate so there are four terms in the spin current. Outside that range, other two-fold degenerate level take over causing a jump in the spin current as indicated. The graph shows how the limit $\alpha = 0$ indicates zero spin current because up down spin symmetry along with inversion symmetry are restored.

The spin current along the ring will again involve the previously derived azimuthal velocity operator (4.38). The general contribution for any single state involved in the current is given by

$$\begin{aligned}
\mathcal{J}^a_\varphi &= \frac{\hbar^2}{2ma}(\lambda n - 1/2)[|A_{\lambda s}|^2\sigma^a_{11} + B^*_{\lambda s}A_{\lambda s}e^{-i\varphi}\sigma^a_{21}] \\
&+ \frac{\hbar^2}{2ma}(\lambda n + 1/2)[A^*_{\lambda s}B_{\lambda s}e^{i\varphi}\sigma^a_{12} + |B_{\lambda s}|^2\sigma^a_{22}] \\
&- \frac{\hbar}{2}\alpha\left(\cos\varphi\ \delta_{x,a} + \sin\varphi\ \delta_{y,a}\right),
\end{aligned} \tag{4.42}$$

where $a = x, y, z$ and we have used notation from Eq. (4.28). Adding contributions from the four degenerate lowest lying levels (again the totally symmetric linear combination) with the

spin orientation in the z direction, one arrives at

$$\begin{aligned}
\mathcal{J}^z_\varphi &= \frac{1}{4}(\Psi^+_{1/2,+})^\dagger \frac{1}{2}\{\mathbf{v}_\varphi, \mathbf{s}^z\}\Psi^+_{1/2,+} + \frac{1}{4}(\Psi^-_{1/2,-})^\dagger \frac{1}{2}\{\mathbf{v}_\varphi, \mathbf{s}^z\}\Psi^-_{1/2,-} \\
&+ \frac{1}{4}(\Psi^-_{-1/2,+})^\dagger \frac{1}{2}\{\mathbf{v}_\varphi, \mathbf{s}^z\}\Psi^-_{-1/2,+} + \frac{1}{4}(\Psi^+_{-1/2,-})^\dagger \frac{1}{2}\{\mathbf{v}_\varphi, \mathbf{s}^z\}\Psi^+_{-1/2,-} \qquad (4.43) \\
&= \frac{\hbar^2}{8ma}\left(\frac{1}{2}\cos\theta - \frac{1}{2}\right) + \frac{\hbar^2}{8ma}\left(\frac{1}{2}\cos\theta - \frac{1}{2}\right) \\
&- \frac{\hbar^2}{8ma}\left(-\frac{1}{2}\cos\theta + \frac{1}{2}\right) - \frac{\hbar^2}{8ma}\left(-\frac{1}{2}\cos\theta + \frac{1}{2}\right), \qquad (4.44) \\
&= \frac{\hbar^2}{4ma}(\cos\theta - 1)\,. \qquad (4.45)
\end{aligned}$$

Such an expression only accounts for α values in the range between the arrows in Fig.28. Outside this range the energies $E^+_{3/2,+}, E^-_{3/2,-}$ are the lowest energies, so we must compute the expectation of the spin current with such two-fold degenerate eigenfunctions. The full spin current for the lowest lying levels is depicted in Fig.29. One can see from the figure, that at $\alpha = 0$ the spin currents vanish, as required by the recovery of the inversion symmetry ($k \to -k$) and, independently, the spin inversion symmetry that were intertwined in the presence of the SO interaction. In the presence of a small scalar potential on the ring, the level crossing in Fig.28 gives way to level repulsion. The abrupt transition in dashed lines in Fig.29 will then be gradual and rounded[37]. Persistent spin currents have yet to measured due to the lack of an appropriate probe.

The spin currents $\mathcal{J}^{x,y}_\varphi$ can also be readily computed along the lines above. In contrast to the spin current $\mathcal{J}^z_\varphi$, such currents for each of the degenerate states of a particular level, are not real valued. Nevertheless, the summation of all the degenerate contribution renders a real spin currents which for the ground state is (in the spin-orbit strength range shown in Fig.28)

$$\begin{aligned}
\mathcal{J}^x_\varphi &= \frac{1}{2}\hbar\alpha(\cos\theta - 1)\cos\varphi, \\
\mathcal{J}^y_\varphi &= \frac{1}{2}\hbar\alpha(\cos\theta - 1)\sin\varphi. \qquad (4.46)
\end{aligned}$$

Such expressions have a φ dependence due to the precession of the spin around the z axis. This means that a particular polarization rotates going through zero and then changing sign, making the whole spin current change sign while the wavevector is constant. Note that the spin persistent currents vanish correctly for $\alpha = 0$ as expected. Figure 30 shows the angular dependence for both spin current components for a value of α within the range shown in Fig.28.

As with charge persistent currents one has to add all occupied levels. Observing figure 28 one sees that the first two levels add constructively while the third level subtracts from the previous two levels. One must then carefully add the corresponding currents taking into account level crossings.

4.5.2 The Dresselhaus SO interaction

The Dresselhaus Hamiltonian of equation (4.6) is another form of SO interaction. Using either of the procedures shown in section 2, keeping only p_φ terms, we express $\boldsymbol{\sigma}_x p_x - \boldsymbol{\sigma}_y p_y$ as $-\boldsymbol{\sigma}_x \sin\varphi\, p_\varphi - \boldsymbol{\sigma}_y \cos\varphi\, p_\varphi$ that we then symmetrize to get

$$\begin{aligned}
\mathbf{V}^{\text{ring}}_{Dresselhaus} &= -\tfrac{1}{2}\beta(\boldsymbol{\sigma}_x\{\sin\varphi, p_\varphi\} + \boldsymbol{\sigma}_y\{\cos\varphi, p_\varphi\}) \\
&= i\hbar\beta a^{-1}[(\boldsymbol{\sigma}_x \sin\varphi + \boldsymbol{\sigma}_y\cos\varphi)\partial_\varphi + \tfrac{1}{2}(\boldsymbol{\sigma}_x\cos\varphi - \boldsymbol{\sigma}_y\sin\varphi)],
\end{aligned} \qquad (4.47)$$

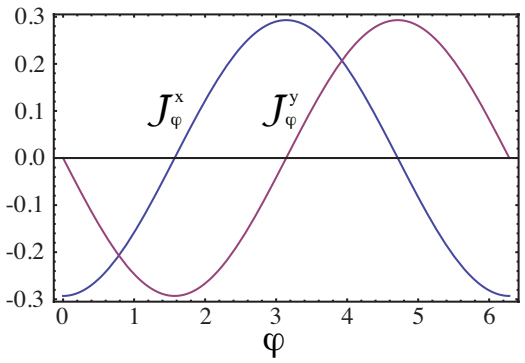

Figure 30: Spin currents for the x, y polarizations in units of $\hbar^2/4ma$ from the lowest lying degenerate levels indicated in Fig.28 as a function of φ and for $\alpha = \frac{\hbar}{2ma}$. Between the arrows in Fig.28, the lowest level is fourfold degenerate so there are four terms in each of the spin currents.

or we define the combination

$$\mathbf{W} = (\boldsymbol{\sigma}_\mathbf{x} \sin\varphi + \boldsymbol{\sigma}_\mathbf{y} \cos\varphi)\mathbf{i}\partial_\varphi + \mathbf{iA}(\boldsymbol{\sigma}_\mathbf{x} \cos\varphi - \boldsymbol{\sigma}_\mathbf{y} \sin\varphi), \tag{4.48}$$

and form the Hermitian conjugate

$$\mathbf{W}^\dagger = (\boldsymbol{\sigma}_x \sin\varphi + \boldsymbol{\sigma}_y \cos\varphi)i\partial_\varphi + i(1 - A^*)(\boldsymbol{\sigma}_x \cos\varphi - \boldsymbol{\sigma}_y \sin\varphi), \tag{4.49}$$

where hermiticity requires $A^* = A = \frac{1}{2}$.

The method of Ref. [33] applied to the Dresselhaus SO interaction would require to express ∂_x and ∂_y in equation (4.6) in terms of ∂_ρ and ∂_φ, then to substitute ρ by a and ∂_ρ by $-(2a)^{-1}$. It obviously leads to the same expression.

Now, completing the square as we have done in the Rashba case, we get for the Dresselhaus SO interaction the more compact expression

$$\mathbf{H}^{\text{ring}}_{Dresselhaus} = \frac{\hbar^2}{2ma^2}\left[\left(i\partial_\varphi \mathbf{1}_{2\times2} + \frac{ma\beta}{\hbar}(\boldsymbol{\sigma}_x \sin\varphi + \boldsymbol{\sigma}_y \cos\varphi)\right)^2 - \left(\frac{ma\beta}{\hbar}\right)^2 \mathbf{1}_{2\times2}\right]. \tag{4.50}$$

This expression is very similar to the Rashba Hamiltonian and only slight modifications are needed to calculate the spin current along the ring. The energy levels are now given by

$$E^\lambda_{n,s} = \frac{\hbar^2}{2ma^2}\left[\left(n - \frac{\lambda s}{2}\sqrt{1 + 4(ma\beta/\hbar)^2}\right)^2 - (ma\beta/\hbar)^2\right], \tag{4.51}$$

i.e. they are obtained from the Rashba eigenenergies via the substitution $\alpha \to \beta$ and time reversal symmetry is preserved. The corresponding eigenspinors become

$$\Psi^+_{n,+} = e^{in\varphi}\begin{pmatrix} \sin\frac{\theta}{2}e^{i\varphi/2} \\ -i\cos\frac{\theta}{2}e^{-i\varphi/2}\end{pmatrix}, \Psi^+_{n,-} = e^{in\varphi}\begin{pmatrix} -\cos\frac{\theta}{2}e^{i\varphi/2} \\ -i\sin\frac{\theta}{2}e^{-i\varphi/2}\end{pmatrix} \tag{4.52}$$

$$\Psi^-_{n,+} = e^{-in\varphi}\begin{pmatrix} \sin\frac{\theta}{2}e^{i\varphi/2} \\ -i\cos\frac{\theta}{2}e^{-i\varphi/2}\end{pmatrix}, \Psi^-_{n,-} = e^{-in\varphi}\begin{pmatrix} -\cos\frac{\theta}{2}e^{i\varphi/2} \\ -i\sin\frac{\theta}{2}e^{-i\varphi/2}\end{pmatrix} \tag{4.53}$$

where now $\cos\theta = 1/\sqrt{1 + 4(ma\beta/\hbar)^2}$. When the SO coupling β is not too strong, we recover the structure of a four-fold degenarate ground state and the spin current polarized in the z direction takes the form

$$\mathcal{J}^z_\varphi = \frac{\hbar^2}{4ma}(1 - \cos\theta). \tag{4.54}$$

Notice that the computed z component of the spin current has the opposite sign to that of the Rashba contribution (see (4.45)), so that given equal SO strengths for both type of interactions the two effects compete to produce a vanishing net spin current.

4.5.3 Spin current and the non-Abelian gauge formalism

The computed spin currents in the previous sections where based on intuitive extensions of the very familiar charge current definition, i.e. the physical quantity being transported times the velocity, along with the necessary symmetrization when the definition involves two non-commuting operators. In this section we make the student realize that a formal, well grounded approach can be used to define the currents based on regarding them as conserved quantities following Noether's theorem. We will depart from a general Lagrangian that will be identified with the corresponding ring Hamiltonian, derived above. New tensor fields will arise, analogous to the gauge potential in electromagnetism but of a non-abelian nature, that will by canonical relations, give us the full expressions of the currents in the theory.

The spin current calculated above is the equivalent of the paramagnetic current in the case of $U(1)$ gauge theory (see e.g. [8]). One can ask about a possible equivalent to the diamagnetic contribution also (such a contribution is called color diamagnetism by Tokatly [40, 41]). The Lagrangian approach is very convenient to investigate this question. To the Hamiltonian given in equation (4.25), we associate a Lagrangian density $\mathcal{L}$ defined according to

$$\begin{aligned} L &\equiv \int ad\varphi\, \mathcal{L}, \\ &= \langle\Psi|i\hbar\partial_t \mathbf{1}_{2\times 2} - \mathbf{H}|\Psi\rangle, \\ &= \int ad\varphi\, [i\hbar\Psi^\dagger\dot{\Psi} - \Psi^\dagger \mathbf{H}\Psi]. \end{aligned} \tag{4.55}$$

After an integration by parts, $\mathcal{L}$ follows,

$$\begin{aligned} &i\hbar\Psi^\dagger\dot{\Psi} \\ &-\frac{1}{2m}\left[\Psi^\dagger(i\hbar a^{-1}\overleftarrow{\partial}_\varphi \mathbf{1}_{2\times 2} - \frac{1}{2}gW^a_\varphi\boldsymbol{\sigma}_a))\right]\left[(-i\hbar a^{-1}\overrightarrow{\partial}_\varphi \mathbf{1}_{2\times 2} - \frac{1}{2}gW^a_\varphi\boldsymbol{\sigma}_a))\Psi\right] \\ &+\frac{1}{8m}g^2\Psi^\dagger(W^b_\varphi\boldsymbol{\sigma}_b)(W^c_\varphi\boldsymbol{\sigma}_c)\Psi, \end{aligned} \tag{4.56}$$

where the arrows above the partials indicate in which direction the derivative is taken and the non-Abelian gauge field

$$\frac{1}{2}gW^a_\varphi\boldsymbol{\sigma}_a = m\alpha\boldsymbol{\sigma}_\rho, \tag{4.57}$$

was introduced with $g = \hbar$ so that W^a_φ has dimensions of $m\alpha/\hbar$. The $SU(2)$ gauge field is then proportional to the SO strength. The contraction on the internal index $a = x, y, z$ is understood. From this Lagrangian, the spin current follows from derivatives with respect to the gauge field components,

$$\mathcal{J}^a_\varphi = \frac{\partial\mathcal{L}}{\partial W^a_\varphi} \tag{4.58}$$

which has the correct dimension of a spin current. A first contribution $\mathcal{J}_{(1)}$ to the spin current follows from the second term at the r.h.s. of equation (4.56),

$$\begin{aligned} \mathcal{J}_{(1)}{}^a_\varphi &= -\frac{1}{2m}\Psi^\dagger(-\frac{1}{2}\hbar\sigma_a)(-i\hbar a^{-1}\partial_\varphi \mathbf{1}_{2\times 2} - m\alpha\boldsymbol{\sigma}_\rho)\Psi \\ &\quad -\frac{1}{2m}\Psi^\dagger(i\hbar a^{-1}\partial_\varphi \mathbf{1}_{2\times 2} - m\alpha\boldsymbol{\sigma}_\rho)(-\frac{1}{2}\hbar\sigma_a)\Psi, \end{aligned} \tag{4.59}$$

and can be explicitly calculated for all three spin components,

$$\mathcal{J}_{(1)}{}^{x}_{\varphi} = -\frac{i\hbar^2}{4ma}[\Psi^\dagger \boldsymbol{\sigma}_x \partial_\varphi \Psi - (\partial_\varphi \Psi^\dagger)\boldsymbol{\sigma}_x \Psi] - \frac{1}{2}\hbar\alpha\Psi^\dagger \cos\varphi\Psi, \tag{4.60}$$

$$\mathcal{J}_{(1)}{}^{y}_{\varphi} = -\frac{i\hbar^2}{4ma}[\Psi^\dagger \boldsymbol{\sigma}_y \partial_\varphi \Psi - (\partial_\varphi \Psi^\dagger)\boldsymbol{\sigma}_y \Psi] - \frac{1}{2}\hbar\alpha\Psi^\dagger \sin\varphi\Psi, \tag{4.61}$$

$$\mathcal{J}_{(1)}{}^{z}_{\varphi} = -\frac{i\hbar^2}{4ma}[\Psi^\dagger \boldsymbol{\sigma}_z \partial_\varphi \Psi - (\partial_\varphi \Psi^\dagger)\boldsymbol{\sigma}_z \Psi]. \tag{4.62}$$

The "diacolor" contribution (linear in α) mentioned above appears only for the x and y spin polarizations. There is nevertheless another term in the Lagrangian, the third term of the r.h.s. in equation (4.56) which plays the role of a *gauge symmetry breaking* term (or a mass term). It brings another contribution $\mathcal{J}_{(2)}$ to the spin current,

$$\mathcal{J}_{(2)}{}^{a}_{\varphi} = \frac{1}{8m} g^2 \Psi^\dagger \left(\sigma_a W^b_\varphi \sigma_b + W^b_\varphi \sigma_b \sigma_a\right) \Psi, \tag{4.63}$$

$$= \frac{1}{4}\hbar\alpha\Psi^\dagger\{\sigma_a, \sigma_\rho\}\Psi, \tag{4.64}$$

so

$$\mathcal{J}_{(2)}{}^{x}_{\varphi} = \frac{1}{2}\hbar\alpha\Psi^\dagger \cos\varphi\Psi, \tag{4.65}$$

$$\mathcal{J}_{(2)}{}^{y}_{\varphi} = \frac{1}{2}\hbar\alpha\Psi^\dagger \sin\varphi\Psi, \tag{4.66}$$

$$\mathcal{J}_{(2)}{}^{z}_{\varphi} = 0, \tag{4.67}$$

that exactly cancels the diacolor contribution in such a way that for all three spin polarizations only the "paracolor" contributions survive. Eventually the total spin current density, given by

$$\mathcal{J}^a_\varphi = -\frac{i\hbar^2}{4ma}[\Psi^\dagger \boldsymbol{\sigma}_a \partial_\varphi \Psi - (\partial_\varphi \Psi^\dagger)\boldsymbol{\sigma}_a \Psi], \tag{4.68}$$

is in agreement with the explicit calculations presented above for the $z-$polarization. In the general case, due to the presence GSB term, it does not coincide with the usual definition of the current in terms of the symmetrized spin-velocity product (4.41). This property is not very well known and deserves special attention.

4.6 Path integral on the ring and voltage quantization

Many questions in the context of mesoscopic rings concern phase effects. When a perpendicular magnetic field is enclosed by the ring there occur peculiar conditions to ensure a single-valued wave function [42]. The well known Aharonov-Bohm effect is a striking consequence of the peculiar phase relations on a multiply connected structure such as a ring. In the presence of SO interactions, phase relations are upgraded to spinor interferences since the wavefunctions are now two component objects. Special attention must be paid when a SO interaction is present, since a new physical effect appears i.e. the spin precession. Spin precession is a two component phase evolution in contrast to the one component phase evolution in electromagnetism or $U(1)$ gauge theory.

There is a simple qualitative picture, which consists in the interpretation of the interaction term as similar to an effective Zeeman term, $\sim -\vec{\boldsymbol{\sigma}} \cdot \vec{\mathrm{B}}_{\mathrm{eff.}}$. In the case of the Rashba SO interaction, the effective magnetic field is

$$\vec{\mathrm{B}}^{\mathrm{eff.}}_{Rashba} = \alpha p_\varphi \vec{e}_\rho \tag{4.69}$$

and the axis around which the spin precesses rotates when the electron moves along the ring.

This condition appears when we consider the $SU(2)-$phase accumulation by the spinor under transport along the loop [43]:

$$\hbar^{-1}\oint \frac{1}{2}g\vec{W}^a\boldsymbol{\sigma}_a d\vec{r} = \frac{m\alpha}{\hbar}\int_0^{2\pi} a\, d\varphi\, \boldsymbol{\sigma}_\rho. \tag{4.70}$$

This expression follows from the gauge formulation of the problem [44, 43], and it is apparent for example in the Rashba case in equation (4.25) where the spin of the electron appears to be minimally coupled to the electric field through the $SU(2)-$kinematic momentum

$$(-i\hbar a^{-1}\partial_\varphi)\mathbf{1}_{2\times 2} - m\alpha\boldsymbol{\sigma}_\rho, \tag{4.71}$$

where $m\alpha\boldsymbol{\sigma}_\rho \equiv \frac{1}{2}g\vec{W}^a\boldsymbol{\sigma}_a$ is a non-Abelian $SU(2)-$gauge field introduced in equation (4.57). When the operator $\exp\left(i\hbar^{-1}\oint \frac{1}{2}g\vec{W}^a\boldsymbol{\sigma}_a d\vec{r}\right)$ constructed from equation (4.70) is applied on $\Psi = \psi_\uparrow|+\rangle_\rho + \psi_\downarrow|-\rangle_\rho$, the condition

$$\cos\tfrac{2\pi m a\alpha}{\hbar}\mathbf{1}_{2\times 2}\Psi + i\boldsymbol{\sigma}_\rho \sin\tfrac{2\pi m a\alpha}{\hbar}\Psi = \Psi \tag{4.72}$$

follows to secure single-valued spinors. We thus obtain a quantization condition

$$\frac{2\pi m a\alpha}{\hbar} = 2\pi \times \texttt{integer}. \tag{4.73}$$

In the case of the standard SO interaction, $\alpha = |e|\hbar E/2m^2c^2$. This condition may be rewritten in terms of a typical voltage in the problem defined by $V = 2\pi aE$ (take care here, the electrons on the ring move in a constant potential and the gate voltage applied externally to produce the electric field is a different quantity V_{gate}),

$$\frac{V}{4\pi mc^2/e} = \texttt{integer}, \tag{4.74}$$

where one can introduce a quantum of voltage, $V_0 = 4\pi mc^2/e$.

The same result also follows from more general arguments based on the path integral formulation on the ring. As the student has learned in graduate quantum mechanics, path integral allow for an alternative and illuminating derivation of quantum mechanics generalizing the action principle of classical mechanics. We will close our description of ring physics in the presence of SO interactions by deriving in detail its path integral and making contact with the quantization conditions derived above.

Let us consider again the Hamiltonian (4.25) and define the eigenstates $|n\rangle$ of the operator $i\partial_\varphi$, $i\partial_\varphi|n\rangle = -n|n\rangle$, such that periodicity along the ring and normalization are satisfied, $\langle\varphi + 2\pi|n\rangle = \langle\varphi|n\rangle$ and $\int_0^{2\pi} d\varphi|\langle\varphi|n\rangle|^2 = 1$. We have

$$\langle\varphi|n\rangle = (2\pi)^{-1/2}e^{in\varphi}, \quad n \in \mathbb{Z}. \tag{4.75}$$

In order to construct the amplitude for an electron to go from a particular state on the ring $|\varphi,\sigma;t\rangle$ to another similar state at different time $|\varphi',\sigma';t'\rangle$, we construct the path integral in discretized time as

$$\mathcal{A}(\varphi,\sigma;t\to\varphi',\sigma';t') = \prod_{i=1}^{N-1}\langle\varphi_{i+1},\sigma_{i+1}|e^{-i\Delta t\mathbf{H}/\hbar}|\varphi_i,\sigma_i\rangle, \tag{4.76}$$

with $\Delta t = t_{i+1} - t_i$. In the limit $\Delta t \to 0$, the evolution operator is expanded to linear order in Δt and one has to evaluate matrix elements of the Hamiltonian between spin states. Expanding on the "plane wave" basis, one has

$$i\partial_\varphi \mathbf{1}_{2\times 2}|\varphi,\sigma\rangle = \sum_{n\in\mathbb{Z}}(-n)(2\pi)^{-1/2}e^{-in\varphi}\mathbf{1}_{2\times 2}|n,\sigma\rangle, \tag{4.77}$$

and the matrix element of the Hamiltonian reads as

$$\langle\varphi',\sigma'|\mathbf{H}|\varphi,\sigma\rangle = \frac{\hbar^2}{2ma^2}\sum_{n\in\mathbb{Z}}\frac{1}{2\pi}[n^2\delta_{\sigma,\sigma'} - 2n\frac{ma\alpha}{\hbar}(\boldsymbol{\sigma}_\rho)_{\sigma,\sigma'}]e^{in(\varphi'-\varphi)}. \tag{4.78}$$

When we pass to the evolution operator, one has to evaluate

$$\langle\varphi',\sigma'|\mathbf{1}_{2\times 2} - \frac{i\Delta t}{\hbar}\mathbf{H}|\varphi,\sigma\rangle = \langle\varphi'|\varphi\rangle\delta_{\sigma,\sigma'} - \frac{i\Delta t}{\hbar}\langle\varphi',\sigma'|\mathbf{H}|\varphi,\sigma\rangle, \tag{4.79}$$

where we make use of the property $\langle\varphi'|\varphi\rangle = \sum_{n\in\mathbb{Z}}\frac{1}{2\pi}e^{in(\varphi'-\varphi)}$ in order to factorize out the term $e^{in(\varphi'-\varphi)}$, and we exponentiate again the Hamiltonian matrix element to get

$$\langle\varphi',\sigma'|\mathbf{1}_{2\times 2} - \frac{i\Delta t}{\hbar}\mathbf{H}|\varphi,\sigma\rangle = \sum_{n\in\mathbb{Z}}\frac{1}{2\pi}\left[e^{-\frac{i\hbar}{2ma^2}\Delta t[n^2\mathbf{1}_{2\times 2} - 2n\frac{ma\alpha}{\hbar}\boldsymbol{\sigma}_\rho]}\right]_{\sigma,\sigma'}e^{in(\varphi'-\varphi)}. \tag{4.80}$$

Completing the square and introducing the classical variable $v_\varphi = a(\varphi'-\varphi)/\Delta t$, one eventually arrives at

$$\langle\varphi_{i+1},\sigma_{i+1}|e^{-i\Delta t\mathbf{H}/\hbar}|\varphi_i,\sigma_i\rangle = \text{const}\left[e^{\frac{i}{\hbar}[\frac{1}{2}m(v_\varphi\mathbf{1}_{2\times 2}-\alpha\boldsymbol{\sigma}_\rho)^2]\Delta t}\right]_{\sigma,\sigma'}, \tag{4.81}$$

such that extended to the whole path, we get the symbolic expression

$$\mathcal{A}(\varphi,\sigma;t\to\varphi',\sigma';t') = \int\mathcal{D}\varphi(t)\mathbf{T}\left[e^{\frac{i}{\hbar}\int\frac{1}{2}m(v_\varphi\mathbf{1}_{2\times 2}-\alpha\boldsymbol{\sigma}_\rho)^2dt}\right]_{\sigma,\sigma'}, \tag{4.82}$$

where $\mathbf{T}$ is a super-operator ordering chronologically all operator products. We note that the path integral representation is only performed at the level of the space degrees of freedom and not for the spin variables for which we still have an evolution operator. Introducing spin coherent states, one could formulate path integrals where both coordinate and spin would be classical variables [45]. From the path integral, we can read a "classical Lagrangian"

$$\mathbf{L} = \frac{1}{2}m(v_\varphi\mathbf{1}_{2\times 2} - \alpha\boldsymbol{\sigma}_\rho)^2. \tag{4.83}$$

When we expand the square, we get three contributions to the spin precession. If we consider the "phase accumulation" for a classical trajectory along a closed path over the ring (one round trip), the first term is simply the dynamical phase, which is path dependent,

$$\frac{1}{\hbar}\int_0^{2\pi}\frac{1}{2}\,mv_\varphi a d\varphi\,\delta_{\sigma,\sigma'} = \frac{\pi m v_\varphi a}{\hbar}\delta_{\sigma,\sigma'}. \tag{4.84}$$

It corresponds to the analogue of the optical phase. The second term, the non-Abelian equivalent to the Aharonov-Bohm phase, is the path independent (for closed paths) contribution discussed in the beginning of this section,

$$\frac{1}{\hbar}\int_0^{2\pi}\,mv_\varphi\alpha(\boldsymbol{\sigma}_\rho)_{\sigma,\sigma'}dt = \frac{2\pi m\alpha(\boldsymbol{\sigma}_\rho)_{\sigma,\sigma'}a}{\hbar}, \tag{4.85}$$

or, using α and V defined above,

$$\frac{V}{2mc^2/e}(\boldsymbol{\sigma}_\rho)_{\sigma,\sigma'}. \tag{4.86}$$

This is the counterpart of the famous Φ/Φ_0 phase in $U(1)$ gauge theory. The third term is an additional path-dependent contribution to the phase which takes its origin in the initial GSB term of equation (4.56),

$$\frac{1}{\hbar}\int_0^{2\pi}\frac{1}{2}\,m\alpha^2(\boldsymbol{\sigma}_\rho^2)_{\sigma,\sigma'}dt = \frac{\pi m\alpha^2\delta_{\sigma,\sigma'}a}{\hbar v_\varphi}. \tag{4.87}$$

This last term produces a phase variation which varies *quadratically* with the gate voltage applied.

Let us note the particular role of the GSB term in the Hamiltonian. In equation (4.82), the transition amplitude is given by a path integral where the action involves a term quadratic in the gauge field. In the simpler case of a particle submitted to the $U(1)$-electromagnetic gauge field, the corresponding transition amplitude would read as

$$\mathcal{A}(\varphi;t\to\varphi';t') = \int \mathcal{D}\varphi(t)e^{\frac{i}{\hbar}\int\left(\frac{1}{2}mv_\varphi^2+ev_\varphi A_\varphi\right)dt}, \tag{4.88}$$

i.e. it would not include any quadratic term in the $U(1)$ gauge field. The presence of such a quadratic term and its contribution (4.87) to the phase accumulation is a direct consequence of the GSB term in the SO case.

5 Derivation of the correct Hamiltonian for 1D ring

One-dimensional ring in the presence of Rashba spin-orbit interaction: Derivation of the correct Hamiltonian

F. E. Meijer, A. F. Morpurgo, and T. M. Klapwijk

The effect of Rashba spin-orbit (SO) interaction [1] on electrons moving in a mesoscopic ring has been studied in several contexts, such as magnetoconductance oscillations, [2,3] Peierls transition, [4,5] and persistent current. [6,7] Essentially all these theoretical studies have employed one-dimensional (1D) model Hamiltonians. Since different Hamiltonians have been used by different authors some ambiguity currently exists with regard to the correct form of the 1D Hamiltonian. For instance, Aronov and Lyanda-Geller, who studied the effect of Rashba SO interaction on the Aharonov-Bohm conductance oscillations, [2] used a non-Hermitean operator as Hamiltonian. [8] Zhou, Li, and Xue [9] noticed this fact and derived a different (Hermitean) Hamiltonian operator. However, in their Hamiltonian the Rashba SO term originates from an electric field pointing in the radial direction and not in the direction perpendicular to the plane of the ring. This is physically not correct. Subsequently others [3,5,7,10] have employed a now commonly used 1D Hamiltonian for electrons on a ring, without explicitly discussing its derivation.

The purpose of this short paper is to identify the origin of the existing ambiguity and to discuss in detail the procedure to obtain the correct 1D Hamiltonian operator for electrons moving on a ring in the presence of Rashba SO interaction. We will show that the subtlety of this seemingly trivial problem has not been fully appreciated so far.

The "conventional" way to obtain the Hamiltonian for a 1D ring from the Hamiltonian in two dimensions consists of two steps. First the Hamiltonian operator is transformed into cylindrical coordinates r and ϕ. Then r is set to a constant and all terms proportional to derivatives with respect to r are discarded (i.e., set to 0). This procedure works correctly in simple cases, such as free electrons or electrons in the presence of a (uniform or textured [11])

magnetic field. However, it does not work in the presence of Rashba SO interaction, as we will illustrate below.

The (2D) Hamiltonian for a (single) electron in the presence of Rashba spin-orbit interaction and a magnetic field is given by

$$\hat{H} = \frac{1}{2m}(\mathbf{p} - e\mathbf{A})^2 + \alpha\hat{\sigma} \cdot \mathbf{E} \times (\mathbf{p} - e\mathbf{A}) + \mu\hat{\sigma} \cdot \mathbf{B},$$

where $\mathbf{A}$ is the vector potential, α is the SO constant, $\mathbf{E}$ and $\mathbf{B}$ are pointing in the $\hat{z}$ direction (perpendicular to the plane). In cylindrical coordinates, with $x = r\cos\phi$ and $y = r\sin\phi$, this operator reads

$$\begin{aligned}\hat{H}(r,\phi) = -\frac{\hbar^2}{2m}\left[\frac{\partial^2}{\partial r^2} + \frac{1}{r}\frac{\partial}{\partial r} - \frac{1}{r^2}\left(i\frac{\partial}{\partial\phi} + \frac{\Phi}{\Phi_0}\right)^2\right] \\ - \frac{\alpha}{r}\left(\cos\phi\sigma_x + \sin\phi\sigma_y\right)\left(i\frac{\partial}{\partial\phi} + \frac{\Phi}{\Phi_0}\right) \\ + i\alpha\left(\cos\phi\sigma_y - \sin\phi\sigma_x\right)\frac{\partial}{\partial r} + \frac{\hbar\omega_B}{2}\sigma_z\end{aligned}$$

with Φ is the magnetic flux through the ring, $\Phi_0 = h/e$, and $\hat{\sigma}_{x,y,z}$ are the usual Pauli spin matrices. Notice also that we have redefined $\alpha\,(\alpha \to \hbar E_z\alpha)$. If we now set r to a constant value $(r = a)$ and neglect the derivative terms, we obtain

$$\hat{H}(\phi) = -\frac{\hbar^2}{2ma^2}\left(i\frac{\partial}{\partial\phi} + \frac{\Phi}{\Phi_0}\right)^2 + \frac{\hbar\omega_B}{2}\sigma_z - \frac{\alpha}{a}\left(\cos\phi\sigma_x + \sin\phi\sigma_y\right)\left(i\frac{\partial}{\partial\phi} + \frac{\Phi}{\Phi_0}\right)$$

This operator, used by Aronov and Lyanda Geller, [2] is not Hermitean, as can be easily shown by calculating its matrix elements in any complete basis (i.e., the "conventional" procedure fails).

In order to find the correct form for the 1D Hamiltonian we go back to the full (2D) Hamiltonian [Eq. (2)]. To this Hamiltonian we add a potential $V(r)$, which forces the electron wave functions to be localized on the ring in the radial direction. Specifically $V(r)$ is small in a narrow region around $r = a$ and large outside this region. For a narrow ring (steep confining potential) the confining energy in the radial direction is much larger than the SO energy, the Zeeman energy, and the kinetic energy in the azimuthal direction. This allows us to solve the Hamiltonian for the radial wave function first and treat $\hat{H}_{\rm SO}$, $\hat{H}_{\rm Zeeman}$, and $\hat{H}_{\rm kin}\,(\phi)$ as a perturbation. Specifically we write $\hat{H} = \hat{H}_0 + \hat{H}_1$, where

$$\hat{H}_0 = -\frac{\hbar^2}{2m}\left[\frac{\partial^2}{\partial r^2} + \frac{1}{r}\frac{\partial}{\partial r}\right] + V(r)$$

and the perturbation Hamiltonian $\hat{H}_1$ is given by

$$\hat{H}_1 = \frac{\hbar^2}{2mr^2}\left(i\frac{\partial}{\partial\phi} + \frac{\Phi}{\Phi_0}\right)^2 + \frac{\hbar\omega_B}{2}\sigma_z - \frac{\alpha}{r}\left(\cos\phi\sigma_x + \sin\phi\sigma_y\right)\left(i\frac{\partial}{\partial\phi} + \frac{\Phi}{\Phi_0}\right) + i\alpha\left(\cos\phi\sigma_y - \sin\phi\sigma_x\right)\frac{\partial}{\partial r}$$

The eigenfunctions of $\hat{H}_0$ are separable in r and ϕ, i.e., $\Psi(r,\phi) = R(r)\Phi(\phi)$, since $\hat{H}_0$ does not depend on ϕ. In the limit of a very narrow (1D) ring all electrons will be in the lowest radial mode $R_0(r)$. We then have an infinitely degenerate set of states $\Psi_n(r,\phi) = R_0(r)\Phi_n(\phi)$ over which we have to diagonalize $\hat{H}_1$ [here, the $\Phi_n(\phi)$ denote a complete set of spinors in the ϕ direction].

The matrix elements of $\hat{H}_1$ are

$$a_{mn} = \langle \Phi_m(\phi)| \langle R_0(r)| \hat{H}_1(r,\phi) |R_0(r)\rangle |\Phi_n(\phi)\rangle ,$$

from which we can read the correct 1D Hamiltonian $\hat{H}(\phi)$ directly

$$\hat{H}_{1\mathrm{D}}(\phi) = \langle R_0(r)| \hat{H}_1(r,\phi) |R_0(r)\rangle .$$

In order to obtain the 1D Hamiltonian explicitly, we have to calculate the lowest radial mode for a given confining potential. If we assume without loss of generality (since we will consider the limit of a truly 1 D ring) a harmonic confining potential $[V(r) = 1/2K(r-a)^2]$, we have to solve

$$-\frac{\hbar^2}{2m}\left[\frac{\partial^2 R(r)}{\partial r^2} + \frac{1}{r}\frac{\partial R(r)}{\partial r}\right] + \frac{1}{2}K(r-a)^2 R(r) = ER(r).$$

In the limit of a 1D ring we may neglect the $(1/r)\times(\partial/\partial r)$ term in comparison to the $\partial^2/\partial r^2$ term and obtain the harmonic-oscillator equation. [12] The lowest energy normalized solutions is then given by

$$R_0(r) = \left(\frac{\gamma}{a\sqrt{\pi}}\right)^{1/2} e^{-(1/2)\gamma^2(r-a)^2}$$

where $\gamma^4 = mK/\hbar^2$ (the 1D limit is achieved by letting γ go to infinity).

From Eqs. (5) and (7) we can now derive the 1D Hamiltonian explicitly. Since $\hat{H}_1$ contains terms dependent or r and derivatives with respect to r we have to calculate their expectation value. We obtain

$$\langle R_0(r)| \frac{1}{r} |R_0(r)\rangle = \int_0^\infty R_0^2(r)dr = \frac{1}{a}$$

and the expectation value of $\partial/\partial r$ is given by

$$\langle R_0(r)| \frac{\partial}{\partial r} |R_0(r)\rangle = \int_0^\infty R_0(r)\frac{\partial R_0(r)}{\partial r} r dr = -\frac{1}{2a}.$$

From this we conclude that we cannot safely disregard the $\partial/\partial r$ term in order to obtain the correct 1D Hamiltonian.

It is worth stressing that it is not essential to choose a harmonic potential, nor to make any approximation as we have done above for simplicity, in order to obtain these results. To show this, let $|\rho_0(r)\rangle$ be the lowest radial mode for an arbitrarily given confining potential. We define $|\rho_0'(r)\rangle = (1/\sqrt{r})\,|\rho_0(r)\rangle$. From direct calculations it follows that $\langle\rho_0|\,(1/2r) + (\partial/\partial r)\,|\rho_0\rangle = \langle\rho_0'|\,(1/r)(\partial/\partial r)\,|\rho_0'\rangle = 1/\,2\rho_0'^2|_0^\infty = 1/\,2r\rho_0^2|_0^\infty = 0$. We then obtain $\langle\rho_0|\,\partial/\partial r\,|\rho_0\rangle = -\langle\rho_0|\,1/2r\,|\rho_0\rangle$. Therefore for the lowest radial mode in the 1D limit we always get $\langle\rho_0|\,\partial/\partial r\,|\rho_0\rangle = -(1/2a)$, independent of the precise form of $|\rho_0(r)\rangle$ and thus of the precise shape of the radial confining potential that is used in the calculation.

Having established the generality of our result, we can now write the 1D Hamiltonian explicitly. From Eqs. (7) and (10) we get

$$\hat{H}_{1\mathrm{D}}(\phi) = \frac{\hbar^2}{2ma^2}\left(i\frac{\partial}{\partial\phi} + \frac{\Phi}{\Phi_0}\right)^2 + \frac{\hbar\omega_B}{2}\sigma_z - \frac{\alpha}{a}\left(\cos\phi\sigma_x + \sin\phi\sigma_y\right)\left(i\frac{\partial}{\partial\phi} + \frac{\Phi}{\Phi_0}\right) - \\ - i\frac{\alpha}{2a}\left(\cos\phi\sigma_y - \sin\phi\sigma_x\right)$$

This is the correct form of the 1D Hamiltonian for electrons on a ring, in the presence of Rashba SO interaction.

The last term in Eq. (12) is neglected if we follow the "conventional" procedure. It is only recovered by following the procedure described above. In the simple cases mentioned earlier (e.g., free electrons), there are no terms present in the Hamiltonian proportional to both $\partial/\partial r$ and some function of ϕ (i.e., the two-dimensional Hamiltonian is separable). In these cases the "conventional" procedure produces the correct result. In all other cases it is necessary to take into account properly the confinement of the wave function in the radial direction as we have shown in this paper in order to obtain the correct 1D Hamiltonian on a ring.

In short, what we have described in this paper is a formally correct procedure to project the original Hamiltonian [Eq. (1)] defined on the Hilbert space of spinors in two dimensions on a restricted Hilbert subspace, spanned by the complete set of spinors $\Phi_n(\phi)$, which are function of the ϕ coordinate only.

6 Spin states and persistent currents in mesoscopic rings: spin-orbit interactions

J. S. Sheng, Kai Chang

Abstract

We investigate theoretically electron spin states in one dimensional (1D) and two dimensional (2D) hard-wall mesoscopic rings in the presence of both the Rashba spin-orbit interaction (RSOI) and the Dresselhaus spin-orbit interaction (DSOI) in a perpendicular magnetic field. The Hamiltonian of the RSOI alone is mathematically equivalent to that of the DSOI alone using an SU(2) spin rotation transformation. Our theoretical results show that the interplay between the RSOI and DSOI results in an effective periodic potential, which consequently leads to gaps in the energy spectrum. This periodic potential also weakens and smoothens the oscillations of the persistent charge current (CC) and spin current (SC) and results in the localization of electrons. For a 2D ring with a finite width, higher radial modes destroy the periodic oscillations of persistent currents.

6.1 Summary

We have conducted a theoretical investigation of the spin states and persistent CC and SC in mesoscopic rings with spin-orbit interactions. We have demonstrated theoretically that the Hamiltonian of the RSOI alone is mathematically equivalent to that of the DSOI alone by a unitary transformation T. This property results in the degenerate energy spectrum for equal strength RSOI and DSOI. The interplay between the RSOI and DSOI leads to an effective periodic potential $\frac{\bar{\alpha}\bar{\beta}}{2}\sin 2\varphi$. This periodic potential results in gaps in the energy spectrum, and smoothens and weakens the oscillations of the persistent CC and SC. The charge density and the local spin orientation $S(\boldsymbol{r})$ are localized along the ring due to the effect of the periodic potential. Higher radical modes become involved as the ring width increases, destroying the periodicity of the persistent CC and SC oscillations.

6.2 Introduction

In recent years, the spin-orbit interaction (SOI) in low-dimensional semiconductor structures has attracted considerable attention due to its potential applications in spintronic devices. [1, 2] There are two types of SOI in conventional semiconductors. One is the Dresselhaus spin-orbit interaction (DSOI) induced by bulk inversion asymmetry, [3] and the other is the Rashba spin-orbit interaction (RSOI) induced by structure inversion asymmetry. [4, 5] The strength of the RSOI can be tuned by external gate voltages or asymmetric doping. Recently, the intrinsic

spin Hall effect (SHE) in a spin-orbit coupled three-dimensional p-doped semiconductor [6] and in a Rashba spin-orbit coupled two-dimensional electron system [7] was predicted theoretically. It provides us a possibility to generate the spin current (SC) electrically without the use of ferromagnetic metal or a magnetic field.

Recently advanced growth techniques make it possible to fabricate high quality semiconductor rings. [8] A quantum ring exhibits the intriguing spin interference phenomenon because of its unique topology. The persistent CC in mesoscopic rings threaded by a magnetic U(1) flux has been studied extensively, neglecting the spin degree of freedom of the electron. [9, 10, 11] It has been experimentally observed both in a gold ring [12] and in a GaAs-AlGaAs ring [13] using standard SQUID magnetometry. As for the persistent SC, the SC-induced electric field that was predicted by several authors[14, 15] may contribute to the successful measurement of the persistent SC in mesoscopic rings in future. The electronic structures and magneto-transport properties of 1D rings with the RSOI alone have attracted considerable interest. [16, 17, 18] Since the strength of the DSOI in thin quantum wells is comparable with that of the RSOI, [19] one should consider both of the SOI's in low dimensional structures. A few works have been done on the effects of the competition between these two types of SOI on the transport properties of 2DEG. [20, 21, 22] The effects of the interplay between the RSOI and DSOI on the spin states and persistent currents (CC and SC) in mesoscopic rings are highly desirable.

In this paper, we investigate theoretically the spin states and persistent CC and SC in mesoscopic rings under a uniform perpendicular magnetic field in the presence of both RSOI and DSOI. We find that the persistent CC and SC, charge density distribution, and local spin orientation are very sensitive to the strength of the RSOI and DSOI. The interplay between the RSOI and DSOI leads to an effective periodic potential. This potential has significant effects on the physical properties of mesoscopic rings, e.g., the energy gaps, the localization of electrons, and weakening and smoothening of persistent CC and SC. Five different cases are considered: (1) a 1D ring with RSOI alone; (2) a 1D ring with DSOI alone; (3) a 1D ring with RSOI and DSOI of equal strengths; (4) a 1D ring with RSOI and DSOI of different strengths; (5) finite-width effects on the energy spectrum, charge density distribution, the persistent CC and SC. The eigenstates of cases one and two are analytically solved and can be connected by a unitary transformation. The paper is organized as follows. In Sec. 6.3 the theoretical model is presented. The numerical results and discussions are given in Sec. 6.4. Finally, we give a brief conclusion in Sec. 6.1.

6.3 Theoretical model

6.3.1 Hamiltonian

In the presence of both RSOI and DSOI, the single-particle Hamiltonian for an electron in a finite-width ring (see Fig. 31(b)) under a uniform perpendicular magnetic field reads

$$H = \frac{\hbar^2 k^2}{2m^*} + \alpha(\sigma_x k_y - \sigma_y k_x) + \beta(\sigma_x k_x - \sigma_y k_y) + \frac{1}{2} g^* \mu_B B \sigma_z + V(r), \tag{6.1}$$

where $\boldsymbol{k} = -i\nabla + e\boldsymbol{A}/\hbar$. $\boldsymbol{A}(\boldsymbol{r}) = B/2(-y, x, 0)$ is the vector potential. m^* is the electron effective mass. The fourth term describes the Zeeman splitting with Bohr magneton $\mu_B = e\hbar/2m_e$ and the effective g factor g^*. $\sigma_i (i = x, y, z)$ are the Pauli matrices. α and β specify the RSOI and DSOI strengths, respectively. $V(r)$ is the radial confining potential,

$$V(r) = \begin{cases} 0 & r_1 \leqslant r \leqslant r_2 \\ \infty & \text{otherwise} \end{cases}, \tag{6.2}$$

where r_1 and r_2 are the inner and outer radii of the ring, respectively.

In the following we take the average radius $a = (r_1 + r_2)/2$ as the length unit and $E_0 = \hbar^2/2m^*a^2$ as the energy unit. The dimensionless Hamiltonian in the polar coordinates becomes

$$H = \begin{bmatrix} H_k + V(r) + \bar{g}b/2 & \bar{\beta}k_+ + i\bar{\alpha}k_- \\ \bar{\beta}k_- - i\bar{\alpha}k_+ & H_k + V(r) - \bar{g}b/2 \end{bmatrix}, \tag{6.3}$$

where $H_k = (\boldsymbol{e}_r k_r + \boldsymbol{e}_\varphi k_\varphi)^2$ is the dimensionless kinetic term; $k_\pm = k_x \pm ik_y = e^{\pm i\varphi}(k_r \pm ik_\varphi)$, with $k_r = -i\frac{\partial}{\partial r}$ and $k_\varphi = -\frac{i}{r}\frac{\partial}{\partial \varphi} + \frac{b}{4}r$; $b = \hbar eB/m^*E_0$ is the dimensionless magnetic field; $\bar{\alpha}(\bar{\beta}) = \alpha(\beta)/E_0 a$ specifies the dimensionless RSOI (DSOI) strength; and $\bar{g} = g^*m^*/2m_e$ is the dimensionless g factor.

The wavefunction $\Psi(\boldsymbol{r})$ of an electron in the ring can be expanded as

$$\Psi(\boldsymbol{r}) = \sum_{nm\sigma} a_{nm\sigma} R_n(r)\Theta_m(\varphi)\chi_\sigma(s_z), \tag{6.4}$$

$$R_n(r)\Theta_m(\varphi)\chi_\sigma(s_z) = \sqrt{\frac{2}{dr}} \sin\left[\frac{n\pi}{d}(r - r_1)\right] \cdot \frac{1}{\sqrt{2\pi}} e^{im\varphi} \cdot \chi_\sigma(s_z), \tag{6.5}$$

where $d = r_2 - r_1$ is the width of the ring and $\chi_\sigma(s_z)(\sigma = \pm 1)$ are the eigenvectors of s_z.

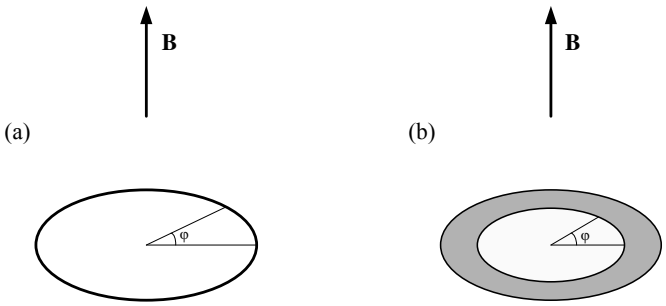

Figure 31: Schematic diagrams for 1D ideal ring (a) and 2D hard-wall ring (b).

Most previous theoretical studies on mesoscopic rings are based on the Hamiltonian of a 1D ring (see Fig. 31(a)), which can be obtained by simply disregarding all the terms proportional to derivatives with respect to r in the 2D Hamiltonian. But this conventional procedure leads to a non-hermitian Hamiltonian in the presence of RSOI or DSOI. [23] We can obtain a hermitian Hamiltonian including both RSOI and DSOI following Ref. [23]. The stationary Schrödinger equation is

$$H\Psi = E\Psi. \tag{6.6}$$

The dimensionless 1D Hamiltonian including both RSOI and DSOI reads

$$H = \left[-i\frac{\partial}{\partial\varphi} + \frac{\Phi}{\Phi_0} + \frac{\bar{\alpha}}{2}\sigma_r - \frac{\bar{\beta}}{2}\sigma_\varphi(-\varphi)\right]^2 - \frac{\bar{\alpha}^2 + \bar{\beta}^2}{4} + \frac{\bar{\alpha}\bar{\beta}}{2}\sin 2\varphi + \frac{1}{2}\bar{g}b\sigma_z, \tag{6.7}$$

where $\sigma_r = \cos\varphi\sigma_x + \sin\varphi\sigma_y$, $\sigma_\varphi = \cos\varphi\sigma_y - \sin\varphi\sigma_x$, $\Phi = B\pi a^2$ is the magnetic flux threading the ring, and $\Phi_0 = h/e$ is the flux unit. Notice that there is a periodic potential term ($\frac{\bar{\alpha}\bar{\beta}}{2}\sin 2\varphi$) induced by the interplay between the RSOI and DSOI.

We introduce a vector function $S(\boldsymbol{r})$ to describe the local spin orientation of a specific eigenstate Ψ in a 1D ring:

$$S(\boldsymbol{r}) = \Psi^\dagger \boldsymbol{s}\Psi = \Psi^\dagger s_x \Psi \mathbf{e}_x + \Psi^\dagger s_y \Psi \mathbf{e}_y + \Psi^\dagger s_z \Psi \mathbf{e}_z. \tag{6.8}$$

When the coupling strength $\bar{\alpha}$ or $\bar{\beta}$ vanishes, the $\sin 2\varphi$ potential accordingly disappears and the analytical solution to the eigenvalue problem is available (see Appendix for details). Generally we have to solve Eq. (6.6) numerically when $\bar{\alpha} \neq 0$ and $\bar{\beta} \neq 0$.

6.3.2 Persistent currents

The charge density operator and the charge current density operator are

$$\begin{aligned}\hat{\rho}(\boldsymbol{r}') &= -e\delta(\boldsymbol{r}'-\boldsymbol{r})\\ \hat{\boldsymbol{j}}_c(\boldsymbol{r}') &= \frac{1}{2}[\hat{\rho}(\boldsymbol{r}')\hat{\boldsymbol{v}}+\hat{\boldsymbol{v}}\hat{\rho}(\boldsymbol{r}'))],\end{aligned} \tag{6.9}$$

where $\boldsymbol{r}'$ refers to the field coordinates and $\boldsymbol{r}$ the coordinates of the electron. We can also introduce the spin density operator and spin current density operator [16] as

$$\begin{aligned}\hat{\boldsymbol{S}}(\boldsymbol{r}') &= \frac{\hbar}{2}\hat{\boldsymbol{\sigma}}\delta(\boldsymbol{r}'-\boldsymbol{r})\\ \hat{\boldsymbol{j}}_s(\boldsymbol{r}') &= \frac{1}{2}[\hat{\boldsymbol{S}}(\boldsymbol{r}')\hat{\boldsymbol{v}}+\hat{\boldsymbol{v}}\hat{\boldsymbol{S}}(\boldsymbol{r}')],\end{aligned} \tag{6.10}$$

where $\hat{\boldsymbol{\sigma}}=\hat{\sigma}_x\mathbf{e}_x+\hat{\sigma}_y\mathbf{e}_y+\hat{\sigma}_z\mathbf{e}_z$ is the vector of the Pauli matrices. The charge current density and spin current density can be obtained by calculating the expectation values of the corresponding operators:

$$\begin{aligned}\boldsymbol{j}_c(\boldsymbol{r}') &= \langle\Psi|\,\hat{\boldsymbol{j}}_c\,|\Psi\rangle = -e\,\mathrm{Re}\left\{\Psi^\dagger(\boldsymbol{r}')\hat{\boldsymbol{v}}'\Psi(\boldsymbol{r}')\right\}\\ \boldsymbol{j}_s(\boldsymbol{r}') &= \langle\Psi|\,\hat{\boldsymbol{j}}_s\,|\Psi\rangle = \mathrm{Re}\left\{\Psi^\dagger(\boldsymbol{r}')\hat{\boldsymbol{v}}'\hat{\boldsymbol{s}}\Psi(\boldsymbol{r}')\right\},\end{aligned} \tag{6.11}$$

where $\Psi(\mathbf{r})$ is the wavefunction of an electron in the ring. For convenience, we note $\boldsymbol{r}', \hat{\boldsymbol{v}}'$ as $\boldsymbol{r}, \hat{\boldsymbol{v}}$ hereafter.

The φ-component of the velocity operator associated with the Hamiltonian in Eq. (6.1) is

$$\hat{\boldsymbol{v}}_\varphi = \mathbf{e}_\varphi\left[\frac{\hbar}{im^*r}\frac{\partial}{\partial\varphi}+\frac{eBr}{2m^*}+\frac{\alpha}{\hbar}\sigma_r-\frac{\beta}{\hbar}\sigma_\varphi(-\varphi)\right]. \tag{6.12}$$

The azimuthal (spin or charge) current can be defined as [10]

$$I_\varphi = \frac{1}{2\pi}\int_0^{2\pi}\mathrm{d}\varphi\int_{r_1}^{r_2}\mathrm{d}r j_\varphi(\boldsymbol{r}). \tag{6.13}$$

We ignore the Coulomb interaction between electrons in this work. At the low temperature, N electrons will occupy the lowest N levels of the energy spectrum. The total (charge or spin) current is the summation over all occupied levels. [16]

For a 1D ring, the eigenstates could be expanded in the basis set $\Theta_m(\varphi)=\exp(im\varphi)/\sqrt{2\pi}$ which is much simpler than that in Eq. (6.4), and we can get the azimuthal component of the velocity operator in a 1D ring by specifying the variable r as the constant a in Eq. (6.12).

Most of the previous investigations of the persistent CC in mesoscopic rings are based on the well-known formula $I_n=-\partial E_n/\partial\Phi$, where I_n denotes the contribution to the persistent CC from the nth state and Φ is the magnetic flux through the ring. [16, 24, 25] In this paper we calculate the persistent CC and SC via Eq. (6.11). Note that for a 1D ring our results are identical with those obtained from the formula $I_n=-\partial E_n/\partial\Phi$.

6.4 Results and discussion

We show the energy spectrum of a 1D ring in Fig. 32 for different g factors. The relevant parameters of the materials used in our calculation are listed in Table 3. Without the spin-orbit couplings, the g factor accounts for the spin splitting. For a material with large g factor such as InSb, although the parabola behavior of the energy levels as functions of the magnetic

Table 3: Parameters used in our calculation are from Ref. [26].

	$m^*(m_e)$	g^*
GaAs	0.067	-0.44
InSb	0.014	-51

fields is still retained, the periodicity of the energy spectrum is severely broken by the g factor, especially at large magnetic fields. For a material with a small g factor, e.g. GaAs, the Zeeman splitting is quite small even in a rather large magnetic field.

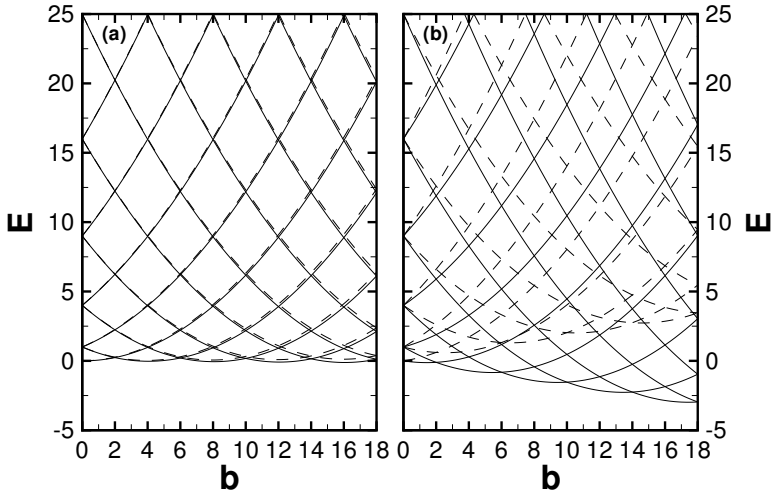

Figure 32: (a) The energy spectrum for 1D GaAs rings. $\bar{\alpha} = \bar{\beta} = 0$, $\bar{g} = -0.01474$; (b) The energy spectrum for 1D InSb ring. $\bar{\alpha} = \bar{\beta} = 0$, $\bar{g} = -0.357$. In Fig. 32(a) and Fig. 32(b) the solid (dashed) lines denote spin-up (spin-down) levels.

6.4.1 1D ring with RSOI alone

As shown in the Appendix, the electron states in a 1D ring with RSOI alone under a uniform magnetic field including the Zeeman splitting can be solved analytically.

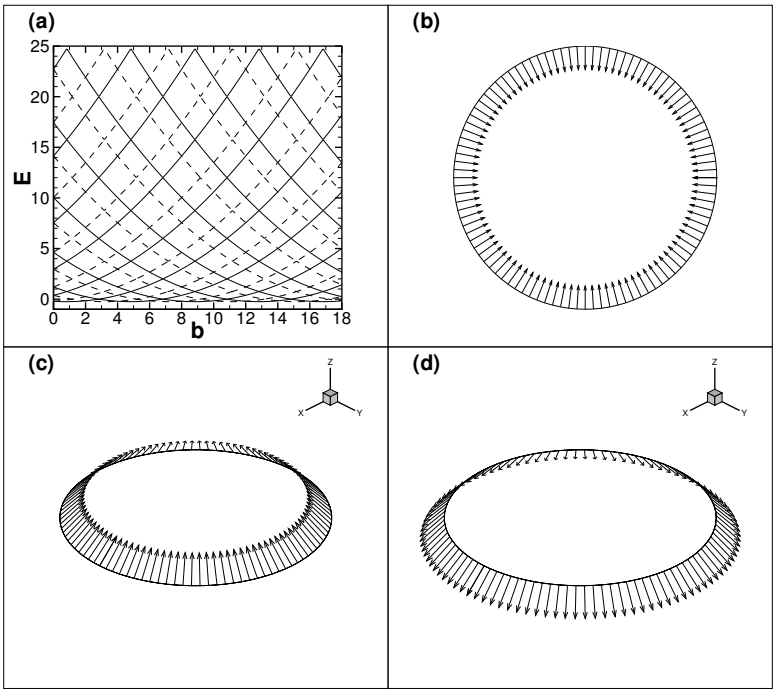

Figure 33: (a) Energy spectrum of 1D ring in the presence of RSOI alone, where the solid lines (dashed lines) denote the spin-up (spin-down) levels; (b) The projection of $S(\boldsymbol{r})^R_\uparrow$ onto the x-y plane; (c) Local spin orientation for all the spin-up levels $S(\boldsymbol{r})^R_\uparrow$; (d) Local spin orientation for all the spin-down levels $S(\boldsymbol{r})^R_\downarrow$. $\bar{\alpha} = 1$, $\bar{\beta} = 0$ and $\bar{g} = 0$.

The energy spectrum in the presence of RSOI alone is plotted in Fig. 33(a). When the g factor is set to be zero, the energy of each level is given by

$$E_{n,\sigma} = \left(n + \frac{b}{4} + \frac{\sigma}{2} - \frac{\sigma}{2\cos\theta}\right)^2 - \frac{\tan^2\theta}{4}, \tag{6.14}$$

where $\theta = \arctan(\bar{\alpha})$ (Eq. (6.34) or Eq. (6.35) represents the corresponding eigenstate so long as $\theta_{n,\sigma}$ is replaced by θ). From the above expression we find that the spin-up and spin-down levels with the same quantum number n are separated in the b axis by $4(1/\cos\theta - 1)$, and both of the spin-up and spin-down levels are pulled down by $\tan^2\theta/4$ compared to the case without SOI.

For the RSOI alone case, the local spin orientation for all the spin-up states along the ring is described as

$$\begin{aligned} S(\boldsymbol{r})^R_\uparrow &= \Psi^{R\dagger}_{n,\uparrow} s_x \Psi^R_{n,\uparrow} \mathbf{e}_x + \Psi^{R\dagger}_{n,\uparrow} s_y \Psi^R_{n,\uparrow} \mathbf{e}_y + \Psi^{R\dagger}_{n,\uparrow} s_z \Psi^R_{n,\uparrow} \mathbf{e}_z \\ &= \frac{\hbar}{4\pi a} \left[\sin(-\theta)(\cos\varphi \mathbf{e}_x + \sin\varphi \mathbf{e}_y) + \cos(-\theta)\mathbf{e}_z\right]. \end{aligned} \tag{6.15}$$

The local spin orientation for all the spin-down states $S(\boldsymbol{r})^R_\downarrow$ is opposite to $S(\boldsymbol{r})^R_\uparrow$ as shown in Fig. 33(c) and Fig. 33(d). In this case, the oblique angle $\theta = \arctan(\bar{\alpha})$ becomes independent from the quantum number n and the magnetic field b. It means that the local spin orientations for all the spin-up (spin-down) states are the same. When there is RSOI alone, the local spin orientation exhibits rotational symmetry for either spin-up or spin-down states.

The contributions to the persistent CC and SC from each level can be easily obtained

explicitly:

$$I_{n,\sigma} = -\left(n + \frac{b}{4} + \frac{\sigma}{2} - \frac{\sigma}{2\cos\theta}\right), \tag{6.16a}$$

$$I^{s_z}_{n,\sigma} = \left(n + \frac{b}{4} + \frac{\sigma}{2} - \frac{\sigma}{2\cos\theta}\right)\sigma\cos\theta. \tag{6.16b}$$

$I_{n,\sigma}$ ($I^{s_z}_{n,\sigma}$) denotes the contribution to the persistent CC (SC) from the eigenstate $\Psi_{n,\sigma}$. $I_{n,\sigma}$ ($I^{s_z}_{n,\sigma}$) is in the units of $2E_0/\Phi_0$ ($E_0/2\pi$). We should notice that these expressions deduced from operators coincide with the formula $I_n = -\partial E_n/\partial\Phi$.

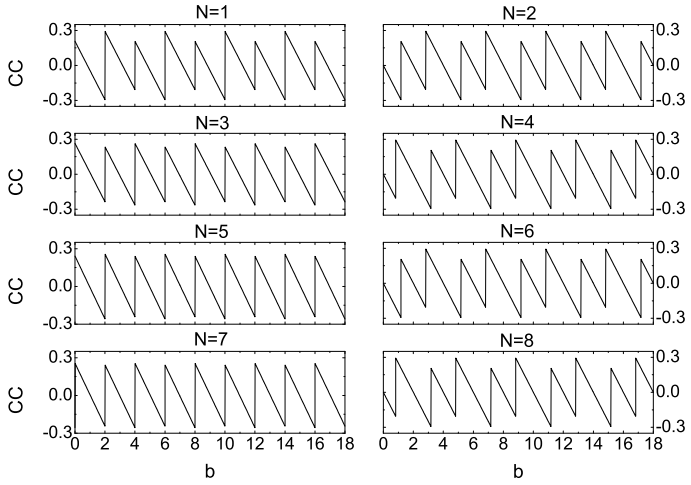

Figure 34: The persistent CC in a 1D ring with different numbers of electrons N *vs* magnetic field b while $\bar{\alpha} = 1$, $\bar{\beta} = 0$, $\bar{g} = 0$. The persistent CC is in units of $2NE_0/\Phi_0$.

Splettstoesser *et al.* analyzed the persistent CC induced by the magnetic flux in the 1D ring with both RSOI and a impurity potential. [16] They demonstrated that the strength of the RSOI can be extracted from the dependence of the persistent CC on the magnetic flux. The number of electrons N in their work was assumed to be large enough. We focus on the case in which there are few electrons in the ring (see Fig. 34). We find that the persistent CC is a periodic function of b exhibiting many linear segments with a slope ratio of $-1/4$ which can be easily deduced from Eq. (6.16a). The periodicity of the persistent CC for an arbitrary N is 4, the same as that of the energy spectrum. For an arbitrary even number of electrons $N = 2\mathbb{m}$, the jumping amplitude is $1/2$ and the neighboring two jumps are shifted along the CC axis. For an odd number of electrons $N = 2\mathbb{m} + 1$, there are two jumping amplitudes which appear alternately at those points where $b = 0, 2, 4, 6, \ldots$ One jumping amplitude is $(\mathbb{m} - 1/\cos\theta + 2)/(2\mathbb{m} + 1)$, while the other is $(\mathbb{m} + 1/\cos\theta - 1)/(2\mathbb{m} + 1)$. When n approaches infinity, the above two amplitudes tend to $1/2$.

The dependence of the persistent SC on the magnetic field b shows interesting behavior. Turning (jumping) points in the persistent SC oscillation for an odd (even) number of electrons are caused by the crossing of levels with opposite (same) spins. When the magnetic field b sweeps, the persistent SC oscillation for an odd (even) number of electrons exhibits saw-tooth (square) wave behavior and the oscillation amplitude of the persistent SC for an even number of electrons is bigger than that for a neighboring odd number of electrons especially when the number of electrons increases. For an odd number of electrons $N = 2\mathbb{m} + 1$, the slope ratios of the persistent SC are $\pm\cos\theta/4(2\mathbb{m} + 1)$ alternately. For an even number of electrons $N = 2\mathbb{m}$, the jumping amplitude is $\cos\theta/2$ for all jumping points.

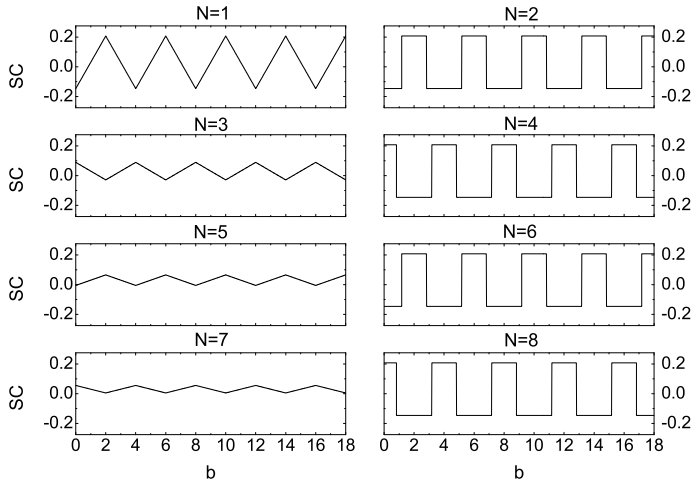

Figure 35: Same as Fig. 34, but for the persistent SC. The persistent SC is in units of $NE_0/2\pi$.

6.4.2 1D ring with DSOI alone

Now we consider a 1D ring with DSOI alone. The eigenstates of the Hamiltonian of a 1D ring with $\bar{\alpha} = a$, $\bar{\beta} = b$, and $\bar{g} = c$ can be connected to those with $\bar{\alpha} = b$, $\bar{\beta} = a$, and $\bar{g} = -c$ by a unitary operator T (see the Appendix). As we will show in the next subsection, T represents a rotational transformation in spin space. b and c are set to be zero and the relationship between the RSOI alone case and DSOI alone case is specified as

$$E^D_{n,\sigma} = E^R_{n,-\sigma}, \tag{6.17a}$$
$$\Psi^D_{n,\uparrow} = \exp[i\pi/4]T\Psi^R_{n,\downarrow}, \tag{6.17b}$$
$$\Psi^D_{n,\downarrow} = \exp[-i\pi/4]T^\dagger\Psi^R_{n,\uparrow}. \tag{6.17c}$$

The energy spectrum while $\bar{\alpha} = 0$, $\bar{\beta} = 1$, and $\bar{g} = 0$ is plotted in Fig. 36(a), which is exactly the same as that of a 1D ring with RSOI alone (see Fig. 33(a)), but the spin orientations of the corresponding eigenstates are different. This feature arises from the sign reversal behavior of σ_z under the unitary transformation T.

Although the eigenstates for the RSOI alone case and those for the DSOI alone case can be connected by the unitary transformation T, the behaviors of $S(\boldsymbol{r})^R_{\uparrow\downarrow}$ and $S(\boldsymbol{r})^D_{\uparrow\downarrow}$ are very different. In the case with DSOI alone, spin-up (spin-down) states with different angular quantum number n or under different magnetic field b share the same local spin orientation $S(\boldsymbol{r})^D_\uparrow$ ($S(\boldsymbol{r})^D_\downarrow$). The angle between $S(\boldsymbol{r})^D_\uparrow$ ($S(\boldsymbol{r})^D_\downarrow$) and the z-axis is $-\theta$ ($\pi - \theta$). The local spin orientations $S(\boldsymbol{r})^D_{\uparrow\downarrow}$ can be obtained by interchanging the x and y components of $S(\boldsymbol{r})^R_{\uparrow\downarrow}$ (see Eqs. (6.15) and (6.18)).

$$\begin{aligned}
&S(\boldsymbol{r})^D_\uparrow \\
&= \Psi^{D\dagger}_{n,\uparrow} s_x \Psi^D_{n,\uparrow}\mathbf{e}_x + \Psi^{D\dagger}_{n,\uparrow} s_y \Psi^D_{n,\uparrow}\mathbf{e}_y + \Psi^{D\dagger}_{n,\uparrow} s_z \Psi^D_{n,\uparrow}\mathbf{e}_z \\
&= \Psi^{R\dagger}_{n,\downarrow} T^\dagger s_x T \Psi^R_{n,\downarrow}\mathbf{e}_x + \Psi^{R\dagger}_{n,\downarrow} T^\dagger s_y T \Psi^R_{n,\downarrow}\mathbf{e}_y \\
&+ \Psi^{R\dagger}_{n,\downarrow} T^\dagger s_z T \Psi^R_{n,\downarrow}\mathbf{e}_z \\
&= -\Psi^{R\dagger}_{n,\downarrow} s_y \Psi^R_{n,\downarrow}\mathbf{e}_x - \Psi^{R\dagger}_{n,\downarrow} s_x \Psi^R_{n,\downarrow}\mathbf{e}_y - \Psi^{R\dagger}_{n,\downarrow} s_z \Psi^R_{n,\downarrow}\mathbf{e}_z \\
&= \Psi^{R\dagger}_{n,\uparrow} s_y \Psi^R_{n,\uparrow}\mathbf{e}_x + \Psi^{R\dagger}_{n,\uparrow} s_x \Psi^R_{n,\uparrow}\mathbf{e}_y + \Psi^{R\dagger}_{n,\uparrow} s_z \Psi^R_{n,\uparrow}\mathbf{e}_z \\
&= \frac{\hbar}{4\pi a}\left[\sin(-\theta)(\sin\varphi\mathbf{e}_x + \cos\varphi\mathbf{e}_y) + \cos(-\theta)\mathbf{e}_z\right].
\end{aligned} \tag{6.18}$$

This interesting feature comes from the behavior of $\sigma_{x(y)}$ under the unitary transformation T, i.e., $T\sigma_{x(y)}T^\dagger = T^\dagger\sigma_{x(y)}T = -\sigma_{y(x)}$. The projections of $S(\boldsymbol{r})^R_\uparrow$ and $S(\boldsymbol{r})^D_\uparrow$ onto the x-y plane are very different (see Fig. 33(b) and Fig. 36(b)). For the RSOI alone case, the vector always points along the radial direction and the locus of the arrowhead is a circle (see Fig. 33(b)). For the DSOI alone case, the vector varies along the ring and the cylindrical symmetry is broken (see Fig. 36(b)).

In the current case, the persistent CC oscillations exhibit the same behavior as those of the RSOI alone case (see Fig. 34) because the corresponding levels are identical as functions of the magnetic field b. We know that the contribution of each level to the persistent SC is related not only to the magnetic field dependence of the eigenenergy but also to the spin orientation of the eigenstate. Since the spin-up and spin-down levels are interchanged compared to those of the RSOI alone case, the persistent SC in the current case can be obtained by changing the sign of the persistent SC for the RSOI alone case.

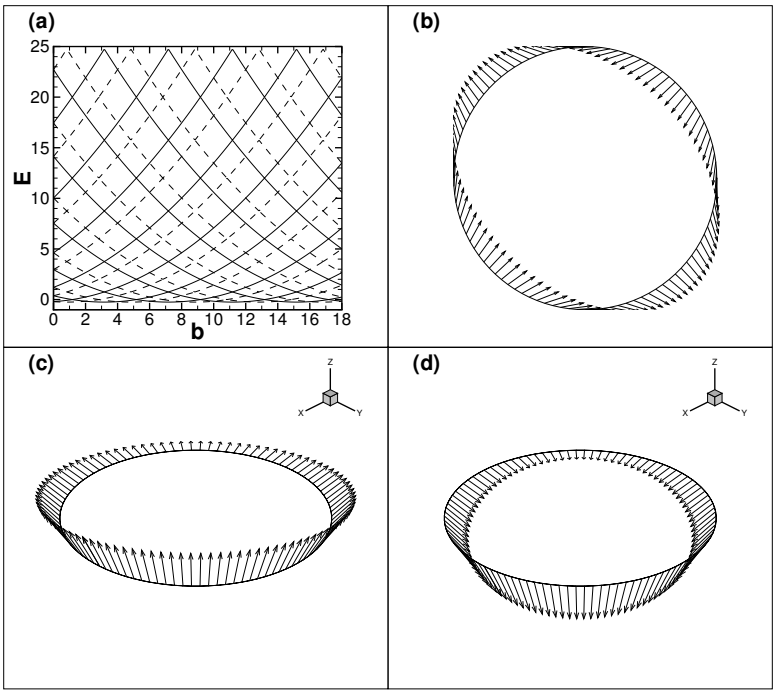

Figure 36: (a) Energy spectrum of 1D ring in the presence of DSOI alone, where the solid lines (dashed lines) denote the spin-up (spin-down) levels; (b) The projection of $S(\boldsymbol{r})^D_\uparrow$ onto the x-y plane; (c) Local spin orientation for all the spin-up levels $S(\boldsymbol{r})^D_\uparrow$; (d) Local spin orientation for all the spin-down levels $S(\boldsymbol{r})^D_\downarrow$. $\bar{\alpha} = 0$, $\bar{\beta} = 1$ and $\bar{g} = 0$.

6.4.3 1D ring with equal strength RSOI and DSOI

The electron energy spectra for $\bar{\alpha} = \bar{\beta} = 1$, $\bar{g} = 0$ and $\bar{\alpha} = \bar{\beta} = 3$, $\bar{g} = 0$ are plotted in Figs. 37(a) and 37(c), respectively. We can see that the energy spectra are spin degenerate. The spin degeneracy comes from the symmetry of the Hamiltonian when $\bar{\alpha} = \bar{\beta}$. In this paper, we use the unitary operator T (see Appendix) to describe the symmetry of the 1D Hamiltonian. When $\bar{\alpha} = \bar{\beta} \neq 0$ and $\bar{g} = 0$, $THT^\dagger = T^\dagger HT = H$. If we have $H\Psi = E\Psi$, in which Ψ is an eigenstate for the eigenenergy E, then the states $T\Psi$ and $T^\dagger\Psi$ are also eigenstates and are equivalent to each other. Thus the energy levels are twofold degenerate. The operator for a φ rotation around the unit vector $\mathbf{n}$ in the Hilbert space reads

$$D(\mathbf{n}, \varphi) = e^{-i\varphi\mathbf{n}\cdot\boldsymbol{L}/\hbar} \otimes e^{-i\varphi\mathbf{n}\cdot\boldsymbol{s}/\hbar}, \tag{6.19}$$

where $\boldsymbol{L}$ and $\boldsymbol{s}$ denote the orbital and spin angular momentum operators, respectively. It is easy to demonstrate that the unitary operator T can be written as $\exp[-i\pi\mathbf{n}_1 \cdot \boldsymbol{s}/\hbar]$ with $\mathbf{n}_1 = (1/\sqrt{2}, -1/\sqrt{2}, 0)$. Then T is actually a rotation operator in the spin space. For a quantum ring in the x-y plane, the orbital angular momentum vector $\boldsymbol{L} = \boldsymbol{r} \times \boldsymbol{p}$ points along the z-axis, and therefore $\mathbf{n}_1 \cdot \boldsymbol{L} = 0$. Thus the unitary operator T is eventually a rotation operator in the whole Hilbert space:

$$T = D(\mathbf{n}_1, \pi). \tag{6.20}$$

That means the unitary transformation T ($T^\dagger$) is actually a rotation by π ($-\pi$) around $\mathbf{n}_1$. Similarly, there are also symmetric operations corresponding to π and $-\pi$ rotations around $\mathbf{n}_2 = (1/\sqrt{2}, 1/\sqrt{2}, 0)$ for the Hamiltonian with $\bar{\alpha} = -\bar{\beta}$. We need to stress that these symmetric operations also exist for a two-dimensional electron gas with equal strength RSOI and DSOI ($\bar{\alpha} = \pm\bar{\beta}$) and $\bar{g} = 0$.

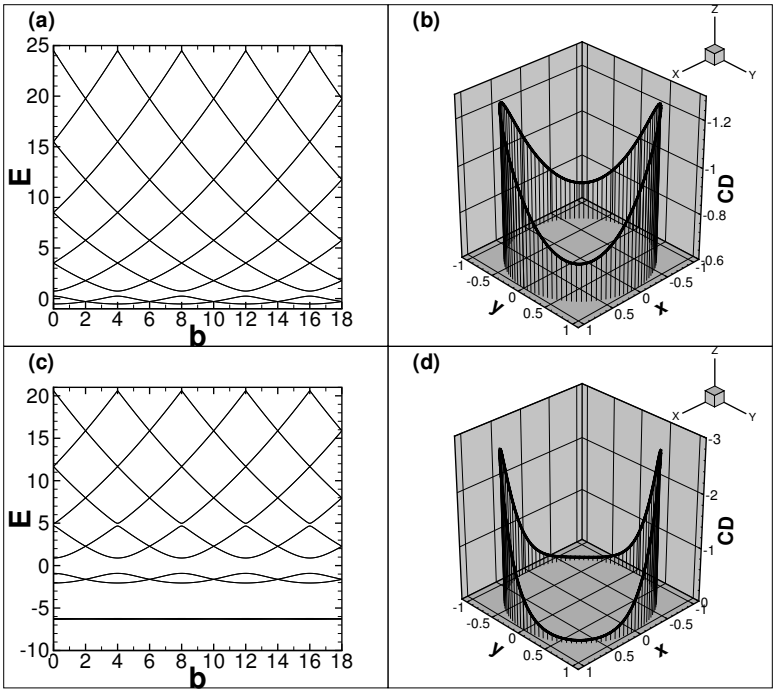

Figure 37: (a) Energy spectrum of 1D ring while $\bar{\alpha} = \bar{\beta} = 1$, $\bar{g} = 0$; (b) The charge density (CD) distribution of the lowest single electron state in a 1D ring while $\bar{\alpha} = \bar{\beta} = 1$, $\bar{g} = 0$, $b = 0$; (c) Energy spectrum of 1D ring while $\bar{\alpha} = \bar{\beta} = 3$, $\bar{g} = 0$; (d) The charge density (CD) distribution of the lowest single electron state in a 1D ring while $\bar{\alpha} = \bar{\beta} = 3$, $\bar{g} = 0$, $b = 0$. The charge density is in units of $e/2\pi a$.

Besides the spin degeneracy, it is interesting to find that gaps appear in the energy spectra. In order to understand this feature, we transform the original Hamiltonian to a simple form via a unitary transformation A as follows:

$$A = \frac{1}{\sqrt{2}} \cdot \begin{bmatrix} \exp[-i\bar{\alpha}f(\varphi)] & \exp[i\bar{\alpha}f(\varphi)] \\ \exp[-i\pi/4]\exp[-i\bar{\alpha}f(\varphi)] & -\exp[-i\pi/4]\exp[i\bar{\alpha}f(\varphi)] \end{bmatrix}, \tag{6.21}$$

with $f(\varphi) = \sin(\varphi + \pi/4)$. The original electron Hamiltonian with $\bar{\alpha} = \bar{\beta}$ and $\bar{g} = 0$ reads

$$H = \left[-i\frac{\partial}{\partial\varphi} + \frac{b}{4} + \frac{\bar{\alpha}}{2}\sigma_r - \frac{\bar{\alpha}}{2}\sigma_\varphi(-\varphi)\right]^2 - \frac{\bar{\alpha}^2}{2} + \frac{\bar{\alpha}^2}{2}\sin 2\varphi. \tag{6.22}$$

After the transformation, the Hamiltonian becomes

$$H' = A^{\dagger} H A = \left(-i\frac{\partial}{\partial\varphi} + \frac{b}{4}\right)^2 - \frac{\bar{\alpha}^2}{2} + \frac{\bar{\alpha}^2}{2}\sin 2\varphi. \tag{6.23}$$

That means the Hamiltonian of a 1D ring with equal strength RSOI and DSOI and zero g factor is equivalent to that of a 1D ring with a periodic potential alone (see the last term in Eq. (6.23)). The potential height is proportional to the square of the SOI strength, and the average of the potential shifts down by about $\bar{\alpha}^2/2$. The eigenvectors of Eq. (6.23) are actually the periodic solutions of the Mathieu equation. [27] The energy gaps, which are proportional to the potential height, decrease with decreasing SOI strengths, especially for higher gaps (see Fig. 37(a)). When the strengths of SOI are fixed, the higher energy gaps are narrower than the lower ones because there is less influence from the potential.

When only one type of SOI (RSOI or DSOI) exists, the charge density distribution will be constant along the ring. But the charge density distribution becomes localized along the ring when both RSOI and DSOI are taken into account. This localization arises from the effective periodic potential, whose height is determined by the product of the strengths of RSOI and DSOI (see Eq. (6.7)). Therefore large SOI strengths lead to strong electron localization. The absolute value of the charge density exhibits maxima at the valleys of the $\sin 2\varphi$ potential ($\varphi = 3\pi/4$ or $\varphi = 7\pi/4$) and minima at the peaks of the $\sin 2\varphi$ potential ($\varphi = \pi/4$ or $\varphi = 5\pi/4$) (see Fig. 37(b) and Fig. 37(d)).

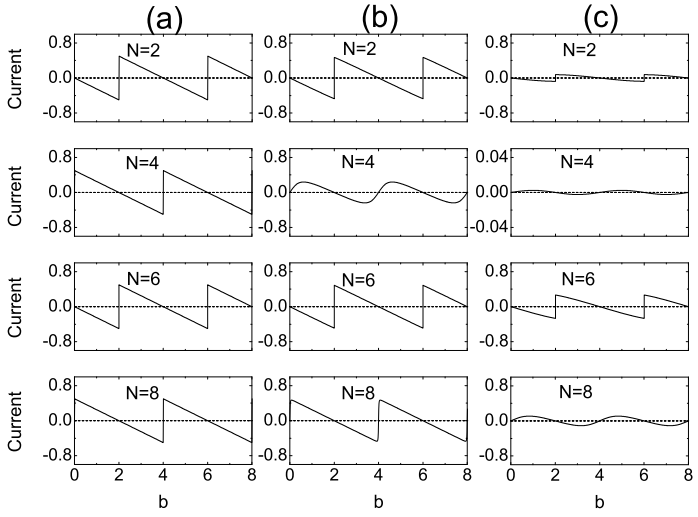

Figure 38: The persistent CC (solid lines) and SC (dashed lines) with different even numbers of electrons N *vs* magnetic field in the degenerate cases (a) $\bar{\alpha} = \bar{\beta} = \bar{g} = 0$; (b) $\bar{\alpha} = \bar{\beta} = 1$, $\bar{g} = 0$; (c) $\bar{\alpha} = \bar{\beta} = 3$, $\bar{g} = 0$. The persistent CC (SC) is in units of $2NE_0/\Phi_0$ ($NE_0/2\pi$).

In the spin degenerate case, we cannot define the local spin orientation $S(\boldsymbol{r})$ for an eigenenergy level and the persistent SC for an odd number of electrons because of the uncertainty of the eigenvectors. The persistent CC oscillation for an odd number of electrons $N = 2\mathrm{n} + 1$ is simply the arithmetic average of that for $N = 2\mathrm{n}$ and that for $N = 2\mathrm{n} + 2$ in a spin degenerate case. Thus we compare the persistent current (CC and SC) oscillations in the three degenerate cases: $\bar{\alpha} = \bar{\beta} = 0$, $\bar{\alpha} = \bar{\beta} = 1$, and $\bar{\alpha} = \bar{\beta} = 3$ only for even numbers of electrons (see Fig. 38). The persistent SC is zero in the two degenerate cases for even numbers of electrons. The $\sin 2\varphi$ potential in Eq. (6.7) accounts for the flatter magnetic dispersion as well as gaps in the energy spectrum when $\bar{\alpha} = \bar{\beta} \neq 0$. Since the contribution to the persistent CC from an energy level

is actually determined by the dependence of the energy level on magnetic field, the oscillation of the persistent CC for the case $\bar{\alpha} = \bar{\beta} \neq 0$ is smoother and smaller than that for the case $\bar{\alpha} = \bar{\beta} = 0$. The interplay between the RSOI and DSOI smoothens and weakens the persistent CC oscillation most obviously when the Fermi level locates near the lowest gap (see the panels labeled $N = 4$ in Fig. 38(b) and Fig. 38(c)). While the number of electrons increases, the oscillation of the persistent CC becomes sharp again since the higher gaps become smaller. This smoothening and weakening effect can even be found again for a large number of electrons when the SOI strengths increase (see Fig. 38(c)).

6.4.4 1D ring with different strength RSOI and DSOI

Generally, the symmetry of the Hamiltonian shown in the previous subsection no longer exists when $|\bar{\alpha}| \neq |\bar{\beta}|$, even for $\bar{g} = 0$. We show the electron spectra for $\bar{\alpha} = 2$, $\bar{\beta} = 1$, $\bar{g} = 0$ and $\bar{\alpha} = 4$, $\bar{\beta} = 3$, $\bar{g} = 0$ in Fig. 39(a) and Fig. 39(c), respectively. The energy gaps increase with increasing SOI strengths. But the spin splitting in the two spectra is quite different. It is interesting to note that the energy spectrum becomes spin degenerate again when the two SOI strengths are tuned to proper values even though they are different. Figs. 39(b) and 39(d) show the distribution of charge density for different strength RSOI and DSOI. The electron is localized along the ring due to the periodic potential $\frac{\bar{\alpha}\bar{\beta}}{2}\sin 2\varphi$. The electron density distribution becomes more localized with increased potential height, i.e., the product of the strengths of RSOI and DSOI (see Eq. (6.7)).

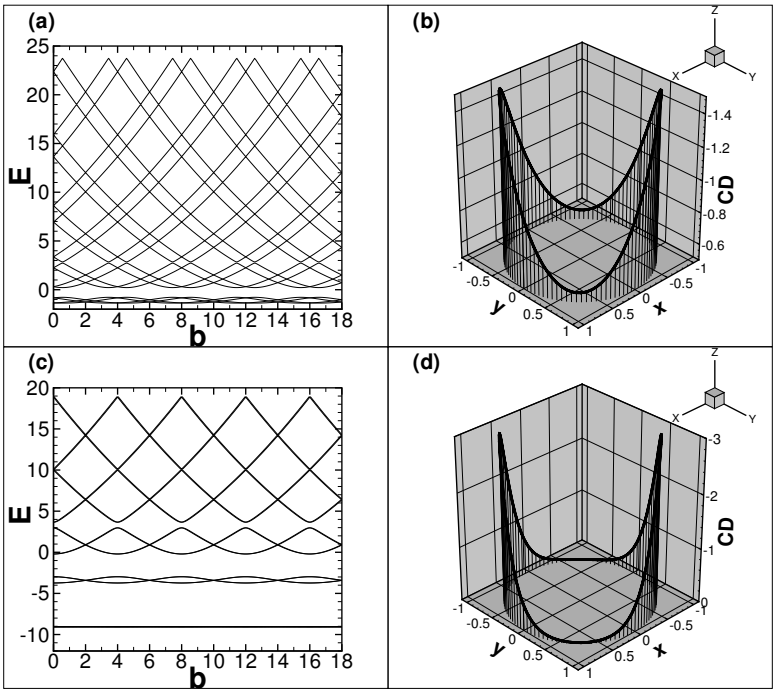

Figure 39: (a) Energy spectrum of 1D ring while $\bar{\alpha} = 2$, $\bar{\beta} = 1$, $\bar{g} = 0$; (b) The charge density (CD) distribution of the lowest single electron state in a 1D ring while $\bar{\alpha} = 2$, $\bar{\beta} = 1$, $\bar{g} = 0$, $b = 0$; (c) Energy spectrum of 1D ring while $\bar{\alpha} = 4$, $\bar{\beta} = 3$, $\bar{g} = 0$; (d) The charge density (CD) distribution of the lowest single electron state in a 1D ring while $\bar{\alpha} = 4$, $\bar{\beta} = 3$, $\bar{g} = 0$, $b = 0$. The charge density is in units of $e/2\pi a$.

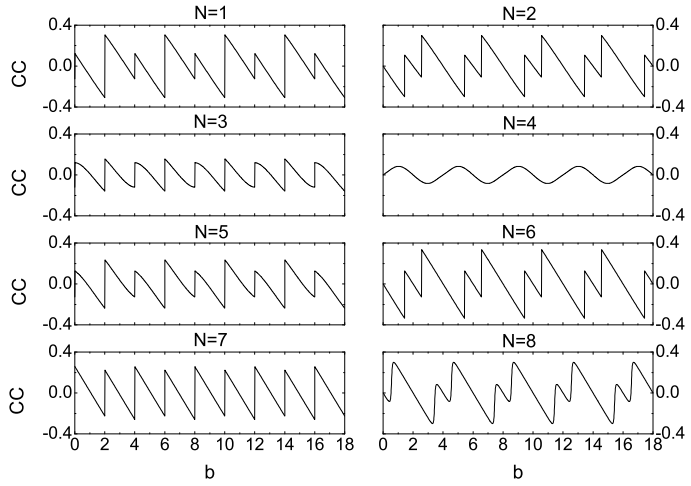

Figure 40: The persistent CC in a 1D ring with different numbers of electrons N *vs* magnetic field b while $\bar{\alpha} = 2$, $\bar{\beta} = 1$, $\bar{g} = 0$. The persistent CC is in units of $2NE_0/\Phi_0$.

The persistent CC and SC are plotted in Fig. 40 and Fig. 41, respectively. We find that the oscillations of the persistent CC and SC become smooth and weak due to the gaps in the energy spectrum, especially when the Fermi level locates near the largest energy gap ($N = 4$). The persistent current (CC or SC) oscillation no longer consists of linear segments since the parabolic behavior of the energy levels disappears due to the periodic potential $\frac{\bar{\alpha}\bar{\beta}}{2}\sin 2\varphi$ in the 1D Hamiltonian (see Eq. (6.7)).

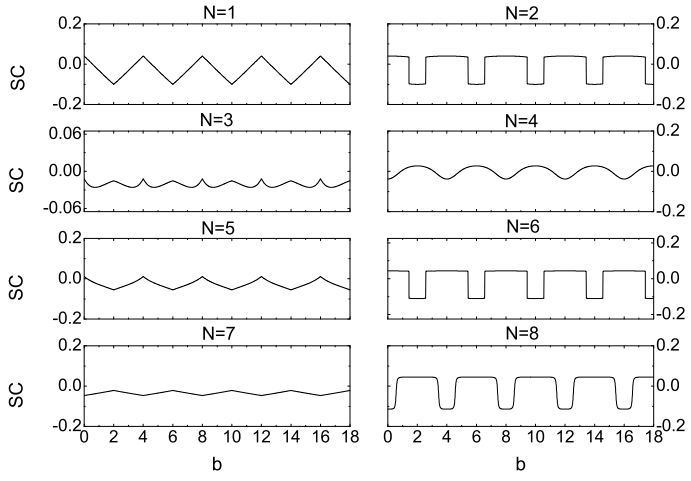

Figure 41: Same as Fig. 40, but for the persistent SC. The persistent SC is in units of $NE_0/2\pi$.

The local spin orientation $S(\boldsymbol{r})$ also reveals the interplay between the RSOI and DSOI since $S(\boldsymbol{r})^R$ is quite different from $S(\boldsymbol{r})^D$. According to Eq. (6.7), the interplay between the RSOI and DSOI is divided into two parts, i.e., $\frac{\bar{\alpha}}{2}\sigma_r - \frac{\bar{\beta}}{2}\sigma_\varphi(-\varphi)$ in the kinetic term and the periodic potential $\frac{\bar{\alpha}\bar{\beta}}{2}\sin 2\varphi$. The first part makes the direction of the local spin orientation vary along the ring, and the second part leads to the electron localization (see Figs. 42(a) and 42(b)). When the SOI strengths increase, the spin orientation exhibits rapid variation due to the enhancement of the interplay between the RSOI and DSOI.

In Fig. 42(c), we plot the persistent SC as a function of RSOI strength $\bar{\alpha}$ and DSOI strength $\bar{\beta}$ for a fixed number of electrons $N = 8$ and magnetic field $b = 2$. The contour plot shows interesting symmetry. It is symmetric (antisymmetric) with respect to the lines $\bar{\alpha} = 0$ and $\bar{\beta} = 0$ ($\bar{\alpha} = \pm\bar{\beta}$). From this figure we find that the maxima and minima of the persistent SC occur while only one of the two types of the SOI exists. That is because the effects of the RSOI and DSOI on spin splitting tend to cancel each other. The persistent SC becomes zero when the strengths of the RSOI and DSOI are equal to each other ($\bar{\alpha} = \pm\bar{\beta}$). This corresponds to the spin degenerate case discussed before. Besides the two orthogonal lines ($\bar{\alpha} = \pm\bar{\beta}$) on the $\bar{\alpha}$-$\bar{\beta}$ plane there are many circle-like closed curves on which the persistent SC disappears. These zero-SC lines intersect the $\bar{\alpha}$ axis at those points $(\pm\sqrt{m^2-1}, 0)$ and the $\bar{\beta}$ axis at $(0, \pm\sqrt{m^2-1})$ where $m = 1, 2, 3, \ldots$. The persistent SC disappears because the energy spectrum becomes degenerate again when the strengths of RSOI and DSOI are tuned to proper values even though they are not equal. The contour plot of the oscillation amplitude of the persistent CC for a fixed number of electrons $N = 8$ is shown in Fig. 42(d). The oscillation amplitude as a function of $\bar{\alpha}$ and $\bar{\beta}$ is symmetric with respect to the lines $\bar{\alpha} = 0$ and $\bar{\beta} = 0$ and $\bar{\alpha} = \pm\bar{\beta}$. When only one type of SOI appears, the maximum of the persistent CC oscillates with increased SOI strength. When both types of SOI are included, the maximum of the persistent CC decays since the interplay between the RSOI and DSOI leads to a periodic potential along the ring which results in the gaps in the energy spectrum, consequently smoothening and weakening the oscillation of the persistent CC.

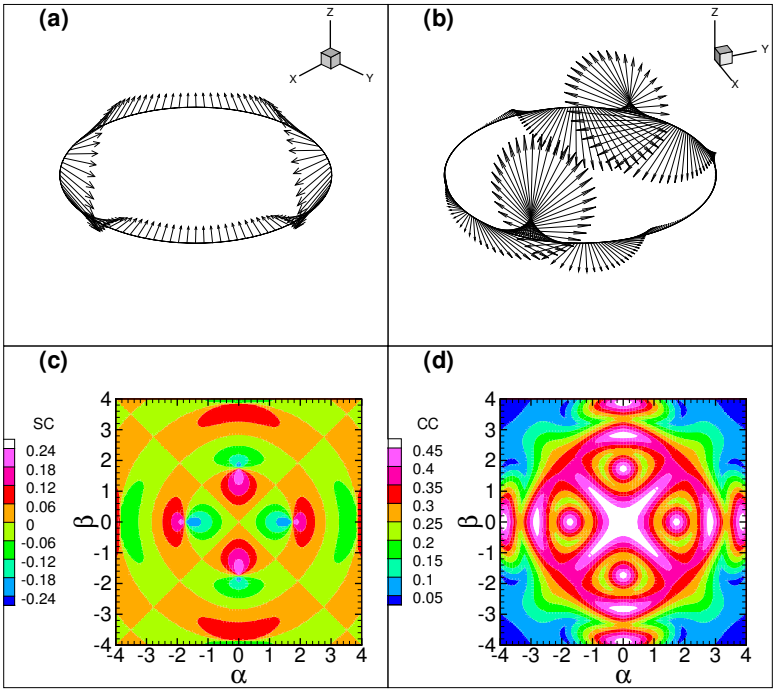

Figure 42: (color online) (a) Local spin orientation $S(\boldsymbol{r})$ for the lowest spin-up level while $\bar{\alpha} = 2$, $\bar{\beta} = 1$, $\bar{g} = 0$, $b = 2$; (b) Local spin orientation $S(\boldsymbol{r})$ for the lowest spin-up level while $\bar{\alpha} = 4$, $\bar{\beta} = 3$, $\bar{g} = 0$, $b = 2$; (c) The persistent SC in a 1D ring with different RSOI and DSOI strengths when the magnetic field b is 2; (d) The oscillation amplitude of the persistent CC in a 1D ring with different RSOI and DSOI strengths. In Fig. 42(c) and Fig. 42(d) we set $\bar{g} = 0$ and $N = 8$. The persistent CC (SC) is in units of $2NE_0/\Phi_0$ ($NE_0/2\pi$).

6.4.5 Finite width effects

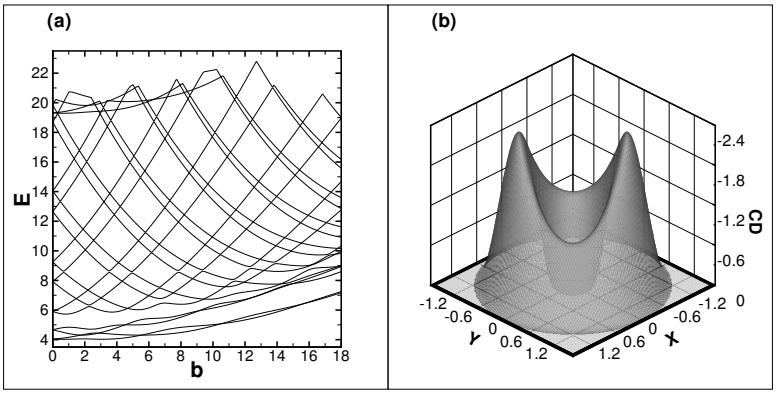

Figure 43: (a) Energy spectrum for 2D hard wall ring with width $d = 1.33$ while $\bar{\alpha} = 2$, $\bar{\beta} = 1$, $\bar{g} = 0$; (b) The charge density (CD) distribution of the lowest single electron state in a 2D hard wall ring with $d = 1.33$ while $\bar{\alpha} = 2$, $\bar{\beta} = 1$, $\bar{g} = 0$, $b = 0$. The charge density is in units of $e/2\pi a^2$.

Now we turn to consider a mesoscopic ring with finite width. When a 2D ring is thin enough, its characteristics are almost the same as those of a 1D ring since the second radial levels are too high to be occupied and the compressing effect of the magnetic field on the radial wave function is negligible. Here we consider the wide ring case.

The energy spectrum for a 2D ring with a finite width while $\bar{\alpha} = 2$, $\bar{\beta} = 1$ and $\bar{g} = 0$ is plotted in Fig. 43(a). The second radial mode can be seen in the top of the energy spectrum. The compressing effect of the magnetic field on the radial wave function accounts for the increase of the energy with increasing magnetic fields. Like the 1D case, the interplay between the RSOI and DSOI leads to an effective periodic potential (see Eq. (6.25)), resulting in energy gaps that depend on the magnetic field. The charge density distribution of a single electron in a 2D ring at $b = 0$ is shown in Fig. 43(b). We find that the electron probability is localized due to the $\sin 2\varphi$ potential arising from the interplay between the RSOI and DSOI.

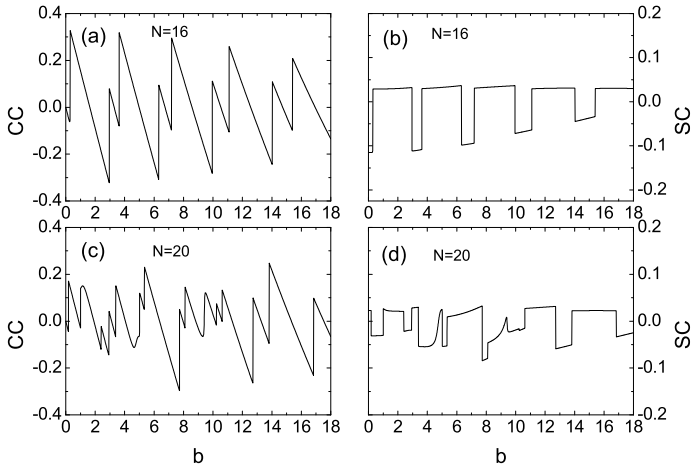

Figure 44: (a) The perisistent CC in a 2D ring *vs* magnetic field b while $\bar{\alpha} = 2$, $\bar{\beta} = 1$, $\bar{g} = 0$, the width $d = 1.33$ and $N = 16$; (b) Same as (a) but for the persistent SC; (c) Same as (a) except $N = 20$; (d) Same as (b) except $N = 20$. The persistent CC (SC) is in units of $2NE_0/\Phi_0$ ($NE_0/2\pi$).

The persistent CC and SC in the 2D wide ring as a function of magnetic field are plotted in Fig. 44. The number of the electrons is tuned to detect the effect of the second radial mode. When we consider the contribution of the lowest 16 levels, the oscillations of the persistent CC and SC have a profile similar to that in the 1D ring because the second radial mode has not been involved yet. But when we increase the number of the electrons to 20, the quasi-periodicity of the persistent CC and SC as functions of the magnetic field b is destroyed. This feature arises from the contribution of the second radial mode.

6.5 The Hamiltonian and available analytical solutions

The dimensionless Hamiltonian for a 2D ring reads

$$H_{2D} = H_k + H_R + H_D + H_Z + V(r), \tag{6.24}$$

where the kinetic term $H_k = (\boldsymbol{e}_r k_r + \boldsymbol{e}_\varphi k_\varphi)^2$, the Rashba term $H_R = \bar{\alpha}(\sigma_r k_\varphi - \sigma_\varphi k_r)$, the Dresselhaus term $H_D = \bar{\beta}[\sigma_r(-\varphi)k_r - \sigma_\varphi(-\varphi)k_\varphi]$, and the Zeeman term $H_Z = \bar{g}b\sigma_z/2$. $V(r)$ is the radial confining potential.

$$\begin{aligned}
H_{2D} = &-\frac{\partial^2}{\partial r^2} - \frac{1}{r}\frac{\partial}{\partial r} + V(r) + k_\varphi^2 + \left[\bar{\alpha}\sigma_r - \bar{\beta}\sigma_\varphi(-\varphi)\right]k_\varphi + \frac{i}{2r}\left[-\bar{\alpha}\sigma_\varphi + \bar{\beta}\sigma_r(-\varphi)\right] + \\
&+ \frac{1}{2}\bar{g}b\sigma_z + \left(k_r - \frac{i}{2r}\right)\left[-\bar{\alpha}\sigma_\varphi + \bar{\beta}\sigma_r(-\varphi)\right] = \\
= &-\frac{\partial^2}{\partial r^2} - \frac{1}{r}\frac{\partial}{\partial r} + V(r) + \left(k_r - \frac{i}{2r}\right)\left[-\bar{\alpha}\sigma_\varphi + \bar{\beta}\sigma_r(-\varphi)\right] + \\
&+ \left[k_\varphi + \frac{\bar{\alpha}}{2}\sigma_r - \frac{\bar{\beta}}{2}\sigma_\varphi(-\varphi)\right]^2 - \left[\frac{\bar{\alpha}}{2}\sigma_r - \frac{\bar{\beta}}{2}\sigma_\varphi(-\varphi)\right]^2 + \frac{1}{2}\bar{g}b\sigma_z = \\
= &-\frac{\partial^2}{\partial r^2} - \frac{1}{r}\frac{\partial}{\partial r} + V(r) + \left(k_r - \frac{i}{2r}\right)\left[-\bar{\alpha}\sigma_\varphi + \bar{\beta}\sigma_r(-\varphi)\right] + \\
&+ \left[k_\varphi + \frac{\bar{\alpha}}{2}\sigma_r - \frac{\bar{\beta}}{2}\sigma_\varphi(-\varphi)\right]^2 - \frac{\bar{\alpha}^2 + \bar{\beta}^2}{4} + \frac{\bar{\alpha}\bar{\beta}}{2}\sin 2\varphi + \frac{1}{2}\bar{g}b\sigma_z.
\end{aligned} \tag{6.25}$$

Specifically we write $H_{2D} = H_0 + H_1$, where $H_0 = -\frac{\partial^2}{\partial r^2} - \frac{1}{r}\frac{\partial}{\partial r} + V(r)$. The correct 1D Hamiltonian H can be obtained by evaluating the expectation of H_1 in the lowest radial mode of H_0. [23] In the limit of a very narrow ring, we can set r to be a constant value ($r = 1$) and the following equation will hold for an arbitrarily given confining potential $V(r)$:

$$\langle\rho_0|\frac{\partial}{\partial r} + \frac{1}{2r}|\rho_0\rangle = 0. \tag{6.26}$$

Here ρ_0 is the lowest radial mode for $V(r)$. Now we can write the 1D Hamiltonian explicitly. We get

$$H = \left[-i\frac{\partial}{\partial\varphi} + \frac{b}{4} + \frac{\bar{\alpha}}{2}\sigma_r - \frac{\bar{\beta}}{2}\sigma_\varphi(-\varphi)\right]^2 - \frac{\bar{\alpha}^2 + \bar{\beta}^2}{4} + \frac{\bar{\alpha}\bar{\beta}}{2}\sin 2\varphi + \frac{1}{2}\bar{g}b\sigma_z. \tag{6.27}$$

A unitary operator $T = \begin{bmatrix} 0 & \exp[-i\pi/4] \\ -\exp[i\pi/4] & 0 \end{bmatrix}$ is defined, and we have $T^\dagger = T^{-1} = -T$. By applying this unitary operator, the Hamiltonian becomes

$$THT^\dagger = \left[-i\frac{\partial}{\partial\varphi} + \frac{b}{4} + \frac{\bar{\beta}}{2}\sigma_r - \frac{\bar{\alpha}}{2}\sigma_\varphi(-\varphi)\right]^2 - \frac{\bar{\alpha}^2 + \bar{\beta}^2}{4} + \frac{\bar{\alpha}\bar{\beta}}{2}\sin 2\varphi - \frac{1}{2}\bar{g}b\sigma_z. \tag{6.28}$$

Thus the Hamiltonian in which $\bar{\alpha} = a$, $\bar{\beta} = b$, $\bar{g} = c$ is mathematically equivalent to that in which $\bar{\alpha} = b$, $\bar{\beta} = a$, $\bar{g} = -c$.

The Hamiltonian in matrix form is

$$\begin{aligned}
H &= \begin{bmatrix} H_{11} & H_{12} \\ H_{21} & H_{22} \end{bmatrix}, \text{ where} \\
H_{11} &= \left(-i\frac{\partial}{\partial\varphi} + \frac{b}{4}\right)^2 + \bar{g}b/2, \\
H_{12} &= \bar{\alpha}e^{-i\varphi}\left(-i\frac{\partial}{\partial\varphi} + \frac{b}{4} - \frac{1}{2}\right) + i\bar{\beta}e^{i\varphi}\left(-i\frac{\partial}{\partial\varphi} + \frac{b}{4} + \frac{1}{2}\right), \\
H_{21} &= \bar{\alpha}e^{i\varphi}\left(-i\frac{\partial}{\partial\varphi} + \frac{b}{4} + \frac{1}{2}\right) - i\bar{\beta}e^{-i\varphi}\left(-i\frac{\partial}{\partial\varphi} + \frac{b}{4} - \frac{1}{2}\right), \\
H_{22} &= \left(-i\frac{\partial}{\partial\varphi} + \frac{b}{4}\right)^2 - \bar{g}b/2.
\end{aligned} \tag{6.29}$$

To solve the equation $H\Psi = E\Psi$, we expand the wavefunction Ψ as $\Psi = \begin{pmatrix} \Psi_1 \\ \Psi_2 \end{pmatrix} = \sum_m \begin{pmatrix} a_m \\ b_m \end{pmatrix} \Theta_m(\varphi)$, where $\Theta_m(\varphi) = \frac{1}{\sqrt{2\pi}} \exp[im\varphi]$. The secular equation becomes

$$\begin{cases} b_{m+1}\bar{\alpha}(m + \frac{b}{4} + \frac{1}{2}) + ib_{m-1}\bar{\beta}(m + \frac{b}{4} - \frac{1}{2}) = \left[E - (m + \frac{b}{4})^2 - \bar{g}b/2\right] a_m \\ a_{m-1}\bar{\alpha}(m + \frac{b}{4} - \frac{1}{2}) - ia_{m+1}\bar{\beta}(m + \frac{b}{4} + \frac{1}{2}) = \left[E - (m + \frac{b}{4})^2 + \bar{g}b/2\right] b_m \end{cases}. \tag{6.30}$$

Generally, we can write the Hamiltonian in an infinite quintuple diagonal matrix form based on Eq. (6.30).

$$\begin{bmatrix}
\ddots & \ddots & 0 & \ddots & 0 & 0 & 0 & 0 \\
\ddots & \left(\frac{b}{4}-1\right)^2 + \frac{\bar{g}b}{2} & 0 & 0 & \bar{\alpha}\left(\frac{b}{4} - \frac{1}{2}\right) & 0 & 0 & 0 \\
0 & 0 & \left(\frac{b}{4}-1\right)^2 - \frac{\bar{g}b}{2} & -i\bar{\beta}\left(\frac{b}{4} - \frac{1}{2}\right) & 0 & 0 & 0 & 0 \\
\ddots & 0 & i\bar{\beta}\left(\frac{b}{4} - \frac{1}{2}\right) & \left(\frac{b}{4}\right)^2 + \frac{\bar{g}b}{2} & 0 & 0 & \bar{\alpha}\left(\frac{b}{4} + \frac{1}{2}\right) & 0 \\
0 & \bar{\alpha}\left(\frac{b}{4} - \frac{1}{2}\right) & 0 & 0 & \left(\frac{b}{4}\right)^2 - \frac{\bar{g}b}{2} & -i\bar{\beta}\left(\frac{b}{4} + \frac{1}{2}\right) & 0 & \ddots \\
0 & 0 & 0 & 0 & i\bar{\beta}\left(\frac{b}{4} + \frac{1}{2}\right) & \left(\frac{b}{4}+1\right)^2 + \frac{\bar{g}b}{2} & 0 & 0 \\
0 & 0 & 0 & \bar{\alpha}\left(\frac{b}{4} + \frac{1}{2}\right) & 0 & 0 & \left(\frac{b}{4}+1\right)^2 - \frac{\bar{g}b}{2} & \ddots \\
0 & 0 & 0 & 0 & \ddots & 0 & \ddots & \ddots
\end{bmatrix}
\begin{bmatrix} \vdots \\ a_{-1} \\ b_{-1} \\ a_0 \\ b_0 \\ a_1 \\ b_1 \\ \vdots \end{bmatrix}
= E
\begin{bmatrix} \vdots \\ a_{-1} \\ b_{-1} \\ a_0 \\ b_0 \\ a_1 \\ b_1 \\ \vdots \end{bmatrix}. \tag{6.31}$$

We consider three different cases. For the first and second cases, in which the quintuple diagonal matrices are reducible, analytical solutions can be obtained.

a) $\bar{\alpha} \neq 0$, $\bar{\beta} = 0$;

$$\begin{bmatrix} (m + b/4)^2 + \bar{g}b/2 & \bar{\alpha}(m + b/4 + 1/2) \\ \bar{\alpha}(m + b/4 + 1/2) & (m + b/4 + 1)^2 - \bar{g}b/2 \end{bmatrix} \begin{bmatrix} a_m \\ b_{m+1} \end{bmatrix} = E \begin{bmatrix} a_m \\ b_{m+1} \end{bmatrix}. \tag{6.32}$$

The eigenvalues are

$$E^R_{n,\sigma} = \left(n + \frac{b}{4} + \frac{\sigma}{2} - \frac{\sigma}{2\cos\theta_{n,\sigma}}\right)^2 - \frac{\tan^2\theta_{n,\sigma}}{4} + \sigma\frac{\bar{g}b}{2\cos\theta_{n,\sigma}}, \tag{6.33}$$

where $\tan\theta_{n,\sigma} = \frac{\bar{\alpha}(n+b/4+\sigma/2)}{n+b/4+\sigma/2-\bar{g}b/2}$. The corresponding eigenvectors are

$$\Psi^R_{n,\uparrow} = \frac{1}{\sqrt{2\pi}} e^{i(n+1/2)\varphi} \begin{pmatrix} \cos\frac{\theta_{n,\uparrow}}{2} e^{-i\varphi/2} \\ -\sin\frac{\theta_{n,\uparrow}}{2} e^{i\varphi/2} \end{pmatrix} \tag{6.34}$$

and

$$\Psi^R_{n,\downarrow} = \frac{1}{\sqrt{2\pi}} e^{i(n-1/2)\varphi} \begin{pmatrix} \sin\frac{\theta_{n,\downarrow}}{2} e^{-i\varphi/2} \\ \cos\frac{\theta_{n,\downarrow}}{2} e^{i\varphi/2} \end{pmatrix}. \tag{6.35}$$

The local spin orientations for eigenstates are

$$S(\boldsymbol{r})^R_{n,\uparrow} = \frac{\hbar}{4\pi a} \left[\sin(-\theta_{n,\uparrow})(\cos\varphi \mathbf{e}_x + \sin\varphi \mathbf{e}_y) + \cos(-\theta_{n,\uparrow})\mathbf{e}_z\right] \tag{6.36}$$

and

$$S(\boldsymbol{r})^R_{n,\downarrow} = \frac{\hbar}{4\pi a} \left[\sin(\pi - \theta_{n,\downarrow})(\cos\varphi \mathbf{e}_x + \sin\varphi \mathbf{e}_y) + \cos(\pi - \theta_{n,\downarrow})\mathbf{e}_z\right]. \tag{6.37}$$

b) $\bar{\alpha} = 0$, $\bar{\beta} \neq 0$;

$$\begin{bmatrix} (m + b/4 + 1)^2 + \bar{g}b/2 & i\bar{\beta}(m + b/4 + 1/2) \\ -i\bar{\beta}(m + b/4 + 1/2) & (m + b/4)^2 - \bar{g}b/2 \end{bmatrix} \begin{bmatrix} a_{m+1} \\ b_m \end{bmatrix} = E \begin{bmatrix} a_{m+1} \\ b_m \end{bmatrix}. \tag{6.38}$$

The eigenvalues are

$$E^D_{n,\sigma} = \left(n + \frac{b}{4} - \frac{\sigma}{2} + \frac{\sigma}{2\cos\eta_{n,\sigma}}\right)^2 - \frac{\tan^2\eta_{n,\sigma}}{4} + \sigma\frac{\bar{g}b}{2\cos\eta_{n,\sigma}}, \tag{6.39}$$

where $\tan\eta_{n,\sigma} = \frac{\bar{\beta}(n+b/4-\sigma/2)}{n+b/4-\sigma/2+\bar{g}b/2}$. The corresponding eigenvectors are

$$\Psi^D_{n,\uparrow} = \frac{1}{\sqrt{2\pi}} e^{i(n-1/2)\varphi} \begin{pmatrix} \cos\frac{\eta_{n,\uparrow}}{2} e^{i\varphi/2} \\ -i\sin\frac{\eta_{n,\uparrow}}{2} e^{-i\varphi/2} \end{pmatrix} \tag{6.40}$$

and

$$\Psi^D_{n,\downarrow} = \frac{1}{\sqrt{2\pi}} e^{i(n+1/2)\varphi} \begin{pmatrix} -i\sin\frac{\eta_{n,\downarrow}}{2} e^{i\varphi/2} \\ \cos\frac{\eta_{n,\downarrow}}{2} e^{-i\varphi/2} \end{pmatrix}. \tag{6.41}$$

The local spin orientations for the eigenstates are

$$S(\boldsymbol{r})^D_{n,\uparrow} = \frac{\hbar}{4\pi a} \left[\sin(-\eta_{n,\uparrow})(\sin\varphi \mathbf{e}_x + \cos\varphi \mathbf{e}_y) + \cos(-\eta_{n,\uparrow})\mathbf{e}_z\right] \tag{6.42}$$

and

$$S(\boldsymbol{r})^D_{n,\downarrow} = \frac{\hbar}{4\pi a} \left[\sin(\pi - \eta_{n,\downarrow})(\sin\varphi \mathbf{e}_x + \cos\varphi \mathbf{e}_y) + \cos(\pi - \eta_{n,\downarrow})\mathbf{e}_z\right]. \tag{6.43}$$

c) $\bar{\alpha} \neq 0$, $\bar{\beta} \neq 0$.

While both RSOI and DSOI have nonvanishing strengths, we cannot reduce the infinite quintuple diagonal matrix shown in Eq. (6.31) into a more compact form. Thus analytical solutions do not exist. We give numerical results instead.

7 Modulating Unpolarized Current in Quantum Spintronics: Visibility of Spin-Interference Effects in Multichannel Aharonov-Casher Mesoscopic Rings

Satofumi Souma and Branislav K. Nikolić

Abstract

The conventional unpolarized current injected into a *quantum-coherent* semiconductor ring attached to two external leads can be modulated from perfect conductor to perfect insulator limit via Rashba spin-orbit (SO) coupling. This requires that ballistic propagation of electrons, whose spin precession is induced by the Aharonov-Casher phase, takes place through a single conducting channel ensuring that electronic quantum state remains a pure separable one in the course of transport. We study the fate of such spin interference effects as more than one orbital conducting channel becomes available for quantum transport. Although the conductance of multichannel rings, in general, does not go all the way to zero at any value of the SO coupling, some degree of current modulation survives. We analyze possible scenarios that can lead to reduced visibility of spin interference effects that are responsible for the zero conductance at particular values of the Rashba interaction: (i) the transmitted spin states remain fully coherent, but conditions for destructive interference are different in different channels; (ii) the transmitted spins end up in partially coherent quantum state arising from entanglement to the environment composed of orbital degrees of freedom of the same particle to which the spin is attached.

7.1 Introduction

Recent attempts in spintronics [1] to harness electron spin for classical and quantum information processing have encountered two major challenges: efficient room temperature spin injection [2] into a semiconductor and quantum-coherent control of spin states. [3] For example, a paradigmatic semiconductor spintronic device, the Datta-Das spin-field-effect transistor [4] where current passing through a two-dimensional electron gas (2DEG) in semiconductor heterostructure is modulated by changing the strength of Rashba SO interaction via gate electrode, [5] requires both problems to be surmounted. The usage of the Rashba SO coupling (which arises due to inversion asymmetry of the confining electric potential for 2DEG) to control spin via electrical means has become one of the most influential concepts in semiconductor spintronics. [2] The injected current can be modulated in this scheme only if it is fully polarized, while precessing spin has to remain quantum coherent during propagation between the two ferromagnetic electrodes. Although spin injection into bulk semiconductors has been demonstrated at low temperatures, [6] creating and detecting spin-polarized currents in high-mobility 2DEG has turned out to be a much more demanding task. In addition, the 2DEG region of spin-FET would be very sensitive to the stray fields induced by the ferromagnetic electrodes. [7]

For devices pushed into the mesoscopic realm, [8, 9] it becomes possible to modulate even unpolarized currents by exploiting spin-dependent quantum interference effects in phase-coherent transport. This is due to the fact that at low temperature $T \ll 1K$ and at nanoscales full electron quantum state $|\Psi\rangle \in \mathcal{H}_o \otimes \mathcal{H}_s$ remains pure in the tensor product of orbital and spin Hilbert spaces, respectively. The conductors in the shape of multiply-connected geometries have been an essential playground since the dawn of mesoscopic physics [8, 10] to explore how quantum interference effects, involving topological quantum phases [11] acquired by a particle moving in the presence of electromagnetic potentials, leave signatures on the measurable transport properties. The typical example is a metallic ring in the magnetic field where transported electron encircling magnetic flux acquires Aharonov-Bohm topological phase which induced conductance oscillations. [10] The electromagnetic duality entails an analogous effect—a neutral magnetic moment going around a charged line acquires Aharonov-Casher (AC) phase that can be manifested in a multitude of ways in mesoscopic transport quantities. [12, 13, 13, 15]

In recently proposed spintronic ring device [16] containing the Rashba SO coupling, the difference between AC phases of opposite spin states traveling clockwise and counterclockwise around the ring generates spin interference effects that can be observed in its transport properties. Since the ring conductance directly depends on this difference, [16, 17] such mesoscopic quantum interference effects can be exploited to modulate conductance of unpolarized charge

transport through a one-dimensional (1D) ring (attached to two 1D leads) between 0 and $2e^2/h$ by changing the Rashba electric field via gate electrode covering the structure. [5] The attractiveness of such *all-electrical* and *all-semiconductor* device comes from the fact that evades usage of any ferromagnetic elements or magnetic fields. However, its envisaged operation necessitates that quantum transport takes place through *only* a single Landauer conducting channel. [9] The theoretical analysis thus far has been confined to strictly 1D rings, [16, 18] or 2D rings where only the lowest transverse propagating mode is open for quantum transport. [17] In both of these cases of single-channel transport similar pattern of complete conductance modulation between 0 and $2e^2/h$ is found, even though higher unoccupied modes in 2D rings can affect the lowest open channel. [19, 20]

On the other hand, despite advances in nanofabrication technology, it is quite challenging to fabricate single channel quantum wires. When unpolarized current, consisting of both spin-$\uparrow$ and spin-$\downarrow$ electrons is injected through more than one propagating modes, defined by the transverse quantization in the leads of a realistic multichannel ring device, each channel will carry its own phase. Moreover, during quantum transport involving more than one conducting channel, any spin-independent scattering of charge (at interfaces or boundaries in the case of a clean system) subjected to SO coupling will lead to a loss of coherence of spin quantum state due to the possibility to entangle spin and orbital degrees of freedom (i.e., within the entangled state, spin subsystem cannot be described by a pure state spinor). [19] The multichannel nature of quantum transport in realistic rings employed in experiments is also part of the controversy surrounding recent fundamental pursuits [11, 22] of the observable effect of spin Berry phase. The analysis of spin-dependent features in conductance oscillations as a function of the magnetic field in disordered rings is not as transparent as in the case of strictly 1D systems. [22] The AC phase acquired by electrons propagating through the 1D ring, subjected to the Rashba electric field orthogonal to the ring plane (Fig. 45), was shown [15] to consist of a dynamical Rashba phase (which depends on the cycle duration) and the geometrical Aharonov-Anandan (AA) phase (which depends only on the path traced in the parameter space) characterizing any nonadiabatic cyclic evolution. [11] In the adiabatic limit, when spin becomes aligned with the effective momentum-dependent Rashba magnetic field $\mathbf{B}_{\rm Rashba}(\mathbf{k})$ in the reference frame of transported electron (Fig. 45), [17] the AA phase becomes the spin-orbit Berry phase introduced in Ref. [13].

Here we address the problem of unpolarized current modulation in clean mesoscopic 2D rings with Rashba SO coupling by studying how the pattern of conductance oscillations changes as one opens conducting channels, one-by-one, for quantum transport. The paper is organized as follows. In Sec. 7.2 we discuss the issue of suitable Hamiltonian description of the ring with SO interactions. Then we introduce a model for the multichannel ring which makes it possible to efficiently implement real$\otimes$spin space Green function technique in order to obtain both the spin and the charge properties of *coupled spin-charge* transport. [19] Section 7.3 studies the conductance modulation in strictly 1D rings as a function of the Fermi energy E_F of the zero-temperature quantum transport. We also establish in this section the connection between the orientation of spin polarization vector and spin precession induced by the Rashba SO interaction, pointing out at spin-switch device properties of the AC rings when injected current is fully polarized. In Sec. 7.4 we discuss conductance modulation in 2D rings with two and three open conducting channels. Although we find that the ring conductance, in general, is not diminished to zero in the multichannel transport at any strength of the SO coupling, it still displays oscillations as we tune the strength of the Rashba interaction. In order to relate such "incomplete" conductance modulation to spin interference effects of states which are not pure (but are instead described by the density matrices), we analyze in Sec. 7.4.2 transport through 2D rings within the picture of transmission eigenchannels. [9] This makes it possible to view the multichannel transport as if occurring through a set of "independent" 1D rings whose channels,

however, can have complicated spin coherence properties. We conclude in Sec. 7.5.

7.2 Hamiltonian models for ring with Rashba Spin-Orbit interaction

In the absence of external magnetic field, the ballistic semiconductor ring structure subjected to the Rashba SO coupling is described by the following effective mass single-particle Hamiltonian

$$\hat{H}_{2D} = \frac{\hat{\mathbf{p}}^2}{2m^*} + \frac{\alpha}{\hbar}\left(\hat{\boldsymbol{\sigma}} \times \hat{\mathbf{p}}\right)_z + V_{\text{conf}}(r), \tag{7.1}$$

where $\hat{\boldsymbol{\sigma}}$ is the vector of the Pauli spin operators, $\hat{\mathbf{p}}$ is the momentum vector in 2D space, and α is the strength of the Rashba SO coupling. The last term $V_{\text{conf}}(r)$ represents the potential which confines electrons to a finite ring region within 2DEG. The analytical expressions for the ring conductance as a function of α have been obtained only for a strictly 1D ring geometry—in this limit one can find the eigenstates of a closed ring and then compute the transmission coefficients by opening the ring to the attached leads where electrons are injected at the Fermi energy equal to the eigenenergies. [16, 17, 18] However, a search for the correct 1D ring Hamiltonian, which includes the Rashba interaction, has turned out to be an ambiguous task yielding several apparent solutions. For example, some of the recent studies have employed non-Hermitian Hamiltonians. [13, 16] It was pointed in Ref. [33] that performing the limit from 2D to 1D carefully, by taking into account the radial wavefunctions in the presence of narrow confinement, leads to a unique Hermitian single-particle Hamiltonian in cylindrical coordinates

$$\hat{H}_{1D}(\phi) = \frac{-\hbar^2}{2m^*R^2}\frac{\partial^2}{\partial\phi^2} - \frac{i\alpha}{R}\left(\cos\phi\sigma_x + \sin\phi\sigma_y\right)\frac{\partial}{\partial\phi} - \frac{i\alpha}{2R}\left(\cos\phi\sigma_y - \sin\phi\sigma_x\right). \tag{7.2}$$

Here R is the radius of the 1D ring, and ϕ is the angular coordinate. The last term in Eq. (7.2), which disappears if we simply take the radial coordinate $r = R$ in the cylindrical coordinate representation of the 2D Hamiltonian, is actually indispensable for this Hamiltonian to be a usual Hermitian operator corresponding to quantum observable.

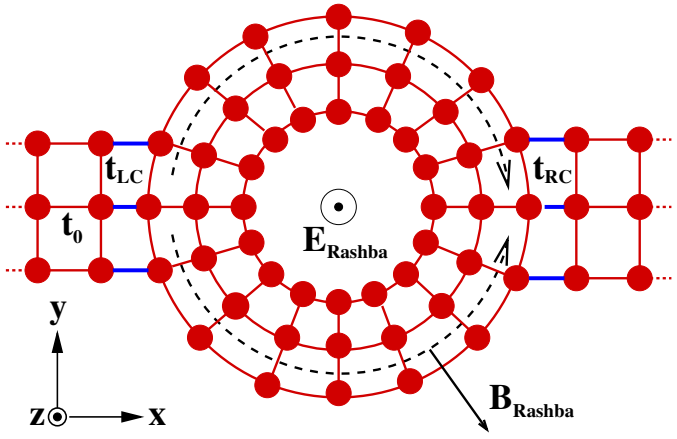

Figure 45: Schematic illustration of the finite-width ring mesoscopic conductor modeled by a concentric tight-binding lattice, where the values of the parameters M and N in the Hamiltonian Eq. (7.4) are chosen to be 3 and 16, respectively. In the actual numerical calculations, we use M =1–3 and N = 200. Here $\mathbf{E}_{\text{Rashba}}$ is the confining electric field for 2DEG (which induces the Rashba SO interaction) and $\mathbf{B}_{\text{Rashba}}$ is the corresponding effective (momentum-dependent) magnetic field in the reference frame of transported spin.

While the 1D Hamiltonian Eq. (7.2) provides a simplest starting point to study quantum transport through the ring within the Landauer-Bütikker transmission formalism, [8] for efficient and *numerically exact* treatment of multichannel transport through finite width 2D rings attached to the leads it is advantageous to switch to a local orbital basis representation that makes is possible to employ real⊗spin space Green function technique and obtain. [19] Therefore, we introduce here a concentric tight-binding lattice Hamiltonian, composed of $M = 1, 2, \ldots$ concentrically connected tight-binding ring chains, as sketched in Fig. 45. The two ideal semi-infinite leads with $\alpha = 0$, of the same width as the ring itself, are attached symmetrically to the ring thereby breaking the rotational invariance of the closed ring problem. The $M = 1$ case corresponding to a single ring chain, which represent a lattice version of the correct 1D Hamiltonian in Eq. (7.2), has frequently been employed to study the Aharonov-Bohm effect in mesoscopic ring-shaped conductors. [24] The $M = 2$ case has appeared in the studies of the influence of finite ring width on the Aharonov-Bohm oscillations of magneto-conductance. [25] Here we introduce the Rashba SO interaction into the concentric tight-binding lattice with arbitrary number M of ring chains. One of the advantages of our model over the conventional square lattice discretization of the finite width rings [26] is that the width of the ring can be controlled precisely by varying the number of the ring chains one-by-one. This makes it possible to study the effects of multichannel transport systematically. The maximum number of open channels in a structure consisting of M ring chains is equal to M. The Hamiltonian corresponding to the set-up depicted in Fig. 45 contains five terms

$$\hat{H} = \hat{H}_{\rm ring} + \hat{H}_{\rm L} + \hat{H}_{\rm R} + \hat{V}_{\rm L,ring} + \hat{V}_{\rm R,ring}. \tag{7.3}$$

The first term, which describes electrons in an isolated (i.e., closed to the environment) ring that are subjected to the Rashba SO coupling, is given by

$$\begin{aligned}\hat{H}_{\rm ring} &= \sum_{n=1}^{N}\sum_{m=1}^{M}\sum_{\sigma=\uparrow,\downarrow}\varepsilon_{nm}\hat{c}^{\dagger}_{nm;\sigma}\hat{c}_{nm;\sigma} - \sum_{n=1}^{N}\sum_{m=1}^{M}\sum_{\sigma,\sigma'=\uparrow,\downarrow}\left[t_{\phi}^{n,n+1,m;\sigma,\sigma'}\hat{c}^{\dagger}_{nm;\sigma}\hat{c}_{n+1,m;\sigma'} + \text{h.c.}\right] \\ &\quad - \sum_{n=1}^{N}\sum_{m=1}^{M-1}\sum_{\sigma,\sigma'=\uparrow,\downarrow}\left[t_{r}^{m,m+1,n;\sigma,\sigma'}\hat{c}^{\dagger}_{nm;\sigma}\hat{c}_{n,m+1;\sigma'} + \text{h.c.}\right].\end{aligned} \tag{7.4}$$

Here $n = 1, 2, \ldots, N$ and $m = 1, 2, \ldots, M$ are the lattice site indices along the azimuthal (ϕ) and the radial (r) directions, respectively. The operator $c_{nm;\sigma}$ ($c^{\dagger}_{nm;\sigma}$) annihilates (creates) a spin σ electron at the site (n, m) of the ring. In our notation $m = 1$ corresponds to the innermost ring chain, while $m = M$ stands for the outermost ring chain to which the external leads are attached. The operator $c_{N+1,m;\sigma}$ ($c^{\dagger}_{N+1,m;\sigma}$) is identified with $c_{1,m;\sigma}$ ($c^{\dagger}_{1,m;\sigma}$) due to the periodic boundary condition. In Eq. (7.3) ε_{nm} is the on-site potential, while $t_{\phi}^{n,n+1,m;\sigma,\sigma'}$ and $t_{r}^{m,m+1,n;\sigma,\sigma'}$ are the nearest neighbor hopping energies along the radial and the angular directions, respectively. Those hopping energies have been generalized to include the SO coupling terms, which are given in the 2×2 matrix form as

$$\begin{aligned}t_{\phi}^{n,n+1,m} &= \frac{1}{(r_m/a)^2\Delta\phi^2}t_0\hat{I}_s - i\frac{t_{\rm so}}{(r_m/a)\Delta\phi}(\cos\phi_{n,n+1}\sigma_x + \sin\phi_{n,n+1}\sigma_y), \\ t_{r}^{m,m+1,n} &= t_0\hat{I}_s + it_{\rm so}(\cos\phi_n\sigma_y - \sin\phi_n\sigma_x).\end{aligned} \tag{7.5}$$

Here $\phi_n \equiv 2\pi(n-1)/N$, $\phi_{n,n+1} \equiv (\phi_n + \phi_{n+1})/2$, $\Delta\phi \equiv 2\pi/N$, $r_m \equiv r_1 + (m-1)a$, $t_0 \equiv \hbar^2/2ma^2$ with a being the lattice spacing constant along the radial direction, $t_{\rm so} \equiv \alpha/2a$ is the tight-binding SO coupling energy with α being the SO coupling strength of the original Hamiltonian Eq. (7.1), and $\hat{I}_s$ is the 2×2identity matrix. We further assume that the lattice spacing along

the azimuthal direction in the outermost ring chain ($m = M$) is the same as that of the radial direction, such that $r_M \Delta\phi (= 2\pi r_M/N) \equiv a$. In order to avoid the negative value of r_1 (the radius of the innermost chain), the value of M has to satisfy the condition $M < N/2\pi + 1$.

In Eq. (7.3), the second term is the Hamiltonian for the left lead

$$\hat{H}_{\rm L} = -t_0 \sum_{i=1}^{\infty} \sum_{j=1}^{M-1} \sum_{\sigma=\uparrow,\downarrow} \left[\hat{b}^{\dagger}_{{\rm L},i,j;\sigma} \hat{b}_{{\rm L},i+1,j,\sigma} + {\rm h.c.} \right], \tag{7.6}$$

where i and j are the lattice indices along the x (current flowing) and the y (transverse) directions, respectively. The operators $b_{{\rm L},i,j,\sigma}$ ($b^{\dagger}_{{\rm L},i,j,\sigma}$) annihilate (create) spin σ electron at the site (i, j) in the left lead. The Hamiltonian of the right lead $\hat{H}_{\rm R}$ has the same form as Eq. (7.6). Finally, the coupling between the leads and ring is described by the following Hamiltonians

$$\hat{V}_{\rm L,ring} = -t_{\rm LC} \sum_{k=1}^{M} \sum_{\sigma=\uparrow,\downarrow} \left[\hat{b}^{\dagger}_{{\rm L},1,k;\sigma} \hat{c}_{k,M;\sigma} + {\rm h.c.} \right], \tag{7.7}$$

$$\hat{V}_{\rm R,ring} = -t_{\rm RC} \sum_{k=1}^{M} \sum_{\sigma=\uparrow,\downarrow} \left[\hat{b}^{\dagger}_{{\rm R},1,k;\sigma} \hat{c}_{\frac{N}{2}+k,M;\sigma} + {\rm h.c.} \right]. \tag{7.8}$$

Here $t_{{\rm L(R)}C}$ is the coupling strength between the left (right) lead and the ring. It is assumed that the left and the right lead are attached to the ring symmetrically, where we neglect the finite curvature of the outermost ring at the interface between the ring and the leads (this is justified if when the condition $N \gg M$ is satisfied).

Once the Hamiltonian Eq. (7.3) is given, one can evaluate the matrix of spin-resolved conductance by using the Landauer-Büttiker's formula generalized to include the spin-degree of freedom

$$\mathbf{G} = \begin{pmatrix} G^{\uparrow\uparrow} & G^{\uparrow\downarrow} \\ G^{\downarrow\uparrow} & G^{\downarrow\downarrow} \end{pmatrix} = \frac{e^2}{h} \sum_{p,p'=1}^{M} \begin{pmatrix} |\mathbf{t}_{p'p,\uparrow\uparrow}|^2 & |\mathbf{t}_{p'p,\uparrow\downarrow}|^2 \\ |\mathbf{t}_{p'p,\downarrow\uparrow}|^2 & |\mathbf{t}_{p'p,\downarrow\downarrow}|^2 \end{pmatrix}, \tag{7.9}$$

where $\mathbf{t}_{p'p,\sigma'\sigma}$ is a transmission matrix element determining the probability amplitude that electron injected in orbital channel $|p\rangle$ with spin σ in the left lead would end up in a conducting channel $|p'\rangle$ of the right lead with spin σ' (the index $p = 1, 2, \ldots$ labels the quantized transverse propagating modes in the leads, while $\sigma = \uparrow, \downarrow$ describes the spin state). The transmission matrix is calculated using the real⊗spin space Green function technique. [19] Note that the spin-quantization axis can be chosen arbitrarily. For example, for the spin-quantization axis chosen along the x-direction, $G^{\downarrow\uparrow}$ can be interpreted as the conductance for a two-probe set-up where the electrodes are half-metallic ferromagnets—magnetization of the left lead is parallel while the magnetization of the right lead is antiparallel to the x-axis. The *total* conductance characterizing conventional unpolarized charge transport

$$G^{\rm tot} = G^{\uparrow\uparrow} + G^{\uparrow\downarrow} + G^{\downarrow\uparrow} + G^{\downarrow\downarrow} \tag{7.10}$$

is independent of the arbitrariliy chosen spin-quantization axis for the calculation of spin-resolved transport properties.

If a quantum system is fully coherent, its state is described by a density matrix $\hat{\rho}^2 = \hat{\rho}$. The decrease of the degree of quantum coherence due to entanglement to environment (*decoherence*) or other dephasing processes (such as classical noise) can be quantified by the purity [27]

$\zeta = \mathrm{Tr}\,\hat{\rho}^2$. Since in the case of the spin-$\frac{1}{2}$ particle $\zeta_s = (1 + |\mathbf{P}|^2)/2$ depends solely on the modulus of the spin-polarization (Bloch) vector $\mathbf{P}$

$$\hat{\rho}_s = \begin{pmatrix} \rho_{\uparrow\uparrow} & \rho_{\uparrow\downarrow} \\ \rho_{\downarrow\uparrow} & \rho_{\downarrow\downarrow} \end{pmatrix} = \frac{\hat{I}_s + \mathbf{P}\cdot\hat{\boldsymbol{\sigma}}}{2}, \tag{7.11}$$

$|\mathbf{P}|$ can be used to measure the degree of coherence retained in spin states in the course of their transport through complicated semiconductor environment. [19]

While the conductance formula Eq. (7.9) requires to evaluate only the amplitude of the complex transmission matrix element $\mathbf{t}_{p'p,\sigma'\sigma}$, the evaluation of the spin-polarization vector $\mathbf{P}$ requires not only the amplitude but also the phase of the transmission matrix elements. Suppose that we inject 100% spin-σ polarized current from the left lead. Then the density matrix of the spin degree of freedom for the outgoing current is given by [19]

$$\hat{\rho}^{\sigma} = \frac{e^2/h}{G^{\uparrow\sigma} + G^{\downarrow\sigma}} \sum_{p,p'=1}^{M} \begin{pmatrix} |\mathbf{t}_{p'p,\uparrow\sigma}|^2 & \mathbf{t}_{p'p,\uparrow\sigma}\mathbf{t}^*_{p'p,\downarrow\sigma} \\ \mathbf{t}_{p'p,\downarrow\sigma}\mathbf{t}^*_{p'p,\uparrow\sigma} & |\mathbf{t}_{p'p,\downarrow\sigma}|^2 \end{pmatrix}. \tag{7.12}$$

The measurement of any observable quantity on the spin subsystem in the right lead is evaluated using such spin density matrix. An example is the *current spin polarization vector*, which is obtained as the expectation value the spin operator $\hat{\boldsymbol{\sigma}}$

$$\mathbf{P}^{\sigma} = \mathrm{Tr}_{\mathrm{s}}\left[\hat{\rho}^{\sigma}\hat{\boldsymbol{\sigma}}\right], \tag{7.13}$$

where Tr_{s} is the trace in the spin Hilbert space. For example, if the injected current is spin-$\uparrow$ polarized along

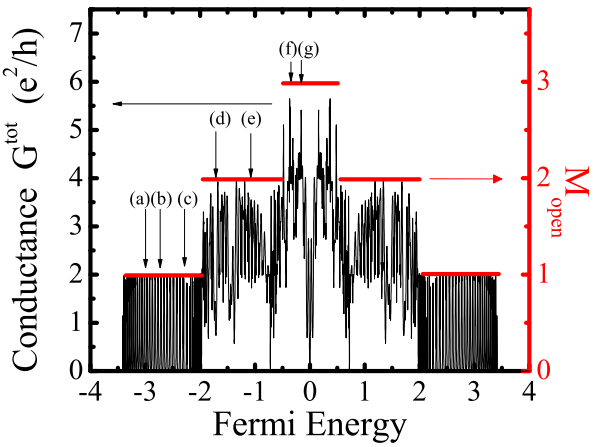

Figure 46: Fermi energy dependence of the total conductance $G^{\mathrm{tot}} = G^{\uparrow\uparrow} + G^{\downarrow\uparrow} + G^{\uparrow\downarrow} + G^{\downarrow\downarrow}$ of a finite width AC ring $(M, N) = (3, 200)$, for a chosen Rashba SO coupling strength $Q_{\mathrm{R}} = 6$ $[Q_{\mathrm{R}} \equiv t_{\mathrm{so}}N/t_0\pi]$. The red line shows the number of open (orbital) conducting channels M_{open} at E_F. The vertical arrows label the values of the Fermi energy selected for Fig. 49 (Sec. 7.3) and Fig. 50 (Sec. 7.4).

the x-direction, the spin polarization vector $\mathbf{P}^{\uparrow} = (P_x^{\uparrow}, P_y^{\uparrow}, P_z^{\uparrow})$ in the right lead is given by

$$P_x^{\uparrow} = \frac{G^{\uparrow\uparrow} - G^{\downarrow\uparrow}}{G^{\uparrow\uparrow} + G^{\downarrow\uparrow}}, \tag{7.14}$$

$$P_y^{\uparrow} = \frac{2e^2/h}{G^{\uparrow\uparrow} + G^{\downarrow\uparrow}} \sum_{p=1}^{M} \mathrm{Re}\left[\mathbf{t}_{p'p,\uparrow\uparrow}\mathbf{t}^{*}_{p'p,\downarrow\uparrow}\right], \tag{7.15}$$

$$P_z^{\uparrow} = \frac{2e^2/h}{G^{\uparrow\uparrow} + G^{\downarrow\uparrow}} \sum_{p'p=1}^{M} \mathrm{Im}\left[\mathbf{t}_{p'p,\uparrow\uparrow}\mathbf{t}^{*}_{p'p,\downarrow\uparrow}\right], \tag{7.16}$$

where $G^{\uparrow\uparrow}$ and $G^{\downarrow\uparrow}$ are the spin conserved and the spin flipped conductance matrix elements. The x-axis is chosen arbitrarily as the spin-quantization axis, $\hat{\sigma}_x = +|\uparrow\rangle$ and $\hat{\sigma}_x = -|\downarrow\rangle$, so that Pauli spin algebra has the following representation

$$\hat{\sigma}_x = \begin{pmatrix} 1 & 0 \\ 0 & -1 \end{pmatrix}, \hat{\sigma}_y = \begin{pmatrix} 0 & 1 \\ 1 & 0 \end{pmatrix}, \hat{\sigma}_z = \begin{pmatrix} 0 & i \\ -i & 0 \end{pmatrix}. \tag{7.17}$$

specifies the particular form of the expectation values of $\mathbf{P}$. One can obtain analogous expressions for (P_x, P_y, P_z) when injected current is polarized along other directions, as well as for the injection of partially polarized current. [19] Thus, studying $\mathbf{P}$, in addition to the ring conductance, will allow us to understand spin orientation and degree of spin coherence that corresponds to modulation of the charge current.

As an example of quantum transport properties of our model Hamiltonian Eq. (7.3), Fig. 46 plots the total conductance of the finite width ring $(M, N) = (3, 200)$ as a function of E_F. The strength of the Rashba SO coupling is fixed at $Q_{\mathrm{R}} = 6$, where we introduce the dimensionless Rashba SO parameter $Q_{\mathrm{R}} \equiv 2m\alpha r_M/\hbar^2 = (t_{\mathrm{so}}/t_0)N/\pi$ with r_M as the radius of the outermost ring. Furthermore, we assume that the system is free from impurities $\varepsilon_{nm} = 0$, and that coupling energies between the conductor and the leads are set to be the same as the hopping energy in the leads $t_{\mathrm{LC}} = t_{\mathrm{RC}} = t_0$. The calculated conductance $G^{\mathrm{tot}}(Q_R = 6, E_F)$ exhibits rapid oscillations with peaks occurring at eigenenergies of the corresponding closed 2D ring. While the conductance oscillates regularly in the single-channel regime, the oscillation pattern in the multichannel regime is rather intricate since the occupation of the higher radial modes gives rise to new conductance peaks in addition to the ones originating from the lowest radial mode.

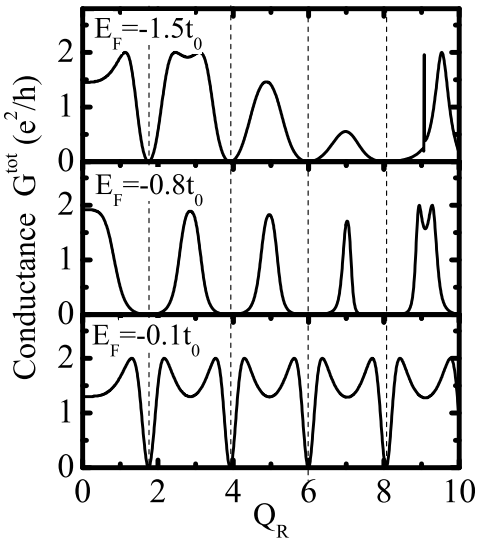

Figure 47: The total conductance $G^{\rm tot}(Q_R, E_F)$ of a strictly 1D ring $(M, N) = (1, 200)$, attached to two 1D semi-infinite ideal leads, as a function of the Rashba SO interaction $Q_{\rm R}$, for three different values of the Fermi energy as a parameter. The vertical dotted lines denote the position of the conductance minima $G^{\rm tot} \simeq 0$, which do not depend on E_F at which the zero-temperature quantum transport takes place.

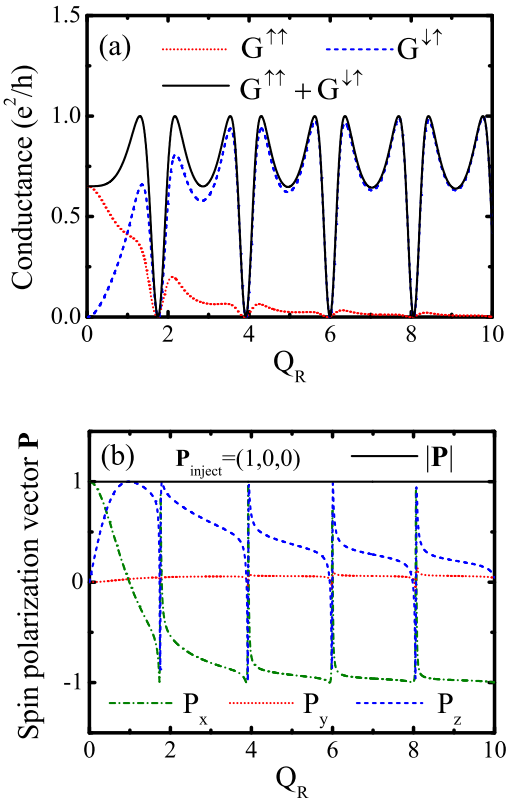

Figure 48: The spin-resolved conductances (a) $G^{\sigma,\sigma'}(Q_R, E_F)$ and the outgoing current spin polarization vector (b) $\mathbf{P}(Q_R, E_F)$ versus the Rashba SO interaction $Q_{\rm R}$ for a strictly 1D ring conductor with $(M, N) = (1, 200)$ and Fermi energy $E_F = -0.1t_0$. The spin-quantization axis is chosen to be the x-axis.

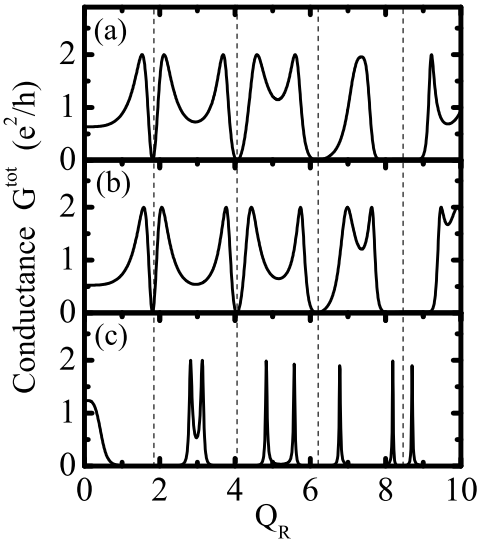

Figure 49: The total conductance $G^{\rm tot}$ vs. the Rashba SO interaction $Q_{\rm R}$ of a finite-width ring conductor with $(M, N) = (3, 200)$ for three different values of the Fermi energy: (a) $E_F = -3.0t_0$, (b) $E_F = -2.7t_0$, and (c) $E_F = -2.2t_0$, which allow only one channel to propagate (see Fig. 46). The vertical dotted lines indicate the minima of the conductance $G^{\rm tot} \simeq 0$, which do not depend on E_F.

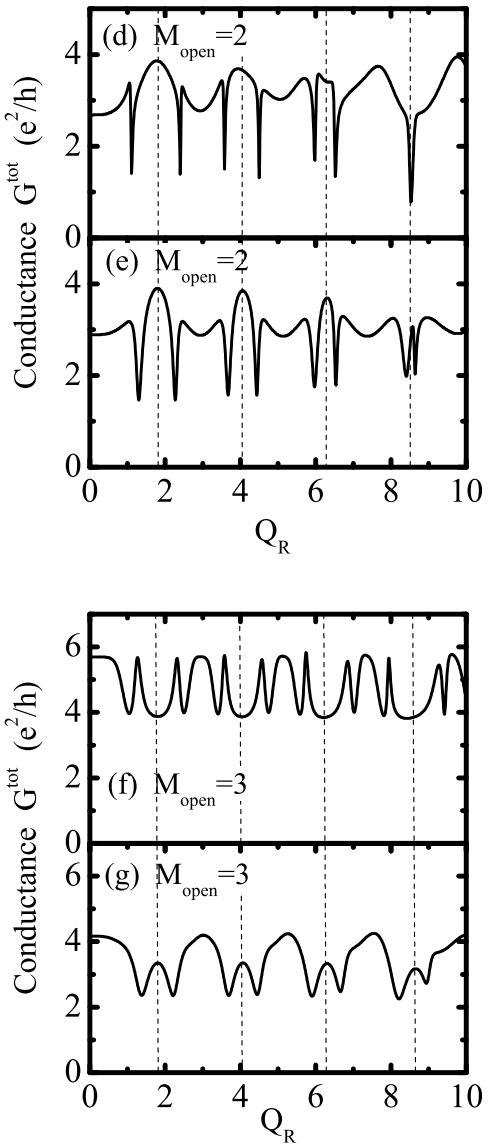

Figure 50: The total conductance $G^{\rm tot}$ vs. the Rashba SO interaction $Q_{\rm R}$ (upper panel) for a finite-width ring conductor $(M, N) = (3, 200)$ at two different values of the Fermi energy: (d) $E_F = -1.8t_0$ and (e) $E_F = -1.0t_0$ at which the number of open conducting channels is $M_{\rm open} = 2$. In the lower panel the selected Fermi energies, (f) $E_F = -0.35t_0$ and (g) $E_F = -0.1t_0$, determine $M_{\rm open} = 3$ (see arrows in Fig. 46).

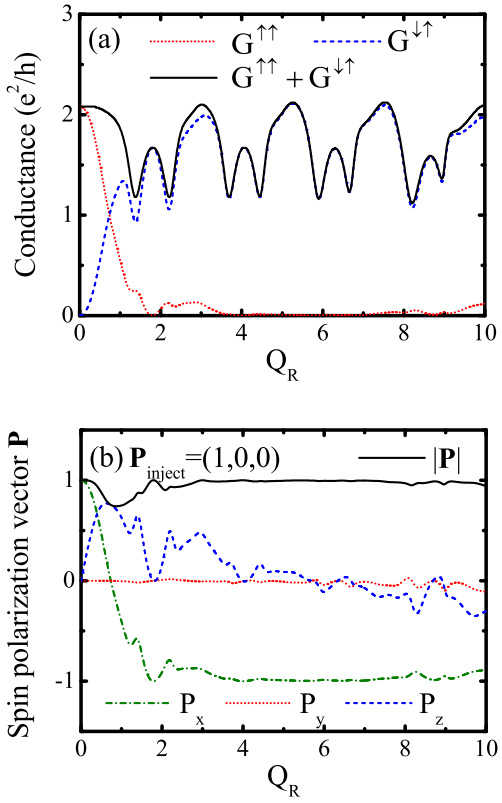

Figure 51: The spin-resolved conductances (a) $G^{\sigma,\sigma'}(Q_R, E_F)$ and the outgoing current spin polarization vector (b) $\mathbf{P}(Q_R, E_F)$ versus the Rashba SO interaction $Q_{\rm R}$ for a strictly 1D ring conductor with $(M, N) = (3, 200)$ and Fermi energy $E_F = -0.1t_0$. The spin-quantization axis is chosen to be the x-axis.

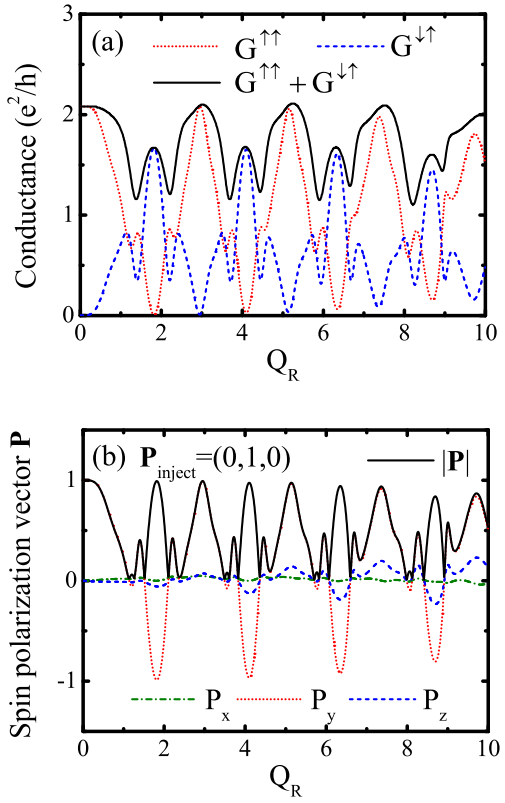

Figure 52: The spin-resolved conductances (a) $G^{\sigma,\sigma'}(Q_R, E_F)$ and the outgoing current spin polarization vector (b) $\mathbf{P}(Q_R, E_F)$ versus the Rashba SO interaction $Q_{\rm R}$ for a strictly 1D ring conductor with $(M, N) = (3, 200)$ and Fermi energy $E_F = -0.1t_0$. The spin-quantization axis is chosen to be the y-axis.

7.3 Spin-interference effects in single-channel quantum transport through AC rings

In this section we study how $G^{\rm tot}$ can be modulated as we change the strength of the Rashba SO coupling Q_R in both strictly 1D rings and single open channel of 2D rings. The transport through phase-coherent 1D rings, described by the correct Hamiltonian [33] Eq. (7.2) has been analyzed recently, [17] in terms of the expressions for $G^{\rm tot}$ of the ring of radius R that does not involve dependence on the Fermi energy

$$G^{\rm tot} = e^2/h \left\{ 1 + \cos\left[\pi \left(\sqrt{Q_\alpha^2 + 1} - 1 \right) \right] \right\}. \tag{7.18}$$

Here $Q_\alpha = 2m\alpha R/\hbar^2$ has the meaning of the spin precession angle over the circumference of 1D ring. However, such simplified expression neglects the back scattering at the interface between the ring and the leads. A more involved treatment that takes into account such effects has been undertaken in Ref. [18]. Nevertheless, no analytical expression has been obtained for single-channel transport in 2D rings.

We confirm [18] in Figure 47 that the exact pattern of zero-temperature $G^{\rm tot}$ versus Rashba SO coupling strength depends on the Fermi energy of transported electrons. This is due to the back scattering effects at the interfaces between the ring and the leads, which can strongly affect the transport. Nevertheless, all of the calculated conductance curves have dips $G^{\rm tot} = 0$ at specific values of Q_R that are spaced quasi-periodically [17] in a way which does not depend on E_F. Thus, the zeros of the conductance in Fig. 47 agree well with those predicted by Eq. (7.18), i.e., their position is insensitive to the lead-ring back scattering effects.

In order to understand the origin of the conductance modulation in more detail, we plot the spin-resolved conductances for a given Fermi energy $E_F = -0.1t_0$ in Fig. 48. Here we consider the conductances corresponding to the injection of current which is fully spin-↑ polarized along the x-axis. As $Q_{\rm R}$ increases, $G^{\uparrow\uparrow}$ decays while the spin-flipped conductance $G^{\downarrow\uparrow}$ increases. That is, at the interface between the ring and the left lead, the injected spin-↑ (along the x-axis) finds itself to be parallel or antiparallel to the effective $\mathbf{k}$-dependent Rashba magnetic field $\mathbf{B}_{\rm Rashba}(\mathbf{k})$ that appears in the frame of electrons circulating along the ring (see Fig. 45). In the presence of large enough Rashba SO coupling, the injected spin-↑ polarized current will change its spin polarization by following the direction of $\mathbf{B}_{\rm Rashba}(\mathbf{k})$ adiabatically. The corresponding outgoing current will appear in the right lead as spin-↓ polarized current. The summation of those two components $G^{\uparrow\uparrow} + G\downarrow\uparrow$ is equal to half of the total conductance $G^{\rm tot}$ plotted in Fig. 47.

The spin polarization vector $\mathbf{P} = (P_x, P_y, P_z)$ of the transmitted current in Fig. 48 further clarifies this insight. We see that with increasing SO coupling, $\mathbf{P}$ in the right lead rotates from $\mathbf{P} = \mathbf{P}_{\rm inject} = (1, 0, 0)$ at $Q_R \to 0$ to the asymptotic value $\mathbf{P} \approx (-1, 0, 0)$ at large Q_R. The functions $P_x(Q_R)$ and $P_z(Q_R)$ are, however, not monotonous since there are abrupt changes of their directions at specific values of Q_R for which $G^{\rm tot}(Q_R) = 0$. Thus, one can also exploit the AC ring in schemes where the spin-polarization of fully polarized injected current is switched to the opposite direction via external electric field applied through a gate electrode covering the ring. [28] For quantum-interference effects, it is important to note that the purity of transported spins $|\mathbf{P}| = 1$ remains one. Therefore, preservation of full quantum coherence ensures complete visibility of the destructive spin-interference effects that give rise to $G^{\rm tot}(Q_R) = 0$.

Furthermore, our framework makes it possible to study single-channel transport through 2D ring, as shown in Figure 49 which plots the $Q_{\rm R}$-dependence of $G^{\rm tot}$ for the finite-width rings $(M, N) = (3, 200)$ and at different Fermi energies selected by the vertical arrows (a)–(c) in Fig. 46. At these values E_F, only one conducting channel is available for quantum transport. We emphasize that the single-channel transport in finite width conductors $M \geq 2$ is not equivalent to the transport in strictly 1D rings [16, 17, 18] since the presence of unoccupied modes (evanescent modes) can influence the transport flowing through the open channel in a way which depends on the confinement potential and the geometry of the conductor. [19, 20] While Fig. 49 shows that the calculated conductance still exhibits zeros at approximately the same values of $Q_{\rm R}$ as in the strictly 1D case, [17] we emphasize that such zeros can be washed out for transport occurring at specific Fermi energies (see also Fig. 53). Also, the conductance oscillation patterns are rather irregular compared with the strictly 1D case, especially in the large $Q_{\rm R}$ regime.

7.4 Visibility of spin-interference effects in multichannel quantum transport through AC rings

7.4.1 Injecting current through spin-polarized conducting channels

In Fig. 50 we show the conductance of the finite width ring $M = 3$ for various Fermi energies which are indicated by vertical arrows (d)–(g) in Fig. 46. More than one transverse propagating mode in the leads exist at these Fermi energies. Therefore, one can view the injected current as being comprised of electrons prepared in all of different quantum state $|p\rangle \otimes |\sigma\rangle$ $(p \leq M)$. For non-magnetic leads, both $|p\rangle \otimes |\uparrow$ and $|p\rangle \otimes |\downarrow$ electrons are injected into the ring. The number of the conducting channels $M_{\rm open} \leq M$ is denoted in the Figure. Although conductance continues to display oscillating behavior as a function of Q_R even in the multichannel transport, its pattern is rather different from the single channel case due to lack of $G_R(Q_R) \simeq 0$ points. Furthermore, the conductance oscillation pattern is significantly more sensitive to the Fermi energy than in the single channel case.

The spin-resolved conductances in Fig. 51 for a given Fermi energy $E_F = -0.1t_0$ (at which $M_{\text{open}} = 3$) provide a more detailed information about such "incomplete" conductance modulation. Here we consider the conductances corresponding to the injection of spin-↑ polarized current. Similarly to the case of strictly 1D ring, the spin-conserved conductance $G^{\uparrow\uparrow}$ decays while the spin-flipped conductance $G^{\downarrow\uparrow}$ increases as increasing Q_{R}. Their sum $G^{\uparrow\uparrow} + G^{\downarrow\uparrow}$ is just half of the total conductance G^{tot} plotted in Fig. 50. Despite the fact that multichannel AC rings are not able to modulate (i.e., $G^{\text{tot}}(Q_R) \neq 0$ at any Q_R) unpolarized current to the extent found in 1D rings (where $G^{\text{tot}}(Q_R) = 0$ at specific values of Q_R), the properties of current spin-polarization vector in Fig. 51 suggest that they can serve as, even better than 1D rings, [28] spin-switch devices. That is, at large Q_R such device flips the spin-↑ of an incoming electron in the left lead into spin-↓ of the outgoing electron in the right lead.

The most prominent distinction between the single and the multichannel cases is that the modulus of the spin polarization $|\mathbf{P}|$ can drop below one—the spin state injected into the multichannel ring loses its purity for $Q_R \neq 0$. This is very contrastive to the single channel transport case where the $|\mathbf{P}| = 1$ is exactly satisfied at any Q_R. Such a reduction of $|\mathbf{P}|$ is attributed to the fact that finite Rashba SO coupling can induce entanglement between the spin state of transported electron and its orbital state, leaving a spin in a mixed quantum state $\hat{\rho}_s^2 \neq \hat{\rho}_s$.

The spin-resolved conductances and spin polarization vector behave rather differently depending on the polarization of the injected spin, as demonstrated by comparing Fig. 51 and Fig. 52, where we change the direction of polarization of injected spin-↑ current to lie along the y-axis. In this case, both the spin conserved conductance $G^{\uparrow\uparrow}$ and the spin flipped conductance $G^{\downarrow\uparrow}$ oscillate and contribute to the total conductance on any interval of Q_{R}. This is because the polarization of injected current in this case is orthogonal to the direction of $\mathbf{B}_{\text{Rashba}}(\mathbf{k})$ field at the interface between the left lead and the ring (see Fig. 45). Thus, the injected spin will be transported through the ring as a superposition of ↑ and ↓ spin states along the radial direction which causes the oscillations of $G^{\downarrow\uparrow}$ and $G^{\uparrow\uparrow}$. When the y-polarized current is injected, P_x and P_z characterizing the spin current are close to zero, while P_y exhibits quasi-periodic oscillation (note that, according to Eq. (7.13) oscillations in P_y are in one-to-one correspondence with oscillations of $G^{\downarrow\uparrow}$ and $G^{\uparrow\uparrow}$). Since $P_x, P_z \simeq 0$, the purity of the transported spin state is approximately given by $|\mathbf{P}| \approx |P_y|$.

7.4.2 Injecting current through eigenchannels

In strictly 1D rings (or transport through a single open channel of a 2D ring) the conductance goes to zero $G^{\text{tot}} = 0$ (or $G^{\text{tot}} \simeq 0$, see Fig. 53 in the regime $M_{\text{open}} = 1$) at specific values of the Rashba SO coupling due to destructive interference effects in coherent superpositions $a|\uparrow\rangle + b|\downarrow\rangle$, as discussed in Sec. 7.3. When current is injected also through higher transverse modes, the analysis of the ring transport properties becomes much more involved. Nevertheless, one can envisage unfolding of three plausible scenarios:

1. The difference in AC phases acquired by spin states is the upper and lower branches of the ring is independent of the wave vector of transverse modes, so that electron remains in a separable quantum state $\left(\sum_{p=1}^{M} c_p|p\rangle\right) \otimes (a|\uparrow\rangle + b|\downarrow\rangle)$ (i.e., the transmission matrix can be decoupled into a tensor product of spin-dependent part and a spatial scattering part [12]); in this case the conditions for destructive interference remain the same as in single-channel quantum transport, [16]

2. The transmitted spins through different channels, each of which has its own orbital phase, pick up different AC phases so that conditions for a destructive interference $G^{\text{tot}} = 0$ cannot be satisfied simultaneously in all channels,

3. The transmitted spins lose their coherence due to coupling to environment, i.e., the off-diagonal elements of the spin density matrix are decaying in the course of transport; [19] if they do not diminish all the way to zero, the transported spin will end up in a *partially coherent* quantum state. [29, 30]

   In both the first and the second scenario, the spin is described by a pure quantum state in the course of transport. Although the second and the third scenario lead to the same observable consequences—the ring conductance never reaches zero since visibility [29] of the spin-interference effects is reduced below one—they are fundamentally different. In the second scenario, spin states remain fully coherent, while in the third one transmitted spins are partially coherent due to coupling to the environment. Even when all other (usually many-body [30]) decoherence mechanisms are suppressed, single spin of an electron can still be entangled to the environment composed of its orbital channels. This mechanism becomes operable in the clean ring when spin-independent charge scattering off boundaries and interfaces occurs in the presence of SO coupling. [19] The partially coherent states, as an outcome of entanglement of spin of transmitted electron with the spin in a quantum dot, were also found in recent experiments on Aharonov-Bohm ring interferometers where quantum dot is embedded in one ring arms. [30]

   Here we explore possibility of the same partially coherent outgoing spin state to appear in the AC ring, where physical mechanism of entanglement is different and single-particle in nature. [19] This makes investigation of ring transport properties in terms of

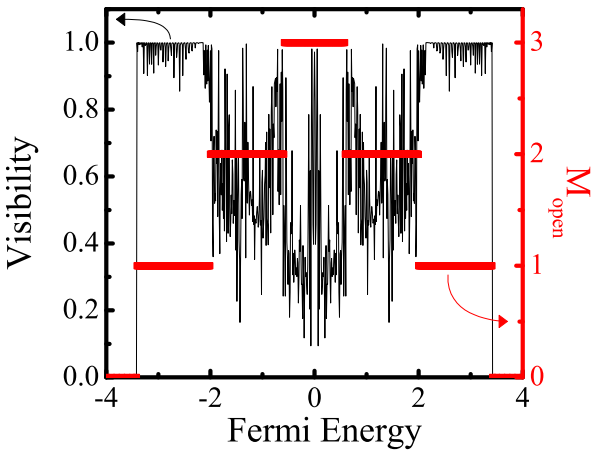

Figure 53: The visibility of spin-interference effects, defined by Eq. (7.19), for a finite width ring conductor $(M, N) = (3, 200)$. The number of the open orbital channels $M_{\rm open}$ is indicated on the right y-axis of the plot.

the AC phases acquired by circulating spins rather difficult since one has to extract geometric phase of an open spin quantum system described by the density matrix rather than by a pure state. [31] It is insightful to define the *visibility* of quantum interference effects in the AC ring

$$\mathcal{V}(E_F) = \frac{G^{\rm tot}_{\rm max}(E_F) - G^{\rm tot}_{\rm min}(E_F)}{G^{\rm tot}_{\rm max}(E_F)}. \tag{7.19}$$

Here $G^{\rm tot}_{\rm max}$ and $G^{\rm tot}_{\rm min}$ are the maximum and the minimum values of the total conductance found in the first period of the conductance oscillations vs. Q_R, for a given Fermi energy and corresponding number of open channels $M_{\rm open} < M$. The visibility $\mathcal{V}(E_F)$ in 2D rings allowing for a maximum of three open channels is plotted in Fig. 53, which shows that $\mathcal{V}(E_F) \approx 1$ in the

single-channel transport regime, i.e., the unpolarized charge transport can be fully modulated by changing the strength of the Rashba SO interaction (except at particular Fermi energies). However, as soon as the second channel starts contributing to the transport, $\mathcal{V}(E_F)$ decreases below one.

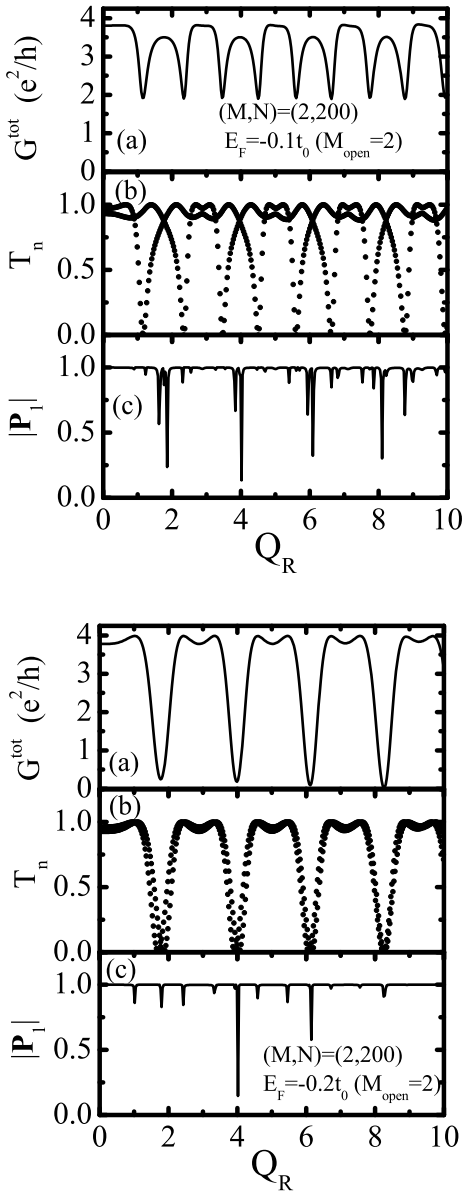

Figure 54: The total conductance (a) $G^{\mathrm{tot}}(Q_R, E_F)$, (b) transmission eigenvalues $T_n(Q_R, E_F)$, and (c) modulus of spin-polarization vector $|\mathbf{P}_1|(Q_R, E_F)$ corresponding to the first eigenchannel of a *two-channel* ring conductor with $(M, N) = (2, 200)$ and at the Fermi energies $E_F = -0.1t_0$ (upper panel) or $E_F = -0.2t_0$ (lower panel). Note that due to Kramers degeneracy (in the presence of SO interaction, but absence of magnetic fields, rings Hamiltonian Eq. (7.2) is time-reversal invariant) there are only two different T_n at each Q_R.

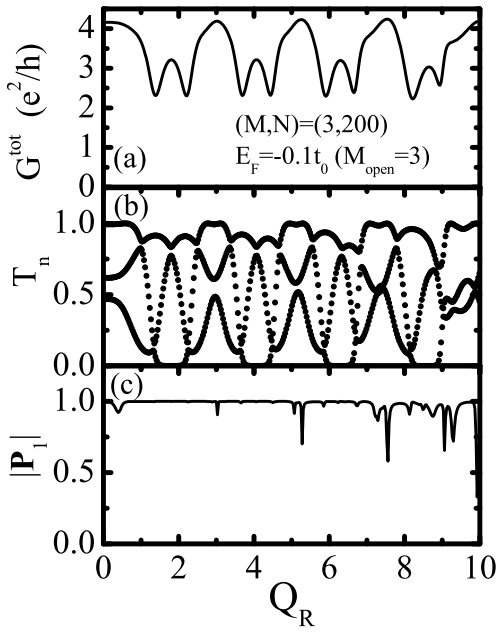

Figure 55: The total conductance (a) $G^{\rm tot}(Q_R, E_F)$, (b) transmission eigenvalues $T_n(Q_R, E_F)$, and (c) modulus of spin-polarization vector $|\mathbf{P}_1|(Q_R, E_F)$ corresponding to the first eigenchannel of a *three-channel* ring conductor $(M, N) = (3, 200)$ and at the Fermi energies $E_F = -0.1t_0$ (upper panel) or $E_F = -0.2t_0$ (lower panel). Due to the Kramers degeneracy there are only three distinctive points plotted at each Q_R.

To investigate which of the above scenarios is realized in the transport through multichannel rings, it is advantageous to invoke as much as possible transparent picture of spin-interference effects in 1D rings. [16, 17, 18] Thus, to be able to consider the transport through multichannel ring as if taking place through a system of independent single-channel rings, we switch to the representation of eigenchannels. In general, the basis of eigenchannels, in which $\mathbf{t}\mathbf{t}^\dagger$ is a diagonal matrix, offers a simple intuitive picture of the transport in a mesoscopic conductor that can be viewed as a parallel circuit of independent channels characterized by channel-dependent transmission probabilities T_n. The computation of T_n as eigenvalues of $\mathbf{t}\mathbf{t}^\dagger$ in the case of conventional unpolarized charge transport allows one to obtain a plethora of transport quantities beyond just the conductance through simple expressions. [9] However, the rotation to the diagonal $\mathbf{t}\mathbf{t}^\dagger$ matrix is inapplicable [19] in spintronics where usually the spin density matrix of injected electrons is non-trivial in the incoming channels of the leads. Nevertheless, when both spin-↑ and spin-↓ are injected into the ring in equal proportion, the basis of eigenchannels allows us to "deconstruct" 2D ring into $M_{\rm open}$ single-channel rings. Moreover, in systems with SO interaction, which are time-reversal invariant in the absence of external magnetic field, due to the Kramers degeneracy all transmission eigenvalues are double degenerate. [9] In the case of single-channel rings of Sec. 7.3 this correspond to both spin-↑ and spin-↓ electrons giving identical contribution to $G^{\rm tot}$. The observable transport properties of a multichannel ring cannot differentiate between injection of unpolarized current through spin-polarized channels defined by the leads as a boundary condition (which were utilized in Sec. 7.4.1) or through the eigenchannels.

The spin properties of eigenstates of $\mathbf{t}\mathbf{t}^\dagger$ can be described by assigning the density matrix to each eigenchannel $|n\rangle = \sum_{p,\sigma} \epsilon^n_{p,\sigma} |p\rangle \otimes |\sigma\rangle$

$$\hat{\rho}^n = \sum_{pp'\sigma\sigma'} \epsilon^n_{p,\sigma} \epsilon^{n*}_{p',\sigma'} |p\rangle\langle p'| \otimes |\sigma\rangle\langle\sigma'|, \tag{7.20}$$

and then taking the partial trace over the orbital degrees of freedom to get the reduced density matrix for the spin subsystem of an eigenchannel

$$\hat{\rho}_s^n = \sum_{p\sigma\sigma'} \epsilon_{p,\sigma}^n \epsilon_{p,\sigma'}^{n*} |\sigma\rangle\langle\sigma'|. \tag{7.21}$$

This allows us to extract the purity $|\mathbf{P}_n|$ of the spin subsystem of an eigenchannel from $\mathbf{P}_n = \mathrm{Tr}\,[\hat{\rho}_s^n \hat{\boldsymbol{\sigma}}]$.

Figure 54 shows the total conductance, the eigenchannel transmissions, and the spin purity $|\mathbf{P}|$ of an eigenchannel of the two-channel $(M, N) = (2, 200)$ ring conductor at two different values of the Fermi energy ensuring that both conducting channels in the leads are open for transport. Here we plot only the spin purity $|\mathbf{P}_1|$ corresponding to the first eigenchannel (spin purity of other eigenchannels display similar behavior). Since the eigenchannel transmissivities are twofold degenerate, one can observer only two different values of T_n at each Q_R in Fig. 54. When $E_F = -0.1t_0$, the total conductance shows incomplete modulation $\mathcal{V} \simeq 0.5$ since the conductance never reaches zero value. It is possible to recognize in Fig. 54 that the eigenchannel transmissions form two distinctive curves as a function of Q_R. Furthermore, each of them exhibits full-modulation characterized by $T_n = 0$ at particular values of Q_R. However, these two oscillating patterns are shifted with respect to each other, thereby preventing total conductance $G^\mathrm{tot}(Q_R) = 2e^2/h\,[T_1(Q_R) + T_2(Q_R)] > 0$ from reaching zero value at any strength of the SO interaction. This can be explained as a realization of the second scenario introduced above. On the other hand, at $E_F = -0.25t_0$ the total conductance shows almost complete modulation $\mathcal{V} \simeq 1$ because: (i) the individual eigenchannel transmissions are akin to the ones found in single-channel rings; and (ii) they almost completely overlap with each other. This case, albeit found rarely in multichannel AC rings, represents quite a good example of the first scenario mechanism. Interestingly enough, $|\mathbf{P}_1|$ drops below one (meaning that an electron is "injected" into the conductor in an entangled state of spin and orbital channels) at those values of Q_R where one would expect destructive interference effects of pure spin states in single-channel rings or system of such independent rings.

Figure 55 plots the same eigenchannel physical quantities for the transport through a three-channel ring $(M, N) = (3, 200)$, where $E_F = -0.1t_0$ is set to allow all three channels to be opened. The total conductance in this case also displays incomplete modulation $\mathcal{V} \simeq 0.3$. However, in this case only one $T_n(Q_R)$ curve can isolated that oscillates between 0 and 1, while the other two never reach zero values. Moreover, these three patterns of $T_n(Q_R)$ are shifted with respect to each other. This observation within the picture of three independent single channels explains why the oscillations of the total conductance end up having a rather small amplitude $G^\mathrm{tot}_\mathrm{max}$ - $G^\mathrm{tot}_\mathrm{max}$.

7.5 Conclusion

In conclusion, we have investigated how the conductance of unpolarized electron transport through two-dimensional rings changes as we increase the strength of the Rashba SO coupling. Moreover, we connect the properties of the charge transport to the orientation of spin of injected electrons as well as its coherence properties. In order to take into account the effect the finite width of the ring and the leads systematically, we model the ring using concentric tight-binding lattice Hamiltonian as the starting point for the calculation of charge and spin transport properties based using the Landauer transmission matrix for a two-probe device.

Our analysis suggests that conductance oscillations, induced by changing the Rashba SO coupling, will persist to some extent even in the multichannel transport through mesoscopic ring-shaped conductors. However, the oscillation patterns are rather different from the single-channel case, or from the anticipated oscillations in multichannel rings where spin-interference

effects would be equivalent in all channels and simply add up. The conductance of single-channel transport through the ring displays full modulation, where $G^{\rm tot}(Q_R) = 0$ appears quasi-periodically as a function of the Rashba SO coupling. This effect is explained in simple terms [16, 17, 18] as a result of destructive spin-interference effects between opposite spin states circulating in the clockwise and counterclockwise direction around the ring, where they acquire Aharonov-Casher phase in the presence of the Rashba electric field. On the other hand, quantum transport in most of the cases occurring in multichannel rings does not lead to zero conductance at any Rashba coupling. Using the picture of quantum transport through independent eigenchannels, we identify different scenarios washing out $G^{\rm tot}(Q_R) = 0$ feature of the single-channel transport, which involve either pure or mixed transported spin states. As the number of conducting channels increases, it becomes more likely to generate partially coherent transported spin (which is described by the density matrix rather than the pure state vector) due to entanglement of electron spin to its orbital degrees of freedom. [19]

8 Electronic charge and spin density distribution in a quantum ring with spin-orbit and Coulomb interactions

Csaba Daday, Andrei Manolescu, D. C. Marinescu, Vidar Gudmundsson.

Abstract

Charge and spin density distributions are studied within a nano-ring structure endowed with Rashba and Dresselhaus spin orbit coupling (SOI). For a small number of interacting electrons, in the presence of an external magnetic field, the energy spectrum of the system is calculated through an exact numerical diagonalization procedure. The eigenstates thus determined are used to estimate the charge and spin densities around the ring. We find that when more than two electrons are considered, the charge-density deformations induced by SOI are dramatically flattened by the Coulomb repulsion, while the spin density ones are amplified.

8.1 Conclusions

We calculated the many-body states of a system of $N = 2, 3$, and 4 interacting electrons located in a ring of finite width with Rashba and Dresselhaus spin-orbit coupling, in the presence of a magnetic field perpendicular on the surface of the ring. The Coulomb effects are fully included in the calculation via the "exact diagonalization" method. We obtained inhomogeneous charge densities, or CDD's, around the ring due to the combined effect of the two types of SOI. When the Coulomb interaction is included the charge deformation is amplified for $N = 2$, as also shown by other authors.[10, 9] For $N > 2$ we find that the CDD is dramatically flattened out in the presence of the Coulomb interaction. We interpret the result as a screening effect. On the contrary, the spin inhomogeneities, or SDD's, are amplified by Coulomb effects for all $N > 1$.

8.2 Introduction

The possibility of controlling the flow of the electron spins in semiconductor structures by external electric means through spin-orbit interaction (SOI) has dominated the recent past of spintronics research. This fundamental principle, first explored in the Datta-Das spin transistor configuration,[1] has been guiding a sustained effort in understanding all the phenomenological

implications of this interactions on systems of electrons. The coupling between spin and orbital motion results either from the two-dimensional confinement (Rashba)[4] or from the inversion asymmetry of the bulk crystal structure (Dresselhaus).[3] The usual expression of the the spin-orbit Hamiltonian H_{SO} retains only the linear terms in the electron momentum $\mathbf{p} = (p_x, p_y)$ and is given by

$$H_{SO} = \frac{\alpha}{\hbar}(\sigma_x p_y - \sigma_y p_x) + \frac{\beta}{\hbar}(\sigma_x p_x - \sigma_y p_y) \ . \tag{8.1}$$

The Rashba and Dresselhaus coupling constants are α and β, respectively, while $\sigma_{x,y,z}$ are the Pauli matrices. In general, the two interactions are simultaneously present and often have comparable strengths. While α, the coupling constant of the Rashba interaction, can be modified by external electric fields induced by external gates, the strength of the Dresselhaus SOI, β, is fixed by the crystal structure and by the thickness of the quasi two-dimensional electron system.[4, 5] In many situations of interest, an additional energy scale is introduced by the Zeeman interaction of the electron spin with an external magnetic field, proportional to the effective gyromagnetic factor, g^*, which depends on the material energy-band structure. While $g^* = -0.44$ is very small in GaAs, it can be more that 100 times larger in InSb.

The interplay between the two types of SOI, which have competing effects on the precession of the electron spin as they rotate it in opposite directions, and the Zeeman splitting, which minimizes the energy by aligning the spin parallel to the external field, determines the ground state polarization of the electron system and the characteristics of spin transport. The investigation of such problems in mesoscopic rings has been pursued intensively by several authors.[6, 7, 8, 9, 10] In particular, it was noticed that, in the absence of the Coulomb interaction among the electrons, the interference between the Rashba and Dresselhaus precessions relative to the orbital motion, leads to the creation of an inhomogeneous spin and charge distribution around the ring.[8] The charge inhomogeneity created in this situation has a symmetric structure with two maxima and two minima around the ring and will be called here a charge-density deformation (CDD). The effect of the Coulomb interaction on this type of charge distribution has been considered for two electrons. It was obtained that, on account of the electrostatic repulsion, the two electrons become even more localized in the potential minima associated to the CDD, leading to an amplitude increase.[10, 9]

In this work we obtain an estimate of the effect of the Coulomb interaction on the charge and spin distribution associated with $N = 2, 3$ and 4 electrons in a ring with SOI coupling by an exact diagonalization procedure that uses the configuration interaction method. Our results indicate that when the number of electrons increases, the mutual repulsion leads to more uniform charge distribution around the ring, generating a dramatically flattened CDD. In contrast, the spin-density deformation (SDD) is amplified by the Coulomb effects. This can be explained by the appearance of a stronger repulsion between same spin electrons, leading to more favorable spin orientations.

8.3 The Ring model

The system of interest in our problem is a two-dimensional quantum ring of exterior and interior radii, R_{ext} and R_{int} respectively. The ring is placed in a perpendicular magnetic field B associated in the symmetric gauge with a vector potential $\mathbf{A} = B/2(-y, x, 0)$. The single-particle Hamiltonian of an electron of momentum $\mathbf{p} = -i\hbar\nabla + e\mathbf{A}$ and effective mass m^* is written as the sum of an orbital term $H_O = \mathbf{p}^2/2m^*$, a Zeeman contribution $H_Z = (1/2)g^*\mu_B B\sigma_z$ and the spin-orbit coupling given in Eq. (8.1). The ensuing expression,

$$H = H_O + H_Z + H_{SO} \ , \tag{8.2}$$

is discretized in a standard manner[6, 7, 11] on a grid[12] defined by N_r radial and N_φ angular sites, as shown in Fig. 56. The radial coordinate of each site is $r_k = R_{ext} - (k-1)\delta r$, with

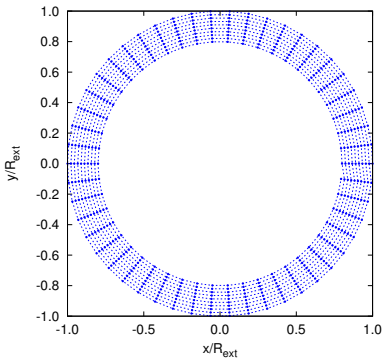

Figure 56: The discretized ring with $R_{int} = 0.8R_{ext}$, and 10 radial $\times$ 50 angular sites. The sites are shown with circular points. The thin dotted lines connection sites are for guiding the eye.

$k = 1, 2, ..., N_r$, while $\delta r = (R_{ext} - R_{int})/(N_r - 1)$ is the distance between adjacent sites with the same angle. Similarly, the angular coordinate is $\varphi_j = (j-1)\delta\varphi$, where $j = 1, 2, ..., N_\varphi$ and $\delta\varphi = 2\pi/N_\varphi$ is the angle between consecutive sites with the same radius. The Hilbert space is spanned by the ket-vectors $|kj\sigma\rangle$, where the first integer, k, stands for the radial coordinate, the second one, j, for the angular coordinate, and $\sigma = \pm 1$ denotes the spin projection in the z direction.

In this basis $\{|kj\sigma\rangle\}$, the matrix elements of the orbital Hamiltonian are given by:

$$\begin{aligned}
&\langle kj\sigma|H_O|k'j'\sigma'\rangle = \\
&T\delta_{\sigma\sigma'}\Bigg\{\left[t_\varphi + t_r + \frac{1}{2}t_B^2\left(\frac{r_k}{4R_{ext}}\right)^2\right]\delta_{kk'}\delta_{jj'} \\
&-\left[t_\varphi + t_B\frac{i}{4\delta\varphi}\right]\delta_{kk'}\delta_{jj'+1} + t_r\delta_{kk'+1}\delta_{jj'}\Bigg\} + h.c.\ .
\end{aligned} \tag{8.3}$$

$T = \hbar^2/(2m^*R_{ext}^2)$ is the energy unit, while R_{ext} is the length unit. In T units, we obtain $t_\varphi = [R_{ext}/(r_k\delta\varphi)]^2$ the angular hopping energy, $t_r = (R_{ext}/\delta r)^2$ the radial hopping energy, and $t_B = \hbar eB/(m^*T)$ the magnetic cyclotron energy. ($h.c.$ denotes the Hermitian conjugate.)

In the same basis, the Zeeman Hamiltonian is simply diagonal in the spatial coordinates,

$$\langle kj\sigma|H_Z|k'j'\sigma'\rangle = \frac{1}{2}Tt_B\gamma(\sigma_z)_{\sigma\sigma'}\delta_{kk'}\delta_{jj'}\ , \tag{8.4}$$

where $\gamma = g^*m^*/(2m_e)$ is the ratio between the Zeeman gap and the cyclotron energy, m_e being the free electron mass.

For the spin-orbit Hamiltonian we obtain:

$$\begin{aligned}
\langle kj\sigma|H_{SO}|k'j'\sigma'\rangle = &\frac{1}{2}Tt_\alpha\Bigg[t_B\frac{r_k}{4R_{ext}}(\sigma_r^j)_{\sigma\sigma'}\delta_{kk'}\delta_{jj'} \\
&+ it_\varphi^{1/2}\ \frac{(\sigma_r^j + \sigma_r^{j+1})_{\sigma\sigma'}}{2}\delta_{kk'}\delta_{jj'+1} - it_r^{1/2}\ (\sigma_\varphi^j)_{\sigma\sigma'}\delta_{kk'+1}\delta_{jj'}\Bigg] \\
&+ Tt_\beta\sum_{k,j}\left[\sigma_r^j \to (\sigma_\varphi^j)^* \text{ and } \sigma_\varphi^j \to -(\sigma_r^j)^*\right] + h.c.\ ,
\end{aligned} \tag{8.5}$$

where $t_\alpha = \alpha/(R_{ext}T)$ and $t_\beta = \beta/(R_{ext}T)$ are the two types of spin-orbit relative energies, while $\sigma_r(\varphi) = \sigma_x\cos\varphi + \sigma_y\sin\varphi$ and $\sigma_\varphi(\varphi) = -\sigma_x\sin\varphi + \sigma_y\cos\varphi$ are the radial and angular Pauli

matrices, respectively. We used the slightly shorter notations $\sigma_r^j = \sigma_r(\varphi_j)$ and $\sigma_\varphi^j = \sigma_\varphi(\varphi_j)$ for the matrices at the particular angles on our lattice. The Rashba spin-orbit terms are all included in the first square bracket. The Dresselhaus terms are very similar to the Rashba ones, being given by the substitutions indicated in the second square bracket.

The single particle states of the noninteracting Hamiltonian (8.2), $H\psi_a = \epsilon_a\psi_a$, are computed as eigenvalues and eigenvectors of the matrices (8.3)-(8.5), $\psi_a(r_k, \varphi_j) = \sum_\sigma \Psi_{a,\sigma}(k,j)|\sigma\rangle$. where $\Psi_{a,\sigma}(k,j)$ are $c-$numbers.

In the basis provided by $\{\psi_a\}$ the *interacting* many-body Hamiltonian is written in the second quantization as

$$\mathcal{H} = \sum_a \epsilon_a c_a^\dagger c_a + \frac{1}{2}\sum_{abcd} V_{abcd} c_a^\dagger c_b^\dagger c_d c_c \,, \tag{8.6}$$

where $c_a^\dagger$ and c_a are the creation and annihilation operators on the single-particle state a. The matrix elements of the Coulomb potential $V(\mathbf{r}-\mathbf{r}') = e^2/(\kappa|\mathbf{r}-\mathbf{r}'|)$, κ being the dielectric constant of the material, are in general give by

$$V_{abcd} = \langle \psi_a(\mathbf{r})\psi_\mathbf{b}(\mathbf{r}')|\mathbf{V}(\mathbf{r}-\mathbf{r}')|\psi_\mathbf{c}(\mathbf{r})\psi_\mathbf{d}(\mathbf{r}')\rangle \ . \tag{8.7}$$

In the present discrete model the double scalar product is in fact a double summation over all the lattice sites and spin labels

$$V_{abcd} = Tt_C \sum_{\substack{kj\sigma \\ k'j'\sigma'}} \Psi^*_{a,\sigma}(kj)\Psi^*_{b,\sigma'}(k'j')\frac{R_{ext}}{|\mathbf{r}_{jk}-\mathbf{r}_{j'k'}|}\Psi_{c,\sigma}(kj)\Psi_{d,\sigma'}(k'j') \ . \tag{8.8}$$

The new energy parameter introduced by the Coulomb repulsion is $t_C = e^2/(\kappa R_{ext}T)$. In the above summation over the sites, the contact terms ($k = k', j = j'$) are avoided, as their contribution vanishes in the continuous limit.

The many-body states Φ_μ are found by solving the eigenvalue problem for the Hamiltonian (8.6),

$$\mathcal{H}\Phi_\mu = E_\mu\Phi_\mu \ .$$

A potential solution of the equation is written in the configuration interaction representation [13, 14, 15] as a linear combination of the non-interacting system eigenstates (Slater determinants),

$$\Phi_\mu = \sum_\alpha c_{\mu\alpha}|\alpha\rangle \ , \tag{8.9}$$

with $\{|\alpha\rangle = |i_1^\alpha, i_2^\alpha, ..., i_K^\alpha\rangle\}$ where $i_a^\alpha = 0, 1$ is the occupation number of the single-particle state ψ_a and K is the number of single-particle states considered. The occupation numbers i_K^α are listed in the increasing energy order, so ϵ_K is the highest energy of the single-particle state included in the many-body basis. For any $|\alpha\rangle$ we have $\sum_a i_a^\alpha = N$, which is the number of electrons in the ring. It is straightforward to derive the matrix elements of $\mathcal{H}_{\alpha\alpha'}$ using the action of the creation and annihilation operators on the many-body basis. In practice Eq. (8.9) is convergent with K for a sufficiently small number of electrons, and sufficiently small ratio of Coulomb to confinement energy, t_C. This procedure, also known as "exact diagonalization", does not rely on any mean field description of the Coulomb effects, like Hartree, Hartree-Fock, or DFT. [16]

To be able to carry the numerical calculations in a reasonable amount of time, we choose a small ring of radii $R_{ext} = 50$ nm and $R_{int} = 0.8R_{ext}$, containing $N \leq 4$ electrons. The discretization grid has 10 radial and 50 angular points (500 sites), as shown in Fig. 56. Two common semiconductor materials used in the experimental spintronics are used for the selection of the material constants needed: InAs with $m^* = 0.023m_e$, $g^* = -14.9$, $\kappa = 14.6$, and

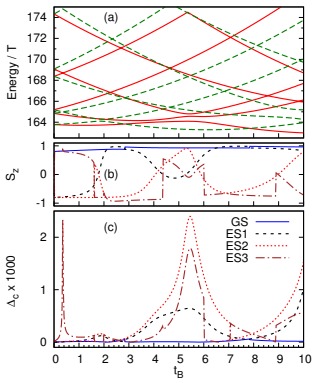

Figure 57: (a) The lowest 12 energies of the single particle states vs. the magnetic energy t_B. The solid (red) and the dashed (green) lines show the states with positive and negative parity, respectively. (b) The expected value of the spin projection along the z direction S_z, in units of $\hbar/2$, for the first four states on the energy scale. (c) The standard deviation Δ_c of the charge distribution around the circle with radial site index $k = 6$, for the first four energy states: ground state (GS), first, second, and third exited states (ES1, ES2, ES3). The same association of line types with states is used in panel (b).

estimated (or possible) values for the spin-orbit interactions $\alpha \approx 20$ and $\beta \approx 3$ meVnm; InSb with $m^* = 0.014m_e, g^* = -51.6, \kappa = 17.9$, and $\alpha \approx 50$, $\beta \approx 30$ meVnm.[4, 5] The relative energies which we defined are: for InAs $t_\alpha = 0.60$, $t_\beta = 0.09$, $t_C = 2.9, \gamma = -0.17$; for InSb $t_\alpha = 0.92$, $t_\beta = 0.55$, $t_C = 1.5, \gamma = -0.36$. In our calculations we have considered material parameters somewhere in between these two sets: $t_\alpha = 0.7$, $t_\beta = 0.3$, $t_C = 2.2, \gamma = -0.2$

8.4 Results

8.4.1 Single particle calculations

In the absence of the SOI, ($\alpha = \beta = 0$), the single particle Hamiltonian (8.2) shares its eigenstates ψ_a with the $\hat{z}$ components of the angular momentum L_z and spin $S_z = \hbar\sigma_z/2$. In the presence of only one type of SOI, either $\alpha \neq 0$ or $\beta \neq 0$, the Hamiltonian commutes with the $\hat{z}$ component of the total angular momentum, $L_z + S_z$, which is conserved. When both $\alpha \neq 0$ and $\beta \neq 0$, the angular momentum is no longer conserved. However, ψ_a continue to be eigenstates of the parity operator $\mathcal{P} = \Pi\sigma_z$, Π being the (three dimensional) spatial inversion operator. Indeed, the general Hamiltonian (8.2) commutes with $\mathcal{P}$, which can be easily verified by using $\Pi\mathbf{p} = -\mathbf{p}\Pi$ and the commutation rules of the Pauli matrices. So in general $\mathcal{P}\psi_a = s\psi_a$, and thus the parity $s = \pm 1$ of any state a is conserved, i. e. it is independent on the magnetic field. In particular, when $\alpha = \beta$ and $g^* = 0$, all states become parity-degenerate at any magnetic field. [8, 10, 17] We identify the parity of the single particle states calculated on our discrete ring model by looking at the relation $\psi_{a,\sigma}(k, j) = s\sigma\psi_{a,\sigma}(k, \bar{j}))$ where (k, j) and $(k, \bar{j})$ are diametrically opposed sites, with angular coordinates $\varphi_{\bar{j}} = \varphi_j + \pi$.

In Fig. 57 we show the single particle states energy for $0 < t_B < 10$ (units of T), which corresponds to a magnetic field strength between 0 and 1.32 Tesla. Further increment of the magnetic field requires an augmentation of the number of sites on the ring in order to maintain the discrete model as a reasonable approximation of a physically continuous ring. At zero magnetic field all states are parity degenerate, which is just the ordinary spin degeneracy. The degeneracy is in general lifted by a finite magnetic field. There are, however, some particular values of t_B where the degeneracy persist. This situation is represented in Fig. 57(a) by all intersection points of two lines corresponding to the two possible parities. Such intersections do not occur between states with the same parity. Due to the spin-orbit coupling, the orbital

momentum of one state depends on the spin of the other state and vice versa, and, consequently, states of same parity do in fact interact and thus avoid intersections.[10] Although in Fig. 57(a) many states represented by the same line type apparently cross each other, in reality there are always tiny gaps between them, similar to those visible at $t_B \approx 2$ between the first and the second excited states or at $t_B \approx 5.5$ between the first, second, and third excited states. The magnitude of these gaps depends on the $g-$factor, reducing in size for a smaller g^* parameter.

In Fig. 57(b) the evolution of the expected spin in the z direction, $S_z = \hbar\langle\psi_a|\sigma_z|\psi_a\rangle/2$ is presented for the first four states in the energy order. One can see how the spin flips for states avoiding the crossing, like those with negative parity at $t_B \approx 2$ (dashed and dotted lines in Fig. 57(b)).

Only one type of SOI, either Rashba or Dresselhaus, is sufficient to avoid the crossing of states with the same parity, but in this case the charge and the spin densities are uniform around the ring. When *both* SOI types are present the charge and spin densities become nonuniform. This situation is equivalent with the presence of a potential with two maxima and two minima around the ring, having reflection symmetry relative to the axes $y = x$ (or $\varphi = \pi/4$, corresponding to the crystal direction [110]) and $y = -x$ (or $\varphi = -\pi/4$, corresponding to the crystal direction $[1\bar{1}0]$).[8, 10] The amplitude of the CDD is illustrated in Fig. 57(c) where the standard deviation (in the statistical sense) Δ_c of the charge density calculated around one circle on the ring, close to the mean radius, with radial site index $k = 6$, is plotted for the lowest four energy states. The density deformation occurs on account of the two combined SOI types which lead to spin interference and additional interaction between states with the same parity. Consequently, the amplitude of the CDD for a certain state is maximum at those magnetic fields where the parity degeneracy is lifted (the state avoids a crossing with another state of the same parity). In Fig. 57(c) this is clearly seen at $t_B \approx 2$, for the excited state. In this example the CDD in the ground state is very weak. The sharp peak at $t_B \approx 0.4$ indicates the existence of a narrow gap between the 4-th and 5-th energy states that avoid crossing.

8.4.2 Many particle calculations

In the following considerations, we will include more than one electron. In Fig. 58 we compare the energy spectra for the first 12 states vs. the magnetic energy for $N = 2, 3$, and 4 electrons, without and with Coulomb interaction. Since the Coulomb interaction is invariant at spatial inversion (and independent on spin) the parity s is also conserved in the many-body states. Spectra drawn for $t_C = 0$ and $t_C = 2.2$ have similar features. The interacting spectrum presents a shift to higher energies, on account of the additional Coulomb energy, and a slight increase of the gaps at high magnetic fields. Moreover, the crossings and the anti-crossings (points where the crossings were avoided) of the energy levels have a tendency to shift slightly to higher magnetic fields. Similarly, the gap between the ground state and the excited states increases at high t_B.

The total spin S_z for each of the first three energy states is shown in Fig. 59. At zero magnetic field, for an even number of electrons, here $N = 2$ or $N = 4$, the ground state is non-degenerate and has total spin $S_z = 0$, i. e. the spin-up and spin-down states of individual electrons compensate. When the field is applied, the first spin flip in the interacting ground state, as well as the spin saturation, occur at lower magnetic fields than in the absence of the Coulomb repulsion. This is a result of the mixing of spin states with the same parity produced by the interaction. For $N = 3$ the ground state is spin (double) degenerate at zero field. In the presence of the Coulomb interaction, the total spin in the ground state and the higher state is reversed.

Similar to the case of one electron ($N = 1$, Fig. 57), the charge deformation of each state is maximized for those magnetic fields where the state has an anti-crossing (or repulsion) with

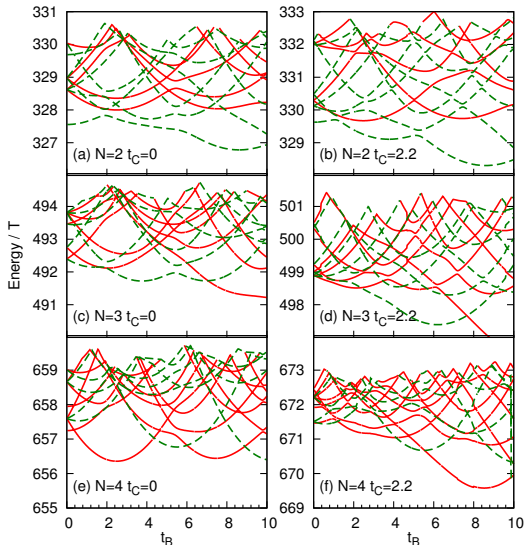

Figure 58: Energy spectra of the first 12 states for $N = 2, 3$, and 4 electrons without Coulomb interaction, $t_C = 0$ in panels (a),(c),(e), and with Coulomb interaction, $t_C = 2.2$, in panels (b),(d),(f). The solid (red) and the dashed (green) lines show the states with positive and negative parity, respectively.

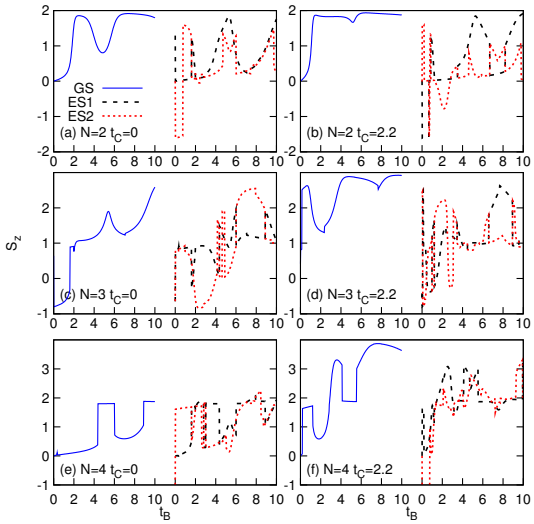

Figure 59: The total spin projection in the z direction, in units of $\hbar/2$, for the many body states with $N = 2, 3, 4$ electrons. Without interaction, i. e. $t_C = 0$ in panels (a),(c),(e), and with interaction, with $t_C = 2.2$, in panels (b),(d),(f). Only the first three states are shown here, the ground state (GS), the 1-st excited states (ES1), and the 2-nd excited state (ES2). The magnetic energy t_B varies between 0 and 10 and the lines showing the excited states are shifted to the right, for clarity.

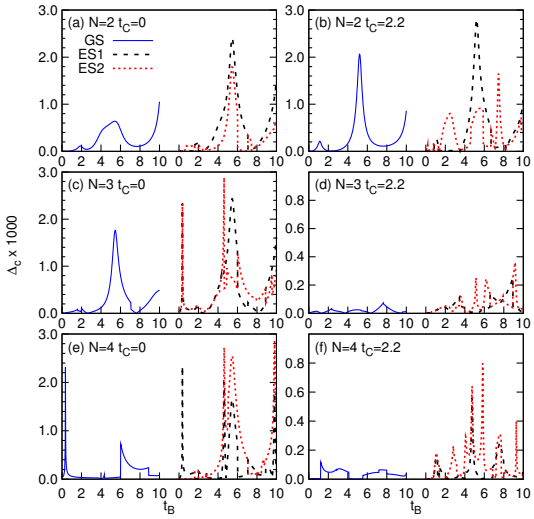

Figure 60: The standard deviation Δ_c of the charge on the circle $k = 6$ around the ring, as a measure of the amplitude of the charge deformation. Shown are the results for the ground state (GS), the 1-st excited states (ES1), and the 2-nd excited state (ES2), for $N = 2, 3, 4$ electrons without without ($t_C = 0$), and with interaction ($t_C = 2.2$). The amplitude of the CDD's is strongly reduced by the Coulomb effects for $N = 3, 4$; notice the different scales used in the paired panels (c),(d) and (e),(f). The magnetic energy t_B varies between 0 and 10 and the lines corresponding to the excited states are shifted to the right, for clarity.

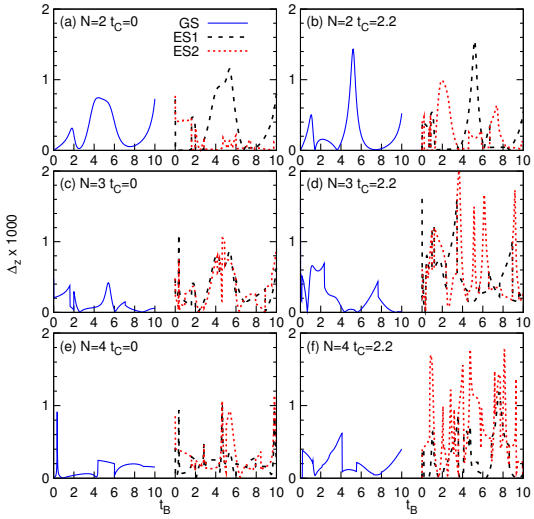

Figure 61: The standard deviation Δ_z of the spin projection along the z direction on the circle $k = 6$ around the ring, as a measure of the amplitude of the spin-density wave. Like in the previous figures GS, ES1, and ES2 in the legend indicate the ground state, the 1-st excited states, and the 2-nd excited states, respectively. The results are shown for $N = 2, 3, 4$ electrons without ($t_C = 0$), and with interaction ($t_C = 2.2$). Unlike the CDD's, the SDD's are amplified by the Coulomb interactions for all N. The magnetic energy t_B varies between 0 and 10 and the lines corresponding to the excited states are shifted to the right, for clarity.

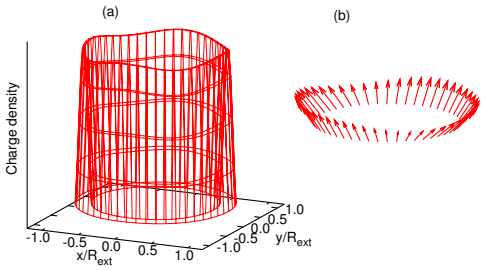

Figure 62: (a) The charge density for $N = 4$ electrons with interaction ($t_C = 2.2$), in the second excited state, i. e. ES2 in Fig.60(f), with magnetic energy energy $t_B = 4.5$. (b) The corresponding total spin distribution along the ring $k = 6$ where the standard deviation of the z component is calculated and shown in Fig.61(f).

another state of the same parity. The charge deformation parameter Δ_c is shown in Fig. 60. For $N = 2$ the amplitude of the CDD increases with the Coulomb interaction. There is a simple reason for that: the potential associated with the charge deformation has two minima diametrically opposite on the ring and each of the two electrons tends be localized in one of these minima. The mutual Coulomb repulsion fixes the electrons in those places better.[10, 9] The situation changes, however, for $N > 2$. The Coulomb forces spread the electrons differently, more or less uniformly, such that the charge deformation created by the SOI is drastically reduced. In other words, the associated potential is strongly screened even by one extra electron above $N = 2$. This effect can be clearly seen in Fig. 60, comparing panels (c) with (d) and (e) with (f). The vertical scale of panels (d) and (e) has been magnified three times, for visibility.

In principle, the screening of the charge deformation is not particularly related to the spin-orbit effects. SOI only generates the specific effective potential which determines the CDD. In the absence of SOI ($\alpha = \beta = 0$), we checked that a similar screening effect occurs in the presence of a potential that induces a charge deformation comparable to that obtained with the SOI. It is, however, surprising that by adding only one extra electron such a drastic effect ensues.

Next, we investigate the effect of the Coulomb interaction on the spin distribution around the ring. The standard deviation of the spin density projected along the z direction, Δ_z, is plotted in Fig. 61 where we show the results calculated as before for the circle corresponding to the sites with radial coordinate $k = 6$. The spin density deformation (SDD) is actually amplified by the Coulomb interaction for all $N = 2, 3, 4$. As the CDD's, the SDD's reach their maximum at the magnetic fields where level repulsion occurs and remains prominent even when the gaps are very small. The Coulomb enhancement is a result of the mixing of states with the same parity, but with different spin orientation produced by the Coulomb potential. Consequently the SDD's have in general a richer structure than the CDD's.

Finally, in Fig. 62 we display an example of CDD and SDD, obtained for $N = 4$ interacting particles. The charge and spin distributions corresponding to the second excited state and $t_B = 4.5$ are illustrated in Figs. 60(f) and 61(f), respectively. The CDD is weak, but still it has four visible maxima. For two electrons the CDD has only two maxima which are along the directions $x = y$ or $x = -y$, depending on the state and on the magnetic field, both with and without the Coulomb interaction. In particular, for a strictly one-dimensional ring model and $N = 2$, in the ground state, the maxima are always along the line $x = -y$, [8, 9] whereas for a two-dimensional model they can also be along $x = y$.[10] But in general, for $N > 2$ electrons, screening effects may distribute the charge in more complicated configurations. Similar profiles with multiple local oscillation may be obtained for the spin density, eventually becoming spin-

density waves around the ring.

9 Persistent current in ballistic mesoscopic rings with Rashba spin-orbit coupling

Janine Splettstoesser, Michele Governale, Ulrich Zülicke

Abstract

The presence of spin–orbit coupling affects the spontaneously flowing persistent currents in mesoscopic conducting rings. Here we analyze their dependence on magnetic flux with emphasis on identifying possibilities to prove the presence and extract the strength of Rashba spin splitting in low–dimensional systems. Effects of disorder and mixing between quasi–onedimensional ring subbands are considered. The spin-orbit coupling strength can be inferred from the values of flux where sign changes occur in the persistent charge current. As an important consequence of the presence of spin splitting, we identify a nontrivial persistent spin current that is not simply proportional to the charge current. The different flux dependences of persistent charge and spin currents are a *unique* signature of spin–orbit coupling affecting the electronic structure of the ring.

9.1 Introduction

The interplay between spin-orbit (SO) coupling and quantum confinement in semiconductor heterostructures has recently attracted great interest. It provides a useful tool to manipulate the spin degree of freedom of electrons by coupling to their orbital motion, and vice versa. As a result, spin-orbit coupling has become one of the key ingredients for phase-coherent spintronics applications[1, 2]. Various sources of broken inversion symmetry give rise to intrinsic (zero–field) spin splitting in semiconductor heterostructures[3]. We focus here on the one induced by structural inversion asymmetry, i.e., the Rashba effect[4]. It is typically important in small-gap zinc–blende–type semiconductors and can be tuned by external gate voltages[5, 6, 7].

Many proposals have been put forward recently for devices based on spin-dependent transport effects due to the Rashba SO coupling in low-dimensional systems[8]. To explore possibilities for their realization, it is desirable to have a reliable way to determine experimentally the strength α of the Rashba SO coupling. Transport experiments have been performed in two-dimensional (2D) electron systems, and α was extracted from beating patterns in the Shubnikov-de Haas oscillations[5, 6, 7] as well as the SO relaxation time obtained from weak–antilocalization behavior in the resistance[9]. The only previous experimental studies of SO coupling in *quasi–1D* systems have measured transport through mesoscopic rings[10, 11]. Beating patterns in the Aharonov-Bohm (AB) oscillations of the ring's conductance are expected to arise from quantum phases[12, 13, 14, 15] induced by the presence of SO coupling.

In practice, it turns out[16], however, that the signature of the Rashba effect in AB oscillations can be masked by features arising due to the ring's nonideal coupling to external leads. As an alternative, we explore here the possibility to obtain a direct measure of the Rashba SO coupling strength from the persistent current[17, 18] induced by a magnetic flux perpendicular to the ring. This approach would have the advantage of circumventing entirely any problems arising from contacting the ring.

There is a vast literature of theoretical[17, 18, 19, 20, 21, 22, 23, 24, 25] and experimental[26, 27, 28] studies on persistent currents. From the theoretical point of view, the effect of SO coupling on the Fourier transform of observables has been addressed in Refs. [22, 23, 24]. Measurements of the persistent charge current have been performed both in an ensemble of metallic rings[26] and on single isolated rings realized in nanostructured 2D electron systems[27,

28]. So far, persistent currents have not yet been studied in rings where the Rashba effect is likely to be important. From our study, we find features in the flux dependence of the persistent charge current that allow for a direct quantitative determination of the Rashba SO coupling strength. We discuss how averaging over rings with different numbers of particles and mixing between different 1D subbands affects these features. An unambiguous signature of SO coupling is obtained from a comparison of the persistent *spin* current with the persistent *charge* current. In the absence of SO coupling, the persistent spin current is finite only for an odd number of particles in the ring and is proportional to the persistent charge current. With SO coupling, the persistent spin current is finite also for an even electron number. For an odd number of electrons in the ring, the persistent spin current is sizeable only for small values of the SO coupling strength. The flux dependence of the persistent spin current is generally strikingly different from that of the charge current. Observability of the persistent spin current by its induced electric field[29, 30, 31, 32] should enable the unambiguous identification of SO effects in low–dimensional mesoscopic rings.

The paper is organized as follows. In Section 9.2, we write down and discuss the model Hamiltonian used to describe the ring. Electronic properties and persistent currents of a purely 1D ring are computed in the following Sec. 9.3. Section 9.4 is devoted to the effect of higher radial subbands. Conclusions are presented in Sec. 9.5.

9.2 Model of a mesoscopic ring with Rashba spin–orbit coupling

For completeness and to introduce notation used later in our work, we outline here briefly the derivation of the Hamiltonian describing the motion of an electron in a realistic quasi–1D ring[33]. We consider 2D electrons in the xy plane that are further confined to move in a ring by a radial potential $V_{\rm c}(r)$. The electrons are subject to the Rashba SO coupling, which reads

$$H_{\rm so} = \frac{\alpha}{\hbar}\left(\sigma_x\,(\vec{p}-e\vec{A})_y - \sigma_y\,(\vec{p}-e\vec{A})_x\right). \tag{9.1}$$

Here $\vec{A}$ is the vector potential of an external magnetic field applied in the z direction. The coupling strength α defines the spin-precession length $l_{\rm so} = \pi\hbar^2/(m\alpha)$. The full single-electron Hamiltonian reads

$$H = \frac{(\vec{p}-e\vec{A})_x^2 + (\vec{p}-e\vec{A})_y^2}{2m} + V_{\rm c}(r) + H_{\rm so} + \hbar\omega_{\rm z}\sigma_z, \tag{9.2}$$

where the Zeeman splitting from the external magnetic field is included as the last term. Due to the circular symmetry of the problem, it is natural to rewrite the Hamiltonian in polar coordinates:[33]

$$H = -\frac{\hbar^2}{2m}\left[\frac{\partial^2}{\partial r^2} + \frac{1}{r}\frac{\partial}{\partial r} - \frac{1}{r^2}\left(i\frac{\partial}{\partial\varphi} + \frac{\Phi}{\Phi_0}\right)^2\right] + V_{\rm c}(r) - \frac{\alpha}{r}\sigma_r\left(i\frac{\partial}{\partial\varphi} + \frac{\Phi}{\Phi_0}\right) + i\alpha\sigma_\varphi\frac{\partial}{\partial r} + \hbar\omega_{\rm z}\sigma_z,$$

where Φ is the magnetic flux threading the ring, Φ_0 the flux quantum, $\sigma_r = \cos\varphi\,\sigma_x + \sin\varphi\,\sigma_y$ and $\sigma_\varphi = -\sin\varphi\,\sigma_x + \cos\varphi\,\sigma_y$. In the case of a thin ring, i.e., when the radius a of the ring is much larger than the radial width of the wave function, it is convenient to project the Hamiltonian on the eigenstates of $H_0 = -\frac{\hbar^2}{2m}\left[\frac{\partial^2}{\partial r^2} + \frac{1}{r}\frac{\partial}{\partial r}\right] + V_{\rm c}(r)$. To be specific, we use a parabolic radial confining potential,

$$V_{\rm c}(r) = \frac{1}{2}m\omega^2(r-a)^2, \tag{9.3}$$

for which the radial width of the wave function is given by $l_\omega = \sqrt{\hbar/m\omega}$. In the following, we assume $l_\omega/a \ll 1$ and neglect contributions of order l_ω/a. In this limit, H_0 reduces to

$$H_0 = -\frac{\hbar^2}{2m}\left[\frac{\partial^2}{\partial r^2}\right] + \frac{1}{2}m\omega^2(r-a)^2. \tag{9.4}$$

We now calculate matrix elements of the Hamiltonian in the basis of eigenfunctions of Eq. (9.4) that correspond to quasi–1D radial subbands, labeled here by the quantum number n. The diagonal matrix elements are given by

$$H_{n,n} = \tfrac{\hbar^2}{2ma^2}\left(i\tfrac{\partial}{\partial\varphi} + \tfrac{\Phi}{\Phi_0}\right)^2 - \tfrac{\alpha}{a}\sigma_r\left(i\tfrac{\partial}{\partial\varphi} + \tfrac{\Phi}{\Phi_0}\right) - i\tfrac{\alpha}{2a}\sigma_\varphi + \hbar\omega_z\sigma_z + \hbar\omega(n+\tfrac{1}{2}). \tag{9.5}$$

The only nonvanishing offdiagonal matrix elements are those coupling adjacent radial subbands:

$$H_{n,n+1} = H^\dagger_{n+1,n} = i\sigma_\varphi\sqrt{\frac{n+1}{2}}\frac{\alpha}{l_\omega}. \tag{9.6}$$

9.3 Properties of ideal 1D rings

The ideal 1D limit for a mesoscopic ring is realized when only the lowest radial subband is occupied by electrons and all relevant energy scales as, e.g., temperature, voltage, and disorder broadening are small enough such that interband excitations can be neglected. In the following Section, we focus on this situation that can be realized in recently fabricated ring structures[34, 35, 36].

9.3.1 Energy spectrum of 1D ring with impurity

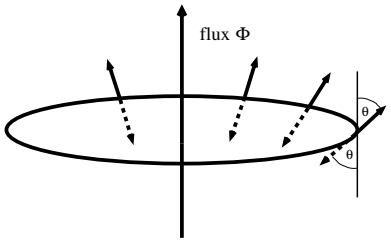

Figure 63: Schematic illustration of the spin texture exhibited by the eigenstates of the ideal one-dimensional ring.

Straightforward algebra yields the eigenenergies of $H_{0,0}$ which are usually labeled by an integer number q:

$$E_{q,\pm} = \hbar\omega_a\left(q - \frac{\Phi}{\Phi_0} + \frac{1}{2} \mp \frac{1}{2\cos\theta_q}\right)^2 + \frac{\hbar\omega_a}{4}\left(1 - \frac{1}{\cos^2\theta_q}\right) \pm \frac{\hbar\omega_z}{\cos\theta_q}. \tag{9.7}$$

Here we have introduced the frequency $\omega_a = \hbar/(2ma^2)$ and omitted the constant energy shift of the radial subband bottom. The eigenvectors corresponding to the eigenenergies given in Eq. (9.7) are

$$\Psi_{q,\pm} = e^{i(q+\frac{1}{2})\varphi}\chi_{q,\pm}, \tag{9.8}$$

with the spinors

$$\chi_{q,+} = \begin{pmatrix} \cos(\frac{\theta_q}{2})e^{-i\frac{1}{2}\varphi} \\ \sin(\frac{\theta_q}{2})e^{i\frac{1}{2}\varphi} \end{pmatrix}, \tag{9.9a}$$

$$\chi_{q,-} = \begin{pmatrix} -\sin(\frac{\theta_q}{2})e^{-i\frac{1}{2}\varphi} \\ \cos(\frac{\theta_q}{2})e^{i\frac{1}{2}\varphi} \end{pmatrix}. \tag{9.9b}$$

The angle θ_q is given by[13]

$$\tan(\theta_q) = -\frac{\frac{\alpha}{a}(q - \frac{\Phi}{\Phi_0} + \frac{1}{2})}{\hbar\omega_{\rm a}(q - \frac{\Phi}{\Phi_0} + \frac{1}{2}) - \hbar\omega_{\rm z}}. \tag{9.10}$$

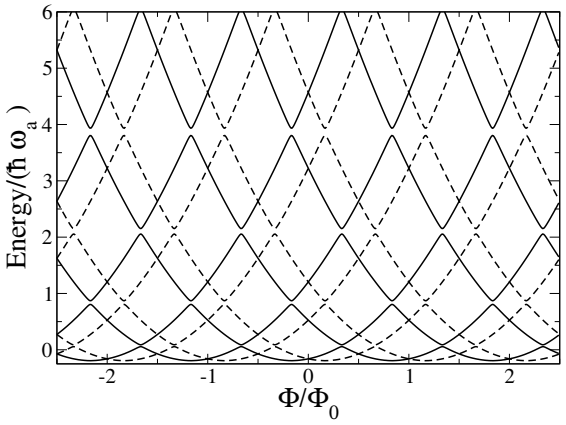

Figure 64: Single-particle energy spectrum of an ideal 1D ring with a model delta–barrier impurity. Parameters are $\cos\theta = 2/5$, and $A = 0.1$. Energy levels for states corresponding to spin-up (solid line) and spin-down (dashed line) in the local-spin-frame basis are shifted, in flux direction, by $1/\cos\theta$.

The spinors $\chi_{q,\pm}$ are the eigenstates of the operator

$$\sigma_{\theta_q} = \sigma_z \cos\theta_q + \sigma_r \sin\theta_q, \tag{9.11}$$

and constitute a basis in spin space with space-dependent quantization direction, as shown in Fig. 63. We will refer to this φ-dependent spin basis as the *local spin frame*. θ_q is the angle between the local quantization axis and the direction perpendicular to the ring (z axis). The tilt angle described by Eq. (9.10) becomes independent of the quantum number q when the Zeeman energy is negligible, i.e., when $\left|\hbar\omega_{\rm a}(q - \frac{\Phi}{\Phi_0} + \frac{1}{2})\right| \gg \hbar\omega_{\rm z}$. For typical realizations of mesoscopic rings with many electrons present, states contributing importantly to the persistent current fulfill this requirement. Therefore, in the following, we focus exclusively on the limit where Zeeman splitting vanishes and $\theta_q \to \theta = \lim_{\omega_{\rm z}\to 0}\theta_q$. Then all eigenstates have the same local spin frame, to which we can transform using the SU(2) matrix

$$\mathcal{U} = \begin{pmatrix} e^{-i\varphi/2}\cos\frac{\theta}{2} & -e^{-i\varphi/2}\sin\frac{\theta}{2} \\ e^{i\varphi/2}\sin\frac{\theta}{2} & e^{i\varphi/2}\cos\frac{\theta}{2} \end{pmatrix}. \tag{9.12}$$

This yields $H_{\rm 1D} \equiv \mathcal{U}^\dagger\,(H_{0,0} - \hbar\omega/2)_{\omega_z=0}\,\mathcal{U}$ where

$$H_{\rm 1D} \;=\; \hbar\omega_{\rm a}\left(-i\frac{\partial}{\partial\varphi} - \frac{\Phi}{\Phi_0} - \frac{1}{2\cos\theta}\sigma_z\right)^2 + \frac{\hbar\omega_{\rm a}}{4}(1 - \frac{1}{\cos^2\theta}). \tag{9.13}$$

Here $\cos\theta$ parameterizes the strength of the SO coupling. The eigenstates in the local spin frame are simply $e^{i(q+\frac{1}{2})\varphi}|\pm\rangle$, where $|\pm\rangle$ denote the eigenspinors of σ_z, and the eigenenergies are given by Eq. (9.7) with $\theta_q \to \theta$ and $\omega_{\rm z} = 0$. Note that the orbital part of the eigenstates obeys antiperiodic boundary conditions to compensate for the antiperiodicity of the spinors of Eq. (9.9).

To discuss the effect of a nonmagnetic impurity, we exploit the formal analogy between a ring with an impurity and a 1D periodic potential[17]. The latter is described by a Kronig–Penney

model[37], with the magnetic flux playing the role of the quasimomentum of the 1D crystal. The impurity is modeled by its energy–dependent transmission amplitude $t = |t| \exp(i\delta)$. The energy spectrum for the electrons with spin $|\pm\rangle$ can now be obtained by solving the transcendental secular equation

$$|t| \cos\left[2\pi\left(\frac{\Phi}{\Phi_0} \pm \frac{1}{2\cos(\theta)}\right)\right] = -\cos\left(2\pi\kappa_\pm + \delta\right), \tag{9.14}$$

complemented by the relation

$$E_\pm = \hbar\omega_\mathrm{a}\left[\kappa_\pm^2 + \frac{1}{4}(1 - \frac{1}{\cos^2\theta})\right]. \tag{9.15}$$

In general, the secular equation (9.14) cannot be solved analytically for arbitrary transmission function t. To simplify the problem, we will now assume that the impurity is a delta-function barrier $V_0\delta(\varphi)$. The transmission coefficient for a state $\exp(i\kappa\varphi)|\pm\rangle$ is $t = 2\kappa/[2\kappa + iV_0/(\hbar\omega_\mathrm{a})]$. For states close to the Fermi level, Eq. (9.14) can be written as

$$\cos\left(2\pi\frac{\Phi_\pm}{\Phi_0}\right) = \cos\left(2\pi\kappa_\pm\right) + \mathrm{sign}(\kappa_\pm) A \sin\left(2\pi\kappa_\pm\right), \tag{9.16}$$

with a constant $A = V_0/(\hbar\omega_\mathrm{a}\mathcal{N})$, where $\mathcal{N}$ is the total number of electrons. We also defined the effective fluxes

$$\Phi_\pm = \Phi + \Phi_0\left(\frac{1}{2} \pm \frac{1}{2\cos(\theta)}\right). \tag{9.17}$$

Equation (9.16) with constant A would be exact for a barrier with energy-independent transmission amplitude $t = [1 - i\,A\,\mathrm{sign}(\kappa)]/(A^2+1)$. The approximated secular equation (9.16) has the solution

$$\kappa_{q,\pm} = q + \frac{1}{2\pi}\arccos\left[\frac{\cos(2\pi\frac{\Phi_\pm}{\Phi_0}) - \mathrm{sign}(q)\sqrt{A^2\left(\sin^2(2\pi\frac{\Phi_\pm}{\Phi_0}) + A^2\right)}}{1 + A^2}\right]. \tag{9.18}$$

Equation (9.18) together with Eq. (9.15) yields the single-particle energy spectrum for the ring with an idealized impurity. Note that, in the representation of the local spin frame, the impurity problem maps to that of electrons without SO coupling but with an effective spin–dependent flux[22, 23] given by Eq. (9.17). This is illustrated in an example spectrum shown in Fig. 64.

9.3.2 Persistent charge currents

Having calculated the single-particle electronic properties of the ring, we proceed to evaluate the persistent charge current. At zero temperature, it is given by[17]

$$I = -\frac{\partial E_\mathrm{gs}}{\partial\Phi} = -\sum_{i\in\mathrm{occupied}}\frac{\partial E_i}{\partial\Phi}, \tag{9.19}$$

where E_gs is the ground state energy, and E_i are the single particle eigenenergies. Here i stands for a set of quantum numbers used to label corresponding eigenstates, including here the spin projection in the local spin frame. The second equality in Eq. (9.19) is valid only in the absence of electron-electron interactions, which we neglect here. The zero-temperature formula applies when the thermal energy $k_\mathrm{B}T$ is smaller than the energy difference between the last occupied

state and the first unoccupied one. In the following, we will always consider the number $\mathcal{N}$ of electrons in the ring to be fixed, i.e., work in the canonical ensemble. This is the relevant situation for an isolated ring.

For spinful electrons, the flux dependence of the persistent charge current is distinctly different for the following cases:[19] i) $\mathcal{N} = 4N$, ii) $\mathcal{N} = 4N + 2$, and iii) $\mathcal{N} = 2N + 1$, where N denotes a positive integer. When $\mathcal{N}$ is large enough, the persistent charge current in units of $I_0 = \hbar\omega_a\mathcal{N}/\Phi_0$ has a universal behavior independent of $\mathcal{N}$. We start discussing the weak barrier limit (small A in our model), shown in Fig. 65. In the case i) where $\mathcal{N} = 4N$, the numbers of spin-up and spin-down electrons (spin projection in the local spin frame!) are both even, resulting in jumps of the persistent current at $\Phi/\Phi_0 = M + 1/2 \pm 1/(2\cos\theta)$, with M being integer. This is simply the superposition of the even–number spinless–electron persistent–current characteristics for each spin direction, shifted in flux by $\pm 1/(2\cos\theta)$. Case ii) corresponds to an odd number of spin-up and spin-down electrons and exhibits jumps of the persistent charge current at $\Phi/\Phi_0 = M \pm 1/(2\cos\theta)$, which is the analogous superposition of the appropriately flux–shifted spinless odd-electron currents for each spin direction. Note that the case $\mathcal{N} = 4N + 2$ is obtained from the $\mathcal{N} = 4N$ case simply by shifting flux by $1/2\Phi_0$. It is apparent that, for both cases i) and (ii), the minimum distance between jumps of the persistent charge current within the periodic flux interval is a measure of $1/\cos\theta$ and, hence, of the SO coupling strength. In contrast, for case iii), i.e., an odd number of electrons in the ring, jumps appear at the same values of flux ($\Phi/\Phi_0 = 0$ and $\pm 1/2$) as in the absence of spin–orbit coupling. The only effect of SO coupling turns out to be a suppression of impurity rounding for these jumps. This can be explained quite easily. Inspection shows that, for finite SO coupling, jumps in the persistent charge current in the case of an odd number of electrons are due to crossing of levels with opposite spin, while those in the case of even electron number arise from crossings of levels having the same spin. As a spin-independent impurity cannot couple levels with opposite spin, only the jumps in the case of even electron number get rounded because of impurity-induced anticrossings. For an odd number of electrons, jumps in the persistent charge current get broadened only by temperature. The effect of increasing impurity (barrier) strength can be seen comparing Fig. 65 and Fig. 66, where the persistent charge current is shown for different SO coupling strengths, occupancy of the ring, and disorder.

Measurements are often performed on ensembles of many rings[26]. The measured persistent charge current is then an average over different occupation numbers, with even and odd occupation occurring with the same probability. Among cases with even electron numbers, $\mathcal{N} = 4N$ and $4N + 2$ would also be equiprobable. An example of average persistent charge current is shown in Fig. 67. It exhibits the well–known period halving[20, 21] which must occur irrespective of the presence of SO coupling. Most importantly, however, all the features present for the single ring and discussed above for different occupancy are still visible. It should therefore be possible to obtain the Rashba SO coupling strength from a measurement of the ensemble-averaged persistent charge current.

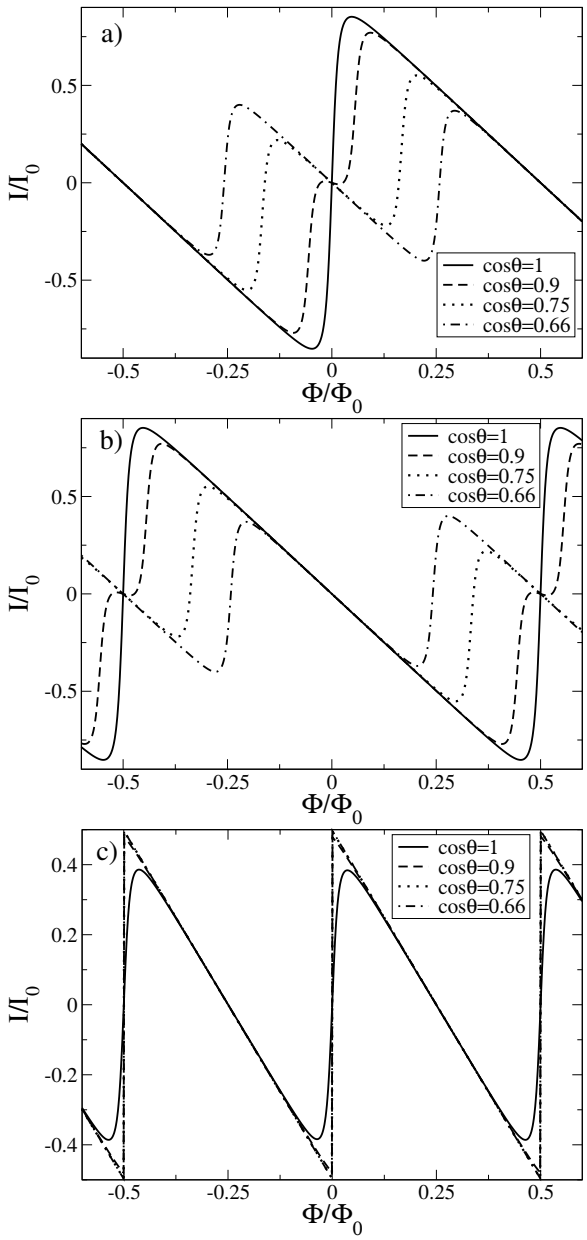

Figure 65: Persistent charge current vs. magnetic flux for a set of values for the spin-orbit coupling strength. The total number of electrons is set to $4N$ in panel a), to $4N+2$ in panel b), and to $2N+1$ in panel c) in the regime of large-enough N such that the persistent current is universal. A dimensionless barrier strength of $A = 0.1$ was assumed. The persistent current is measured in units of $I_0 = \hbar\omega_{\rm a}\mathcal{N}/\Phi_0$.

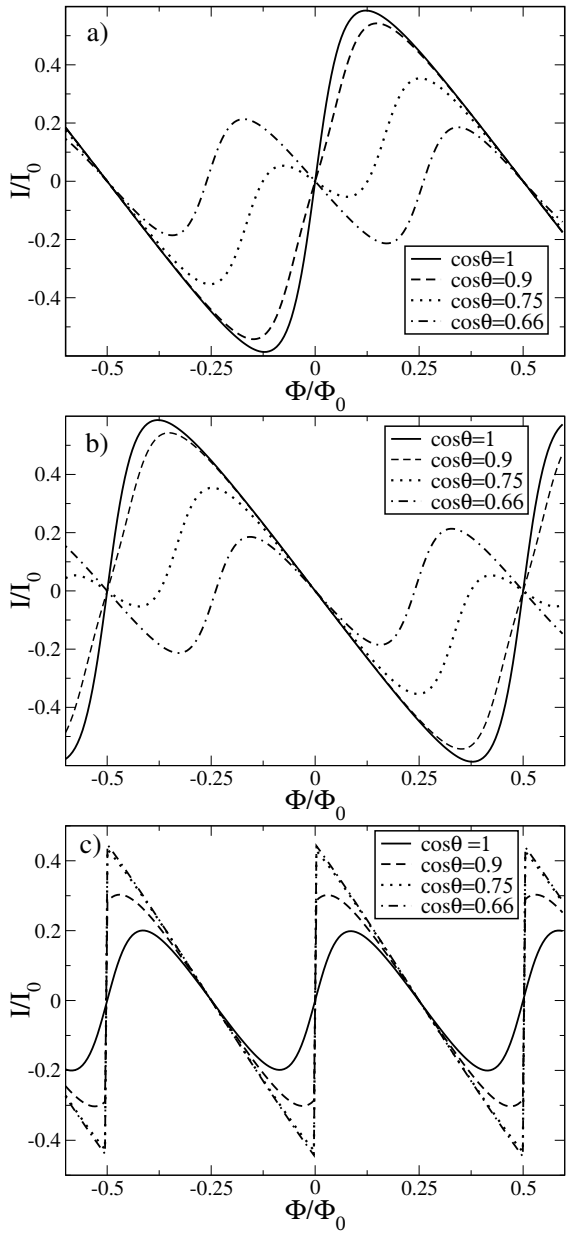

Figure 66: Same as Fig. 65 but with different impurity parameter $A = 0.5$. Note the remaining sharpness of jumps in the case of odd electron number even at this rather large value of A.

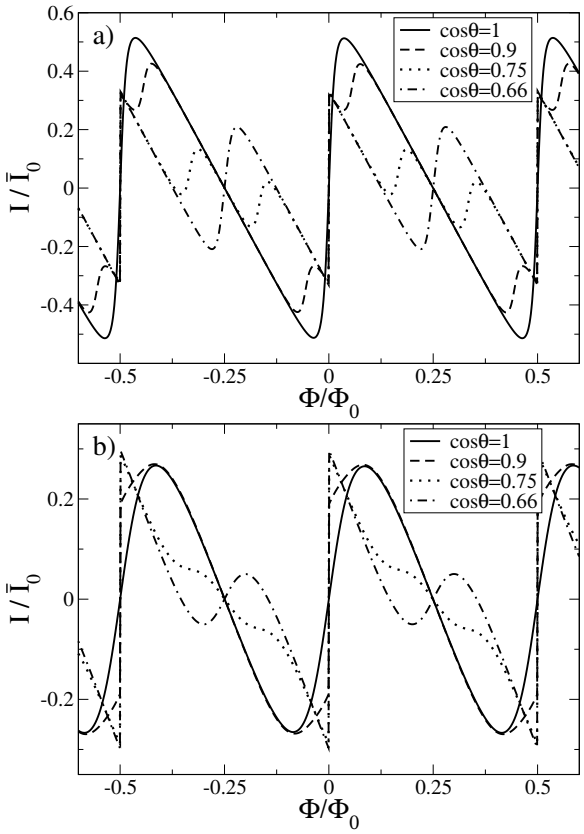

Figure 67: Average persistent charge current for an ensemble of identical rings with different electron numbers, shown as function of magnetic flux for different values of the spin-orbit coupling strength. The impurity parameter is $A = 0.1$ in panel a) and $A = 0.5$ in panel b). The current unit is $\bar{I}_0 = \hbar\omega_a\bar{\mathcal{N}}/\Phi_0$, where $\bar{\mathcal{N}}$ denotes the average number of electrons.

9.3.3 Persistent spin currents

As electrons carry spin as well as charge, their motion gives rise also to a spin current besides the charge current. Very often, the difference of charge currents carried by spin-up and spin-down electrons is identified with the spin current. While this is appropriate in many contexts, it has to be kept in mind[12, 32] that the spin current is actually a tensor. A particular case where this fact matters is the one to be considered here. As the electron velocity in the presence of SO coupling turns out to be an operator in spin space[38], and eigenstates for electrons of the ring correspond to eigenspinors of a spatially varying spin matrix [σ_θ as defined in Eq. (9.11)], the proper expression for the spin current has to be derived carefully. After presenting details of this derivation, we proceed to show results for the persistent spin currents of electrons in a ring with Rashba SO coupling.

The operator of the ν component of spin density in real-space representation is given by $s_\nu(\vec{r}) = \sigma_\nu(\vec{r'})\,\delta(\vec{r}-\vec{r'})$, with σ_ν being the SU(2) spin matrix whose eigenstates form the basis for projection of spin in ν direction. In general, this projection direction can vary in space. The equation of motion for the spin-density operator is given by the familiar Heisenberg form

$$\frac{d}{dt}\,s_\nu(\vec{r}) = \frac{i}{\hbar}\,[H\,,\,s_\nu(\vec{r})]\,, \tag{9.20a}$$

$$= \left(\frac{d}{dt}\,\sigma_\nu(\vec{r'})\right)\,\delta(\vec{r}-\vec{r'}) - \vec{\nabla}_{\vec{r}}\cdot\left(\sigma_\nu(\vec{r'})\,\vec{v}(\vec{r})\right). \tag{9.20b}$$

Here $\vec{\nabla}_{\vec{r}}$ denotes the gradient operator acting on the coordinate $\vec{r}$, and $\vec{v}(\vec{r})$ is the electron velocity operator. The latter differs from its expression $\vec{v}_0$ in the absence of SO coupling by a

spin–dependent term:[38] $\vec{v} = \vec{v}_0 + \alpha(\hat{z} \times \vec{\sigma})/\hbar$.

Straightforward calculation for the case of *spatially constant* σ_ν and vanishing Zeeman splitting yields the continuity equation

$$\frac{d}{dt}\, s_\nu(\vec{r}) + \vec{\nabla} \cdot \vec{j}_\nu(\vec{r}) = \frac{2\alpha}{\hbar^2}\, (\hat{\nu} \times (\hat{z} \times \vec{\sigma})) \cdot \left(\vec{p} - e\vec{A}\right), \tag{9.21a}$$

with the ν component of the spin-current tensor given by

$$\vec{j}_\nu(\vec{r}) = \vec{v}(\vec{r})\, \sigma_\nu. \tag{9.21b}$$

We have used the symbols $\hat{z}$ and $\hat{\nu}$ to denote unit vectors in z and ν direction, respectively. Note that the expression (9.21b) and the source term on the r.h.s. of Eq. (9.21a) have been written in the usual shorthand notation where it is understood that the real part has to be taken in the expectation value. As an example, we fix $\nu = z$ and consider the case of electrons moving in the lowest quasi-1D radial ring subband. We find, after transformation into the representation of the local spin frame, for the continuity equation (9.21a) the simple expression

$$\frac{d}{dt}\, s_z(\varphi) + \frac{1}{a}\frac{\partial}{\partial\varphi}\, j_z^\varphi(\varphi) = 2\omega_\mathrm{a}\, \sigma_y \left(i\frac{\partial}{\partial\varphi} + \frac{\phi}{\phi_0}\right) \tan\theta. \tag{9.22a}$$

The only nonvanising (φ) component of the spin current turns out to be

$$\begin{aligned} j_z^\varphi(\varphi) \;=\; & \frac{\hbar}{ma} \left\{ \left(-i\frac{\partial}{\partial\varphi} - \frac{\phi}{\phi_0} - \frac{1}{2\cos\theta}\, \sigma_z\right) \sigma_z \cos\theta \right. \\ & \left. - \left(-i\frac{\partial}{\partial\varphi} - \frac{\phi}{\phi_0}\right) \sigma_x \sin\theta \right\}. \end{aligned} \tag{9.22b}$$

Eigenstates on the ring which are labeled by quantum numbers q and σ carry a current for the z projection of spin given by

$$I_z^{(q\sigma)} = \frac{1}{2\pi a}\, \langle j_z^\varphi(\varphi) \rangle_{q\sigma} = -\frac{1}{e}\frac{\partial E_{q,\sigma}}{\partial\Phi}\, \sigma \cos\theta, \tag{9.23}$$

which is just the charge current multiplied by the magnetization in z direction of the corresponding state[39].

As an important example for the current of a spatially varying projection of the magnetization, we consider the case of the local spin frame, i.e., $\sigma_\nu(\vec{r}) = \sigma_\theta(\varphi)$. [See Eq. (9.11).] Additional terms arising from derivatives of σ_θ w.r.t. polar angle φ appear in the continuity equation for $s_\theta(\vec{r})$. After transformation into the local spin frame, it has the extremely simple form

$$\frac{d}{dt}\, s_\theta(\varphi) + \frac{1}{a}\frac{\partial}{\partial\varphi}\, j_\theta^\varphi(\varphi) = 0, \tag{9.24a}$$

with the current

$$j_\theta^\varphi(\varphi) = \frac{\hbar}{ma} \left(-i\frac{\partial}{\partial\varphi} - \frac{\phi}{\phi_0} - \frac{1}{2\cos\theta}\, \sigma_z\right) \sigma_z. \tag{9.24b}$$

The current of magnetization parallel to the quantization axis in the local spin frame carried by eigenstates is therefore given by

$$I_\theta^{(q\sigma)} = -\frac{1}{e}\frac{\partial E_{q,\sigma}}{\partial\Phi}\, \sigma. \tag{9.25}$$

Comparison with results from above yield the relation $I_z^{(q\sigma)} = I_\theta^{(q\sigma)} \cos\theta$, and we have derived also the related one $I_r^{(q\sigma)} = I_\theta^{(q\sigma)} \sin\theta$.

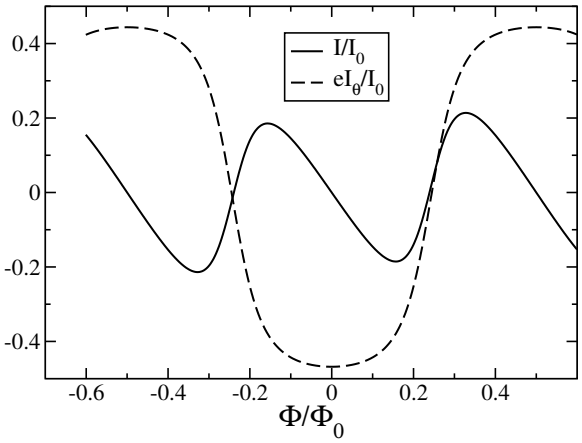

Figure 68: Persistent spin current for spin projection onto the local spin frame (dashed curve) and persistent charge current (solid curve) vs. magnetic flux for the case with electron number $4N+2$. The barrier strength is $A = 0.5$, and $\cos\theta = 0.66$. The current is measured in units of $I_0 = \hbar\omega_a \mathcal{N}/\Phi_0$.

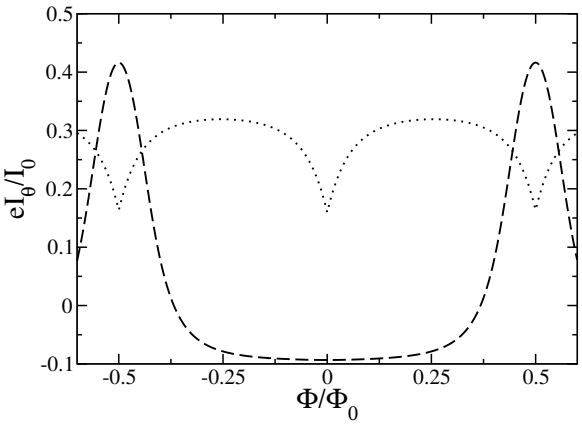

Figure 69: Comparison of persistent spin currents for electron number equal to $4N+2$ (dashed curve) and $2N+1$ (dotted curve). The barrier strength is $A = 0.5$, and $\cos\theta = 0.9$ corresponding to a small spin-orbit coupling strength. The magnitude of persistent spin current decreases rapidly for odd electron number as $\cos\theta$ approaches 0.66.

We now present results for the total persistent spin current $I_\theta = \sum_{q\sigma} I_\theta^{(q\sigma)}$ for the projection onto the quantization axis of the local spin frame. As shown above, spin currents for certain other projections can be easily obtained from I_θ. The fact that flux dependences for the persistent-current contributions from opposite-spin eigenstates are shifted according to Eq. (9.17) results in large spin currents at certain flux values. In particular, this is realized when the currents carried by electrons with opposite spin flow in opposite directions. In Fig. 68, we show the persistent spin current for an even number of electrons. For comparison, the persistent charge current is plotted as well. Both exhibit strikingly different flux dependences. Note also that, in the absence of SO coupling, the persistent spin current vanishes for even electron number in the ring. Only the relative shift of energy bands in flux direction caused by SO coupling enables a finite persistent spin current in this case. For an odd number of electrons, the persistent spin current is finite both with and without SO coupling present. We find it to be sizable, however, only for small values of SO coupling strength. We show a comparison of even and odd electron number cases in Fig. 69.

The persistent spin current would be a mere theoretical curiosity if no detectable effect of it could be found. Fortunately, this is not so. Recently, it has been pointed out by several

authors[29, 30, 31, 32] that a spin current, being a magnetization current, gives rise to an electric field. This is easily proved by making a Lorenz transform to the rest frame of spin. For example, the electrostatic potential for a point at a distance $z \ll a$ from the plane of the ring on the vertical from the center of the ring is

$$\phi(z) \approx \frac{\mu_0}{4\pi} g\mu_B I_\theta \sin\theta \frac{a}{z^2}, \tag{9.26}$$

where μ_0 is the vacuum permeability, g the gyromagnetic ratio, μ_B the Bohr magneton, a the radius of the ring, and θ the tilt angle due to SO coupling. This result is identical with the one derived in Ref. [30] for the electric field resulting from persistent spin currents in Heisenberg rings.

9.4 Effect of many radial subbands

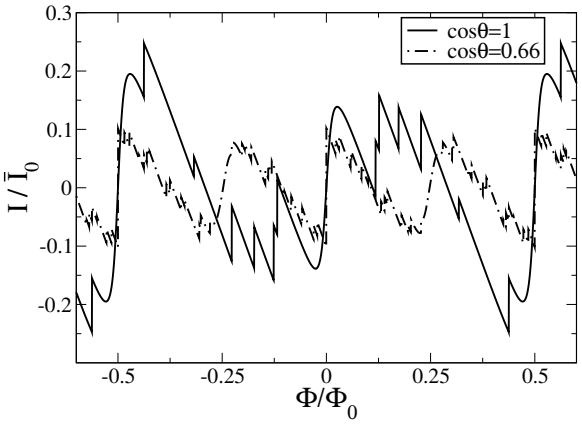

Figure 70: Average persistent current vs. magnetic flux for a ring with two occupied radial subbands. The barrier strength is $A = 0.1$. The average is performed on an ensemble containing rings with occupancy ranging from 60 to 80 electrons.

In the previous section, we have analyzed the persistent current in a strictly 1D ring, i.e., a ring with only the lowest radial subband occupied by electrons and a sufficiently large subband-energy splitting. We now generalize this discussion to the case where higher subbands are important. SO coupling introduces coupling between neighboring radial subbands as described in Eq. (9.6). More specifically, the Hamiltonian Eq. (9.6) couples radial subbands with opposite spin in the local spin frame, leading to non-parabolicity of energy dispersions and to hybridization of opposite-spin bands. The physics in the limit of strong subband coupling is analogous to what happens in a quantum wire with Rashba SO coupling; this has been discussed in Refs. [41, 40]. Here it is sufficient to notice that $H_{n,n+1}$ is negligible if $l_\omega/l_{so} \ll 1$, i.e., if the radial width of the wave function is much smaller than the spin-precession length. This condition is fulfilled in realistic samples. Therefore, we neglect in the following the coupling term Eq. (9.6). For the sake of simplicity we now consider only the two lowest subbands. Furthermore we introduce a barrier in the same way as in Section 9.3.1. Assuming that the barrier does not couple different subbands, and that the transmission coefficient is the same for both radial subbands and is given by $t = [1 - i\mathrm{sign}(\kappa)A]/(A^2+1)$, we find for the energy spectrum

$$E_{q,\pm,n} = \hbar\omega_a \left[\kappa_{q,\pm}^2 + \frac{1}{4}(1 - \frac{1}{\cos^2\theta})\right] + \hbar\omega\left(n + \frac{1}{2}\right), \tag{9.27}$$

where $n = 0, 1$ is the subband index, and $\kappa_{q,\pm}$ is still given by Eq. (9.18). In Fig. 70, we show the average persistent current with and without SO coupling. In comparison to the single-subband

case, additional fine structure appears due to crossing of levels with different radial quantum numbers. The jumps arising from these extra crossings are very sharp due to the way we model the barrier, and occur at flux values that are strongly dependent on the ring occupancy. All other features discussed for the strictly 1D case occur at the same flux values for all radial subbands. Hence, upon averaging, the latter are magnified and the former demagnified, as it is evident comparing Fig. 70 with Fig. 67 a. The dependence of the average persistent current on the SO coupling and barrier strength is the same as for the 1D case, hence, we do not show it again for the many-subband case. The presence of many radial subbands, although it introduces some additional fine structure, essentially yields, after averaging over different electron numbers, the same SO-related features discussed in the purely 1D case.

9.5 Conclusions

We have investigated the effect of Rashba spin-orbit coupling on the persistent spin and charge currents circling in ballistic quasi-onedimensional rings. The flux dependence of persistent charge currents exhibits features that allow for a direct measurement of the spin-orbit coupling strength. These features survive averaging over different electron-number configurations as well as the inclusion of higher subbands. The most striking effect of spin-orbit coupling discussed here is the occurrence of finite persistent *spin* currents for even electron numbers. We have carefully derived the correct general form of spin currents in the presence of spin-orbit coupling. The possibility to measure persistent *spin* currents via the electric field generated by their transported magnetization should make it possible to unambiguously verify the presence and magnitude of spin-orbit coupling, namely by the different flux dependences of persistent spin and charge currents.

10 Examples and Solved Problems

A Adds

A.1 Дополнения

A.1.1 Литература

B Bibliography

References

From Mesoscopic rings with Spin-Orbit interactions

References

[1] Y. Imry, *Introduction to mesoscopic physics*, Oxford University Press, Oxford 2002.

[2] M. König, A. Tschetschetkin, E.M. Hankiewicz, J. Sinova, V. Hock, V. Daumer, M. Schäfer, C.R. Becker, H. Buhmann and L.W. Molenkamp, *Direct Observation of the Aharonov-Casher Phase*, Phys. Rev. Lett. **96**, 076804 (2006).

[3] A.A. Kovalev, M. F. Borunda, T. Jungwirth, L. W. Molenkamp and J. Sinova, *Aharonov-Casher effect in a two-dimensional hole ring with spin-orbit interaction*, Phys. Rev. B **76**, 125307 (2007).

[4] M. Zivkovic, M. Jääskeläinen, C.P. Search, and I. Djuric, *Sagnac rotational phase shifts in a mesoscopic electron interferometer with spin-orbit interactions*, Phys. Rev. B **77**, 115306 (2008).

[5] D. Frustaglia and K. Richter, *Spin interference effects in ring conductors subject to Rashba coupling*, Phys. Rev. B **69**, 235310 (2004).

[6] M. Harmer, *Spin filtering on a ring with the Rashba Hamiltonian*, J. Phys. A **39**, 14329 (2006).

[7] N. Hatano, R. Shirasaki and H. Nakamura, *Non-Abelian gauge field theory of the spin-orbit interaction and a perfect spin filter*, Phys. Rev. A **75**, 032107 (2007).

[8] B. Berche, N. Bolívar, A. López and E. Medina, *Gauge field theory approach to spin transport in a 2D electron gas*, Cond. Matt. Phys. **12**, 707 (2009).

[9] A. López, E. Medina, N. Bolívar and B. Berche, *A perfect spin filtering device through Mach-Zehnder interferometry in a GaAs/AlGaAs electron gas*, J. Phys.: Condens. Matter **22**, 115303 (2010).

[10] P. Recher, B. Trauzettel A. Rycerz, Ya.M. Blanter, C.W.J. Beenakker and A. F. Morpurgo, *Aharonov-Bohm effect and broken valley degeneracy in graphene rings*, Phys. Rev. B **76**, 235404 (2007).

[11] Z.-Y. Zhang, *Spin accumulation on a one-dimensional mesoscopic Rashba ring*, J. Phys. Condens. Matter **18**, 4101 (2006).

[12] P. Földi, O. Kálmán, M. G. Benedict and F.M. Peeters, *Quantum rings as electron spin beam splitters*, Phys. Rev. B **73**, 155325 (2006).

[13] R. Citro and F. Romeo, *Pumping in a mesoscopic ring with Aharonov-Casher effect*, Phys. Rev. B **73**, 233304 (2006).

[14] J. Nitta, T. Bergsten, Y. Kunihashi and M. Kohda, *Electrical manipulation of spins in the Rashba two dimensional electron gas systems*, J. Appl. Phys. **105**, 122402 (2009).

[15] B. Molnár, P. Vasilopoulos, and F. M. Peeters, *Spin-dependent transmission through a chain of rings: Influence of a periodically modulated spinâorbit interaction strength or ring radius*, Appl. Phys. Lett. **85**, 612 (2004).

[16] Z.-Y. Zhang, *Andreev reflection in a mesoscopic hybrid four-terminal Rashba ring*, J. Phys. Condens. Matter **19**, 236212 (2007).

[17] P. Földi, M.G. Benedict, O. Kálmán and F.M. Peeters, *Quantum rings with time-dependent spin-orbit coupling: Spintronic Rabi oscillations and conductance properties*, Phys. Rev. B **80**, 165303 (2009).

[18] J. Splettstoesser, M. Governale and U. Zülicke, *Persistent current in ballistic mesoscopic rings with Rashba spin-orbit coupling*, Phys. Rev. B **68**, 165341 (2003).

[19] Q.-f. Sun, X.C. Xie and J. Wang, *Persistent Spin Current in a Mesoscopic Hybrid Ring with Spin-Orbit Coupling*, Phys. Rev. Lett. **98**, 196801 (2007).

[20] G.-Y. Huang and S.-D. Liang, *Orbital magnetic phase and pure persistent spin current in spin-orbit coupling mesoscopic rings*, EPL **86**, 67009 (2009).

[21] O. Kálmán, P. Földi, M.G. Benedict and F.M. Peeters, *Magnetoconductance of rectangular arrays of quantum rings*, Phys. Rev. B **78**, 125306 (2008).

[22] I.A. Shelykh, G. Pavlovic, D.D. Solnyshkov and G. Malpuech, *Proposal for a Mesoscopic Optical Berry-Phase Interferometer*, Phys. Rev. Lett. **102**, 046407 (2009).

[23] P. Földi B. Molnár, M.G. Benedict and F. M. Peeters, *Spintronic single-qubit gate based on a quantum ring with spin-orbit interaction*, Phys. Rev. B **71**, 033309 (2005).

[24] J. J. Sakurai, Modern Quantum Mechanics, Addison Wesley, Reading 1994.

[25] J.D. Bjorken and S.D. Drell, *Relativistic quantum mechanics*, Mac Graw Hill, New-York 1964.

[26] E. Merzbacher, *Quantum Mechanics*, John Wiley and Sons, Inc., New York 1970.

[27] E.I. Rashba, *Properties of semiconductors with an extremum loop*, Sov. Phys. Solid State **2**, 1109 (1960).

[28] Y.A. Bychkov and E.I. Rashba, *Properties on 2D electron-gas with lifted spectrum degeneracy*, JETP Lett. **39**, 78 (1984).

[29] S. D. Ganichev, V.V. Bel'kov, L.E. Golub, E.L. Ivchenko, Petra Schneider, S. Giglberger, J. Eroms, J. De Boeck, G. Borghs, W. Wegscheider, D. Weiss, and W. Prettl, *Experimental separation of Rashba and Dresselhaus spin splittings in semiconductor quantum wells*, Phys. Rev. Lett. **92**, 256601 (2004).

[30] H.A. Engel, E. I. Rashba and B.I. Halperin, *Theory of Spin Hall Effects in Semiconductors*, in Handbook of Magnetism and Advanced Magnetic Materials, H. Kronmüller and S. Parkin, eds. (John Wiley & Sons, Chichester, UK, 2007) Vol. 5, pp 2858-2877. Cond-mat/0603306

[31] R. Winkler, *Spin-Orbit Coupling Effects in Two Dimensional Electron and Hole Systems*, (Springer) 2003.

[32] E.I. Rashba, *Semiconductors spintronics: Progress and Challenges*, arXiv:cond-mat/0611194

[33] F.E. Meijer, A.F. Morpurgo and T.M. Klapwijk, *One-dimensional ring in the presence of Rashba spin-orbit interaction: Derivation of the correct Hamiltonian*, Phys. Rev. B **66**, 033107 (2002).

[34] G. Paz, *On the connection between the radial momentum operator and the Hamiltonian in n dimensions*, Eur. J. Phys. **22**, 337 (2001).

[35] B. Molnár, F. M. Peeters and P. Vasilopoulos, *Spin-dependent magnetotransport through a ring due to spin-orbit interaction*, Phys. Rev. B **69**, 155335 (2004).

[36] M. Peskin and D. Shroeder, *An Introduction to Quantum Field Theory*, (Boulder, Westview Press) 1996.

[37] M. Buttiker, Y. Imry, and R. Landauer, *Josephson behavior in small normal one dimensional rings*, Phys. Lett. **96A**, 365 (1983).

[38] P. Mohanty, *Persistent currents in normal metals*, Ann. Phys. (Leipzig) **8**, 549 (1999).

[39] N. Ashcroft, D. Mermin, *Solid State Physics*, (Holt, Rinehart and Winston) 1976.

[40] I.V. Tokatly, *Equilibrium Spin Currents: Non-Abelian Gauge Invariance and Color Diamagnetism in Condensed Matter*, Phys. Rev. Lett. **101**, 106601 (2008).

[41] A. López, E. Medina, N. Bolívar and B. Berche, *Comment on Equilibrium Spin Currents: Non-Abelian Gauge Invariance and Color Diamagnetism in Condensed Matter* arxiv/0902.46352009 (2009).

[42] N. Byers and C.N. Yang, *Theoretical considerations concerning quantized magnetic flux in superconducting cylinders*, Phys. Rev. Lett. **7**, 46 (1961).

[43] E. Medina, A. López, and B. Berche, *Gauge symmetry breaking and topological quantization for the Pauli Hamiltonian*, Europhys. Lett. **83**, 47005 (2008).

[44] P.Q. Jin, Y.Q. Li and F.C. Zhang, $SU(2) \times U(1)$ *unified theory for charge, orbit and spin currents*, J. Phys. Math Gen. **39**, 7115 (2006).

[45] P. Lucignano, D. Giuliano, A. Tagliacozzo, *Quantum Rings with Rashba spin orbit coupling: a path integral approach*, Phys. Rev. B **76**, 045324 (2007).

From Modulating Unpolarized Current in Quantum Spintronics

References

[1] I. Žutić, J. Fabian, and S. Das Sarma, *Rev. Mod. Phys.* **76**, 323 (2004).

[2] E.I. Rashba, Physica E **20**, 189 (2004).

[3] D.D. Awschalom and J.M. Kikkawa, Phys. Today **52**, 33 (1999).

[4] S. Datta and B. Das, Appl. Phys. Lett. **56**, 665 (1990).

[5] J. Nitta, T. Akazaki, H. Takayanagi, and T. Enoki, Phys. Rev. Lett. **78**, 1335 (1997).

[6] Y. Ohno, D.K. Young, B. Beschoten, F. Matsukura, H. Ohno, D.D. Awschalom, Nature **402**, 790 (1999); R. Fiederling, M. Keim, G. Reuscher, W. Ossau, G. Schmidt, A. Waag, and L. W. Molenkamp, Nature **402**, 790 (1999).

[7] F.G. Monzon, M. Johnson, and M.L. Roukes, Appl. Phys. Lett. **71**, 3087 (1997).

[8] Y. Imry, *Introduction to mesoscopic physics* (Oxford University Press, Oxford, 2002).

[9] C.W.J. Beenakker, Rev. Mod. Phys. **69**, 731 (1997).

[10] S. Washburn and R.A. Webb, Rep. Prog. Phys. **55**, 1311 (1992).

[11] A. Bohm, A. Mostafazadeh, H. Koizumi, Q. Niu, and J. Zanziger, *The geometric phase in quantum systems* (Springer-Verlag, Berlin, 2003).

[12] Y. Meir, Y. Gefen, O. Entin-Wohlman, Phys. Rev. Lett. **63**, 798 (1989).

[13] H. Mathur and A.D. Stone, Phys. Rev. Lett. **68**, 2964 (1992).

[14] A.G. Aronov and Y.B. Lyanda-Geller, Phys. Rev. Lett. **70**, 343 (1993).

[15] T.-Z. Qian and Z.-B. Su, Phys. Rev. Lett. **72**, 2311 (1994).

[16] J. Nitta, F.E. Meijer, and H. Takayanagi, Appl. Phys. Lett. **75**, 695 (1999).

[17] D. Frustaglia and K. Richter, `cond-mat/0309228`.

[18] B. Molnár, and F.M. Peeters, P. Vasilopoulos, Phys. Rev. B **69**, 155335 (2004).

[19] B.K. Nikolić and S. Souma, `cond-mat/0402662`.

[20] W. Häusler, Physica E **18**, 337 (2003).

[21] J.B. Yau, E.P. De Poortere, and M. Shayegan, Phys. Rev. Lett. **88**, 146801 (2002).

[22] M.J. Yang, C.H. Yang, K.A. Cheng, and Y.B. Lyanda-Geller, `cond-mat/0208260`.

[23] F.E. Meijer, A.F. Morpurgo, and T.M. Klapwijk, Phys. Rev. B **66**, 033107 (2002).

[24] J.L. D'Amato, H.M. Pastawski, and J.F. Weisz, Phys. Rev. B **39**, 3554 (1989).

[25] A. Aldea, P. Gartner, and I. Corcotoi, Phys. Rev. B **45**, 14122 (1992).

[26] K.N. Pichugin and A.F. Sadreev, Phys. Rev. B **56**, 9662 (1997).

[27] W. Zurek, Rev. Mod. Phys. **75**, 715 (2003).

[28] S.-Q. Shen, Z.-J. Li, and Z. Ma, Appl. Phys. Lett. **84**, 996 (2004).

[29] Y. Gefen, in *Strongly Correlated Fermions and Bosons in Low-Dimensional Disordered Systems*, edited by I.V. Lerner, B.L. Altshuler, V.I. Fal'ko, and T. Giamarchi (Kluwer, Dodrecht, 2002) (`cond-mat/0207440`).

[30] H. Aikawa, K. Kobayashi, A. Sano, S. Katsumoto, and Y. Iye, Phys. Rev. Lett. **92**, 176802 (2004).

[31] A. Carollo, I. Fuentes-Guiridi, M. França Santos, and V. Vedral, Phys. Rev. Lett. **90**, 160402 (2003); R.S. Whitney and Y. Gefen, Phys. Rev. Lett. **90**, 190402 (2003).

From Spin states and persistent currents in mesoscopic rings

References

[1] S. A. Wolf, D. D. Awschalom, R. A. Buhrman, J. M. Daughton, S. von Molnár, M. L. Roukes, A. Y. Chtchelkanova, and D. M. Treger, Science **294**, 1488 (2001).

[2] E. Tsitsishvili, G. S. Lozano, and A. O. Gogolin, Phys. Rev. B **70**, 115316 (2004).

[3] G. Dresselhaus, Phys. Rev. **100**, 580 (1955).

[4] E. I. Rashba, Sov. Phys. Solid State **2**, 1109 (1960).

[5] Y. A. Bychkov and E. I. Rashba, J. Phys. C **17**, 6039 (1984).

[6] S. Murakami, N. Nagaosa, and S. C. Zhang, Science **301**, 1348 (2003).

[7] J. Sinova, D. Culcer, Q. Niu, N. A. Sinitsyn, T. Jungwirth, and A. H. MacDonald, Phys. Rev. Lett. **92**, 126603 (2004).

[8] A. Fuhrer, S. Lüescher, T. Ihn, T. Heinzel, K. Ensslin, W. Wegscheider, and M. Bichler, Nature **413**, 822 (2001).

[9] M. Büttiker, Y. Imry, and R. Landauer, Phys. Lett. **96A**, 365 (1983).

[10] L. Wendler, V. M. Fomin, and A. A. Krokhin, Phys. Rev. B **50**, 4642 (1994).

[11] T. Chakraborty and P. Pietiläinen, Phys. Rev. B **50**, 8460 (1994).

[12] V. Chandrasekhar, R. A. Webb, M. J. Brady, M. B. Ketchen, W. J. Gallagher, and A. Kleinsasser, Phys. Rev. Lett. **67**, 3578 (1991).

[13] D. Mailly, C. Chapelier, and A. Benoit, Phys. Rev. Lett. **70**, 2020 (1993).

[14] F. Meier and D. Loss, Phys. Rev. Lett. **90**, 167204 (2003).

[15] F. Schütz, M. Kollar, and P. Kopietz, Phys. Rev. Lett. **91**, 017205 (2003).

[16] J. Splettstoesser, M. Governale, and U. Zülicke, Phys. Rev. B **68**, 165341 (2003).

[17] B. Molnár, F. M. Peeters, and P. Vasilopoulos, Phys. Rev. B **69**, 155335 (2004).

[18] S. Souma and B. K. Nikolić, Phys. Rev. Lett. **94**, 106602 (2005).

[19] G. Lommer, F. Malcher, and U. Rössler, Phys. Rev. Lett. **60**, 728 (1988).

[20] S. D. Ganichev, V. V. Bel'kov, L. E. Golub, E. L. Ivchenko, P. Schneider, S. Giglberger, J. Eroms, J. De Boeck, G. Borghs, W. Wegscheider, et al., Phys. Rev. Lett. **92**, 256601 (2004).

[21] M. C. Chang, Phys. Rev. B **71**, 085315 (2005).

[22] W. Yang and K. Chang, Phys. Rev. B **73**, 045303 (2006).

[23] F. E. Meijer, A. F. Morpurgo, and T. M. Klapwijk, Phys. Rev. B **66**, 033107 (2002).

[24] T. Chakraborty, in *Adv. in Solid State Phys.*, edited by B. Kramer (Springer-Verlag, Berlin Heidelberg, 2003), vol. **43**, pp. 79–94.

[25] G. S. Lozano and M. J. Sánchez, Phys. Rev. B **72**, 205315 (2005).

[26] O. Madelung, ed., *Physics of Group IV Elements and III- V Compounds*, Landolt-Börnstein (New Series) Group III Condensed Matter Vol. **17**, Pt. a (Springer-Verlag, Berlin, 1982).

[27] I. S. Gradshteyn and I. M. Ryzhik, eds., *Tables of Integrals,Series, and Products* (Academic Press, New York, 1980).

From Electronic charge and spin density distribution ...

References

[1] S. Datta and B. Das, Appl. Phys. Lett. **56** (1990).

[4] Y. Bychkov and E. I. Rashba, JETP Lett. **39**, 78 (1984).

[3] G. Dresselhaus, Phys. Rev. **100**, 580 (1955).

[4] R. Winkler, *Spin orbit coupling effects in two-dimensional electron and hole systems* (Springer-Verlag Berlin, Heidelberg, New York, 2003).

[5] T. Ihn, Semiconductor nanostructures. Quantum states and electronic transport (Oxford University Press, 2010).

[6] J. Splettstoesser, M. Governale, and U. Zülicke, Phys. Rev. B **68**, 165341 (2003).

[7] S. Souma and B. K. Nikolić, Phys. Rev. B **70**, 195346 (2004).

[8] J. S. Sheng and K. Chang, Phys. Rev. B **74**, 235315 (2006).

[9] Y. Liu, F. Cheng, X. J. Li, F. M. Peeters, and K. Chang, Phys. Rev. B **82**, 045312 (2010).

[10] M. P. Nowak and B. Szafran, Phys. Rev. B **80**, 195319 (2009).

[11] F. E. Meijer, A. F. Morpurgo, and T. M. Klapwijk, Phys. Rev. B **66**, 033107 (2002).

[12] The first and second derivatives of any generic function $f(x)$, are approximated as $f'(x) \approx [f(x+h) - f(x-h)]/h$ and $f''(x) \approx [f(x+h) + f(x-h) - 2f(x)]/h^2$, respectively, where h is considered sufficiently small.

[13] P. Hawrylak and D. Pfannkuche, Phys. Rev. Lett. **70**, 485 (1993).

[14] N. T. T. Nguyen and F. M. Peeters, Phys. Rev. B **83**, 075419 (2011).

[15] N. T. T. Nguyen and F. M. Peeters, Phys. Rev. B **78**, 045321 (2008).

[16] D. Pfannkuche, V. Gudmundsson, and P. Maksym, Phys. Rev. B **47**, 2244 (1993).

[17] J. Schliemann, J. C. Egues, and D. Loss, Phys. Rev. Lett. **90**, 146801 (2003).

From Persistent current in ballistic mesoscopic rings with Rashba spin-orbit coupling

References

[1] *Semiconductor Spintronics and Quantum Computation*, D. D. Awschalom, D. Loss, and N. Samarth (eds.), Series Nanoscience and Technology (Springer, Berlin, 2002).

[2] S. A. Wolf *et al*, Science **294**, 1488 (2001).

[3] G. Lommer, F. Malcher, and U. Rössler, Phys. Rev. Lett. **60**, 728 (1988).

[4] E. I. Rashba, Fiz. Tverd. Tela (Leningrad) **2**, 1224 (1960), [Sov. Phys. Solid State **2**, 1109 (1960)].

[5] J. Nitta, T. Akazaki, H. Takayanagi, and T. Enoki, Phys. Rev. Lett. **78**, 1335 (1997).

[6] T. Schäpers *et al.*, J. Appl. Phys. **83**, 4324 (1998).

[7] D. Grundler, Phys. Rev. Lett. **84**, 6074 (2000).

[8] S. Datta and B. Das, Appl. Phys. Lett. **56**,665 (1990); E. A. de Andrada e Silva and G. C. La Rocca, Phys. Rev. B **59**, R15583 (1999); A. A. Kiselev and K. W. Kim, Appl. Phys. Lett. **78**, 775, (2001); T. Koga *et al*, Phys. Rev. Lett. **88**, 126601 (2001); M. Governale *et al.*, Phys. Rev. B **65**, 140403(R) (2002); J. C. Egues, G. Burkard, and D. Loss, Phys. Rev. Lett. **89**, 176401 (2002); M. Governale, Phys. Rev. Lett. **89**, 206802 (2002); R. Ionicioiu and I. D'Amico, Phys. Rev. B **67**, 041307(R) (2003); L. S. Levitov and E. I. Rashba, Phys. Rev. B **67**, 115324 (2003).

[9] T. Koga, J. Nitta, T. Akazaki, and H. Takayanagi, Phys. Rev. Lett. **89**, 046801 (2002).

[10] A. F. Morpurgo *et al.*, Phys. Rev. Lett. **80**, 1050 (1998).

[11] J.-B. Yau, E. P. De Poortere, and M. Shayegan, Phys. Rev. Lett. **88**, 146801 (2002).

[12] D. Loss, P. Goldbart, and A. V. Balatsky, Phys. Rev. Lett. **65**, 1655 (1990); D. Loss and P. Goldbart, Phys. Rev. B **45**, 13544 (1992).

[13] A. G. Aronov, Y. B. Lyanda-Geller, Phys. Rev. Lett. **70**, 343 (1993).

[14] T.-Z. Qian and Z.-B. Su, Phys. Rev. Lett. **72**, 2311 (1994).

[15] D. Frustaglia and K. Richter, preprint.

[16] M. J. Yang, C. H. Yang, K. A. Cheng, Y. B. Lyanda-Geller, cond-mat/0208260.

[17] M. Büttiker, Y. Imry, and R. Landauer, Phys. Lett. **96A**, 365 (1983).

[18] H. F. Cheung, Y. Gefen, E. K. Riedel, and W. H. Shih, Phys. Rev. B **37**, 6050 (1988).

[19] D. Loss and P. Goldbart, Phys. Rev. B **43**, 13762 (1991).

[20] H. Bouchiat and G. Montambaux, J. Phys. France **50**, 2695 (1989).

[21] G. Montambaux, H. Bouchiat, D. Sigeti, and R. Friesner, Phys. Rev. B **42**, 7647 (1990).

[22] Y. Meir, Y. Gefen, and 0. Entin-Wohlman, Phys. Rev. Lett. **63**, 798 (1989).

[23] O. Entin-Wohlmann, Y. Gefen, Y. Meir, and Y. Oreg, Phys. Rev. B **45**, 11890 (1992).

[24] H. Mathur and A. D. Stone, Phys. Rev. B **44**, 10957 (1991).

[25] T.-Z. Qian, Y.-S. Yi, and Z.-B. Su, Phys. Rev. B **55**, 4065 (1997).

[26] L. P. Lévy, G. Dolan, J. Dunsmuir, and H. Bouchiat, Phys. Rev. Lett. **64**, 2074 (1990)

[27] V. Chandrasekhar, R. A. Webb, M. J. Brady, M. B. Ketchen, W. J. Gallagher, and A. Kleinsasser, Phys. Rev. Lett. **67**, 3578 (1991).

[28] D. Mailly, C. Chapelier, and A. Benoit, Phys. Rev. Lett. **70**, 2020 (1993).

[29] F. Meier and D. Loss, cond-mat/0209521.

[30] F. Schütz, M. Kollar and P. Kopietz, cond-mat/0301351.

[31] Q.-F. Sun, H. Guo, and J. Wang, cond-mat/0301402.

[32] F. S. Nogueira and K.-H. Bennemann, cond-mat/0302528.

[33] F. E. Meijer, A. F. Morpurgo, and T. M. Klapwijk, Phys. Rev. B **66**, 033107 (2002).

[34] A. Lorke, R. J. Luyken, A. O. Govorov, J. P. Kotthaus, J. M. Garcia, and P. M. Petroff, Phys. Rev. Lett. **85**, 1694 (2000).

[35] A. Fuhrer, S. Lüscher, T. Ihn, T. Heinzel, K. Ensslin, W. Wegscheider, and M. Bichler, Nature (London) **413**, 822 (2001).

[36] U. F. Keyser, S. Borck, R. J. Haug, M. Bichler, G. Abstreiter, and W. Wegscheider, Semicond. Sci. Technol. **17**, L22 (2002).

[37] N. W. Ashcroft and N. D. Mermin, *Solid State Physics* (Saunders College, Philadelphia, 1988).

[38] See, e.g., U. Zülicke and C. Schroll, Phys. Rev. Lett. **88**, 029701 (2002).

[39] In a related model of electrons on a ring subject to a textured external magnetic field, additional constant terms contributing to the spin current were reported[12]. For the case of electrons on a ring with Rashba SO coupling which is considered here, no such terms appear.

[40] F. Mireles and G. Kirczenow, Phys. Rev. B **64**, 024426 (2001).

[41] M. Governale and U. Zülicke, Phys. Rev. B **66**, 073311 (2002).

From One-dimensional ring in the presence of Rashba spin-orbit interaction: Derivation of the correct Hamiltonian

[1] E. I. Rashba, Sov. Phys. Solid State 2, 1109 (1960).
[2] A. G. Aronov and Y. B. Lyanda-Geller, Phys. Rev. Lett. 70, 343 (1993).
[3] Y. S. Yi, T. Z. Qian, and Z. B. Su, Phys. Rev. B 55, 10631 (1997).
[4] L. Hu, H. Li, and G. He, Phys. Rev. B 62, 16744 (2000).
[5] Y. S. Yi and A. R. Bishop, Phys. Rev. B 58, 4077 (1998).
[6] S. L. Zhu, Y. C. Zhou, and H. Z. Li, Phys. Rev. B 52, 7814 (1995).
[7] T. Z. Qian, Y. S. Yi, and Z. B. Su, Phys. Rev. B 55, 4065 (1997).

[8] We note that the Hamiltonian used by Aronov and Lyanda-Geller becomes Hermitean in the limit of large angular momentum
($\langle i\partial/\partial\phi + \Phi/\Phi_0\rangle \gg 1$). In this limit, the eigenfunctions of the Hamiltonian calculated by these authors are correct.

[9] Y. C. Zhou, H. Z. Li, and X. Xue, Phys. Rev. B 49, 14010 (1994).

[10] T. Choi, S. Y. Cho, C. M. Ryu, and C. K. Kim, Phys. Rev. B 56, 4825 (1997).

[11] D. Loss, P. Goldbart, and A. V. Balatsky, Phys. Rev. Lett. 65, 1655 (1990); A. Stern, ibid. 68, 1022 (1992).

[12] Using the resulting approximate radial wave function, Eq. (9), we obtain $\langle(1/r)(\partial/\partial r)\rangle/\langle\partial^2/\partial r^2\rangle = e^{-(\gamma a)^2/(\gamma a\sqrt{\pi})}$. This is a small quantity when the radius of the ring is much larger than the width of the arms that goes to zero for a truly 1D ring ($\gamma \to \infty$). Therefore $\langle(1/r)(\partial/\partial r)\rangle$ can be neglected in the 1D limit.